

DESIGN OF SINGLE-SIDED FILLET WELDS UNDER TRANSVERSE LOADING

by

Justin H. Thomas

Submitted in partial fulfilment of the requirements
for the degree of Master of Applied Science

at

Dalhousie University
Halifax, Nova Scotia
August 2021

© Copyright by Justin H. Thomas, 2021

TABLE OF CONTENTS

| | |
|--|------|
| List of Tables | v |
| List of Figures | vii |
| Abstract | xii |
| Abbreviations and Symbols | xiii |
| Acknowledgements..... | xvii |
| Chapter 1: Introduction..... | 1 |
| 1.1. General..... | 1 |
| 1.1.1. Types of Welding Processes | 1 |
| 1.1.2. Types of Welds and Weld Joints | 2 |
| 1.2. Fillet Welds..... | 4 |
| 1.3. Single-Sided Fillet Welds | 5 |
| 1.4. Research Program Overview | 7 |
| Chapter 2: Background/ Literature Review | 8 |
| 2.1. Effect of Loading Angle on Fillet Weld Behaviour..... | 8 |
| 2.2. Experimental and Theoretical Studies on Transverse Fillet Welds | 8 |
| 2.2.1. Butler and Kulak (1971) | 8 |
| 2.2.2. Lesik and Kennedy (1988)..... | 8 |
| 2.2.3. Miazga and Kennedy (1989)..... | 9 |
| 2.2.4. Lesik and Kennedy (1990)..... | 11 |
| 2.2.5. Ng et al. (2002) | 12 |
| 2.2.6. Deng et al. (2003) | 12 |
| 2.2.7. Luo et al. (2020) | 13 |
| 2.3. Experimental and Numerical Studies on Single-Sided Welds | 15 |
| 2.3.1. Rasmussen et al. (1999)..... | 15 |
| 2.3.2. Chen et al. (2001) | 16 |
| 2.3.3. Packer et al. (2016)..... | 17 |
| 2.3.4. Tousignant and Packer (2017)..... | 18 |
| 2.3.5. Tuominen et al. (2018)..... | 19 |
| Chapter 3: Design Criteria for Fillet Welds..... | 22 |

| | | |
|------------|---|----|
| 3.1. | General..... | 22 |
| 3.2. | According to CSA S16:19 | 22 |
| 3.3. | According to CSA S16-14 | 23 |
| 3.4. | According to AISC 360-16 | 23 |
| 3.5. | According to EN1993-1-8:2005..... | 24 |
| 3.5.1. | Directional Method..... | 24 |
| 3.5.2. | Simplified Method | 26 |
| 3.6. | Summary | 27 |
| Chapter 4: | Experimental Program | 28 |
| 4.1. | Scope..... | 28 |
| 4.2. | Test Specimens | 28 |
| 4.2.1. | Test Specimen Description | 28 |
| 4.2.2. | Test Specimen Design Procedure | 29 |
| 4.2.3. | Test Specimen Fabrication Process | 30 |
| 4.3. | Geometric Property Measurement Procedure | 32 |
| 4.3.1. | Overall Specimen Cross-section Dimensions..... | 32 |
| 4.3.2. | Fillet Weld Cross Sectional Dimensions and Lengths..... | 33 |
| 4.4. | Mechanical Property Measurement Procedures..... | 38 |
| 4.4.1. | Base Metal Tensile Coupon Tests | 38 |
| 4.4.2. | Weld Metal Tensile Coupon Tests..... | 41 |
| 4.5. | Test Set-Up and Instrumentation | 42 |
| 4.5.1. | Test Set-Up..... | 42 |
| 4.5.2. | Instrumentation | 43 |
| 4.5.3. | Testing/ Loading Strategy..... | 43 |
| 4.6. | ETLCC Test Results | 44 |
| 4.6.1. | CSA S16:19 | 44 |
| 4.6.2. | AISC 360-16..... | 45 |
| 4.6.3. | EN1993-1-8:2005 | 46 |
| Chapter 5: | Evaluation of Results | 48 |
| 5.1. | Influence of Connection Parameters | 48 |
| 5.1.1. | Weld Size..... | 48 |
| 5.1.2. | Branch Plate Thickness..... | 49 |
| 5.1.3. | Eccentricity (Magnitude/Direction)..... | 50 |
| 5.1.4. | Weld Size-to-Branch Plate Thickness Ratio..... | 51 |
| 5.2. | Evaluation of Current Design Criteria | 51 |
| 5.2.1. | Reliability Analysis | 51 |

| | | |
|-------------|---|-----|
| 5.2.2. | Evaluation Procedure..... | 53 |
| 5.2.3. | Evaluation of Results..... | 56 |
| 5.3. | Comparison of Results to Tests on Double-Sided Welds..... | 60 |
| 5.3.1. | Comparison to Fillet Welded Lapped Splice and Cruciform Test Results..... | 60 |
| 5.3.2. | Comparisons to Fillet Welded HSS Test Results..... | 62 |
| 5.4. | Introduction and Evaluation of New Theoretical Model..... | 63 |
| Chapter 6: | Conclusions and Recommendations..... | 67 |
| 6.1. | Introduction..... | 67 |
| 6.2. | Summary..... | 67 |
| 6.3. | Conclusions..... | 67 |
| 6.4. | Recommendations and Future Work..... | 69 |
| References | | 70 |
| Appendix A: | ETLCC Specimen & Metal Coupon Fabrication Drawings..... | 74 |
| Appendix B: | Weld Pre-rupture and Post-rupture measurements..... | 86 |
| B.1. | Pre-Rupture Measurements..... | 86 |
| B.2. | Post-Rupture Measurements..... | 92 |
| Appendix C: | Material Property Test Results..... | 99 |
| Appendix D: | ETLCC Experimental Test Results..... | 101 |
| Appendix E: | Digital Image Correlation & Strain Gage Results..... | 105 |
| E.1. | Digital Image Correlation Results..... | 105 |
| E.2. | Strain Gage Results..... | 113 |
| Appendix F: | Other Experimental Program Test Data..... | 119 |
| Appendix G: | Macro-etch Examinations..... | 123 |
| Appendix H: | Documentation From Marid Industries Ltd..... | 163 |
| H.1. | Welder Qualification..... | 163 |
| H.2. | Mill Test Reports..... | 164 |
| H.3. | Welding Procedure Specification..... | 169 |

LIST OF TABLES

| | |
|---|-----|
| Table 1.1. Types of Welds (Gallow 2019) | 3 |
| Table 4.1. Nominal and actual cross-sectional dimensions of the welded ETLCC specimens..... | 33 |
| Table 4.2. Preliminary measurements of fillet weld cross sectional dimensions..... | 35 |
| Table 4.3. Post-rupture macro-etch examination measurements of fillet weld cross sectional dimensions..... | 37 |
| Table 4.4. Comparison between nominal properties and actual properties of the CSA G40.21 350W base metal coupons..... | 40 |
| Table 4.5. Summary of weld metal coupon tests | 42 |
| Table 5.1. Reliability indexes, resistance factors, and load factors..... | 53 |
| Table 5.2. Measured-to-nominal ratios of tensile strength of weld metal (Lesik and Kennedy 1990) | 55 |
| Table 5.3. Summary of δ_P and V_P values for CSA S16-19, AISC 360-16, and EN1993-1-8:2005..... | 55 |
| Table 5.4. Summary of δ_d and V_d for fillet weld throat and leg sizes from CISC handbook and AISC manual..... | 56 |
| Table 5.5. Reliability index values (CSA S408-11/CSAS6:19 approach) for each branch plate offset (S) using CSA S16:19, AISC 360-16 & EN1993-1-8:2005 design codes..... | 58 |
| Table 5.6. Reliability index values (separation factor approach) for each branch plate offset (S) using CSA S16:19, AISC 360-16 & EN1993-1-8:2005 design codes..... | 60 |
| Table 5.7. Summary of δ_P and V_P values for CSA S16-19, AISC 360-16, and EN1993-1-8:2005 for single-sided fillet welds and double-sided welds for lapped-splice and cruciform connections..... | 61 |
| Table 5.8. Summary of δ_P and V_P values for CSA S16-19, AISC 360-16, and EN1993-1-8:2005 for single-sided fillet welds and welds in HSS-to-rigid end plate connections | 62 |
| Table 5.9. Summary of δ_P and V_P values using the new theoretical model and β values according to CSA S408-11/ CSA S6:19 and the Separation-factor approach for single-sided fillet welds..... | 65 |
| | |
| Table A.1. List of ETLCC specimen fabrication drawings..... | 74 |
| Table B.1. Pre-rupture measurements for ETLCC specimens | 86 |
| Table B.2. Post-rupture measurements of ETLCC specimens | 92 |
| Table D.1. ETLCC experimental test results with comparison to CSA S16:19, AISC 360-16 and EN1993-1-8:2005..... | 101 |
| Table D.2. ETLCC experimental test results with comparison to new theoretical model | 103 |
| Table F.1. Experimental program test data for fillet welded RHS-to-rigid end plate connection tests | 119 |

Table F.2. Experimental program test data for fillet welded CHS-to-rigid end plate connection tests 120

Table F.3. Experimental program test data for fillet welded lapped-splice and cruciform connection tests..... 121

LIST OF FIGURES

| | |
|--|----|
| Fig. 1.1. Loading angle on a fillet welded connection..... | 4 |
| Fig. 1.2. Fillet weld geometry..... | 4 |
| Fig. 1.3. Fillet welded connections | 6 |
| Fig. 2.1 Diagram of an eccentrically loaded fillet weld connection (Lesik and Kennedy 1988)..... | 9 |
| Fig. 2.2. Eccentrically loaded welded connections (Lesik and Kennedy 1990) | 11 |
| Fig. 2.3. Finite element models for PJP and fillet welds (Luo et al. 2020) | 13 |
| Fig. 2.4. Test specimen and set-up for testing eccentricity in PJP (Rasmussen et al. 1999) | 15 |
| Fig. 2.5. Relationship of weld strength versus eccentricity for PJP welds (Rasmussen et al. 1999)..... | 16 |
| Fig. 2.6. Experimental segment for single-sided fillet weld specimen (Chen et al. 2001) | 16 |
| Fig. 2.7. HSS-to-rigid end-plate connection specimen (with RHS or CHS member) (Tousignant and Packer 2017)..... | 17 |
| Fig. 2.8. Single-sided fillet weld connection (Tuominen et al. 2018) | 20 |
| Fig. 2.9. Types of specimens used for experimental tests (Tuominen et al. 2018)..... | 20 |
| Fig. 3.1. Stress components of a fillet weld for the directional method (Newcomb and Tousignant 2021)..... | 25 |
| Fig. 4.1. Welded ETLCC connections and test specimens | 29 |
| Fig. 4.2. Mitigating branch plate deflection of welded ETLCC connections | 31 |
| Fig. 4.3. Macro-etch examination with measurements | 36 |
| Fig. 4.4. Sheet-type coupon specimen to test base metal..... | 38 |
| Fig. 4.5. Stress versus strain curve for 6.4 mm thick base metal coupons | 39 |
| Fig. 4.6. Testing of rectangular base metal coupons..... | 40 |
| Fig. 4.7. Drawings to fabricate weld coupon specimens. | 41 |
| Fig. 4.8. Stress versus strain curves for weld metal coupons | 42 |
| Fig. 4.9. Test set-up and instrumentation for the ETLCC specimens..... | 43 |
| Fig. 4.10. Comparison of actual strengths and predicted strengths using CSA S16:19..... | 45 |
| Fig. 4.11. Comparison of actual strengths and predicted strengths using AISC 360-16 | 46 |
| Fig. 4.12. Comparison of actual strength and predicted strengths using EN1993-1-8:2005 | 47 |
| Fig. 5.1. Effect of weld throat size on single sided fillet weld strength..... | 48 |
| Fig. 5.2. Effect of plate thickness on single-sided fillet weld strength..... | 49 |
| Fig. 5.3. Digital image correlation plots for y-axis strain (ϵ_{yy}) | 50 |

| | |
|--|-----|
| Fig. 5.4. Effect of eccentricity on single-sided fillet weld strength..... | 50 |
| Fig. 5.5. Effect of weld throat-to-branch plate thickness ratio on single-sided fillet weld strength..... | 51 |
| Fig. 5.6. Actual-to-measured weld throat size ratio versus weld throat size for ETLCC tests..... | 54 |
| Fig. 5.7. Discretization Factor (δ_d) for fillet weld throat and leg sizes from the CISC handbook and fillet weld leg sizes from the AISC manual..... | 56 |
| Fig. 5.8. Reliability index (β) plots for CSA S16:19..... | 57 |
| Fig. 5.9. Reliability index (β) plots for AISC 360-16..... | 58 |
| Fig. 5.10. Reliability index (β) plots for EN1993-1-8:2005..... | 59 |
| Fig. 5.11. Comparison of single-sided weld versus fillet welded lapped splice and cruciform test strengths using CSA S16:19..... | 61 |
| Fig. 5.12. Comparison of single-sided weld versus fillet welded HSS test strengths using CSA S16:19..... | 63 |
| Fig. 5.13. Correlation of new theoretical method to ETLCC tests..... | 64 |
| Fig. 5.14. Relationship between stiffness factor (λ) and weld throat-to-branch thickness ratio (t_w/t_v)..... | 65 |
| Fig. 5.15. Comparison of actual strengths and predicted strengths & reliability using the new theoretical model..... | 66 |
| | |
| Fig. A.1. Welded section overview..... | 75 |
| Fig. A.2. S6-30a & S6-15a sections..... | 76 |
| Fig. A.3. S6-0 & S6-15b sections..... | 77 |
| Fig. A.4. S6-30b & S20-30a sections..... | 78 |
| Fig. A.5. S20-15a & S20-0 sections..... | 79 |
| Fig. A.6. S20-15b & S20-30b sections..... | 80 |
| Fig. A.7. S9-0 section..... | 81 |
| Fig. A.8. S14-0 section..... | 82 |
| Fig. A.9. Test & trial specimens..... | 83 |
| Fig. A.10. Instrumentation..... | 84 |
| Fig. A.11. Base metal & weld metal test coupons..... | 85 |
| Fig. C.1. Base metal rectangular tensile coupon results..... | 99 |
| Fig. C.2. Weld metal round tensile coupon results..... | 100 |
| Fig. E.1. DIC strain plots for test S6-L-30a..... | 105 |
| Fig. E.2. DIC strain plots for test S6-S-15a..... | 106 |
| Fig. E.3. DIC strain plots for test S6-S-0..... | 106 |
| Fig. E.4. DIC strain plots for test S6-S-15b..... | 107 |
| Fig. E.5. DIC strain plots for test S6-S-30b..... | 107 |
| Fig. E.6. DIC strain plots for test S6-M-30b..... | 108 |
| Fig. E.7. DIC strain plots for test S6-L-30b..... | 108 |
| Fig. E.8. DIC strain plots for test S9-XS-0..... | 109 |

| | |
|---|-----|
| Fig E.9. DIC strain plots for test S9-L-0 | 109 |
| Fig. E.10. DIC strain plots for test S14-XS-0..... | 110 |
| Fig. E.11. DIC strain plots for test S14-L-0 | 110 |
| Fig. E.12. DIC strain plots for test S20-S-30a..... | 111 |
| Fig. E.13. DIC strain plots for test S20-L-15a..... | 111 |
| Fig. E.14. DIC strain plots for test S20-S-0..... | 112 |
| Fig. E.15. DIC strain plots for test S20-S-15b..... | 112 |
| Fig. E.16. DIC strain plots for test S20-S-30b..... | 113 |
| Fig. E.17. Legend for locations of strain gages for ETLCC tests..... | 113 |
| Fig. E.18. Strain gage graphs for S6-L-30a & S6-S-15a..... | 114 |
| Fig. E.19. Strain gage graphs for S6-S-0 & S6-S-15b..... | 114 |
| Fig. E.20. Strain gage graphs for S6-S-30b & S6-M-30b | 115 |
| Fig. E.21. Strain gage graphs for S6-L-30b..... | 115 |
| Fig. E.22. Strain gage graphs for S9-XS-0 & S9-L-0..... | 116 |
| Fig. E.23. Strain gage graphs for S14-XS-0 & S14-L-0..... | 116 |
| Fig. E.24. Strain gage graphs for S20-S-30a & S20-S-15a | 117 |
| Fig. E.25. Strain gage graphs for S20-L-15a & S20-S-0..... | 117 |
| Fig. E.26. Strain gage graphs for S20-S-15b & S20-S-30b..... | 118 |
| Fig. G.1. Macro-etch examinations for specimen S6-S-30a..... | 123 |
| Fig. G.2. Macro-etch examinations for specimen S6-M-30a | 124 |
| Fig. G.3. Macro-etch examinations for specimen S6-L-30a | 125 |
| Fig. G.4. Macro-etch examinations for specimen S6-S-15a..... | 126 |
| Fig. G.5. Macro-etch examinations for specimen S6-M-15a | 127 |
| Fig. G.6. Macro-etch examinations for specimen S6-L-15a | 128 |
| Fig. G.7. Macro-etch examinations for specimen S6-S-0 | 129 |
| Fig. G.8. Macro-etch examinations for specimen S6-M-0 | 130 |
| Fig. G.9. Macro-etch examinations for specimen S6-L-0 | 131 |
| Fig. G.10. Macro-etch examinations for specimen S6-S-15b | 132 |
| Fig. G.11. Macro-etch examinations for specimen S6-M-15b | 133 |
| Fig. G.12. Macro-etch examinations for specimen S6-L-15b | 134 |
| Fig. G.13. Macro-etch examinations for specimen S6-S-30b | 135 |
| Fig. G.14. Macro-etch examinations for specimen S6-M-30b | 136 |
| Fig. G.15. Macro-etch examinations for specimen S6-L-30b | 137 |
| Fig. G.16. Macro-etch examinations for specimen S9-XS-0..... | 138 |
| Fig. G.17. Macro-etch examinations for specimen S9-S-0 | 139 |
| Fig. G.18. Macro-etch examinations for specimen S9-M-0 | 140 |

| | |
|--|-----|
| Fig. G.19. Macro-etch examinations for specimen S9-L-0 | 141 |
| Fig. G.20. Macro-etch examinations for specimen S9-XL-0 | 142 |
| Fig. G.21. Macro-etch examinations for specimen S9-XXL-0 | 143 |
| Fig. G.22. Macro-etch examinations for specimen S14-XS-0..... | 144 |
| Fig. G.23. Macro-etch examinations for specimen S14-S-0 | 145 |
| Fig. G.24. Macro-etch examinations for specimen S14-M-0 | 146 |
| Fig. G.25. Macro-etch examinations for specimen S14-L-0 | 147 |
| Fig. G.26. Macro-etch examinations for specimen S14-XL-0 | 148 |
| Fig. G.27. Macro-etch examinations for specimen S14-XXL-0 | 149 |
| Fig. G.28. Macro-etch examinations for specimen S20-S-30a..... | 150 |
| Fig. G.29. Macro-etch examinations for specimen S20-M-30a | 151 |
| Fig. G.30. Macro-etch examinations for specimen S20-L-30a | 152 |
| Fig. G.31. Macro-etch examinations for specimen S20-S-15a..... | 153 |
| Fig. G.32. Macro-etch examinations for specimen S20-M-15a | 154 |
| Fig. G.33. Macro-etch examinations for specimen S20-L-15a | 155 |
| Fig. G.34. Macro-etch examinations for specimen S20-S-0 | 156 |
| Fig. G.35. Macro-etch examinations for specimen S20-M-0 | 157 |
| Fig. G.36. Macro-etch examinations for specimen S20-L-0 | 158 |
| Fig. G.37. Macro-etch examinations for specimen S20-S-15b | 159 |
| Fig. G.38. Macro-etch examinations for specimen S20-M-15b | 160 |
| Fig. G.39. Macro-etch examinations for specimen S20-L-15b | 161 |
| Fig. G.40. Macro-etch examinations for specimen S20-S-30b | 162 |
| Fig. H.1. Welder's certification from Marid Industries Ltd..... | 163 |
| Fig. H.2. Mill test report for 6.4 mm plate steel | 164 |
| Fig. H.3. Mill test report for 9.5 mm plate steel | 165 |
| Fig. H.4. Mill test report for 15.9 mm plate steel | 166 |
| Fig. H.5. Mill test report for 19.1 mm plate steel..... | 167 |
| Fig. H.6. Mill test report for 25.4 mm plate steel..... | 168 |
| Fig. H.7. Welding Procedure Specification (Pg. 1) | 169 |
| Fig. H.8. Welding Procedure Specification (Pg. 2) | 170 |
| Fig. H.9. Welding Procedure Specification (Pg. 3) | 171 |
| Fig. H.10. Welding Procedure Specification (Pg. 4) | 172 |
| Fig. H.11. Welding Procedure Specification (Pg. 5) | 173 |
| Fig. H.12. Welding Procedure Specification (Pg. 6) | 174 |
| Fig. H.13. Welding Procedure Specification (Pg. 7) | 175 |
| Fig. H.14. Welding Procedure Specification (Pg. 8)..... | 176 |

Fig. H.15. Welding Procedure Specification (Pg. 9)..... 177

ABSTRACT

In North American steel design codes, a “directional strength enhancement” (or “ $\sin\theta$ ”) factor is used to increase the predicted strength of fillet welds subjected to tension-induced shear. CSA and AISC code committees have expressed concerns about this factor being potentially unsafe for single-sided fillet welds; however, due to a paucity of physical tests on such welds, only cautionary, but vague, statements to address this issue exist in codes.

An experimental program was therefore developed at Dalhousie University to test 40 single-sided fillet welds in cruciform connections subjected to branch axial tension. The connections varied the fillet weld size, branch-plate thickness, and loading eccentricity, to investigate the effects of these parameters on the weld strength. Using ultimate loads, a first-order reliability analysis was performed to determine the inherent safety index (β) of North American fillet weld design procedures over a practical range of live-to-dead load (L/D) ratios for elements in steel buildings ($0 \leq L/D \leq 3$). The results show that current provisions meet/exceed the target safety index (i.e. $\beta = 4.0$) specified by North American codes (e.g. CSA S16 and AISC 360) provided that: (i) the “ $\sin\theta$ ” factor is not used and (ii) tension at the weld root is avoided. A new theoretical model for single-sided fillet welds is also introduced to account for weld eccentricity (i.e. induced stress due to the bending of the weld).

ABBREVIATIONS AND SYMBOLS

| | | |
|------------|---|--|
| AISC | = | American Institute of Steel Construction |
| ASTM | = | American Society for Testing and Materials |
| AWS | = | American Welding Society |
| CEN | = | European Committee for Standardization |
| CISC | = | Canadian Institute of Steel Construction |
| CSA | = | Canadian Standards Association |
| | | |
| CHS | = | circular hollow section |
| CJP | = | complete joint penetration groove weld |
| DIC | = | digital image correlation |
| ETLCC | = | eccentrically Tension-Loaded Cruciform Connection |
| FCAW | = | flux cored arc welding |
| GMAW | = | gas metal arc welding |
| HSS | = | hollow structural section |
| LVDT | = | linearly varying differential transformer |
| PJP | = | partial joint penetration groove weld |
| RHS | = | rectangular hollow section |
| SMAW | = | shield metal arc welding |
| SAW | = | submerged arc welding |
| TC | = | tensile coupon |
| | | |
| A | = | cross-sectional area of the HSS chord |
| A_θ | = | area of fracture surface of fillet weld at loading angle θ |
| a | = | weld throat size (according to EN 1993-1-8); factor expressing eccentricity in terms of weld length (in Lesik and Kennedy 1988). |
| A_w | = | effective throat area of weld ($= t_w \times l_w$) |
| B_b | = | width of RHS branch member |
| b | = | the length of the weld (and joint) (in Tuominen 2018) |
| C | = | tabulated coefficient for eccentrically loaded weld group |
| D | = | weld leg size |
| d | = | substitute for denominator of new theoretical model |
| D_b | = | diameter of CHS branch member |
| E | = | Young's modulus |

| | | |
|---------------|---|--|
| E_{avg} | = | average Young's modulus for tensile coupon tests |
| e | = | centre-to-centre distance between the branch plate and the weld throat plane (Tuominen 2018 & New theoretical model) |
| e/l_{wn} | = | eccentricity (for Rasmussen et al. 1999) |
| F_{EXX} | = | ultimate tensile strength of weld metal (in AISC 360) |
| F_{nw} | = | nominal strength of weld metal at failure (in AISC 360) |
| F_u | = | ultimate tensile strength for the base metal |
| $F_{u,avg}$ | = | average ultimate tensile strength for the base metal |
| f_w | = | applied load per weld throat area ($= P/A_w$) (New theoretical model) |
| F_w | = | load capacity (Tuominen 2018) |
| F_y | = | yield strength |
| $F_{y,avg}$ | = | average yield strength for base metal |
| k | = | 6 (for elastic distribution) and 4 (for plastic distribution) (in Tuominen 2018 & New theoretical model); factor expressing weld separation in terms of the weld length (in Lesik and Kennedy 1988). |
| L | = | basic length of fillet weld group; transverse distance from force to weld (in Tuominen 2018) |
| L/D | = | live-to-dead load ratio |
| l_{eff} | = | effective length of weld |
| l_h | = | weld leg (measured along the tension face) |
| l_v | = | weld leg (measured along the shear face) |
| l_w | = | total length of weld |
| M | = | moment of an adjacent member |
| M_w | = | strength reduction factor for multi-orientation fillet welds (in CSA S16) |
| n | = | number of load bearing (web) plates (in Tuominen 2018) |
| P | = | applied load |
| P_a | = | actual strength for single-sided fillet weld (from ETLCC experimental tests) |
| P_0 | = | ultimate strength of weld with loading angle of 0° |
| P_{nw} | = | nominal strength of fillet weld(s) |
| P_{nwl} | = | nominal strength of longitudinal fillet welds |
| P_{pr} | = | predicted strength for single-sided fillet weld (from CSA S16:19, AISC 360-16 or EN1993-1-8:2004 equations for fillet welds subject to tension-induced shear) |
| P_u/Af_{uw} | = | actual divided by predicted strength (for Rasmussen et al. 1999) |
| P_{wnt} | = | nominal strength of transverse fillet welds |
| P_θ | = | ultimate strength of weld with loading angle θ |
| S | = | branch plate offset (for ETLCC specimens) |

| | | |
|--------------------|---|---|
| t | = | plate thickness |
| t_b | = | wall thickness of HSS branch member |
| t_h | = | thickness of horizontal plates in ETLCC specimens |
| t_p | = | end-plate thickness |
| t_v | = | thickness of vertical (flange) plates in ETLCC specimen |
| t_w | = | weld throat size (in CSA S16 and AISC 360) |
| t_{wa} | = | actual weld throat size (from macro-etch examinations) |
| t_{wm} | = | measured weld throat size (from weld gage measurements) |
| V_d | = | coefficient of variation (discretization) |
| V_D | = | coefficient of variation for dead load |
| V_G | = | coefficient of variation (geometry) |
| V_L | = | coefficient of variation for live load |
| V_M | = | coefficient of variation (material) |
| V_P | = | coefficient of variation (professional) |
| V_r | = | factored shear resistance |
| V_R | = | coefficient of variation for resistance |
| V_{rw} | = | factored resistance of fillet weld |
| V_S | = | coefficient of variation for load effects |
| X_u | = | ultimate tensile strength of weld metal (in CSA S16) |
| X_{un} | = | nominal tensile strength of weld metal (in CSA S16) |
| $X_{u,avg}$ | = | average tensile strength of weld metal |
| α | = | average angle of inclination of fracture surface (Miazga and Kennedy 1989); angle of inclination of the weld throat plane (measured perpendicular to weld axis) (Tuominen 2018 and new theoretical model) |
| α_R | = | coefficient of separation (= 0.55) |
| β | = | reliability index |
| β_w | = | correlation factor for fillet welds (in EN 1993-1-8) |
| γ_D | = | load factor for dead load (associated with the LRFD or LSD method) |
| γ_L | = | load factor for live load (associated with the LRFD or LSD method) |
| γ_{M2} | = | partial safety factor for the resistance of welds (= 1.25 in EN 1993-1-8) |
| δ_d | = | discretization factor |
| δ_G | = | geometry factor |
| δ_M | = | material factor |
| δ_P | = | professional factor |
| ϵ_f | = | fracture strain |
| $\epsilon_{f,avg}$ | = | average fracture strain |

| | | |
|-----------------------|---|---|
| ε_{xx} | = | x-axis strain (from DIC plots) |
| ε_{xy} | = | shear strain (from DIC plots) |
| ε_{yy} | = | y-axis strain (from DIC plots) |
| ε_y | = | yield strain |
| $\varepsilon_{y,avg}$ | = | average yield strain |
| θ | = | angle between the axis of a weld segment and the line of action of the applied force (in degrees) |
| θ_i | = | branch inclination angle |
| λ | = | angle of inclination of the weld throat plane (measured perpendicular to weld axis); frame stiffness factor for bending moment in the load bearing web plate (in Tuominen 2018); stiffness factor for single-sided fillet welded connection (New theoretical model) |
| ρ_D | = | bias coefficient for dead load |
| ρ_L | = | bias coefficient for live load |
| ρ_r | = | bias coefficient for resistance |
| σ_{\perp} | = | normal stress perpendicular to the weld throat |
| τ_{\parallel} | = | shear stress (in plane of throat) parallel to the longitudinal axis of the weld |
| τ_{\perp} | = | shear stress (in plane of throat) perpendicular to the longitudinal axis of the weld |
| ϕ | = | resistance factor (associated with the LRFD or LSD method) |
| ϕ_w | = | resistance factor for weld metal |
| Ψ | = | local dihedral angle (angle between the base metal fusion faces) |

ACKNOWLEDGEMENTS

First, I would like to thank my supervisor, Dr. Kyle Tousignant, for all the support he has given me with my thesis and developing my professional career. I would also like to thank the lab technicians in the Department of Civil and Resource Engineering at Dalhousie University: Mr. Jordan Maerz, Mr. Jesse Keane, and Mr. Dean Grijm.

Financial support for this research was provided by the Canadian Institute of Steel Construction (CISC), the Natural Sciences and Engineering Research Council of Canada (NSERC), and the Nova Scotia Graduate Scholarship (NSGS) program.

Thanks are extended to Marid Industries Ltd., Windsor Junction, Nova Scotia, for fabricating the Eccentrically Tension-Loaded Cruciform Connection (ETLCC) specimens, and Mr. T. Parsons, for his ongoing interest in this work. Fabrication work by Mr. S. Butler is gratefully acknowledged.

Finally, I would like to give thanks to my family, who have been the greatest support to me while getting my education.

Chapter 1: INTRODUCTION

1.1. GENERAL

Steel structures are generally constructed of members connected by welds, bolts, or some combination of the two. Welding is a process done by applying heat and/or pressure between two (or more) pieces of metal to fuse them together. This can be done with, or without, the use of additional filler metal, as described in Section 1.1.1.

1.1.1. TYPES OF WELDING PROCESSES

Welding, as a process, has evolved over time and takes many forms. In its simplest form, it can be done by heating metals in ovens and joining them together by hammering. In more complex forms, various heat sources such as electrical heat generation (arc welding and electron beam welding), electric resistance (resistance welding such as spot welding), electromagnetic radiation (laser beam welding), chemical heat generation (exothermic welding), and mechanical heat generation (oxy-fuel or gas-flame welding) and filler metals can be used (Linnert 1967).

The most common welding methods are the arc-welding and oxy-gas flame welding methods. The former method (i.e. arc welding) is most widely used – especially in structures – for its low cost and accuracy. The heat in arc welding is generated by an electric current from an electrode attached to the metal pieces that need to be welded. An ionized column is created between the negatively charged cathode (electrode) held by the welder, and the positively charged anode (i.e. the work pieces to be welded). This results in an arch-shaped central plasma, like what happens when lightning is formed. The plasma is used to generate a large amount of heat, which is used to promote fusion of the two (or more) metal pieces together. In most cases, the electrode is also a *consumable*, which acts as a *filler metal* for the welded connection. This filler metal – when molten – needs to be shielded from oxidization, and from forming nitrates. This is typically done using a *shielding gas*.

Common types of arc welding processes (which differ based on electrode and shielding gas used) include shielded metal arc welding (SMAW), gas metal arc welding (GMAW), flux-cored arc welding (FCAW), and submerged arc welding (SAW) (EFIG 1995).

The electrode rod used in SMAW consists of a filler metal protected by a shielding cover. During welding, the shielding cover vaporizes and forms a gas shield to protect the arc and molten metal from the atmosphere. In GMAW, the electrode is the filler, and a shielding gas is externally applied to protect the arc. FCAW's














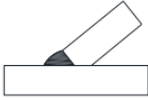
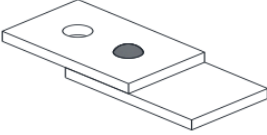
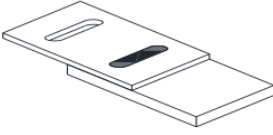
electrode is tubular in nature. The filler metal is within the external tubular portion, and the flux (powered metals) exists inside of it. When heat is applied, and the weld is formed, the flux covers the weld in a protective slug. For SAW, the arc and weld pool are continually shielded by granular fusible flux that is applied right before the welding (O'Brien, 1991).

The most common welding process used in the fabrication of structural steel is the FCAW process. The research herein focuses on joints made using that process (rather than equivalent joints made using SMAW, GMAW, or SAW).

1.1.2. TYPES OF WELDS AND WELD JOINTS

Classification of welds varies based on the connection details and the weld location. Welds can be classified groove welds (complete- or partial-joint-penetration), plug welds, slot welds, or fillet welds. These different types of welds are shown, diagrammatically, in Table 1.1 on the following page. Fillet welds are – by far – the most desirable type of weld in structures. This is because fillet welds require less preparation of the base metal(s) when compared to plug and slot welds, making them simpler and more cost effective.

Table 1.1. Types of Welds (Gallow 2019)

| Fillet Welds | | | |
|---|--|--|---|
|  T-Joint |  Lap Joint |  Corner Joint | |
|  Skewed Beveled T-Joint | |  Skewed Square T-Joint | |
| Complete Joint Penetration (CJP) Groove Welds | | | |
|  Square But Weld |  Single V-But Weld |  Double V-But Weld | |
|  Skewed T-Joint without Backing | |  Skewed T-Joint with Backing | |
| Partial Joint Penetration (PJP) Groove Weld | | | |
|  Square But Weld |  Single V-But Weld |  Double V-But Weld |  Skewed T-Joint |
| Plug Weld | | Slot Weld | |
|  | |  | |

As shown in Table 1.1, a complete-joint-penetration (CJP) groove weld is a condition in which weld metal extends through the entire joint thickness (CSA 2018). Partial-joint-penetration (PJP) groove welds are like CJP welds, except the weld metal only extends through a part of the joint thickness. Plug welds are made in a circular hole(s) in one member of a joint in order to fuse that member to another, adjacent member. Slot welds are like plug welds except the weld is made in an elongated (rather than a circular) hole. It is worth noting that plug welds and slot welds are not commonly used in structures.

Fillet welds (e.g. as shown at the top of Table 1.1) are welds of approximately triangular cross section joining two surfaces approximately at right angles to each other in a lap joint, T-joint, or corner joint. There are

generally considered to be two loading conditions: a longitudinal loading condition, where the applied load is along the longitudinal axis of the weld, and a transverse loading condition, where the load is applied perpendicular to the weld axis as shown in Fig. 1.1. As discussed below in Section 1.2., design criteria exist for these two loading conditions, as well as cases where the direction of the applied load falls between these two extremes.

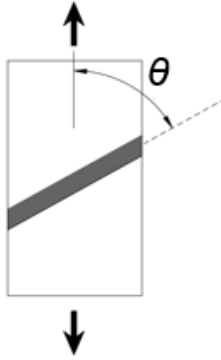


Fig. 1.1. Loading angle on a fillet welded connection.

1.2. FILLET WELDS

The strength of a fillet weld is governed by the weld material (filler metal) shear strength. When the load on a joint exceeds the fillet weld capacity (shear strength), failure generally occurs by weld rupture along a plane through the effective weld throat (Fig. 1.2.).

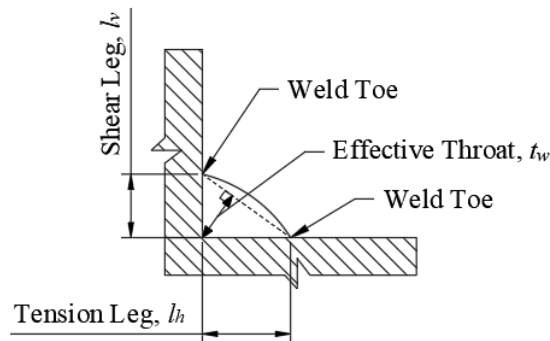


Fig. 1.2. Fillet weld geometry

The effective weld throat is defined as the shortest distance from the root of the weld to the face of the largest triangle which can be inscribed within the weld profile. Another common weld measurement is the weld leg(s). Fillet welds, by definition, have two “legs”, which are measured as the distance from the weld root to the “toe” of the weld, along the fusion face, in either direction. Weld sizes (e.g. as cited in North American

codes and standards) are generally given as the weld leg dimension(s) for fillet weld joining two pieces or material at 90°. Both leg dimensions are usually assumed to be equal.

To simplify calculations, the strength of a fillet weld in North American codes is generally based on the shear strength of the filler metal and the effective throat area of the weld – regardless of the loading direction or the angle of the actual failure plane.

For example, until CSA S16:19 (CSA 2019), the factored resistance (V_r) of a fillet weld for direct shear and tension- or compression-induced shear could be taken as (CSA 2014):

$$V_r = 0.67\phi_w A_w X_u (1.00 + 0.50\sin^{1.5}\theta) \quad (1.1)$$

where ϕ_w = weld metal resistance factor; A_w = effective throat area of weld; and X_u = strength of matching electrode; and θ = angle, in degrees, of axis of weld segment with respect of the line of action of applied force (e.g., 0° for a longitudinal weld and 90° for a transverse weld). The term $(1.00+0.5\sin^{1.5}\theta)$ in Eq. (1.1) is herein referred to as the “directional strength-increase” or “ $\sin\theta$ ” factor.

As seen from the $\sin\theta$ factor, it is generally accepted that, at a loading perpendicular to the weld axis (i.e. for transverse welds), the fillet weld strength is about 50% stronger than the longitudinal loading condition (AISC 2016; Butler and Kulak 1971; Callele et al. 2009; Dale and Laurie 1988; Iwankiw 1997; Lesik and Kennedy 1988; Miazga and Kennedy 1989; Miller 1998).

Conversely, transversely loaded fillet welds tend to exhibit lower ductility than longitudinally loaded welds. In CSA S16-14 (CSA 2014), for example, the resistance (V_r) of each weld segment in a fillet weld group that is concentrically loaded and consists of weld segments in different orientations [i.e. in multi-orientation fillet weld (MOFW) groups] was multiplied by a reduction factor, M_w , which is given by the following:

$$M_w = \frac{0.85 + \theta_1/600}{0.85 + \theta_2/600} \quad (1.2)$$

where θ_1 = orientation of the weld segment under consideration; and θ_2 = orientation of the weld segment in the joint that is nearest to 90°.

For MOFW joints, M_w can vary be 0.85 and 1.0 depending on the orientation of the weld segments. This M_w factor aimed to take into account that, in an MOFW joint, transverse weld(s) prevent a longitudinal weld(s) from reaching their full strength (due to deformation incompatibility) before failure of the entire joint takes place. For joints with a single weld orientation (such as those covered herein), M_w is equal to 1.0.

1.3. SINGLE-SIDED FILLET WELDS

As discussed so far, in North America, fillet welds connecting structural elements can be designed using a directional strength-increase or $\sin\theta$ factor [i.e. $(1.00+0.5\sin^{1.5}\theta)$ in Eq. (1.1)] that permits engineers to take

advantage of a 50% “strength increase” when load is applied perpendicular (i.e. at $\theta = 90^\circ$) to the weld axis. At present, this factor is included in CSA S16:19 Clause 13.13.2.2 (CSA 2019), AISC 360-16 Section J2.4b (AISC 2016), and AWS D1.1-15 Clause 2.6.4.2 (AWS 2015). The $\sin\theta$ factor is based on testing of lapped splice and cruciform connections (Figs. 1.3.a and 1.3.b), where fillet welds were made on both sides of a plate loaded in tension (Figs. 1.3.a, b). These tests are discussed, in detail, in Section 2.3.

Recently, CSA S16 and AISC 360 code committees have expressed concerns about the $\sin\theta$ factor being potentially unsafe for transversely loaded single-sided fillet welds (i.e. welds made on one side of a structural element, connected to an element in tension) (Fig. 1.3.c).

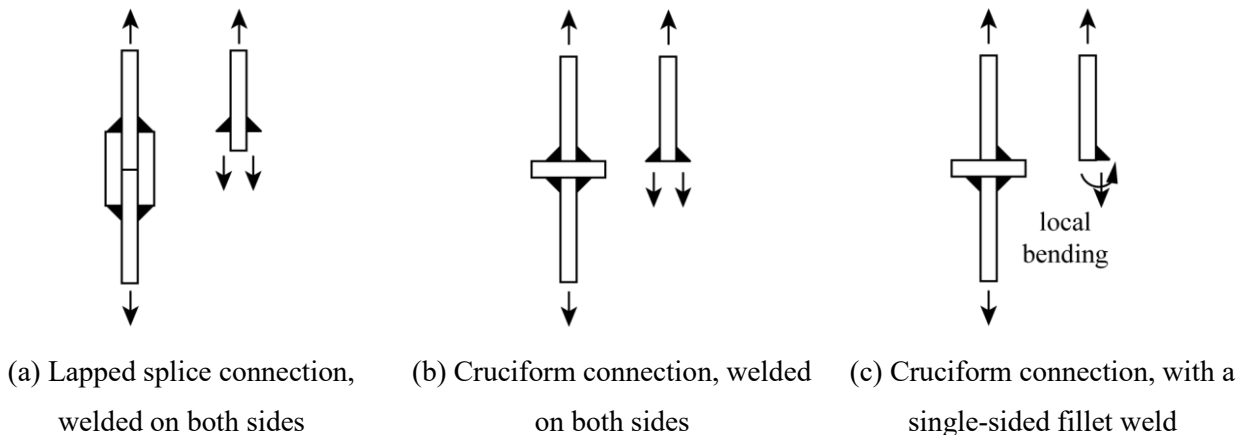


Fig. 1.3. Fillet welded connections

The application of single-sided welds includes but are not limited to: HSS-to-HSS connections, wide flange beam to column connections and HSS column-to-base plate connections. Unlike their two-sided counterparts (Figs. 1.3.a, b), single-sided fillet welds are inherently “eccentrically loaded”, and prone to local bending about their axis (or rotation about the weld toe) (Fig. 1.3.c). This can subject the weld to additional tensile stress at its root, and significantly reduce its capacity (AISC 2015, CEN 2005). Cautionary (but vague) comments addressing this issue are found in modern steel design codes. For example:

1. AISC 360-16 (2016) Commentary to Section J2b: “The use of single-sided fillet welds in joints subject to rotation around the toe of the weld is discouraged.”
2. AWS D1.1-15 (2015) Section 2.6.2: “In the design of welded joints, the calculated stresses shall include those due to eccentricity caused by alignment of the connected parts, size, and type of weld(s)”
3. CSA W59-18 (2018) Clause 4.1.3.3.2: “Single fillet and single partial joint penetration groove welds shall not be subjected to bending about the longitudinal axis of the weld if it produces tension at the root of the weld”; and

4. EN 1993-1-8 (2005) Clause 4.12: “local eccentricity should be taken into account where a tensile force transmitted perpendicular to the longitudinal axis of the weld produces a bending moment, resulting in a tension force at the root of the weld”.

Recent experiments and numerical (finite element) analysis on single-sided fillet welds around the ends of hollow structural sections (HSS) has confirmed that bending about the weld axis occurs when the HSS is in tension (Packer 2016; Tousignant and Packer 2017). Furthermore, it has been shown that such welds, to rectangular HSS, do not develop the 50% strength increase at failure predicted by the $\sin\theta$ factor.

Based on this evidence, the CSA S16 Code Committee has opted to exclude/prohibit the $(1.00+0.5\sin^{1.5}\theta)$ factor for the design of *all* single-sided fillet welds to an element in tension (i.e. not just those to the ends of rectangular HSS members) in CSA S16:19 (Packer 2019; CSA 2019). In contrast, AISC Task Committee 6 (Connection Design) has recommended to exclude the $\sin\theta$ factor only for the design of fillet welds to tension-loaded rectangular HSS walls in AISC 360-22 (Tousignant and Packer 2019; AISC 2021). While both restrictions are rational, the one being imposed by CSA (covering all single-sided fillet welds) stands to increase weld sizes in many connections (by up to 50%). Presently, there is a paucity of physical tests on such welds to substantiate this requirement.

1.4. RESEARCH PROGRAM OVERVIEW

Hence, the research presented herein covers an experimental program developed and executed at Dalhousie University to investigate the strength of single-sided fillet welds under transverse loading.

Relevant experimental and numerical studies on the strength and behaviour of double- and single-sided fillet welds are reviewed in Chapter 2.

In Chapter 3, modern design criteria for fillet welds (i.e. criteria in steel codes) are discussed. The use of the “directional strength enhancement” in North American design codes (CSA S16:19 and AISC 360-16) is illustrated, and the European steel design code (EN1993-1-8:2004) methods for the design of fillet welds, known as the Directional Method and the Simplified Method, are discussed.

Chapter 4 details the development and execution of the experimental program covering tests on 40 transversely loaded single-sided fillet welds in cruciform connections. The connections varied the fillet weld size (D), branch-plate thickness (t_v), and loading eccentricity (S) to investigate the effects of these parameters on the weld strength.

In Chapter 5, a first-order reliability analysis is performed to determine the inherent safety index (β) of North American fillet weld design procedures – applied to the results of the experiments – over a practical range of live-to-dead load (L/D) ratios for elements in steel buildings ($0 \leq L/D \leq 3$). The results are compared to previous tests on fillet-welded lapped splice, cruciform and HSS connections.

Conclusions of this study, and recommendations for CSA S16 and AISC 360, are discussed in Chapter 6.

Chapter 2: BACKGROUND/ LITERATURE REVIEW

2.1. EFFECT OF LOADING ANGLE ON FILLET WELD BEHAVIOUR

As the loading angle (θ) on a fillet weld increases, the strength of the fillet weld increases as well. When the weld is loaded longitudinally (i.e. at $\theta = 0^\circ$), the strength of the fillet weld is governed by the shear strength of the filler metal. When the weld is loaded transversely (i.e. $\theta = 90^\circ$), the strength of the fillet is more dependant on the tensile strength of the filler. To take this behaviour into account (simply), a “directional strength enhancement” factor is used in North American codes. Experimental and numerical studies that contributed to the derivation of this factor are discussed in Section 2.2.

2.2. EXPERIMENTAL AND THEORETICAL STUDIES ON TRANSVERSE FILLET WELDS

2.2.1. BUTLER AND KULAK (1971)

Butler and Kulak (1971) conducted a series of 23 concentrically loading fillet weld lapped splice specimens. Five specimens were loaded parallel to the weld axis and ones loaded at 30° , 60° , and 90° to the weld axis each had six. The objective of this research was to establish a load-deformation relationship for a length of fillet weld. The specimens were made using CSA G40.12 steel plates and E60XX weld metal [with a specified yield strength of 44 ksi (approx. 300 MPa) and a minimum tensile strength of 62 ksi (approx. 450 MPa)]. Results showed that the strength and the deformation of the welds change with changes in loading direction. Fillet welds saw an approximate strength increase of 44%, and a loss in ductility, when changing the loading angle from 0° to 90° .

2.2.2. LESIK AND KENNEDY (1988)

The goal of Lesik and Kennedy (1988) was to develop a method for predicting the ultimate strength of eccentrically loaded fillet weld groups loaded in shear, based on previous work of Miazga and Kennedy (1986). One such method was the “instantaneous centre of rotation” method which is an analytical approach based on the load-deformation characteristics of the weld and satisfying the equilibrium and compatibility conditions of the connection. Fig. 2.1. shows an example of an eccentrically loaded fillet weld connection. It is important to note that, unlike the current research, the welds tested by Lesik and Kennedy (1988) were eccentrically loaded *in-plane*.

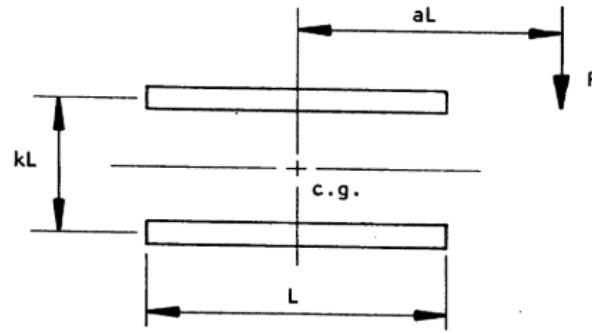


Fig. 2.1 Diagram of an eccentrically loaded fillet weld connection (Lesik and Kennedy 1988)

Values k and a are factors expressing weld separation and eccentricity, respectively, in terms of the weld length (L). In the CISC handbook, a set of tables of C coefficients can be used to determine the capacity of eight different weld groups. Eqn. (2.1) is used to calculate the capacity of these connections:

$$P = CDL \quad (2.1)$$

P = applied load; C = tabulated coefficient for eccentrically loaded weld group; D = weld leg size; and L = basic length of fillet weld group.

Lesik and Kennedy's (1988) results showed that coefficient C , indicative of the weld group strength, is larger when fracture deformation is used as the critical criteria. The proposed tables were shown to be less conservative and less variable than those in previous CISC design guides.

2.2.3. MIAZGA AND KENNEDY (1989)

A rational analytical model for determining the ultimate strength of fillet welds loaded in shear dependent on the angle of loading was later developed by Miazga and Kennedy (1989). This model related the ultimate strength to the inclination of the fracture surface and the restraint conditions of the root of the weld. The weld can be oriented parallel to the load direction (0° to the load direction), perpendicularly to the load direction (90° to the load direction), or in an intermediate direction.

A total of 42 fillet welded specimens were made to test the capacity of fillet welds loaded at different load angles, where 6 of those were loaded in the transverse direction. The weld sizes tested are 5 mm and 9 mm, and the specimens had fillet welds on both sides to reduce the effects of eccentric loading. The welds were also chosen to ensure weld rupture occurred before plate yielding to limit deformation of the plates. The plate sizes used were 9, 18, and 35 mm, and were all from the same heat. The fracture of inclination of the welds were also measured.

The results from Miazga and Kennedy (1989) showed that the average inclination of fracture surface (from the shear face) ranges from 49° for welds subject to longitudinal loading, where it is around 14° for welds subject to transverse loading. The maximum shear stress theory (states failure will occur once the maximum allowable shear stress is achieved) was the best overall predictor of the inclination of fracture angles. The expressions used to derive the predicted fracture angles [Eqns. (2.2) and (2.4)] are as follows:

$$\tau = \frac{P}{A_{\theta}} [(\sin \theta \cos \alpha - a \sin \theta \sin \alpha)^2 + \cos^2 \theta]^{1/2} \quad (2.2)$$

where τ = average shear stress along the fracture plane; P = applied load; A_{θ} = area of fracture surface of fillet weld at loading angle θ ; θ = angle between the axis of a weld segment and the line of action of the applied force (in degrees); α = average angle of inclination of the fracture surface; and a = coefficient applied to stress resultant component $P \sin \theta$ which is described by:

$$a = 0.600 - 0.0036\theta \quad (2.3)$$

Eqn. (2.2) can be differentiated in terms of α and set to zero to maximize τ . The predicted fracture angle α can be determined using Eqn. (2.4).

$$\tan(45^\circ + \alpha) = \frac{(\cos \alpha - a \sin \alpha)^2 + \cot^2 \theta}{(\cos \alpha - a \sin \alpha)(\sin \alpha + a \cos \alpha)} \quad (2.4)$$

Using predicted fracture angles, Miazga and Kennedy (1989) found that the maximum shear stress theory predicts that weld strengths increase to 1.32 times the longitudinal strength as the loading angle increases from 0° to 90°. Lateral restraint at the weld root also contributes to a strength increase with is a function of the loading angle. With increase in weld strength based on the fracture angle with that due to lateral restraint, the weld strength increases 1.50 times as the loading angle increases from 0° to 90°. The mean test/predicted ratio for the 42 specimens they tested was 1.004 with a coefficient of variation of 0.087. The predicted directional strength enhancement factors were determined using the following expression:

$$\frac{P_{\theta}}{P_0} = \sin(45^\circ + \alpha) \sqrt{(\sin \theta \cos \alpha - a \sin \theta \sin \alpha)^2 + \cos^2 \theta}^{-1} \quad (2.5)$$

where P_{θ} = ultimate strength of weld with loading angle θ ; and P_0 = ultimate strength of weld with loading angle of 0°.

2.2.4. LESIK AND KENNEDY (1990)

Fillet weld connections are frequently loaded eccentrically in shear with the externally applied load in the same plane as the weld group (whereas the ETLCC specimens are eccentrically loaded out of plane) as shown in Fig. 2.2. Lesik and Kennedy (1990) compare methods of analysis involving ultimate strengths as well as incorrectly mix inelastic and elastic approaches which were being used in, at the time, current design standards which give conservative and variable margins of safety.

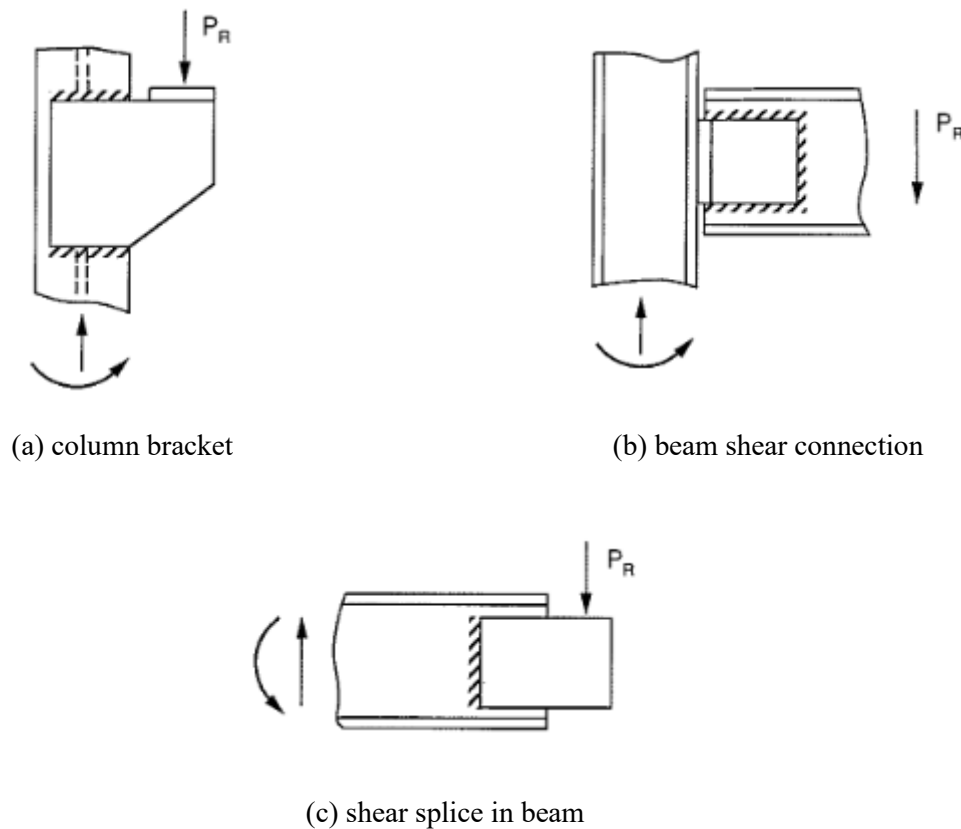


Fig. 2.2. Eccentrically loaded welded connections (Lesik and Kennedy 1990)

Lesik and Kennedy summarize the data for various tests programs on the ultimate strength of fillet welds. These test programs include Butler et al. (1972), Swannell and Skewes (1979a, 1979b), Kulak and Timler (1984), and Miazga and Kennedy (1989). All these programs observed that the ultimate strength of fillet welds increase with loading angle.

A more simplified expression [compared to Miazga and Kennedy (1989)] was proposed for shear resistance (V_r) of concentrically loaded fillet welds at an angle to the load of θ degrees which is:

$$V_r = P_\theta = 0.67\phi_w A_w X_u (1.00 + 0.50 \sin^{1.5} \theta) \quad (2.6)$$

where P_θ = ultimate strength of weld with loading angle θ ; ϕ_w = weld metal resistance factor; A_w = effective throat area of weld; X_u = strength of matching electrode; and θ = angle between the axis of a weld segment and the line of action of the applied force (in degrees).

Lesik and Kennedy (1990) state the empirical relationship between the angle of the load and the weld strength agrees with the work done by Miazga and Kennedy (1989). The deformation capacity (i.e. ductility) of fillet welds decrease as the loading angle increases. Eqn. (2.6) is still used in North American steel design codes to consider the effects loading angle has on fillet weld capacity.

2.2.5. NG ET AL. (2002)

Ng et al. (2002) conducted tests on 102 transverse weld specimens made using the flux core arc welding (FCAW) process (93 specimens) and the shield metal arc welding (SMAW) process (9 specimens). Of the 102 specimens, 96 were lapped-splice specimens and 6 were cruciform connection specimens. The purpose of this study was to expand on the work done by Miazga and Kennedy (1989) by investigating more parameters and their effects on fillet weld strength. The tests were designed to investigate the following parameters: (1) filler metal classification, both with and without a toughness requirement; (2) welding process, SMAW vs. FCAW; (3) weld size and number of passes; (4) welding electrode manufacturers; (5) steel fabricators; (6) low temperature; and (7) root notch orientation fillet weld (i.e. lapped splice vs. cruciform connections). Eqn. 2.6 (with $\phi_w = 1.0$, to give nominal strength) was used to predict the fillet weld strength. Results showed the range of test/predicted ratios were from 1.14 to 2.30 and that the welding process itself (SMAW or FCAW) had little on the weld strength. However, the FCAW specimens had higher penetration leading to larger fracture surface areas (approx. 1.5 to 2.0 times the theoretical throat areas) where the SMAW specimens fracture areas were closer to the theoretical throat areas. Based on a simplified reliability analysis using a separation factor of $\alpha = 0.55$ (see Section 2.2.6), Eqn. (2.6) was shown to provide a reliability index (β) of at least 4.5 (the target value at the time) or greater.

2.2.6. DENG ET AL. (2003)

Deng et al. (2003) conducted an experimental program consisting of 18 lapped-splice fillet weld specimens. Nine had fillet welds orientated longitudinally and the other nine at 45° to the applied load. This was done to compliment the work of Ng et al (2002). Specimens had 12.7 mm fillet welds and were prepared using three FCAW electrodes which included filler metals with and without a specified toughness. Higher toughness was found to improve fillet weld ductility but decrease longitudinal fillet weld strength. The fillet weld strength was found to increase with increasing loading angle. It was also found that the North American design equation for fillet welds provides an adequate safety index for single orientation fillet welds. The reliability index (β) was calculated using the “separation factor approach” (CSA 2001) given by the following expression:

$$\phi = \Phi_{\beta} \rho_R e^{-\beta \alpha_R V_R} \quad (2.7)$$

where ϕ = resistance factor; ρ_R = bias coefficient for resistance; α_R = coefficient of separation (= 0.55); V_R = coefficient of variation for resistance; and Φ_{β} = adjustment factor that modifies ϕ , determined by the following expression:

$$\Phi_{\beta} = 0.0062\beta^2 - 0.131\beta + 1.338 \quad (2.8)$$

The results for the Deng et al. (2003) for the 90°, 45° and 0° loading angle tests showed β values of 6.2, 7.5 and 5.6, respectively. Tests were compared to previous tests done by Miazga and Kennedy (1989) which saw a β value of 4.9.

2.2.7. LUO ET AL. (2020)

Luo et al. (2020) investigated the mechanical behaviour of partial-joint-penetration (PJP) groove welds and fillet welds at different loading angles. As codes traditionally focus on the directional strength increase factor for fillet welds, more research was needed to focus on PJP welds. A series of non-linear finite-element (FE) analyses using Abaqus were used to evaluate the strength of PJP welds under different loading angles, which would be compared with fillet welds. The FE models are shown in Fig. 2.3. These FE analyses were validated by experimental tests.

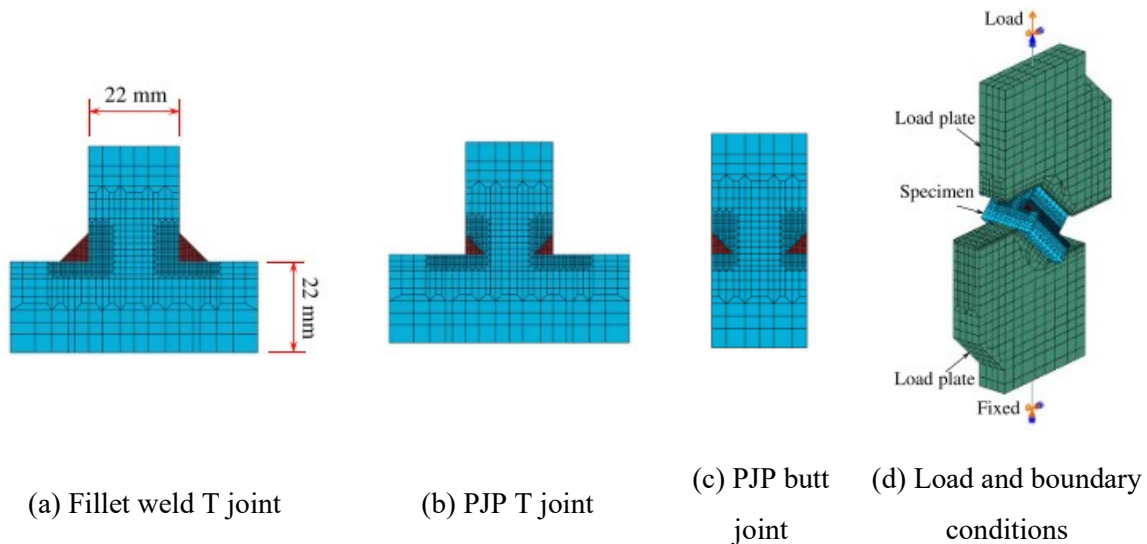


Fig. 2.3. Finite element models for PJP and fillet welds (Luo et al. 2020)

For the fillet weld T joints (Fig. 2.3a), which are similar to the ETLCCs covered in the current study, loading angles from 0° to 90° were tested at 15° increments. The transverse loaded fillet weld (loaded at 90°) was shown to have 1.34 times the strength compared to the fillet weld loaded longitudinally (loaded at 0°).

Results of the FE analyses along with the experimental tests showed that current US design practice for calculating the strength of PJP welds is conservative when the directionality effect is ignored. While this finding is important for the design of welded steel connections, PJP welds are outside the scope of the current study.

2.3. EXPERIMENTAL AND NUMERICAL STUDIES ON SINGLE-SIDED WELDS

This section provides a summary of experimental and numerical studies on the strength and behaviour of single-sided welds. To date, there has been little testing done on single-sided *fillet* welds, except for in the context of hollow structural sections (HSS) joints, in which welds to branch members are inherently single-sided.

2.3.1. RASMUSSEN ET AL. (1999)

The work done by Rasmussen et al. (1999) investigates the strength of eccentricity loaded incomplete penetration butt welds (PJP welds). The purpose was to examine how increasing eccentricity affects the stress on the weld. A total of 9 cruciform specimens were tested where the eccentricity ranges from 0 mm to 30 mm. Offset of the PJP welded plate in both directions were examined. An example of the test specimen and the test-up used can be seen in Fig. 2.4.

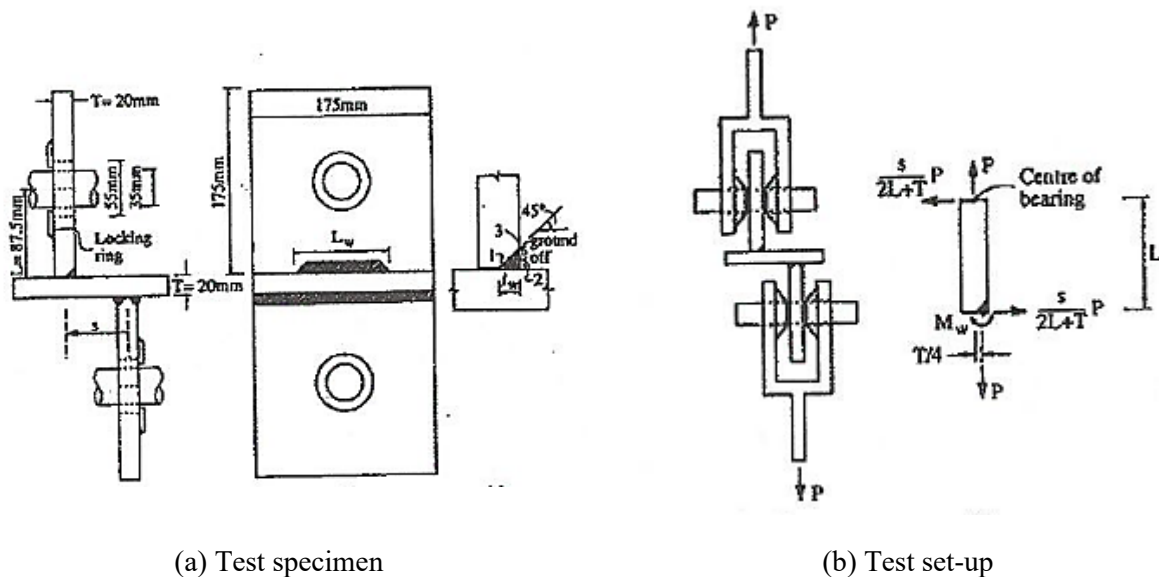


Fig. 2.4. Test specimen and set-up for testing eccentricity in PJP (Rasmussen et al. 1999)

The results saw two types of failure modes emerge. The first one caused the connection to “close-up” which caused compression in the infused parts. The second one caused the connection to “open-up” which caused a separation in the infused parts and large bending strains in the weld. Also, a relationship between eccentricity and strength was derived and the results were compared to the Australian steel structures standard AS4100:1998. A graph of this relationship, comparing P_u/Af_{uw} (strength) on the y-axis to e/l_{wn} (eccentricity) on the x-axis, is shown below, in Fig. 2.5.

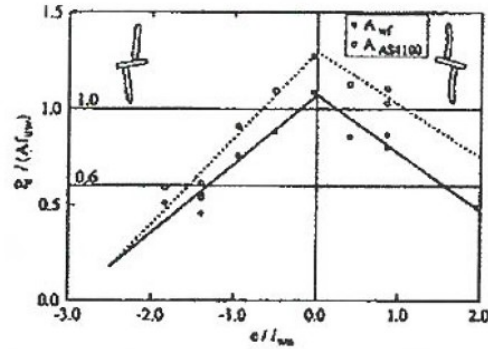


Fig. 2.5. Relationship of weld strength versus eccentricity for PJP welds (Rasmussen et al. 1999)

2.3.2. CHEN ET AL. (2001)

Chen et al. (2001) conducted an experimental program on the performance of single fillet weld joints in H-shape steel members. The authors examined the mechanical performance of single sided welded joints. A total of 57 specimens were studied for the depth of the fusion by metallographic examination. To evaluate the strength of the single-sided weld joints, two sets of specimens were tested: 26 specimens under shear and 20 specimens under tension.

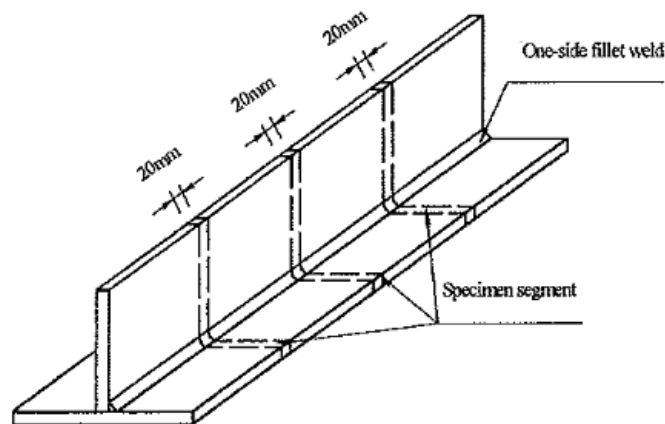


Fig. 2.6. Experimental segment for single-sided fillet weld specimen (Chen et al. 2001)

Results showed that the shear strength of a single-sided fillet weld can be treated the same as a double-sided fillet weld in engineering design. However, when the specimens were subjected to tension (load is applied perpendicular to the weld length), they exhibited reduced strength, since they were subjected, as well, to bending due to the eccentricity in the weld joint. The authors concluded that if the welding procedure can assure good depth of fusion, the reduction of the fillet weld strength due to the eccentricity could be neglected; however, this was in conjunction with an over-simple design model (i.e. one that is inherently conservative).

2.3.3. PACKER ET AL. (2016)

Packer et al. (2016) published the results of 33 total weld-critical HSS-to-rigid end-plate connections tested at the University of Toronto between the mid-1980s and late-2010s. The objective was to assess the reliability associated with the directional strength enhancement factor used by the North American steel design codes. All specimens were tested to failure by axial tension and were designed to be weld critical. The specimens tested along with their parameters can be seen in Fig. 2.7.

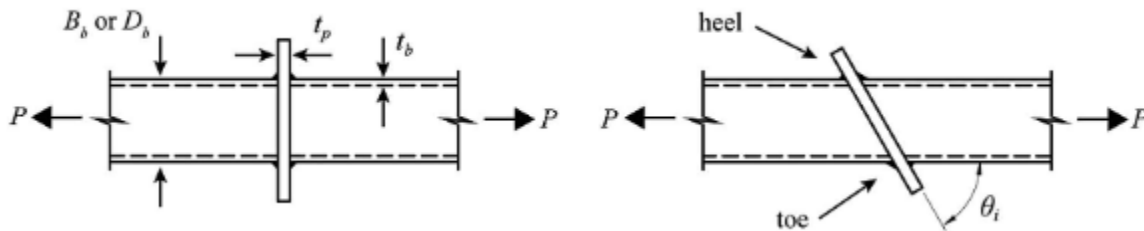


Fig. 2.7. HSS-to-rigid end-plate connection specimen (with RHS or CHS member) (Tousignant and Packer 2017)

Of the 33 connections, thirteen of these tests were done by Frater (1986) on RHS-to-rigid end-plate connections, with fillet weld throat dimensions (t_w) ranging from 0.37 to 1.13 times the branch wall thickness (t_b). Frater (1986) found that, for connections with small welds ($t_w/t_b \leq 0.50$) and a branch inclination angle $\theta_i = 90^\circ$, rupture always occurred through the weld, around the entire branch perimeter. With slightly larger welds ($0.50 < t_w/t_b \leq 0.60$), rupture generally occurred within the weld, but was accompanied by rupture of the end-plate near the middle of the RHS branch member walls. For connections with the largest welds tested ($0.81 \leq t_w/t_b \leq 1.13$), end-plate rupture governed failure, with only some weld rupture occurring at sharp angles around the RHS corners (failure mode P). When $\theta_i = 60^\circ$, Frater (1986) found that only the connection with the smallest weld size ($t_w/t_b = 0.42$) ruptured through the weld, around the entire branch perimeter. The remaining three connections with $\theta_i = 60^\circ$ ruptured in the end-plate, instead of the weld, along the heel of the connection.

Eight additional RHS-to-rigid end-plate connections, with $\theta_i = 90^\circ$ and similar weld sizes to Frater (1986) ($0.46 \leq t_w/t_b \leq 0.76$), were tested by Oatway (2014). In all these tests, rupture occurred through the weld, around the entire branch perimeter. In 12 tests on CHS-to-rigid end-plate connections conducted by the authors, with $0.45 \leq t_w/t_b \leq 0.99$, the same failure mode was observed. Three tests on CHS-to-rigid end-plate connections were also performed at Tongji University, China (Wang et al. 2015); however, only one of them failed entirely by weld rupture. A second test failed by weld rupture combined with branch rupture in the heat-affected zone, and the third test did not reach the ultimate load.

Results showed that using the directional strength enhancement factor led to unsafe predictions in the design strength of these connections. This led to a recommendation to restrict the use of this factor when using

fillet welds on HSS members. When the strength enhancement factor is not used for strength calculations for fillet welds to HSS, both current CSA and AISC specifications achieved adequate reliability indices (i.e. $\beta \geq 4.5$ and 4.0 , respectively, at the time).

2.3.4. TOUSIGNANT AND PACKER (2017)

Tousignant and Packer (2017) performed a finite element (FE) investigation to extend the work of Packer et al. (2016) and examine the behaviour of fillet-welded hollow structural section (HSS) rigid end-plate connections. To validate the FE models used, 33 RHS- and CHS-to-rigid end-plate connection FE models were developed using ANSYS. These tests were designed to replicate the experimental tests done by Packer et al. (2016). The geometric parameters used (as defined, previously, in Section 2.3.1.) were: θ_i , t_w , t_b , and D_b or B_b (diameter of CHS branch member or width of RHS branch member, respectively). These models covered the following ranges of these geometric parameters: $\theta_i = 60$ and 90° , $0.34 \leq t_w/t_b \leq 1.13$, CHS branches with $11.0 \leq D_b/t_b \leq 25.1$, and RHS branches with $13.4 \leq B_b/t_b \leq 16.3$. The specimens tested are as shown, previously, in Fig. 2.2.

Then, a parametric study was performed along with 73 other numerical tests to evaluate the effect of weld size, HSS wall slenderness, and branch inclination on fillet weld strength. A total of 65 90° fillet-welded RHS- and CHS-to-rigid end-plate connection specimens with six values of t_w/t_b (ranging from 0.35 to 1.41), and six values of the branch wall slenderness (9.1 to 50). The effect of θ_i was also examined by conducting eight additional FE analyses with $t_w/t_b = 0.50$: two RHS-to-rigid end-plate connections with $B_b/t_b = 12.5$ and 50 , and $\theta_i = 60^\circ$; two RHS-to-rigid end-plate connections with $B_b/t_b = 12.5$ and 50 , and $\theta_i = 75^\circ$; two CHS-to-rigid end-plate connections with $D_b/t_b = 12.5$ and 50 , and $\theta_i = 60^\circ$; two CHS-to-rigid end-plate connections with $D_b/t_b = 12.5$ and 50 , and $\theta_i = 75^\circ$. These eight analyses were then compared to four previous FE specimens where $t_w/t_b = 0.50$ and $\theta_i = 90^\circ$ (two RHS-to-rigid end-plate connections with $B_b/t_b = 12.5$ and 50 , and two CHS-to-rigid end-plate connections with $D_b/t_b = 12.5$ and 50) to examine the effect on fillet weld strength with respect to branch angle. The HSS width, or diameter, and end plate thickness were kept constant for all joints ($B_b = 200$ mm, $D_b = 168$ mm, and $t_p = 25$ mm).

Results of the FE tests showed: as t_w/t_b increases, the average stress on the weld throat area greatly decreases, as B_b/t_b and D_b/t_b increase, the average stress on the weld throat area slightly decreases. Design methods for fillet welds to HSS members given in ANSI/AISC 360-16 (AISC 2016), CSA S16-14 (CSA 2014), and EN 1993-1-8:2005 (CEN 2005) were evaluated according to North American safety index requirements looking at RHS and CHS-to-rigid end-plate connections independently. When the directional strength-increase factor in ANSI/AISC 360-16 and CSA S16-14 was used, it was found to provide inadequate safety indices when used to design fillet welds to HSS. It was therefore recommended to not use the directional strength increase factor for the design of fillet welds to HSS.

2.3.5. TUOMINEN ET AL. (2018)

Tuominen et al. (2018) examined the effect of bending moment (due to eccentricity) on the capacity of single-sided fillet welds around RHS branches in longitudinal RHS-to-RHS T-connections. Typically, the moment generated by the loading eccentricity was believed to decrease stresses and strains at the root of the weld, which increases the strength and deformation capacity of the weld(s). However, in some cases, it was found that this moment can increase the stresses at the weld root. This study investigated the effect of that so-called eccentricity moment (and its direction) on the static strength of welds.

The theoretical resistance of a single-sided fillet weld was developed by the authors based on the von Mises yield failure criterion and the expression used in EN 1993-1-8 (CEN 2005), as given by Eqn. (2.9).

$$\sigma_v = \sqrt{(\sigma_m + \sigma_b)^2 + 3\tau^2} = \frac{F_u}{\beta_w \gamma_{M2}} \quad (2.9)$$

where σ_v = von Mises stress; σ_m = membrane stress acting normal to the throat area; σ_b = bending stress acting on the critical plane; τ = shear stress; F_u = ultimate strength of the base metal; γ_{M2} = partial safety factor for the resistance of the weld; and β_w = correlation factor for fillet welds.

The stress components were defined by the following Eqns. (2.10a-c).

$$\sigma_b = \frac{k(nM \pm Fe)}{na^2b} \quad (2.10a)$$

$$\sigma_m = \frac{F \cos \alpha}{nab} \quad (2.10b)$$

$$\tau = \frac{F \sin \alpha}{nab} \quad (2.10c)$$

where $k = 6$ (for elastic distribution) and 4 (for plastic distribution); F = applied load; n = the number of load bearing (web) plates; e = centre-to-centre distance between the branch plate and the weld throat plane (described in Fig. 2.8.); a = weld throat size; b = the length of the weld (and joint); M = is the (constant) moment of an adjacent member [see Eqn. (2.11)]; and α = angle of inclination of the weld throat plane (measured perpendicular to weld axis).

$$M = \lambda FL \quad (2.11)$$

where λ = the frame stiffness factor for bending moment in the load bearing web plate; and L = the transverse distance from force to weld.

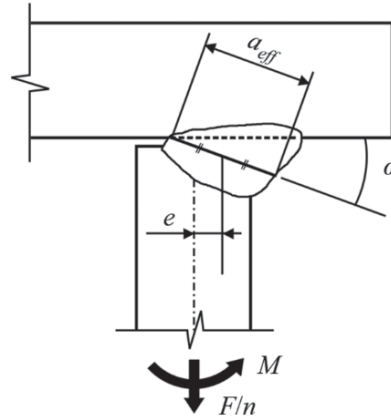
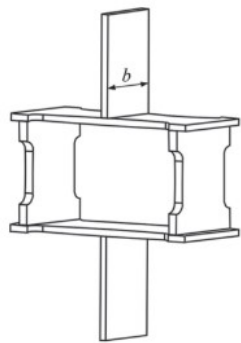


Fig. 2.8. Single-sided fillet weld connection (Tuominen et al. 2018)

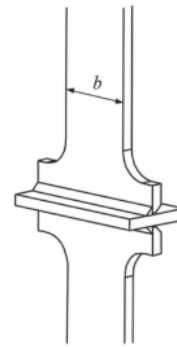
Eqns. (2.10a-c) and (2.11) can be substituted into Eqn. (2.9) to achieve the following expression [Eqn. (2.12)] for the load capacity (F_w) of a single-sided welded joint, in accordance with the European Directional Method (see Section 3.4.1.), where γ_{M2} can be set to 1.0 for nominal strength predictions.

$$F_w = \frac{nabF_u}{\beta_w \sqrt{\left[\cos \alpha + \frac{k(n\lambda L + e)}{a} \right]^2 + 3\sin^2 \alpha}} \quad (2.12)$$

A total of 13 laboratory tests were conducted by Tuominen et al. (2018), including tests on box sections and X-joints. The box sections contained only fillet welds, whereas the X-joints contained both fillet welds and single-bevel welds. The parameters examined were type (box section and X-joint), location and eccentricity of the joint and type of the weld (single bevel weld and fillet weld). The types of test specimens used can be seen in Fig. 2.9.



(a) Box test specimen



(b) X-joint test specimen

Fig. 2.9. Types of specimens used for experimental tests (Tuominen et al. 2018)

The range of λ observed for the experimental tests was between 0 to 0.11. The results of the tests showed that tensile stresses on the root side of the weld due to bending and tension loads resulted in the most critical combination, and the interaction should be calculated according to the theory of elasticity (elastic stress distribution). Otherwise, the interaction of stress components can be taken as the fully plastic stress distribution. It was also recommended that additional bending due to eccentricity and the fillet weld should be avoided in the weld root. This model serves as the basis for the “new theoretical model” for fillet weld strength (which accounts for out-of-plane eccentricity) introduced in Section 5.4.

Chapter 3: DESIGN CRITERIA FOR FILLET WELDS

3.1. GENERAL

Design specifications (i.e. CSA S16 in Canada, AISC 360 in the United States, and EN 1993-1-8 in Europe), which have been largely developed from the previously discussed test programs, provide weld strength design criteria based on the joint type, weld and base-metal strength, and direction of the load with respect to the longitudinal axis of the weld. While these specifications generally allow for under- or over-matched electrodes, this work will cover the case where matched electrodes are used and, hence, failure is generally assumed to occur in the weld metal.

3.2. ACCORDING TO CSA S16:19

In Clause 13.13.2.2 of CSA S16:19 (CSA 2019), the factored resistance for the direct shear and tension- or compression-induced shear of a fillet weld is taken as:

$$V_r = 0.67\phi_w A_w X_u \quad (3.1)$$

where ϕ_w = weld metal resistance factor; A_w = effective throat area of weld; and X_u = strength of matching electrode.

For cases other than single-sided fillet welds connected to an element in tension, the above resistance may be multiplied by the following strength-enhancement factor:

$$(1.00 + 0.50 \sin^{1.5} \theta) \quad (3.2)$$

where θ = angle, in degrees, of axis of weld segment with respect of the line of action of applied force (e.g., 0° for a longitudinal weld and 90° for a transverse weld).

For fillet weld groups concentrically loaded and consisting of welding segments in different orientations, the strength of each weld segment shall be multiplied by the reduction factor, M_w , given as 1.0 for the weld segment with the largest θ and 0.85 for the other weld segments.

3.3. ACCORDING TO CSA S16-14

Prior to CSA S16:19, CSA S16-14 gave the factored resistance for direct shear and tension- or compression-induced shear (V_r) as:

$$V_r = 0.67\phi_w A_w X_u (1.00 + 0.50 \sin^{1.5} \theta) M_w \quad (3.3)$$

where M_w = strength reduction factor for multi-orientation fillet welds. For joints with a single weld orientation, $M_w = 1.0$; for joints with multiple weld orientations, for each segment:

$$M_w = \frac{0.85 + \theta_1/600}{0.85 + \theta_2/600} \quad (3.4)$$

where θ_1 = orientation of the weld segment under consideration; and θ_2 = orientation of the weld segment in the joint that is closer to 90° . Unlike in CSA S16:19 (CSA 2019), in CSA S16-14 (2014), there was no distinction made about joints having single-sided fillet welds.

3.4. ACCORDING TO AISC 360-16

In Section J of AISC 360, a similar approach is taken for the design of fillet welds where the design strength ($V_r = \phi P_{nw}$) is as follows:

$$P_{nw} = F_{nw} A_w \quad (3.5)$$

where P_{nw} = the nominal weld strength; F_{nw} = nominal stress of the weld metal; and A_w = effective throat area of weld. In the above expression:

$$F_{nw} = 0.60 F_{EXX} \quad (3.6)$$

where F_{EXX} = ultimate strength of weld metal (= X_u , in CSA S16:19).

Also, for a linear weld group with a uniform leg size, loaded through the center of gravity (i.e. all welds in the weld group are parallel and have the same deformation capacity), the provisions of Section J2.4(b) allow for the directional strength factor, as shown in CSA S16:19, to be used. In that case, the equation for calculating the strength of the weld segment or group in AISC 360-16 is hence:

$$F_{nw} = 0.60 F_{EXX} (1.0 + 0.50 \sin^{1.5} \theta) \quad (3.7)$$

However, as discussed previously in this thesis, in the cases where welds of different orientations are together in the same welded connection (i.e. in MOFW joints), the longitudinal welds cannot reach their full capacity

(because longitudinal welds are more ductile than transverse welds). Thus, when applying the above equation to MOFW joints, the following adjustment is made:

$$P_{nw} = 0.85P_{nwl} + 1.5P_{nwt} \quad (3.8)$$

where P_{nwl} = total nominal strength of the longitudinal fillet welds; and P_{nwt} = total nominal strength of the transverse fillet welds without the “ $\sin\theta$ ” factor. This is akin to the approach that is now given in CSA S16:19 (using the M_w factor).

3.5. ACCORDING TO EN1993-1-8:2005

3.5.1. DIRECTIONAL METHOD

The EN1993-1-8 Directional Method breaks up the resultant design force transmitted by a unit length of weld into components parallel and perpendicular to the longitudinal axis of the weld and normal and transverse to the plane of the weld throat. The following inequalities must then be met for the strength of the weld to be adequate:

$$\left[\sigma_{\perp}^2 + 3(\tau_{\perp}^2 + \tau_{\parallel}^2) \right]^{0.5} \leq F_u / (\beta_w \gamma_{M2}) \quad (3.9a)$$

$$\text{and } \sigma_{\perp} \leq 0.9F_u / \gamma_{M2} \quad (3.9b)$$

where σ_{\perp} = normal stress perpendicular to the throat; τ_{\perp} = shear stress (in plane of throat) perpendicular to the longitudinal axis of the weld; τ_{\parallel} = shear stress (in plane of throat) parallel to the longitudinal axis of the weld; γ_{M2} = partial safety factor for the resistance of the weld equal to 1.25; and β_w = correlation factor for fillet welds.

The three stress components used for the Directional Method are shown in Fig. 3.1. It can be noted that the applied load (P) causes stress on the weld throat surface which exists, in theory, at the surface angle (λ). The local dihedral angle (between the base metal fusion faces) (Ψ) is assumed to be 90° .

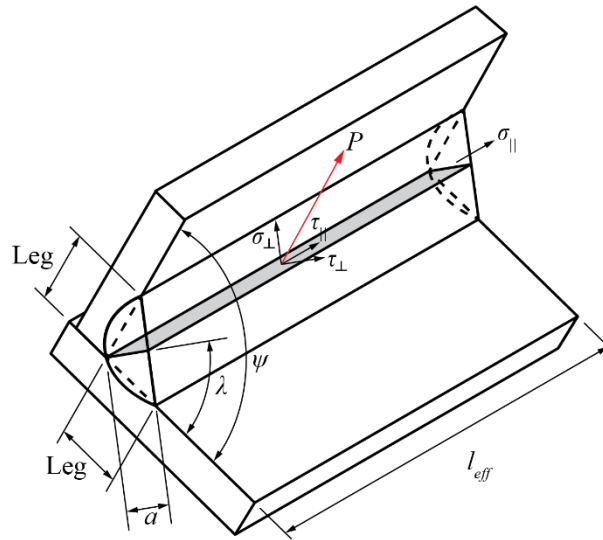


Fig. 3.1. Stress components of a fillet weld for the directional method (Newcomb and Tousignant 2021)

Packer et al. (2016) has shown that Eqns. (3.10a-c) can be used to calculate the stress components on a fillet weld at a load equal to the design resistance (V_{rw}) as follows:

$$\tau_{\parallel} = \frac{V_{rw} \cos \theta}{al_{eff}} \quad (3.10a)$$

$$\sigma_{\perp} = \frac{V_{rw} \sin \theta \cos \lambda}{al_{eff}} \quad (3.10b)$$

$$\tau_{\perp} = \frac{V_{rw} \sin \theta \sin \lambda}{al_{eff}} \quad (3.10c)$$

where V_{rw} = design resistance of the fillet weld; λ = angle of inclination of the weld throat plane, measured in a plane perpendicular to the weld axis; a = throat thickness; and l_{eff} = effective length of weld.

When the stress component equations Eqns. (3.10a-c) for a fillet weld are substituted into Eqn. (3.8a) the following expression, Eq. (3.11), can be derived for the shear resistance of a fillet weld according to EN 1993-1-8:

$$V_{rw} = \frac{F_u}{\beta_w \gamma_{M2}} \frac{a l_{eff}}{\left[\sin^2 \theta \cos^2 \lambda + 3(\sin^2 \theta \sin^2 \lambda + \cos^2 \theta) \right]^{0.5}} \quad (3.11)$$

where F_u = ultimate tensile strength of the base metal.

Eqn. (3.11) can be simplified for 90° equal-legged fillet welds ($\lambda = 45^\circ$). Hence, it can be shown that the design strength for longitudinal welds ($\theta = 0^\circ$) [Eqn. (3.12a)] and transverse welds ($\theta = 90^\circ$) [Eqn. (3.12b)], respectively, are the following:

$$V_{rw} = \left(\frac{F_u}{\sqrt{3} \beta_w \gamma_{M2}} \right) t_w l_w \quad (3.12a)$$

$$V_{rw} = \left(\frac{F_u}{\sqrt{2} \beta_w \gamma_{M2}} \right) t_w l_w \quad (3.12b)$$

where t_w = size of weld throat; and l_w = length of weld segment.

In the case of 90° unequal-legged fillet welds ($\lambda \neq 45^\circ$), Eqn. (3.11) must be used, and the weld throat thickness can be calculated by the following expression [Eqn. (3.13)].

$$a = \frac{l_v l_h}{\sqrt{l_v^2 + l_h^2}} \quad (3.13)$$

where l_v = weld leg (measured along the shear face); and l_h = weld leg (measured along the tension face).

To calculate λ for 90° unequal-legged fillet welds, the following expression [Eqn. (3.14)] can be used:

$$\lambda = \tan^{-1} \left(\frac{l_h}{l_v} \right) \quad (3.14)$$

3.5.2. SIMPLIFIED METHOD

The Simplified Method is an alternative to the Directional Method that assumes the fillet weld strength is independent of the orientation of the weld throat plane relative to the design force. This method is conservative

compared to Eq. (3.11) because the welds are assumed to be loaded in pure shear and proportioned in accordance with Eq. (3.12a).

3.6. SUMMARY

Currently, design specifications (i.e. CSA S16 in Canada, AISC 360 in the United States, and EN 1993-1-8 in Europe) provide weld strength design criteria based on the joint type, weld and base-metal strength, and direction of the load with respect to the longitudinal axis of the weld. For North American design codes (i.e. CSA S16 in Canada, AISC 360 in the United States), a “directional strength enhancement” (or “ $\sin\theta$ ”) factor is used to increase the predicted strength of fillet welds subjected to tension-induced shear. Transverse fillet welds take advantage of a 50% strength increase.

Experiments and numerical (finite element) analysis on single-sided fillet welds around the ends of hollow structural sections (HSS) has confirmed that bending about the weld axis occurs when the HSS is in tension (Packer 2016; Tousignant and Packer 2017). Furthermore, it has been shown that such welds generally do not develop the 50% strength increase at failure predicted by the $\sin\theta$ factor.

Based on this evidence, the CSA S16 Code Committee has opted to exclude/prohibit the $(1.00+0.5\sin^{1.5}\theta)$ factor for the design of all single-sided fillet welds to an element in tension (i.e. not just those to the ends of rectangular HSS members) in CSA S16:19 (Packer 2019; CSA 2019). In contrast, AISC Task Committee 6 (Connection Design) has recommended to exclude the $\sin\theta$ factor only for the design of fillet welds to tension-loaded rectangular HSS walls in AISC 360-22. This can cause confusion for those designing single-sided fillet welded connections which are not HSS connections (examples of other applications in Section 1.3.).

The current research aims to better understand the behaviour of single-sided fillet welds to resolve this disparity between CSA S16 and AISC 360.

Chapter 4: EXPERIMENTAL PROGRAM

4.1. SCOPE

An experimental program was developed at Dalhousie University to examine the parameters that affect the capacity of transversely loaded single-sided fillet welds. The purpose of this program was to address (i.e. validate or modify) restrictions on the “strength increase” factor ($1.00+0.50\sin^{1.5}\theta$) in modern steel codes [principally AISC 360-16 (2016) and CSA S16:19 (2019)].

Forty-two “weld-critical” connections (i.e. connections that failed by weld rupture) were designed and fabricated with variations in the fillet weld size, branch-plate thickness, and loading eccentricity. The specimens, referred to as “eccentrically tension loaded cruciform connections” (or ETLCCs), were tested in the Heavy Structures Lab at Dalhousie University by using a 2-MN Instron Universal Testing Machine to apply tension to the branch plates. Tension load on the plate and the strain adjacent to the weld, on both sides of the plate, were measured, and the ultimate load of each specimen was determined. A combination of both strain gages and digital image correlation (DIC) was used in order to measure strains and bending of the branch plates.

The ETLCC specimens, along with trail specimens, were fabricated at Marid Industries Ltd. (Windsor Junction, Nova Scotia) and all specimens were welded, using a semi-automatic FCAW process, by a certified welder. Steel plate and weld metal samples from the same heat(s) as the specimen were provided for subsequent tensile coupon (TC) testing to determine the mechanical properties of the base metals and the weld metal.

4.2. TEST SPECIMENS

4.2.1. TEST SPECIMEN DESCRIPTION

The ETLCC test specimens were made up of two vertical steel plates welded to a ‘rigid’ 19.1 mm thick horizontal plate, as shown in Fig. 4.1. Each specimen was 630 mm high and 75 mm deep. The top vertical plate was connected through a single-sided fillet weld that was designed to be weld critical (the single-sided weld fails first), while the bottom vertical plate had larger fillet welds on both sides that were not intended to fail. The base metal was comprised of plates made to CSA G20.21 350W steel (2019) and the welds were made from E491T flux-cored electrodes.

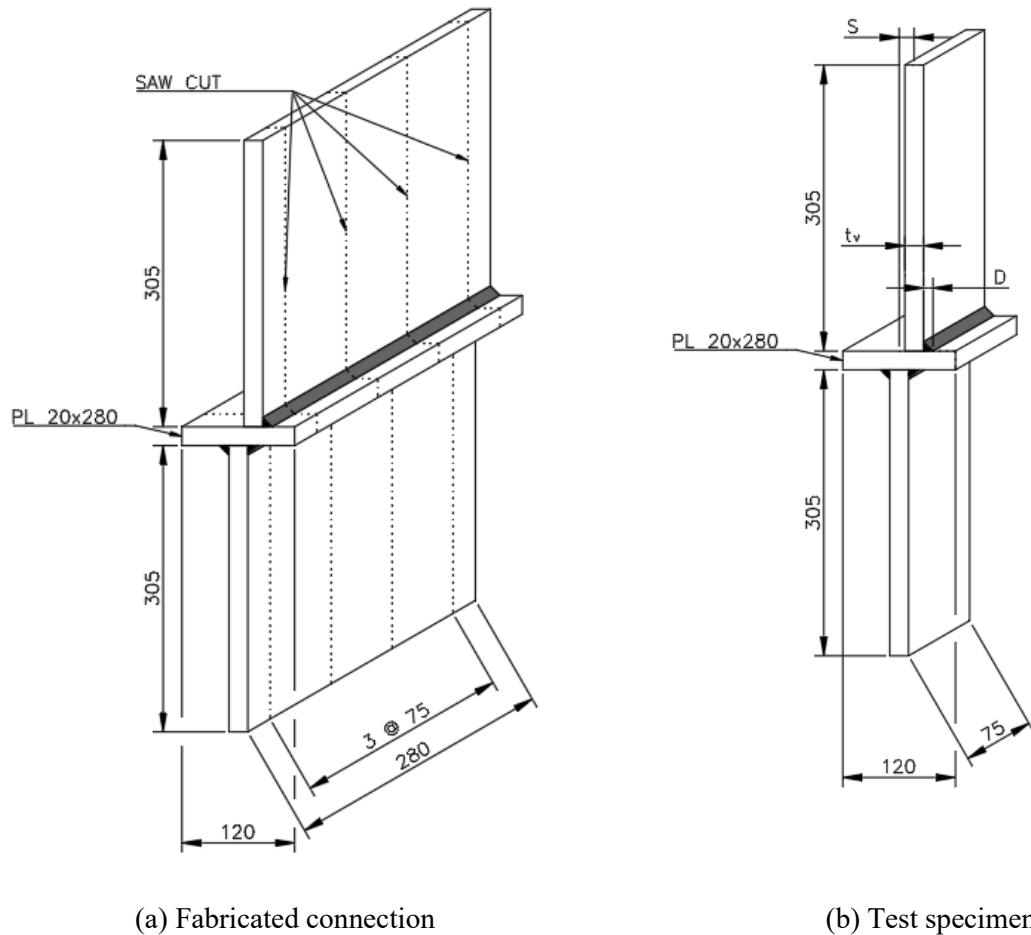


Fig. 4.1. Welded ETLCC connections and test specimens

To create eccentricity, the centerline of the top vertical plate was offset from the centerline of the bottom vertical plate. This was intended to cause concentrated stresses on the weld (resulting from local bending) that produced either tension or compression at the root. The specimens hence varied the vertical plate offsets (S , in Fig. 4.1.) from 30 mm left (producing compression at the weld root) to 30 mm right (producing tension at the weld root), nominal weld leg size (D) from 3 mm to 14 mm, and nominal vertical plate thicknesses (t_v) from 6.4 mm to 19.1 mm. These parameters are summarized in Section 4.3.1 for each of the 40 specimens.

4.2.2. TEST SPECIMEN DESIGN PROCEDURE

To design the ETLCC test specimens, previous literature was reviewed. Branch plate thicknesses, weld sizes, horizontal plate thicknesses and lengths all needed to be designed accordingly to ensure the ETLCC specimens were ‘weld-critical’.

The experimental program on the behavior of transverse fillet welds (Ng, et al. 2002) served as the chief reference for the design of the test specimens. In that program, tests were conducted on concentrically loaded

fillet welds (i.e. to both sides of a plate) in lapped splice and cruciform connection test specimens that were weld critical. The largest plate size used for the cruciform specimens was 19.1 mm (see Section 4.3.1.). The CISC Handbook of Steel Construction (CISC 2016) was used to observe common wall thicknesses used in structural shapes. These were all used to choose an ideal range of branch plate thicknesses (6.4 mm to 19.1 mm).

Once the plate thicknesses were chosen, the weld sizes could be considered. The smallest weld sizes chosen for the ETLCC test specimens were based on the minimum weld sizes in CSA S16-19 (2019) to avoid preheating the base metal. The largest weld sizes were chosen to be as large as possible while still ensuring that the specimens were ‘weld critical’. It is important to note that while all welds were initially made to exceed the minimum required weld size (CSA 2019), subsequent grinding of some welds – as discussed in Section 4.3.2. – reduced the throat sizes to below this threshold. Grinding is a common practice, as discussed in Tousignant and Packer (2015, 2017) and Packer et al. (2016).

For determining the required length of the branch plates, two factors were considered. For the 2-MN Instron Universal Testing Machine to grip the specimens, the jaws required 203 mm (8”) of steel plate to prevent the jaws from slipping. Also, an extra 102 mm (4”) was added to the length to give allowable room to place strain gages to the ETLCC test specimens. Therefore, the total length of the branch plates was 305 mm.

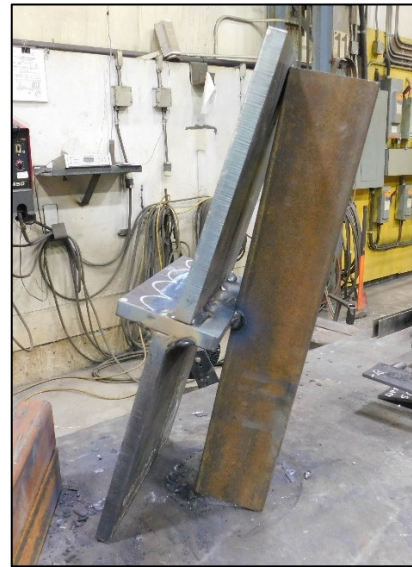
The horizontal ‘rigid’ plate (length and thickness) was designed to reflect similar work was done for eccentrically loaded PJP welds (Rasmussen et al. 1999) (see Section 2.3.1), in which the authors used a ‘rigid’ plate thickness of 19.1 mm (and tested vertical plate offsets up to 30 mm). Similar values were picked to ensure the horizontal plate was ‘rigid’ enough for the offsets that would be tested for the ETLCC specimens. The horizontal plate thickness chosen was 19.1 mm. Branch plate offsets chosen were also up to 30 mm, to mirror the results of this study. Once the offset was established, the length of the ‘rigid’ plate was determined to be 120 mm to leave enough room for the offsets, vertical plates, and the fillet welds.

The width (measured along the weld length) of the ETLCC connections used in the current study were made to be 280 mm (Rasmussen et al. 1999); however, after welding was complete, the ends of the connections were trimmed (to eliminate the weld start/stop locations), and each section was cut into three equally sized ETLCC test specimens (each are 75 mm wide). A schematic of the specimen was shown previously in Fig. 4.1, and the complete set of ETLCC connection fabrication drawings can be found in Appendix A.

4.2.3. TEST SPECIMEN FABRICATION PROCESS

The connections were fabricated by Marid Industries Ltd. (Windsor Junction, Nova Scotia). Before welding, the test specimens, as well as the trail specimens (see Appendix A), were tack welded together. All final welds were performed in the horizontal position, and tack welds were removed before applying the full-length weld.

The first weld completed was the single-sided fillet weld on the trial connection. The purpose of the trials connection(s) was to assess the quality of the welds before moving on to the ETLCC connections to be used for testing. One challenge encountered along the way, with the larger weld specimens, was that the branch plate would tend to tilt to one side/bend due to cooling shrinkage of the weld (see Fig. 4.2.a) making it difficult to fit the plate into the jaws of the testing machine. This was mitigated by added multiple tack welds, and a tie bar on the opposite side (see Fig. 4.2.b). This reduced the deflection of the top branch plate significantly from 6.4 mm (1/4") down to 1.6 mm (1/16"). It's worth noting that restraining the branch plate can cause residual stress in the fillet weld having a minor effect on strength.



(a) Trial connection with no tack welds or tie bar (b) ETLCC connection with tack welds and tie bar

Fig. 4.2. Mitigating branch plate deflection of welded ETLCC connections

Once the trial connection(s) were deemed satisfactory, the ETLCC connections were welded. First, the top branch plates were welded – on one side – to the ‘rigid’ plate. Then, the bottom branch plate was welded on both sides by alternating sides every couple of weld passes to prevent bending (due to cooling shrinkage) until the desired weld sizes were achieved on both sides. This ensured that the double-sided weld would not tilt to one side once the welding was completed. Preparations for the single-sided weld would require adding extra tack welds, and a tie bar on the opposite side, as previously mentioned, to prevent branch plate deflection. Once done, the single sided weld was added. All details of the welding procedure specification can be found in Appendix H.3.

With the welding complete, a portion of the connection was saw-cut off on each end to create a flat edge at the ends of the weld (see Fig. 4.1.a). The remainder of each connection was then saw-cut into three equal sized specimens (42 in total). The saw cuts can be seen, again, in Fig 4.1.a. This allowed for three specimens

with the same plate thicknesses, and same offsets. After the saw-cuts were made, a grinder was used on the specimens to remove any sharp edges. A reference to these ETLCC section drawings can be found in Appendix A.

4.3. GEOMETRIC PROPERTY MEASUREMENT PROCEDURE

4.3.1. OVERALL SPECIMEN CROSS-SECTION DIMENSIONS

All 40 ETLCC test specimens with their nominal cross-sectional dimensions and weld lengths are summarized in Table 4.1. The parameters evaluated are branch plate thickness (t_v), weld leg size (D), and branch plate offset (S). The range of these parameters covered are: $6.4 \text{ mm} \leq t_v \leq 19.1 \text{ mm}$; $3 \text{ mm} \leq D \leq 14 \text{ mm}$; and $0 \text{ mm} \leq S \leq 30 \text{ mm}$ (offsets causing compression at the weld root are denoted with 'a' and compression at the weld root with 'b'). The specimen designations are based on t_v , D , and S , in that order [i.e. S6-S-30a means $t_v = 6.4 \text{ mm}$ (closest imperial size), $D = 3 \text{ mm}$ (small weld for that plate thickness) and $30a = 30 \text{ mm}$ (causing compression at the root)]. The ETLCC specimens are made up of 15 specimens with $t_v = 6.4 \text{ mm}$, six specimens with $t_v = 9.5 \text{ mm}$, six specimens with $t_v = 15.9 \text{ mm}$, and 15 specimens with $t_v = 19.1 \text{ mm}$. The different sized specimens were designed to cover a wide range of D , and S . For S6-X-X specimens, the range of parameters covered are: $3 \text{ mm} \leq D \leq 5 \text{ mm}$; and $0 \text{ mm} \leq S \leq 30 \text{ mm}$. For S9-X-X specimens, the range of parameters covered are: $3 \text{ mm} \leq D \leq 8 \text{ mm}$; and $S = 0 \text{ mm}$. For S14-X-X specimens, the range of parameters covered are: $3 \text{ mm} \leq D \leq 12 \text{ mm}$; and $S = 0 \text{ mm}$. For S20-X-X specimens, the range of parameters covered are: $10 \text{ mm} \leq D \leq 14 \text{ mm}$; and $0 \text{ mm} \leq S \leq 30 \text{ mm}$. The horizontal plate thickness (t_h) is 19.1 mm for all ETLCC specimens. The width for all ETLCC specimens is 75 mm .

Table 4.1. Nominal and actual cross-sectional dimensions of the welded ETLCC specimens.

| Specimen designation ¹ | Nominal | | | Actual | |
|-----------------------------------|------------------------------------|-------------------------|-------------------------------|------------------------------------|------------------|
| | Branch plate thickness, t_v (mm) | Weld leg size, D (mm) | Offset, S (mm) ¹ | Branch plate thickness, t_v (mm) | Offset, S (mm) |
| S6-S-30a | 6.4 | 3 | 30 | 6.40 | -30.2 |
| S6-S-15a | 6.4 | 3 | 15 | 6.28 | -12.4 |
| S6-S-0 | 6.4 | 3 | 0 | 6.41 | +1.1 |
| S6-S-15b | 6.4 | 3 | 15 | 6.41 | +17.4 |
| S6-S-30b | 6.4 | 3 | 30 | 6.45 | +30.5 |
| S6-M-30a | 6.4 | 4 | 30 | 6.39 | -30.9 |
| S6-M-15a | 6.4 | 4 | 15 | 6.41 | -13.1 |
| S6-M-0 | 6.4 | 4 | 0 | 6.42 | +0.9 |
| S6-M-15b | 6.4 | 4 | 15 | 6.42 | +17.3 |
| S6-M-30b | 6.4 | 4 | 30 | 6.46 | +30.3 |
| S6-L-30a | 6.4 | 5 | 30 | 6.52 | -31.6 |
| S6-L-15a | 6.4 | 5 | 15 | 6.40 | -12.9 |
| S6-L-0 | 6.4 | 5 | 0 | 6.35 | +1.1 |
| S6-L-15b | 6.4 | 5 | 15 | 6.43 | +17.4 |
| S6-L-30b | 6.4 | 5 | 30 | 6.42 | +30.0 |
| S9-XS-0 | 9.5 | 3 | 0 | 9.63 | +1.2 |
| S9-S-0 | 9.5 | 4 | 0 | 9.57 | +1.2 |
| S9-M-0 | 9.5 | 5 | 0 | 9.64 | +1.5 |
| S9-L-0 | 9.5 | 6 | 0 | 9.62 | +0.9 |
| S9-XL-0 | 9.5 | 7 | 0 | 9.62 | +1.1 |
| S9-XXL-0 | 9.5 | 8 | 0 | 9.58 | +1.6 |
| S14-XS-0 | 15.9 | 3 | 0 | 15.93 | -0.6 |
| S14-S-0 | 15.9 | 4 | 0 | 15.90 | -0.4 |
| S14-M-0 | 15.9 | 5 | 0 | 15.88 | -0.5 |
| S14-L-0 | 15.9 | 8 | 0 | 15.90 | +0.8 |
| S14-XL-0 | 15.9 | 10 | 0 | 15.88 | +0.6 |
| S14-XXL-0 | 15.9 | 12 | 0 | 15.90 | +1.5 |
| S20-S-30a | 19.1 | 10 | 30 | 19.50 | -27.3 |
| S20-S-15a | 19.1 | 10 | 15 | 19.42 | -13.5 |
| S20-S-0 | 19.1 | 10 | 0 | 19.47 | +2.8 |
| S20-S-15b | 19.1 | 10 | 15 | 19.56 | +15.8 |
| S20-S-30b | 19.1 | 10 | 30 | 19.40 | +30.1 |
| S20-M-30a | 19.1 | 12 | 30 | 19.53 | -28.3 |
| S20-M-15a | 19.1 | 12 | 15 | 19.55 | -13.3 |
| S20-M-0 | 19.1 | 12 | 0 | 19.46 | +3.5 |
| S20-M-15b | 19.1 | 12 | 15 | 19.42 | +16.3 |
| S20-L-30a | 19.1 | 14 | 30 | 19.53 | -27.9 |
| S20-L-15a | 19.1 | 14 | 15 | 19.41 | -14.2 |
| S20-L-0 | 19.1 | 14 | 0 | 19.41 | +3.0 |
| S20-L-15b | 19.1 | 14 | 15 | 19.45 | +16.2 |

¹ ETLCC specimen designations with 'a' represent compression at the root and ETLCC specimen designations with 'b' represent tension at the root (see Section 4.2.2).

4.3.2. FILLET WELD CROSS SECTIONAL DIMENSIONS AND LENGTHS

This section covers both the preliminary (pre-rupture) and macro-etch (post-rupture) fillet weld measurements of the ETLCC specimens. These measurements are shear leg size (l_v), tension leg size (l_h), and weld throat (t_w) [as well as the weld length (l_w)], as shown in Fig. 1.2.

Prior to testing, welds were ground into perfectly triangular shapes to facilitate connection failure by weld fracture (the intended limit state) and provide stronger geometric correlation between the weld leg and throat

sizes. The preliminary and post-rupture measurements herein refer to measurements made after grinding, either immediately before or after the ETLCC tests were performed.

4.3.2.1. Preliminary Measurements

Initially, a weld gage was used to measure weld leg sizes [shear leg (l_v) and tension leg (l_h)] and weld throats (t_w). The weld throat was also calculated based on the weld leg measurements for comparison. These measurements were taken at five different locations along the weld length of each specimen to ensure an accurate measurement. The average of these measurements is summarized in Table 4.2. All measurements taken to acquire these average values can be all found in Appendix B.1.

Table 4.2. Preliminary measurements of fillet weld cross sectional dimensions.

| Specimen designation ¹ | Shear leg, l_v (mm) | Tension leg, l_h (mm) | Weld throat (measured), t_w (mm) | Weld throat (calculated), t_w (mm) | Weld length, l_w (mm) |
|-----------------------------------|-----------------------|-------------------------|------------------------------------|--------------------------------------|-------------------------|
| S6-S-30a | 2.96 | 2.96 | 2.20 | 2.09 | 80.4 |
| S6-S-15a | 3.14 | 3.14 | 2.04 | 2.22 | 74.7 |
| S6-S-0 | 3.10 | 3.24 | 2.40 | 2.24 | 75.0 |
| S6-S-15b | 3.26 | 3.20 | 2.04 | 2.28 | 77.5 |
| S6-S-30b | 3.14 | 2.92 | 2.10 | 2.14 | 75.4 |
| S6-M-30a | 3.94 | 4.06 | 2.98 | 2.83 | 71.4 |
| S6-M-15a | 4.18 | 4.12 | 2.52 | 2.93 | 76.0 |
| S6-M-0 | 3.72 | 3.80 | 2.60 | 2.66 | 76.2 |
| S6-M-15b | 4.02 | 4.02 | 2.78 | 2.84 | 75.0 |
| S6-M-30b | 3.82 | 3.64 | 2.56 | 2.63 | 77.9 |
| S6-L-30a | 4.82 | 4.80 | 3.32 | 3.40 | 73.6 |
| S6-L-15a | 4.90 | 4.92 | 3.12 | 3.47 | 73.5 |
| S6-L-0 | 4.82 | 4.82 | 3.30 | 3.41 | 73.8 |
| S6-L-15b | 5.04 | 4.76 | 3.20 | 3.46 | 73.7 |
| S6-L-30b | 4.62 | 4.60 | 3.16 | 3.26 | 72.4 |
| S9-XS-0 | 3.22 | 3.16 | 2.22 | 2.26 | 74.3 |
| S9-S-0 | 4.12 | 4.04 | 2.72 | 2.88 | 75.8 |
| S9-M-0 | 5.08 | 5.02 | 3.30 | 3.57 | 79.4 |
| S9-L-0 | 5.72 | 5.82 | 4.25 | 4.08 | 72.1 |
| S9-XL-0 | 7.00 | 7.12 | 5.00 | 4.99 | 75.2 |
| S9-XXL-0 | 7.78 | 7.94 | 5.45 | 5.56 | 74.9 |
| S14-XS-0 | 2.94 | 3.16 | 1.90 | 2.15 | 72.7 |
| S14-S-0 | 4.00 | 3.68 | 2.80 | 2.71 | 74.7 |
| S14-M-0 | 4.98 | 4.68 | 3.44 | 3.41 | 78.7 |
| S14-L-0 | 7.96 | 8.00 | 5.48 | 5.64 | 73.5 |
| S14-XL-0 | 10.28 | 9.90 | 6.98 | 7.13 | 76.5 |
| S14-XXL-0 | 11.34 | 11.62 | 8.52 | 8.12 | 71.5 |
| S20-S-30a | 10.14 | 10.28 | 7.04 | 7.22 | 77.5 |
| S20-S-15a | 10.04 | 9.82 | 7.14 | 7.02 | 74.5 |
| S20-S-0 | 9.92 | 9.66 | 6.92 | 6.92 | 77.5 |
| S20-S-15b | 9.96 | 10.06 | 7.14 | 7.08 | 75.0 |
| S20-S-30b | 9.82 | 10.08 | 6.98 | 7.03 | 72.8 |
| S20-M-30a | 11.48 | 11.58 | 8.40 | 8.15 | 75.5 |
| S20-M-15a | 11.90 | 11.90 | 8.44 | 8.41 | 76.5 |
| S20-M-0 | 12.00 | 11.72 | 8.66 | 8.38 | 74.5 |
| S20-M-15b | 12.10 | 12.00 | 8.16 | 8.52 | 75.5 |
| S20-L-30a | 13.90 | 13.82 | 10.02 | 9.80 | 74.5 |
| S20-L-15a | 13.96 | 13.74 | 9.94 | 9.79 | 74.5 |
| S20-L-0 | 13.90 | 13.88 | 9.82 | 9.82 | 75.5 |
| S20-L-15b | 13.78 | 13.80 | 9.94 | 9.75 | 74.5 |

¹ ETLCC specimen designations with ‘a’ represent compression at the root and ETLCC specimen designations with ‘b’ represent tension at the root (see Section 4.2.2).

4.3.2.2. Post-Rupture Macro-Etch Examinations

After the ETLCC specimens were tested (i.e. after the weld had ruptured), each specimen was cut in three places along its width at 90° to the weld root. The resulting four pieces were scanned, and duplicate measurements of the weld leg sizes [shear leg (l_v) and tension leg (l_h)], weld throat (t_w) and weld throat inclination angles (α) were made. This resulted each measurement taken at five different locations for all specimens to ensure accurate results. All t_w 's were measured directly in AutoCAD as the shortest distance from

the root to the face of the diagrammatic weld, and, additionally, calculated based on l_v and l_h measured in AutoCAD, for comparison. See Fig. 4.3. for an example of a macro-etch examination and its measurements.

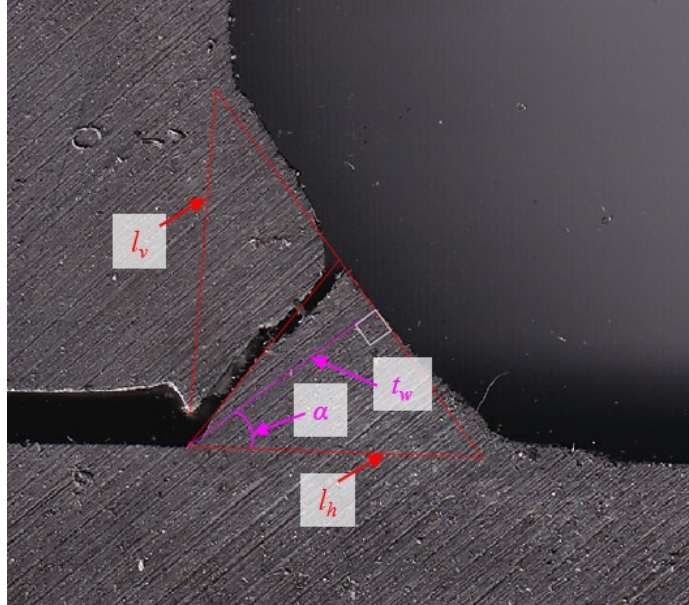


Fig. 4.3. Macro-etch examination with measurements

All values of α were calculated based on the l_v and l_h values measured in AutoCAD by using Eqn. (3.13) (see Section 3.4.1.). The averages of the post-rupture measurements (out of five locations) are shown in Table 4.3. To see all measurements at each location taken, refer to Appendix B.2.

Table 4.3. Post-rupture macro-etch examination measurements of fillet weld cross sectional dimensions.

| Specimen designation ¹ | Shear leg, l_v (mm) | Tension leg, l_h (mm) | Weld throat (measured), t_w (mm) | Weld throat (calculated), t_w (mm) | Angle of inclination of the weld throat plane, α (°) |
|-----------------------------------|-----------------------|-------------------------|------------------------------------|--------------------------------------|---|
| S6-S-30a | 4.10 | 3.30 | 2.58 | 2.55 | 38.7 |
| S6-S-15a | 3.95 | 4.15 | 3.20 | 2.84 | 46.1 |
| S6-S-0 | 4.43 | 4.03 | 3.17 | 2.98 | 42.3 |
| S6-S-15b | 3.34 | 3.76 | 2.54 | 2.47 | 48.4 |
| S6-S-30b | 3.18 | 3.12 | 2.42 | 2.22 | 44.5 |
| S6-M-30a | 4.22 | 3.78 | 2.86 | 2.79 | 41.8 |
| S6-M-15a | 5.63 | 4.17 | 3.43 | 3.35 | 36.4 |
| S6-M-0 | 5.54 | 3.84 | 3.52 | 3.14 | 34.9 |
| S6-M-15b | 4.56 | 4.30 | 3.34 | 3.11 | 43.4 |
| S6-M-30b | 3.30 | 3.46 | 2.46 | 2.35 | 47.4 |
| S6-L-30a | 5.66 | 4.20 | 2.84 | 3.35 | 36.1 |
| S6-L-15a | 6.10 | 4.54 | 3.86 | 3.61 | 36.7 |
| S6-L-0 | 6.10 | 4.68 | 4.04 | 3.69 | 37.5 |
| S6-L-15b | 4.32 | 4.72 | 3.42 | 3.17 | 46.7 |
| S6-L-30b | 4.14 | 4.66 | 3.24 | 3.08 | 48.4 |
| S9-XS-0 | 3.78 | 2.80 | 2.38 | 2.23 | 36.4 |
| S9-S-0 | 4.98 | 3.26 | 2.76 | 2.72 | 33.2 |
| S9-M-0 | 5.60 | 4.58 | 3.70 | 3.50 | 39.0 |
| S9-L-0 | 5.82 | 6.30 | 4.82 | 4.25 | 47.2 |
| S9-XL-0 | 8.16 | 6.78 | 5.68 | 5.20 | 39.8 |
| S9-XXL-0 | 8.36 | 7.44 | 6.00 | 5.52 | 41.8 |
| S14-XS-0 | 2.76 | 2.46 | 1.84 | 1.82 | 41.4 |
| S14-S-0 | 4.90 | 3.22 | 2.72 | 2.68 | 33.2 |
| S14-M-0 | 6.14 | 4.52 | 3.74 | 3.64 | 36.3 |
| S14-L-0 | 7.24 | 7.26 | 5.20 | 5.12 | 45.3 |
| S14-XL-0 | 10.18 | 8.82 | 6.70 | 6.66 | 41.0 |
| S14-XXL-0 | 12.16 | 11.08 | 8.42 | 8.17 | 42.4 |
| S20-S-30a | 12.54 | 9.08 | 7.58 | 7.30 | 35.7 |
| S20-S-15a | 11.60 | 9.28 | 7.58 | 7.21 | 38.3 |
| S20-S-0 | 9.76 | 8.76 | 6.86 | 6.41 | 42.0 |
| S20-S-15b | 9.72 | 11.10 | 7.40 | 7.31 | 48.8 |
| S20-S-30b | 10.76 | 12.08 | 8.22 | 8.02 | 48.3 |
| S20-M-30a | 13.02 | 10.82 | 9.00 | 8.30 | 39.7 |
| S20-M-15a | 12.54 | 11.50 | 9.22 | 8.46 | 42.6 |
| S20-M-0 | 13.16 | 11.90 | 9.74 | 8.81 | 42.1 |
| S20-M-15b | 11.16 | 12.12 | 9.10 | 8.19 | 47.4 |
| S20-L-30a | 12.94 | 11.04 | 9.12 | 8.39 | 40.4 |
| S20-L-15a | 15.36 | 13.28 | 10.88 | 9.99 | 40.9 |
| S20-L-0 | 14.66 | 13.06 | 10.00 | 9.62 | 41.5 |
| S20-L-15b | 14.30 | 13.32 | 10.52 | 9.74 | 43.0 |

¹ ETLCC specimen designations with 'a' represent compression at the root and ETLCC specimen designations with 'b' represent tension at the root (see Section 4.2.2).

4.4. MECHANICAL PROPERTY MEASUREMENT PROCEDURES

4.4.1. BASE METAL TENSILE COUPON TESTS

Base metal tensile coupons (TCs) were cut from 450 mm x 300 mm plates from the same stock material (same heat no.) into 20 mm strips. This was the same CSA G40.21 350W steel used to make the ETLCCs (i.e. nominal thicknesses of 6.4 mm, 9.5 mm, 15.9 mm, and 19.1 mm). The TCs were then tested to determine the actual properties of the base metal (yield strength, ultimate strength, Young's Modulus, and % elongation).

A total of 12 sheet type specimens (three of each plate thickness) were made according to ASTM E8/E8M-21 guidelines (2021). The specimens were 450 mm long with a grip length of 175 mm. A grip length of at least 150 mm was required for the jaws of the testing machine to grip the specimen. An extensometer was used to measure the deformation of the TC and a gage length of 50 mm was used to determine strains. The rate of loading varied depending on the size of the specimen. The target run-time for the tests was between 20 to 30 minutes. The sheet-type specimen can be seen in Fig. 4.4.

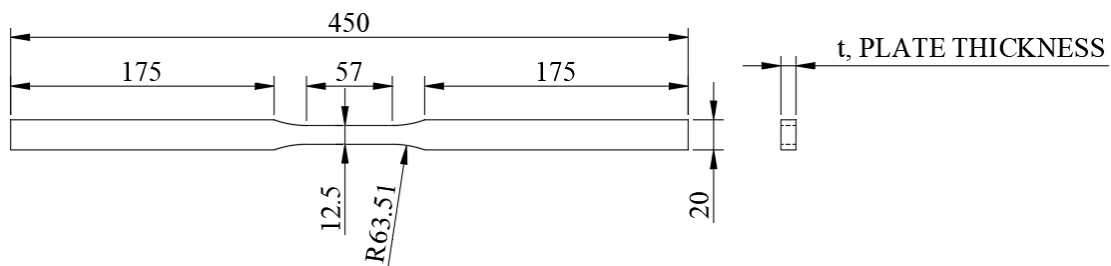


Fig. 4.4. Sheet-type coupon specimen to test base metal

4.4.1.1. Base Metal Tensile Coupon Results

A graph showing a typical stress-strain diagram for the base metal coupons is shown in Fig. 4.4. Due to the initial exported data being “noisy”, a moving average filter was used to gather the overall trend of the data providing a smoother curve. The stress-strain curves for the three coupons were consistent. The yield strength (F_y) and yield strain (ϵ_y) were both determined using the 0.2% offset method. Young's Modulus (E) was then taken as the slope of the 0.2% offset line of the elastic region of the stress-strain curve. The average values (based on all three tests) are shown in Fig. 4.5. for illustration. All TC test results can be found in Appendix C.

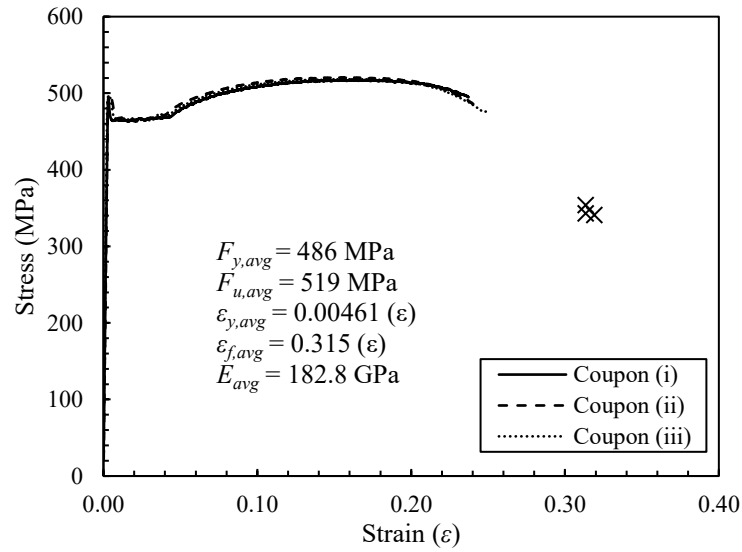


Fig. 4.5. Stress versus strain curve for 6.4 mm thick base metal coupons

The equation to calculate fracture strains (ϵ_f) (which correspond to the x-ordinates of the “X” symbols in Fig. 4.5) was as follows:

$$\epsilon_f = \frac{L_f - L_o}{L_o} \quad (4.1)$$

where L_f is the gage length after failure, and L_o is the gage length before failure.

L_f was measured by joining the fractured pieces back together after the tensile coupon failed and remeasured the gage length. The stress corresponding to ϵ_f was calculated dividing the final load (i.e. just before rupture) by the original cross-sectional area of the TC. Samples of the base metal coupons tested, along with the test set-up, can be seen in Fig. 4.6.



(a) Rectangular base metal coupons



(b) Instron Universal Testing machine set-up

Fig. 4.6. Testing of rectangular base metal coupons.

A comparison table between nominal properties of CSA G40.21 350W steel to the actual properties can be seen in Table 4.4. The actual properties were expressed as a percentage compared to the nominal properties (for exact values, see Appendix C). All actual properties were greater than expected. The actual yield strengths (F_y) for TCs ranged from +10.5% to +38.8%, the ultimate strengths (F_u) ranged from +15.4% to +23.1%, and the fracture strains (ϵ_f) ranged from +5.2% to +23.5%. This behaviour is rather typical, as can also be seen in previous work by Tousignant (2017) and McFadden (2014). Note that the actual material properties of each branch plate thickness represent the average of three TC tests.

Table 4.4. Comparison between nominal properties and actual properties of the CSA G40.21 350W base metal coupons

| Branch Plate Thickness | Nominal | | | Actual | | |
|------------------------|----------------|-------------------|------------------|----------------|-------------------|------------------|
| | Yield Strength | Ultimate Strength | Fracture Strain | Yield Strength | Ultimate Strength | Fracture Strain |
| (mm) | F_y (MPa) | F_u (MPa) | ϵ_f (%) | F_y (%) | F_u (%) | ϵ_f (%) |
| 6.4 | 350 | 450 | 0.300 | +38.8 | +15.4 | +5.2 |
| 9.5 | 350 | 450 | 0.300 | +34.3 | +16.9 | +6.0 |
| 15.9 | 350 | 450 | 0.300 | +10.5 | +18.0 | +25.3 |
| 19.1 | 350 | 450 | 0.300 | +21.0 | +23.1 | +23.5 |

4.4.2. WELD METAL TENSILE COUPON TESTS

Marid Industries made the “mold” for the weld metal test coupons by welding three steel plates together with fillet welds that formed a groove in the center, as shown in Fig. 4.7.a. The groove was then filled with weld metal through multiple passes. The weld metal was grade E491T ($X_u = 490$ MPa), from the same weld coil (same heat) used to weld the ETLCC specimens to determine the actual properties of the weld metal (yield strength, ultimate strength, Young’s Modulus, and % elongation).

The weld sample was then cut into three pieces to be made into rounded test coupons according to ASTM E8/E8M guidelines (2021). The specimens were 218 mm long with a grip length of 75 mm. They were machined to have a 15 mm diameter at the grips, and 12.5 mm at the reduced section. The loading rate used was 0.8 mm/min. The target run-time for the tests was between 20 to 30 minutes. The rounded weld coupon tested is shown in Fig. 4.7.b.

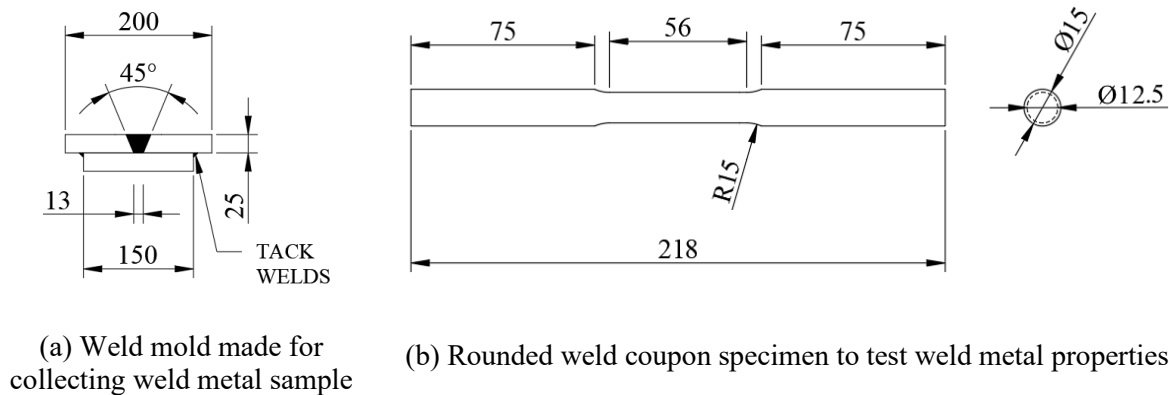


Fig. 4.7. Drawings to fabricate weld coupon specimens.

4.4.2.1. Weld Metal Tensile Coupon Results

A graph showing a typical stress-strain diagram for the weld metal coupons is shown in Fig. 4.8. Like with the base metal TC test results, a moving average filter was used to gather the overall trend of the data to reduce “noise” (hence, providing a smoother overall curve). Again, the stress-strain curves for the three coupons were consistent, which gives credence to the testing procedure. The yield strength (F_y) and yield strain (ϵ_y) were both determined using the 0.2% offset method (which gives similar results to using the yield plateau). The Young’s Modulus (E) was taken as the slope of the offset line, and the fracture strain (ϵ_f) was calculated by using Eqn. (4.1) (shown previously).

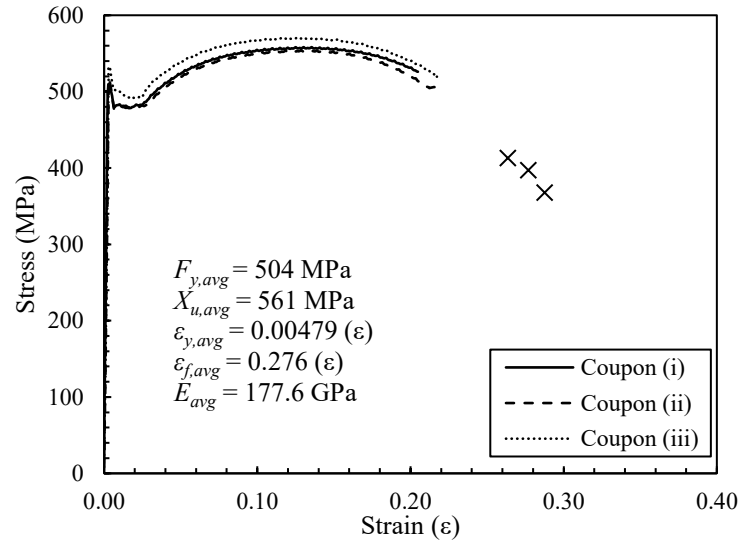


Fig. 4.8. Stress versus strain curves for weld metal coupons

A summary of the weld metal coupon test results can be seen in Table 4.5. The average yield strength ($F_{y,avg}$) was 504 MPa, the electrode ultimate strength ($X_{u,avg}$) was 561 MPa which was 14.5% greater than the nominal strength. The yield strain ($\epsilon_{y,avg}$) was 0.00479, the ultimate strain ($\epsilon_{f,avg}$) was 0.276, and the Young's modulus (E_{avg}) was 177.6 GPa.

Table 4.5. Summary of weld metal coupon tests

| Coupon | Yield Strength | Ultimate Strength | Yield Strain | Ultimate Strain | Young's Modulus |
|---------|----------------|-------------------|--------------------------------|--------------------------------|-----------------|
| | F_y (MPa) | X_u (MPa) | ϵ_y (ϵ) | ϵ_f (ϵ) | E (GPa) |
| (i) | 502 | 558 | 0.00435 | 0.288 | 196.8 |
| (ii) | 497 | 554 | 0.00499 | 0.264 | 166.3 |
| (iii) | 514 | 571 | 0.00501 | 0.277 | 169.6 |
| Average | 504 | 561 | 0.00479 | 0.276 | 177.6 |

4.5. TEST SET-UP AND INSTRUMENTATION

4.5.1. TEST SET-UP

Following the TC tests, the ETLCC specimens were tested using a 2-MN Instron Universal Testing Machine. The specimens were gripped at both ends by the jaws of the machine and tested in tension. The jaws grip 203.2 mm (8 in) of the vertical plate to ensure the jaws did not slip during testing. The ETLCC specimens with offset vertical plates used steel plates as spacers to accommodate the concentric grips of the Instron Universal Testing Machine (see Fig. 4.9.a). During the tests, digital image correlation (DIC) was used to capture

displacements and strains locally throughout 16 (of 40 tested) welded connections. Schematic diagrams of the test setup and instrumentation can be seen in Fig. 4.9.

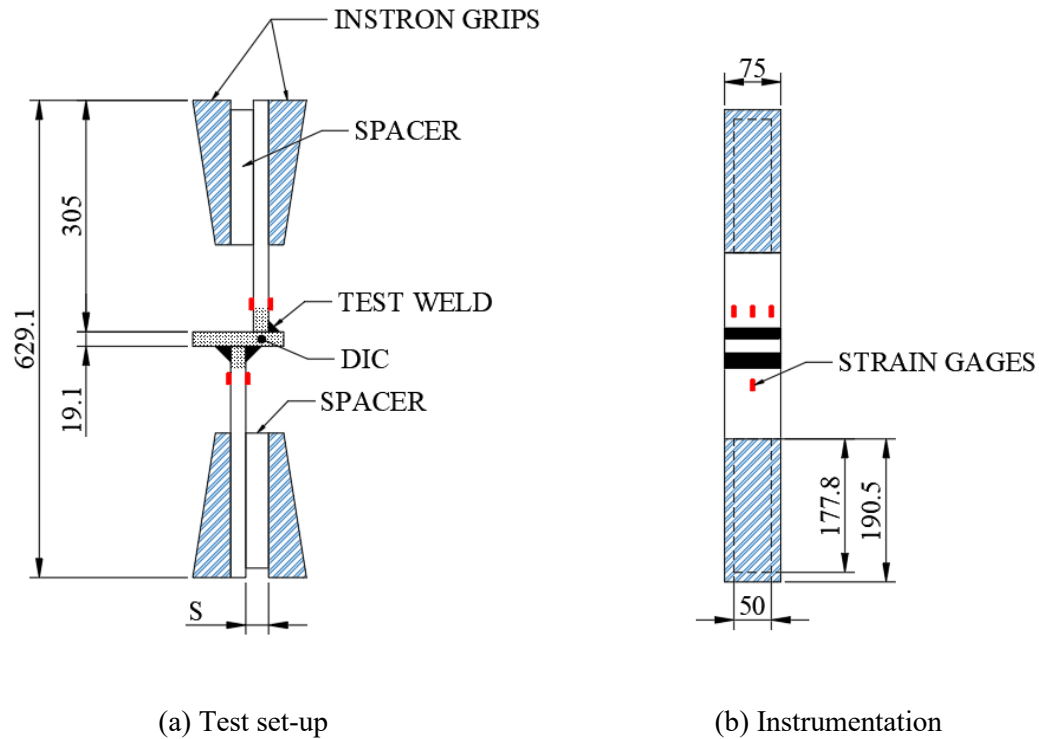


Fig. 4.9. Test set-up and instrumentation for the ETLCC specimens.

4.5.2. INSTRUMENTATION

Strain gages were positioned on both sides of each branch plate to detect any bending in the plate(s). They were evenly spaced at 10 mm from each edge to avoid edge effects, and 15 mm away from the test weld to avoid detecting the high strain region of the weld associated with the notch effect (Cassidy 1993). The three strain gages along both sides of the top branch plate were to demonstrate full effective lengths of the single-sided fillet weld. Once a full effective length was seen for the first few tests, the remaining tests (using DIC) only used one strain gage on both sides of the top branch plate. The DIC paint (see Section 4.5.1) was applied along the face of the specimen around the central portion of the welded connection (refer to Fig. 4.9.) to measure the deformation of the single-sided test weld and detect bending in the branch plates. Results of the strain gages and DIC can be found in Appendix E.

4.5.3. TESTING/ LOADING STRATEGY

The ETLCC specimens were tested by using a 2-MN Instron Testing Machine to apply tension to the vertical branch plates in a quasi-static manner. The time target for the ETLCC tests varied between 5-10 minutes

depending on the specimen size and the anticipated degree of rotation of the transverse plate (i.e. opening/closing of the weld root). These tests were performed under displacement control with a loading rate starting at 1.0 mm/min to 2.0 mm/min. Due to the specimens with a larger eccentricity experiencing more rotation of the transverse plate, a faster loading rate was used for these specimens. The ‘0 mm offset’ specimens were loaded at 1.0 mm/min, the ‘15 mm offset’ specimens were loaded at 1.5 mm/min, and the ‘30 mm offset’ specimens were loaded at 2.0 mm/min.

4.6. ETLCC TEST RESULTS

Ultimately, a total of 40 ETLCC specimens were tested in tension until failure. Two of the fabricated specimens (S20-M-30b & S20-L-30b) were not tested due to slight out-of-straightness that caused them to exceed the dimensional tolerances of the Instron Universal Testing Machine. All 40 specimens tested failed due to weld rupture along a plane through the fillet weld throat, as intended. Strain gages adjacent to the welds showed that the welds were uniformly loaded along their length. In this section, the results in terms of actual versus predicted strength are briefly summarized. Further discussion is provided in Chapter 5.

4.6.1. CSA S16:19

The actual strengths of the specimens are compared to the predicted nominal strengths in accordance with CSA S16:19 with the $\sin\theta$ factor and without the $\sin\theta$ factor in Fig. 4.10., below. Predicted strengths (P_{pr}) therein were hence calculated using Eqn. 3.1 (CSA S16:19 equation for fillet welds subject to tension-induced shear) and Eqn. 3.2 ($\sin\theta$ factor) with $\phi = 1.0$. All predicted strengths of the fillet welds were calculated based on the post-rupture measured weld throats (directly from AutoCAD) (see Section 4.3.2.2. Table 4.3. column 4) and material properties ($X_u = 561$ MPa). The actual strengths (P_a) were based off the measured loads from the ETLCC experimental tests. As shown below, CSA S16:19 with the $\sin\theta$ factor generally overpredicts the single-sided fillet weld strength whether there is compression or tension at the root. CSA S16:19 without the $\sin\theta$ factor more accurately predicts the single-sided fillet weld strength when there is compression at the root.

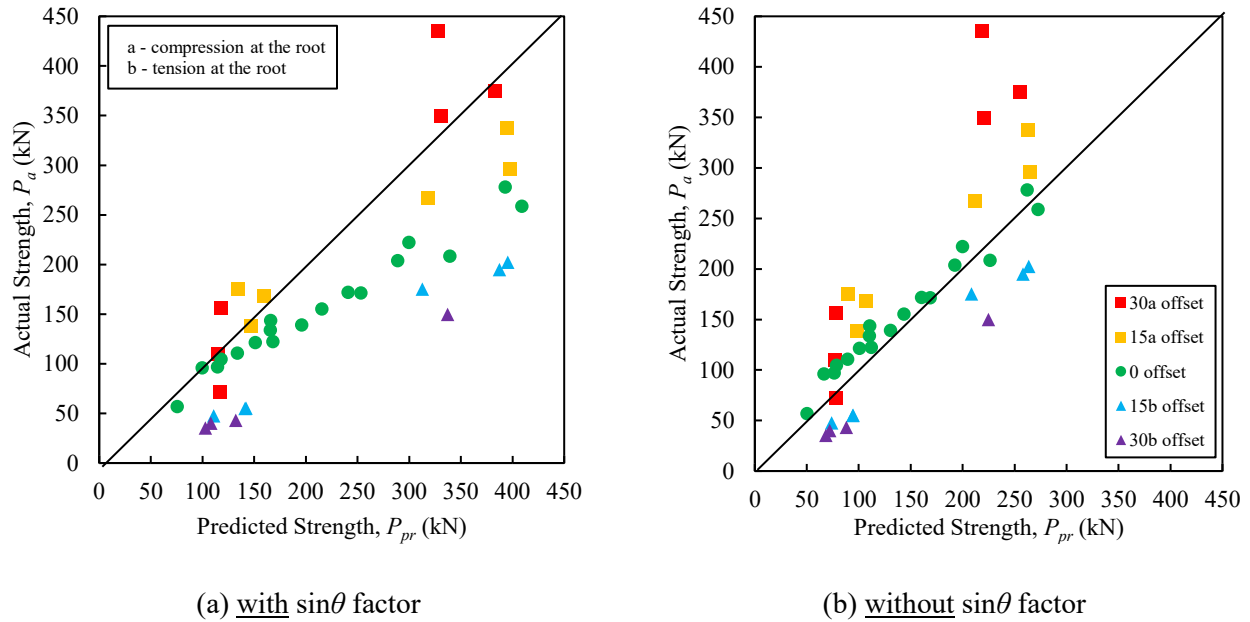


Fig. 4.10. Comparison of actual strengths and predicted strengths using CSA S16:19

4.6.2. AISC 360-16

The actual strengths of the specimens are compared to the predicted strengths in accordance with AISC 360-16 with the $\sin\theta$ factor and without the $\sin\theta$ factor in Fig. 4.11., below. Predicted strengths (P_{pr}) therein were hence calculated using Eqn. 3.5 and 3.6 (AISC 360-16 equation for fillet welds subject to tension-induced shear) and Eqn. 3.5 and 3.7 ($\sin\theta$ factor) with $\phi = 1.0$. All predicted strengths of the fillet welds were again calculated based on the post-rupture measured weld throats (directly from AutoCAD) (see Section 4.3.2.2. Table 4.3. column 4) and material properties ($X_u = 561$ MPa). The actual strengths (P_a) were based off the measured loads from the ETLCC experimental tests. As shown below, AISC 360-16 with the $\sin\theta$ factor generally overpredicts the single-sided fillet weld strength whether there is compression or tension at the root. AISC 360-16 without the $\sin\theta$ factor more accurately predicts the single-sided fillet weld strength when there is compression at the root.

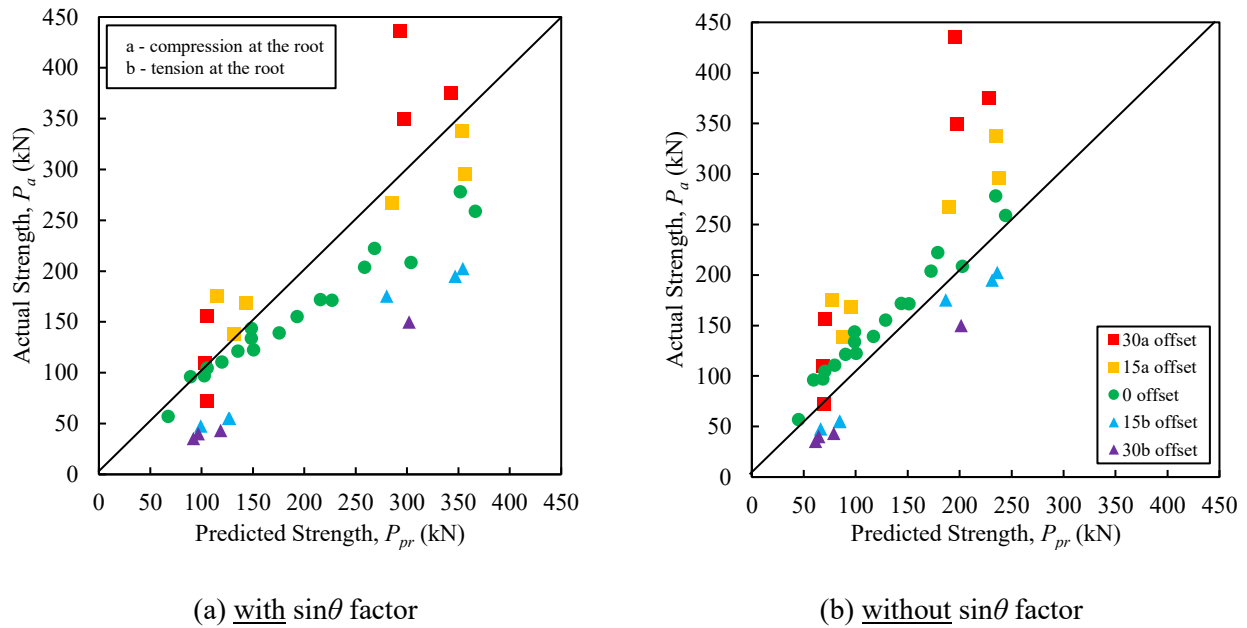
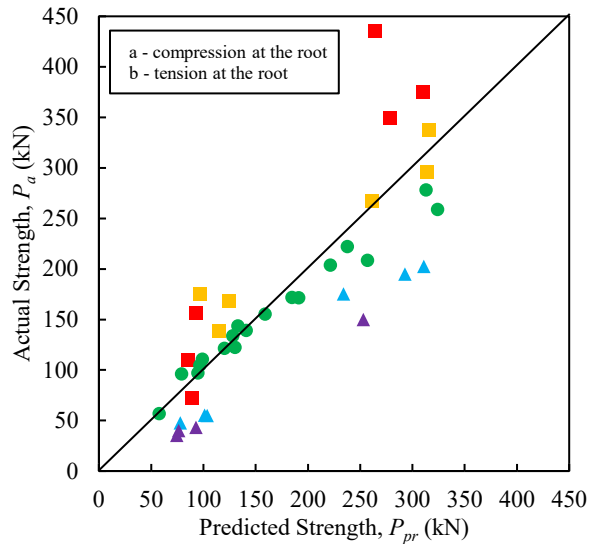


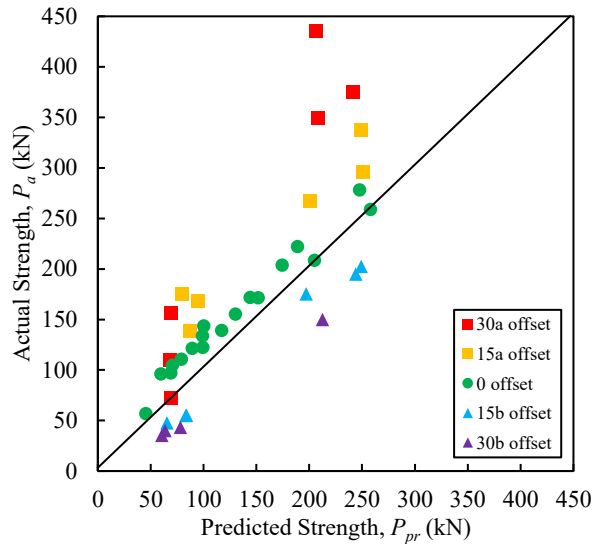
Fig. 4.11. Comparison of actual strengths and predicted strengths using AISC 360-16

4.6.3. EN1993-1-8:2005

The actual strengths and predicted nominal strengths are compared for EN1993-1-8:2005 using the Directional Method and Simplified Method in Fig. 4.12. Predicted strengths were calculated using Eqns. (3.11) (EN1993-1-8:2005 Directional Method) and (3.12a-b) (EN1993-1-8:2005 Simplified Method). All predicted strengths of the fillet welds were calculated based on the post-rupture measured weld throats (directly from AutoCAD) and weld throat inclination angles (calculated using measured weld legs) (see Section 4.3.2.2. Table 4.3. columns 4 & 6) and material properties (F_u = base metal strength of weaker part joined, see Appendix C). In both cases, $\beta_w = 0.9$ and $\gamma_{M2} = 1.0$. The actual strengths (P_a) were based off the measured loads from the ETLCC experimental tests. As shown below, the EN1993-1-8:2005 Directional Method generally overpredicts the single-sided fillet weld strength whether there is compression or tension at the root. The EN1993-1-8:2005 Simplified Method more accurately predicts the single-sided fillet weld strength when there is compression at the root.



(a) Directional Method



(b) Simplified Method

Fig. 4.12. Comparison of actual strength and predicted strengths using EN1993-1-8:2005

Chapter 5: EVALUATION OF RESULTS

5.1. INFLUENCE OF CONNECTION PARAMETERS

In this section, multiple connection parameters are examined to determine their effect(s) on the strength of single-sided fillet welds in the ETLCCs. The comparisons in Section 5.1. show the ratio of actual-to-predicted strength according to CSA S16:19 [Eqn. (3.1)] without the $\sin\theta$ factor. The observed trends are identical for all other North American design methods (i.e. CSA S16:19 with the $\sin\theta$ factor and AISC 360-16 with and without the $\sin\theta$ factor).

5.1.1. WELD SIZE

Weld throat size (t_w) was found to have a small effect on fillet weld strength when observing all ETLCC tests. When observing tests of the same offset (e.g., 0b offset) in Fig. 5.1 as t_w increases, the fillet weld strength slightly decreases. This can be attributed to a slightly greater eccentricity causing tension at the root of the weld. Larger branch plate thickness also contributed minimally to this trend (see Section 5.1.2.), which was less evident for ETLCCs with compression at the root. A plot of P_d/P_{pr} versus t_w for all ETLCC tests can be seen in Fig. 5.1.

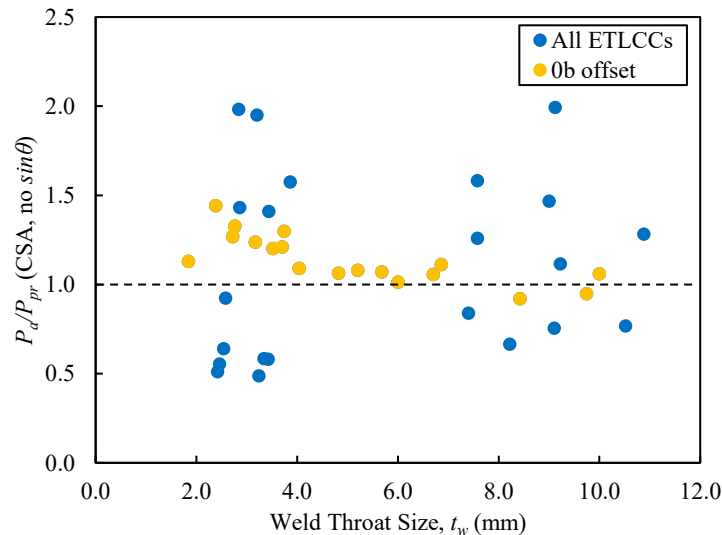


Fig. 5.1. Effect of weld throat size on single sided fillet weld strength

5.1.2. BRANCH PLATE THICKNESS

As noted above, branch plate thickness (t_v) was found to have a small effect on fillet weld strength when observing all ETLCC tests. When observing tests of the same offset (e.g., 0b offset), as t_v increases, the fillet weld strength is shown to slightly decrease, on average. This may again be attributable to a slightly greater eccentricity causing tension at the root of the weld (from both larger branch plate thicknesses plus larger weld sizes). A plot of P_d/P_{pr} versus t_v for all ETLCC tests can be seen in Fig. 5.2.

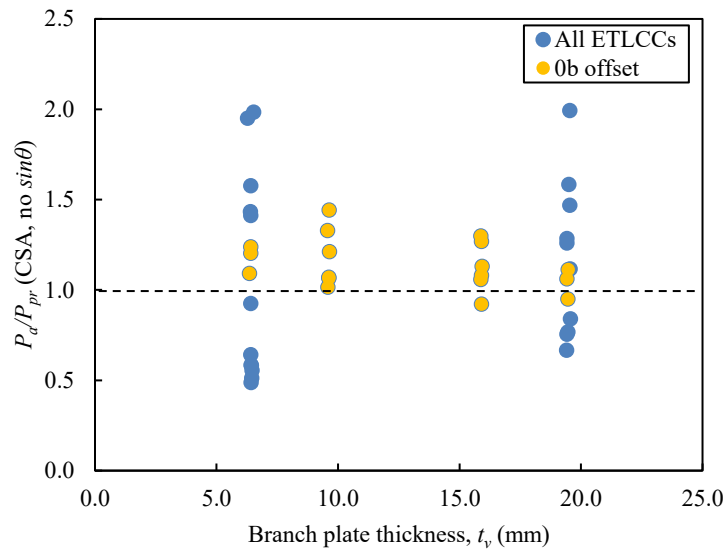


Fig. 5.2. Effect of plate thickness on single-sided fillet weld strength

Despite having only a small effect on strength, less rotation of the connection about the weld axis was observed as t_v increased. In Fig. 5.3., digital image correlation plots for y-axis strain (ϵ_{yy}) are compared for two ETLCC specimens (S6-L-30a and S20-S-30a). Specimens S6-L-30a and S20-S-30a have the same branch plate offset but have a t_v of 6.4 mm and 19.1 mm, respectively. For specimen S20-S-30a, ϵ_{yy} is greatly reduced in the branch plates leading to less rotation of the specimen and the fillet weld under load.

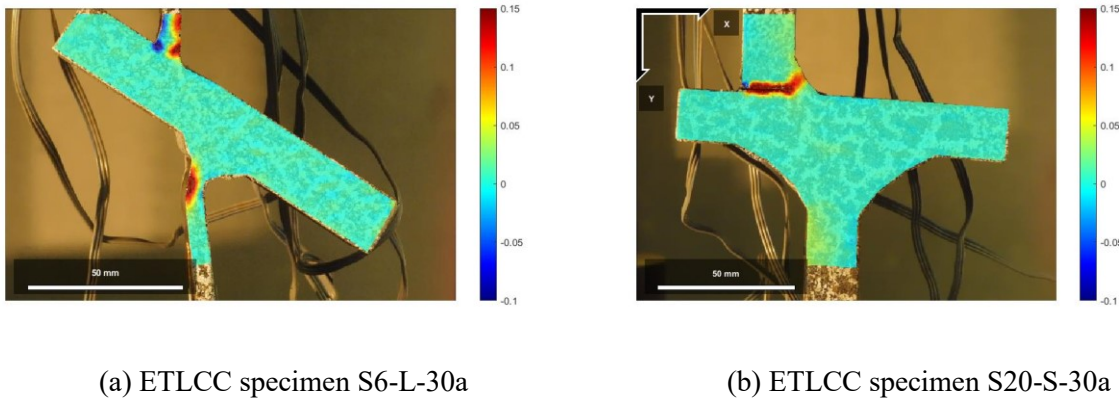


Fig. 5.3. Digital image correlation plots for y-axis strain (ϵ_{yy})

5.1.3. ECCENTRICITY (MAGNITUDE/DIRECTION)

Eccentricity was found to have a significant effect on fillet weld strength when observing all ETLCC tests. As eccentricity increases (causing tension at the weld root), the fillet weld strength decreases. It is also worth noting that, when eccentricity decreases (causing compression at the weld root), single-sided fillet weld strength increases only up to a point (approx. when eccentricity = 15 mm). After that point, single-sided fillet weld strength saw a slight decrease; however, this may be due to the inherent/expected experimental scatter. A plot of P_d/P_{pr} versus eccentricity for all ETLCC tests can be seen in Fig. 5.4.

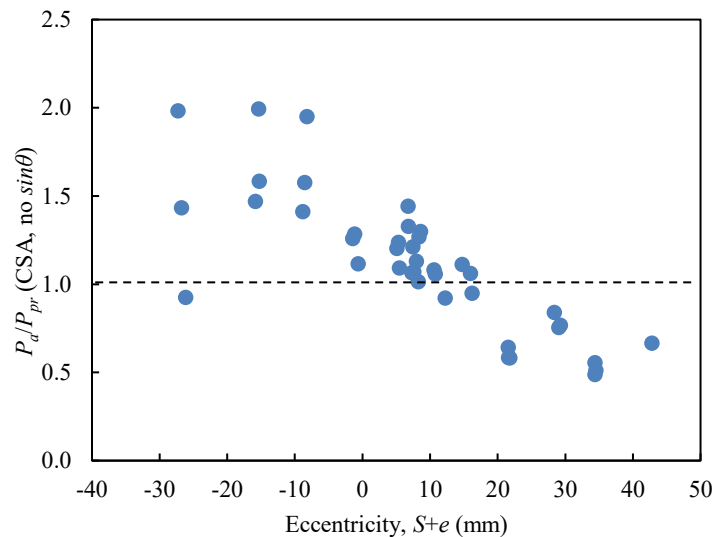


Fig. 5.4. Effect of eccentricity on single-sided fillet weld strength

5.1.4. WELD SIZE-TO-BRANCH PLATE THICKNESS RATIO

Weld size-to-branch plate thickness (t_w/t_v) was found to have no effect on fillet weld strength (based on the current, simple, CSA S16:19 fillet weld strength model) when observing all ETLCC tests or tests of the same offset (i.e. 0b offset). A plot of P_d/P_{pr} versus t_w/t_v for all ETLCC tests can be seen in Fig. 5.5.

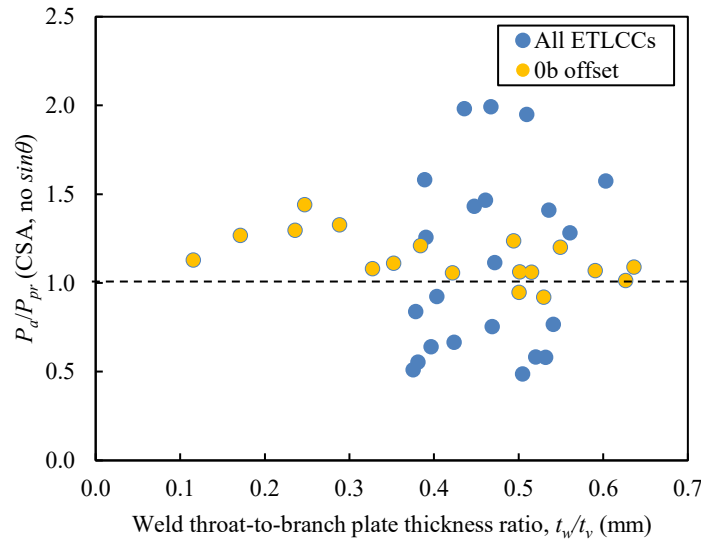


Fig. 5.5. Effect of weld throat-to-branch plate thickness ratio on single-sided fillet weld strength

In Section 5.4, however, it is shown that this ratio, t_w/t_v , bares some significance with respect to other fillet weld strength models (e.g. EN 1993-1-8) and can be used to help predict fillet weld strength according to the new theoretical model proposed herein (see Section 5.4). Similar findings were made by Tousignant and Packer (2017), who related the strength of welds in HSS connections to the ratio t_w/t_b (see Section 2.3.4.). The new model proposed in Section 5.4 considers the induced stress caused by eccentricity on a fillet weld via a stiffness factor (λ) that can be reasonably correlated to t_w/t_v .

5.2. EVALUATION OF CURRENT DESIGN CRITERIA

5.2.1. RELIABILITY ANALYSIS

A reliability analysis was herein performed for the ETLCC specimens to determine the inherent safety indices (β) for the fillet weld design equations discussed in Chapter 3. This analysis was done by using two approaches: (1) a modern approach, in general accordance with CSA S408-11 and CSA S6:19 (incorporating variability in both resistance and load effects), and (2) a simpler, “separation-factor” approach that was historically used for the calibration of LSD/LRFD criteria.

5.2.1.1. CSA S408-11/CSA S6:19 approach

The formula used to determine the reliability index (β) in accordance with CSA S408-11/CSA S6:19 is as shown in Eqn. (5.1) (see Clause 14.15.2.3 in CSA S6:19):

$$\phi = \rho_r \frac{\gamma_D + \gamma_L (L/D)}{\rho_D + \rho_L (L/D)} \exp\left(-\beta \sqrt{V_R^2 + V_S^2}\right) \quad (5.1)$$

where ϕ = resistance factor; ρ_R = bias coefficient for resistance; ρ_D = bias coefficient for dead load; ρ_L = bias coefficient for live load; γ_D = load factor for dead load; γ_L = load factor for live load; β = reliability index; L/D = live-to-dead load ratio; V_R = coefficient of variation for resistance [Eqn. (5.2a)]; and V_S = coefficient of variation (load) [Eqn. (5.2b)].

When calculating V_R and ρ_r , the resistance was broken down into four multiplicative factors including: geometry (G), material (M), professional (P), and discretization (d). The geometry factor incorporates variability in the weld throat size; the material factor incorporates variability in electrode strength; the professional factor incorporates the predictive accuracy of the design equation used (i.e., CSA S16-19, AISC 360-16 or EN1993-1-8:2004); and the discretization factor incorporates the effect of “rounding up” in design. The factors ρ_R and V_R can be calculated by using Eqns. (5.2a-b).

$$\rho_R = \delta_G \delta_M \delta_P \delta_d \quad (5.2a)$$

$$V_R = \sqrt{V_G^2 + V_M^2 + V_P^2 + V_d^2} \quad (5.2b)$$

where δ_G = geometry factor; δ_M = material factor; δ_P = professional factor; δ_d = discretization factor; V_G = coefficient of variation (geometry); V_M = coefficient of variation (material); V_P = coefficient of variation (professional); and V_d = coefficient of variation (discretization).

The load effects considered for the reliability analysis were live and dead load. The coefficient of variation for load (V_S) and load bias coefficient includes live load and dead load only, with V_S calculated by using Eqn. (5.3), below.

$$V_S = \frac{\sqrt{(\rho_D V_D)^2 + (\rho_L V_L (L/D))^2}}{\rho_D + \rho_L (L/D)} \quad (5.3)$$

where V_S = coefficient of variation (load); V_D = coefficient of variation for dead load; and V_L = coefficient of variation for live load.

5.2.1.2. Separation factor approach

The formula used to determine the safety index (β) according to the separation-factor approach is as shown in Eqn. (5.4).

$$\phi = \rho_R \exp(-\alpha_R \beta V_R) \quad (5.4)$$

where ϕ = resistance factor; ρ_R = resistance bias coefficient; α_R = coefficient of separation (= 0.55); β = safety index; and V_R = coefficient of variation for resistance [Eqn. (5.2a)].

The coefficient of variation for resistance (V_R) and the bias coefficient for resistance (ρ_R) are broken down in the same manner described in Section 5.2.1.1. The four factors included were again: geometry (G), material (M), professional (P), and discretization (d). The terms ρ_R and V_R were hence calculated, again, by using Eqns. (5.2a-b). In contrast with Eqn. (2.7), presented earlier, the adjustment factor, Φ_β , is not included. Eqn. (5.4) is generally in accordance with the separation-factor approach introduced in the 1970s.

5.2.2. EVALUATION PROCEDURE

For the CSA S408-11/CSA S6:19 approach, the reliability index (β) was calculated over a practical range of live-to-dead load ratios ($0.0 \leq L/D \leq 3.0$). The governing load combination at any given L/D ratio was used to calculate β . All bias coefficients and variations for dead load and live load (ρ_D , ρ_L , V_D , and V_L) used were extracted from MacPhedran & Grondin (2011). The target β value was taken as 4.0 (for connection design) for all steel design codes (CSA S16-19, AISC 360-16, and EN1993-1-8:2005) in accordance with Annex B.4 of CSA S16:19 (CSA 2019) and Chapter B of the AISC 360-16 Commentary (AISC 2016). A summary of all target reliability indexes, resistance factors, and load factors used, for each code, can be found in Table 5.1.

Table 5.1. Reliability indexes, resistance factors, and load factors

| | CSA S16:19 | | AISC 360-16 | | EN1993-1-8:2005 |
|------------------|-------------------|-------------------|-------------------|-------------------|-------------------|
| β (target) | 4.0 | | 4.0 | | 4.0 |
| ϕ | 0.67 | | 0.75 | | 0.80 ¹ |
| Load Combination | (1) | (2) | (1) | (2) | (1) |
| γ_D | 1.25 | 1.40 | 1.20 | 1.40 | 1.35 |
| γ_L | 1.50 | 0 | 1.60 | 0 | 1.50 |
| | ρ_D | ρ_L | V_D | V_L | |
| | 0.90 ² | 1.05 ² | 0.10 ² | 0.27 ² | |

¹Derived by converting the partial safety factor ($\gamma_{M2} = 1.25$) to its equivalent resistance factor ($\phi = 1/\gamma_{M2}$)

²Values from MacPhedran & Grondin (2011)

All the factors [geometry (G), material (M), professional (P), and discretization (d)] used to calculate ρ_R (shown in Section 5.2.1.1) were determined from the ETLCC test results. The parameter δ_G was found to be 1.13. This was derived by, first, taking in the actual weld throat size (t_w) (macro-etch examinations) and dividing it by the measured throat size (weld gage measurements) (t_{wm}) for each ETLCC test to find the actual-to-measured weld throat size ratio ($= t_w/t_{wm}$). The average of t_w/t_{wm} was found to be 1.10. A graph comparing t_w/t_{wm} to t_{wm} for various weld sizes can be seen in Fig. 5.6. The final value for δ_G (1.13) was then determined by combining the value of 1.10 with that given by Calelle (2009) (1.03), which accounts for fabrication tolerance. The corresponding coefficient of variation was determined by taking the square root of the sum of squares of the statistical variations associated with these two values.

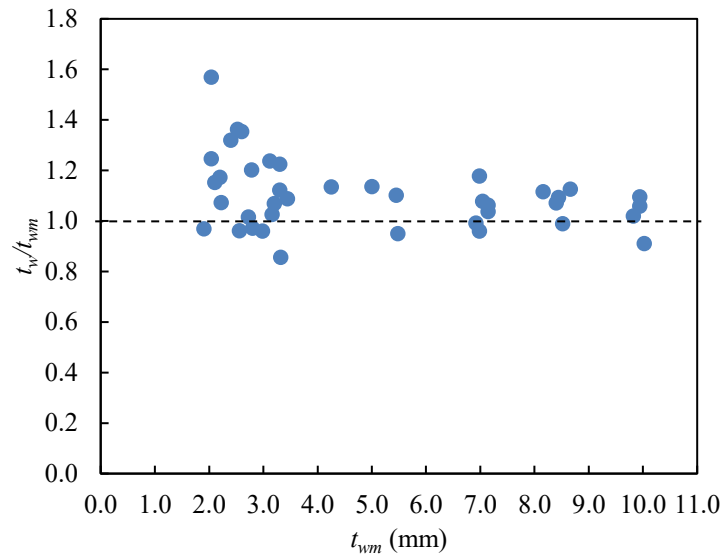


Fig. 5.6. Actual-to-measured weld throat size ratio versus weld throat size for ETLCC tests

The parameter δ_M was taken to be 1.12. This value was obtained from Lesik and Kennedy (1990) who derived a value for δ_M and V_M based on 672 tests for weld metal tensile strength including: Miazga and Kennedy (1986), Gagnon and Kennedy (1987), Swannell and Skewes (1979b) and Fisher et al. (1978). A summary of these tests can be seen in Table 5.2.

Table 5.2. Measured-to-nominal ratios of tensile strength of weld metal (Lesik and Kennedy 1990)

| Source | Sample Size | Nominal Tensile Strength, X_{in} | Mean Tensile Strength, X_u | X_{in}/X_u | Std. dev. | COV |
|-----------------------------|-------------|------------------------------------|------------------------------|--------------|-----------|--------------|
| Miazga and Kennedy (1986) | 3 | 480 MPa | 537.7 MPa | 1.120 | 0.0158 | 0.0141 |
| Gagnon and Kennedy (1987) | 10 | 480 MPa | 579.9 MPa | 1.208 | 0.0428 | 0.0355 |
| Swannell and Skewes (1979b) | 2 | 410 MPa | 538.8 MPa | 1.314 | 0.0262 | 0.0199 |
| Fisher et al. (1978) | 127 | 60 ksi | 66 ksi | 1.100 | 0.0427 | 0.0388 |
| | 138 | 70 ksi | 74.9 ksi | 1.070 | 0.0381 | 0.0356 |
| | 136 | 80 ksi | 87.9 ksi | 1.099 | 0.0543 | 0.0494 |
| | 16 | 90 ksi | 100.2 ksi | 1.113 | 0.048 | 0.0431 |
| | 72 | 110 ksi | 116.9 ksi | 1.063 | 0.0426 | 0.0400 |
| | 128 | 70 ksi | 85.4 ksi | 1.220 | 0.0681 | 0.0559 |
| | 40 | 70 ksi | 86.8 ksi | 1.240 | 0.1411 | 0.1138 |
| All samples | 672 | - | - | 1.123 | 0.087 | 0.077 |

A key finding from the current study is that the parameter δ_P depends on the ETLCC specimen offset (30a, 15a, 0, etc.) [as well as the design method used (CSA S16-19, AISC 360-16, and EN1993-1-8:2005)]. By dividing the actual strength obtained from tests discussed in Chapters 4 and 5 (P_a) by the predicted strength (P_{pr}), the average actual-to-predicted strength ratio $P_a/P_{pr} = \delta_P$, and V_P , was determined for each specimen offset (S). A summary of these values for each design method can be seen in Table 5.3. P_a/P_{pr} values for all the individual ETLCC test specimens can be found in Appendix D.

Table 5.3. Summary of δ_P and V_P values for CSA S16-19, AISC 360-16, and EN1993-1-8:2005

| Offset, S | CSA S16:19 | | AISC 360-16 | | EN1993-1-8:2005 | | |
|-------------|-------------------|----------------------|-------------------|----------------------|-----------------|------------|-------|
| | with $\sin\theta$ | without $\sin\theta$ | with $\sin\theta$ | without $\sin\theta$ | Directional | Simplified | |
| 30a | $\delta_P =$ | 1.043 | 1.564 | 1.164 | 1.746 | 1.314 | 1.706 |
| | $V_P =$ | 0.255 | 0.255 | 0.255 | 0.255 | 0.247 | 0.251 |
| 15a | $\delta_P =$ | 0.955 | 1.432 | 1.066 | 1.599 | 1.232 | 1.573 |
| | $V_P =$ | 0.208 | 0.208 | 0.208 | 0.208 | 0.259 | 0.237 |
| 0b | $\delta_P =$ | 0.761 | 1.141 | 0.849 | 1.274 | 0.979 | 1.260 |
| | $V_P =$ | 0.120 | 0.120 | 0.120 | 0.120 | 0.106 | 0.129 |
| 15b | $\delta_P =$ | 0.463 | 0.695 | 0.517 | 0.776 | 0.624 | 0.756 |
| | $V_P =$ | 0.155 | 0.155 | 0.155 | 0.155 | 0.131 | 0.122 |
| 30b | $\delta_P =$ | 0.370 | 0.555 | 0.413 | 0.620 | 0.511 | 0.615 |
| | $V_P =$ | 0.142 | 0.142 | 0.142 | 0.142 | 0.116 | 0.110 |

The value for δ_d was derived as part of this study, to include the factor of “rounding-up” when designing. To determine δ_d , the shear resistance (V_R) of fillet weld throats and fillet weld leg sizes from the CISC handbook (from Tables 3-23, 3-24a & 3-24b) and fillet weld leg sizes from the AISC manual (Table 8-2). A list of factored shear (V_f) values were arranged in a spreadsheet ranging from 0 kN/mm to 10 kN/mm in 0.05 increments. Each V_f was then assigned the closest design V_R for design (where $V_f < V_R$). V_R/V_f was calculated then averaged to acquire δ_d . A summary of δ_d and V_d for fillet weld throats and leg sizes can be seen in Table 5.4.

Table 5.4. Summary of δ_d and V_d for fillet weld throat and leg sizes from CISC handbook and AISC manual

| | CISC Handbook | | AISC Manual |
|------------|--------------------|---------------|-------------|
| | Throat size, t_w | Leg size, D | Leg size, D |
| | Table 3-23 | Table 3-24a-b | Table 8-2 |
| δ_d | 1.12 | 1.09 | 1.10 |
| V_d | 0.072 | 0.062 | 0.062 |

Ultimately, δ_d (1.09) and V_d (0.062) for fillet weld leg sizes according to CISC handbook (values in bold) were chosen as the δ_d was the lowest, providing the worst case for design. Plots used to derive δ_d for fillet weld throat and leg sizes from the CISC handbook and fillet weld leg sizes from the AISC manual can be seen in Fig. 5.7.

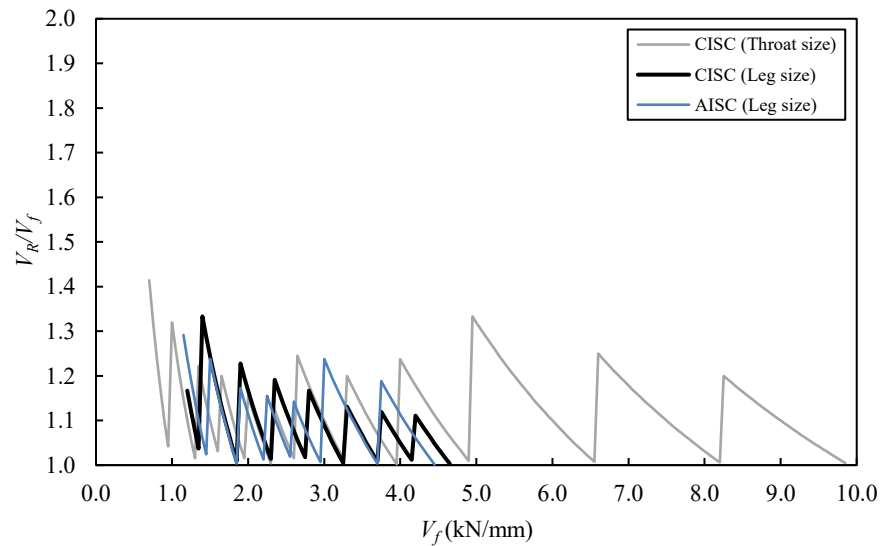


Fig. 5.7. Discretization Factor (δ_d) for fillet weld throat and leg sizes from the CISC handbook and fillet weld leg sizes from the AISC manual

With all the above parameters determined, the reliability index, β , was calculated based on the formulas given in Section 5.2.1.1 (the CSA S408-11/CSA S6:19 approach) and Section 5.2.1.2 (the separation-factor approach). In Section 5.2.3, the resulting β values are compared to the specified target value(s) in North American codes (i.e. $\beta = 4.0$).

5.2.3. EVALUATION OF RESULTS

As previously noted, the reliability indices (β) herein are calculated according to CSA S408-11/CSA S6:19 and separation-factor approaches (see Sections 5.2.1.1. and 5.2.1.2.). The values of β were determined for using CSA S16:19 (with/without the $\sin\theta$ factor), AISC 360-16 (with/without the $\sin\theta$ factor) and EN1993-1-8:2005

(Directional and Simplified methods) for each branch plate offset (S) separately and for all 40 ETLCC specimens together for a practical range of L/D ratios ($0 \leq L/D \leq 3.0$).

5.2.3.1. CSA S408-11/CSA S6:19 approach

Fig. 5.8 shows the reliability indices (β) calculated in accordance with the CSA S408-11/CSA S6:19 approach for CSA S16:19 with and without the use of the $\sin\theta$ factor.

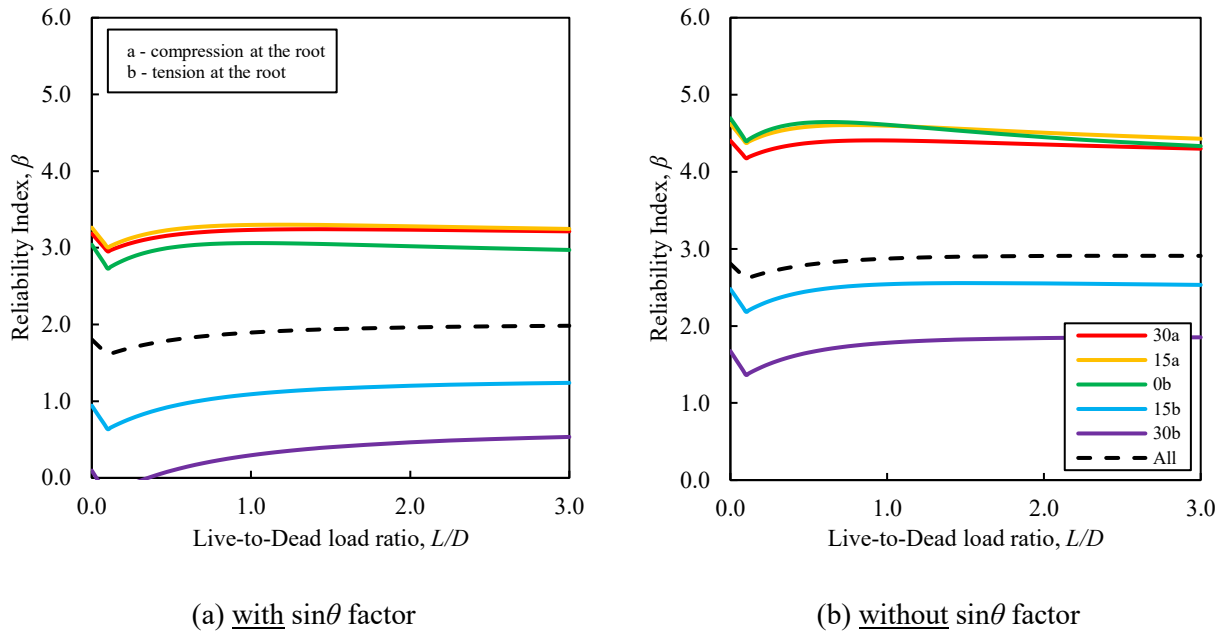


Fig. 5.8. Reliability index (β) plots for CSA S16:19

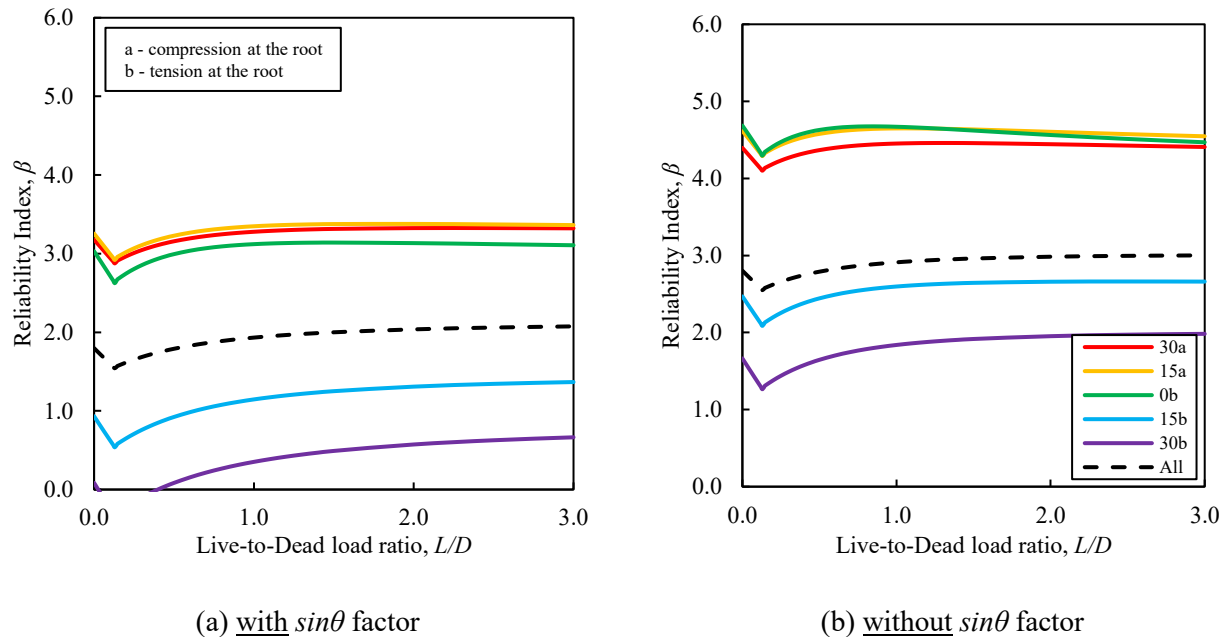
When the $\sin\theta$ factor is used, the target β ($= 4.0$) is not met for any offset. When looking at branch plate offsets causing compression at the root (i.e. 30a & 15a), the reliability index varies from 2.95 to 3.30. When the branch plate offset is 0, the reliability index varies from 2.73 to 3.06. ETLCC specimens with branch plate offsets causing tension at the root (i.e. 15b & 30b) see significantly lower reliability indexes ranging from - 0.23 to 1.24. All ETLCC specimens together have a β ranging from 1.61 to 1.98. These results are summarized in Table 5.5, below.

Table 5.5. Reliability index values (CSA S408-11/CSAS6:19 approach) for each branch plate offset (S) using CSA S16:19, AISC 360-16 & EN1993-1-8:2005 design codes

| Offset, S | CSA S16:19 | | AISC 360-16 | | EN1993-1-8:2005 | |
|-------------|-------------------|----------------------|-------------------|----------------------|------------------|------------------|
| | with $\sin\theta$ | without $\sin\theta$ | with $\sin\theta$ | without $\sin\theta$ | Directional | Simplified |
| 30a | 2.95-3.24 | 4.18-4.41 | 2.88-3.33 | 4.10-4.46 | 3.30-3.56 | 4.06-4.30 |
| 15a | 3.01-3.30 | 4.37-4.62 | 2.92-3.38 | 4.29-4.65 | 3.02-3.28 | 3.94-4.18 |
| 0b | 2.73-3.06 | 4.33-4.69 | 2.62-3.14 | 4.30-4.68 | 3.28-3.60 | 4.08-4.44 |
| 15b | 0.64-1.24 | 2.18-2.56 | 0.54-1.37 | 2.09-2.66 | 1.33-1.75 | 2.13-2.49 |
| 30b | -0.23-1.98 | 1.36-1.85 | -0.33-0.66 | 1.26-1.98 | 0.55-1.11 | 1.32-1.75 |
| All | 1.61-1.98 | 2.61-2.91 | 1.54-2.08 | 2.55-3.00 | 1.97-2.26 | 2.50-2.76 |

When the $\sin\theta$ factor is not used, the target β ($= 4.0$) is met for offset branch plate offsets causing compression at the root. When looking at branch plate offsets causing compression at the root (i.e. 30a & 15a), the reliability index varies from 4.18 to 4.62. When the branch plate offset is 0, the reliability index varies from 4.33 to 4.69. ETLCC specimens with branch plate offsets causing tension at the root (i.e. 15b & 30b) see significantly lower reliability indexes ranging from 1.36 to 2.56 which does not meet the target β . All ETLCC specimens together have a β ranging from 2.61 to 2.91.

For AISC 360-16, the resulting values of β calculated in accordance with the CSA S408-11/CSA S6:19 approach are compared in Fig. 5.9.

**Fig. 5.9.** Reliability index (β) plots for AISC 360-16

When the $\sin\theta$ factor is used, the target β ($= 4.0$) is not met for any offset. When looking at branch plate offsets causing compression at the root (i.e. 30a & 15a), the reliability index varies from 2.88 to 3.38. When

the branch plate offset is 0, the reliability index varies from 2.62 to 3.14. ETLCC specimens with branch plate offsets causing tension at the root (i.e. 15b & 30b) see significantly lower reliability indexes ranging from -0.33 to 1.37. All ETLCC specimens together have a β ranging from 1.54 to 2.08.

When the $\sin\theta$ factor is not used, the target β ($= 4.0$) is met for offset branch plate offsets causing compression at the root. When looking at branch plate offsets causing compression at the root (i.e. 30a & 15a), the reliability index varies from 4.10 to 4.65. When the branch plate offset is 0, the reliability index varies from 4.30 to 4.68. ETLCC specimens with branch plate offsets causing tension at the root (i.e. 15b & 30b) see significantly lower reliability indexes ranging from 1.26 to 2.66 which does not meet the target β . All ETLCC specimens together have a β ranging from 2.55 to 3.00.

Fig. 5.10 shows the calculated values of β for EN1993-1-8:2005 in accordance with the CSA S408-11/CSA S6:19 approach, using both the Directional Method and the Simplified Method.

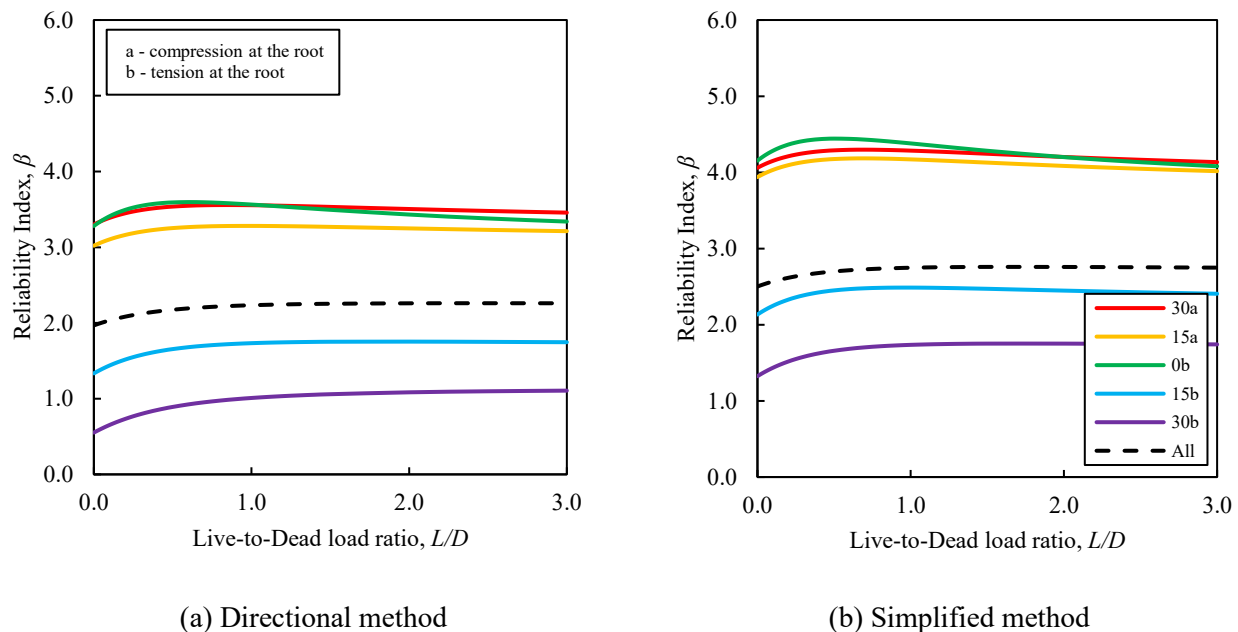


Fig. 5.10. Reliability index (β) plots for EN1993-1-8:2005

When the Directional Method is used, the target β ($= 4.0$) is not met for any offset. When looking at branch plate offsets causing compression at the root (i.e. 30a & 15a), the reliability index varies from 3.02 to 3.56. When the branch plate offset is 0, the reliability index varies from 3.28 to 3.60. ETLCC specimens with branch plate offsets causing tension at the root (i.e. 15b & 30b) see significantly lower reliability indexes ranging from 0.55 to 1.75. All ETLCC specimens together have a β ranging from 1.97 to 2.26.

When the Simplified Method is used, the target β ($= 4.0$) is mostly met for offset branch plate offsets causing compression at the root. When looking at branch plate offsets causing compression at the root (i.e. 30a & 15a), the reliability index varies from 3.94 to 4.30. When the branch plate offset is 0, the reliability index varies from 4.08 to 4.44. ETLCC specimens with branch plate offsets causing tension at the root (i.e. 15b &

30b) see significantly lower reliability indexes ranging from 1.32 to 2.49 which does not meet the target β . All ETLCC specimens together have a β ranging from 2.50 to 2.76.

5.2.3.2. Separation factor approach

A summary of the reliability index values calculated in accordance with separation-factor approach, for each branch plate offset (S), is given in Table 5.6.

Table 5.6. Reliability index values (separation factor approach) for each branch plate offset (S) using CSA S16:19, AISC 360-16 & EN1993-1-8:2005 design codes

| Offset, S | CSA S16:19 | | AISC 360-16 | | EN1993-1-8:2005 | |
|-------------|-------------------|----------------------|-------------------|----------------------|-----------------|------------|
| | with $\sin\theta$ | without $\sin\theta$ | with $\sin\theta$ | without $\sin\theta$ | Directional | Simplified |
| 30a | 4.42 | 6.75 | 4.41 | 6.73 | 4.83 | 6.29 |
| 15a | 4.43 | 7.06 | 4.42 | 7.05 | 4.33 | 6.03 |
| 0b | 3.72 | 7.01 | 3.70 | 6.99 | 4.46 | 6.24 |
| 15b | -0.29 | 2.73 | -0.31 | 2.71 | 0.65 | 2.21 |
| 30b | -2.02 | 1.09 | -2.04 | 1.07 | -0.96 | 0.56 |
| All | 2.05 | 3.93 | 2.04 | 3.92 | 2.49 | 3.53 |

For CSA S16:19 and AISC 360-16, when the $\sin\theta$ factor is used, the target β (= 4.0) is mostly met for branch plate offsets causing compression at the root (with exception for tests with 0b offsets) and is not met for branch plate offsets causing tension at the root. When β is calculated for all ETLCCs, β is close to meeting the target β . When the $\sin\theta$ factor is not used, the target β (= 4.0) is completely met for branch plate offsets causing compression at the root and is not met for branch plate offsets causing tension at the root. When β is calculated for all ETLCCs, β is close to meeting the target value.

For EN1993-1-8:2005, using the Directional Method or the Simplified Method meets the target β (= 4.0) for branch plate offsets causing compression at the root and is not met for branch plate offsets causing tension at the root. When β is calculated for all ETLCCs, β is close to meeting the target β when using both methods.

5.3. COMPARISON OF RESULTS TO TESTS ON DOUBLE-SIDED WELDS

5.3.1. COMPARISON TO FILLET WELDED LAPPED SPLICE AND CRUCIFORM TEST RESULTS

To evaluate the behaviour of single-sided fillet welds in relation to double-sided fillet welds, the ETLCC test results produced as part of this research program are compared to fillet welded lapped splice and cruciform connections from Ng & Driver (2002) and Miazga & Kennedy (1989). The databases compiled for tests by these authors are provided in Appendix F. In Fig. 5.11, the actual strength (P_a) is plotted versus the predicted strength (P_{pr}) according to CSA S16:19 both with and without the $\sin\theta$ factor. Table 5.7 summarizes the mean values of COVs for the tests. It is clear from Fig. 5.11 and Table 5.7 that single-sided fillet welds are almost

always weaker than double-sided fillet welds, regardless of whether there is tension or compression at the weld root in the former.

Table 5.7. Summary of δ_P and V_P values for CSA S16-19, AISC 360-16, and EN1993-1-8:2005 for single-sided fillet welds and double-sided welds for lapped-splice and cruciform connections

| Offset, S | | | CSA S16:19 | | AISC 360-16 | | EN1993-1-8:2005 | |
|------------------------|------------|---|-------------------|----------------------|-------------------|----------------------|-----------------|--------------|
| | | | with $\sin\theta$ | without $\sin\theta$ | with $\sin\theta$ | without $\sin\theta$ | Directional | Simplified |
| 30a | δ_P | = | 1.043 | 1.564 | 1.164 | 1.746 | 1.314 | 1.706 |
| | V_P | = | 0.255 | 0.255 | 0.255 | 0.255 | 0.247 | 0.251 |
| 15a | δ_P | = | 0.955 | 1.432 | 1.066 | 1.599 | 1.232 | 1.573 |
| | V_P | = | 0.208 | 0.208 | 0.208 | 0.208 | 0.259 | 0.237 |
| 0b | δ_P | = | 0.761 | 1.141 | 0.849 | 1.274 | 0.979 | 1.260 |
| | V_P | = | 0.120 | 0.120 | 0.120 | 0.120 | 0.106 | 0.129 |
| 15b | δ_P | = | 0.463 | 0.695 | 0.517 | 0.776 | 0.624 | 0.756 |
| | V_P | = | 0.155 | 0.155 | 0.155 | 0.155 | 0.131 | 0.122 |
| 30b | δ_P | = | 0.370 | 0.555 | 0.413 | 0.620 | 0.511 | 0.615 |
| | V_P | = | 0.142 | 0.142 | 0.142 | 0.142 | 0.116 | 0.110 |
| All single-sided welds | δ_P | = | 0.748 | 1.123 | 0.836 | 1.253 | 0.967 | 1.234 |
| | V_P | = | 0.343 | 0.343 | 0.343 | 0.343 | 0.329 | 0.345 |
| Double-sided welds | δ_P | = | 1.493 | 2.240 | 1.668 | 2.502 | - | - |
| | V_P | = | 0.237 | 0.237 | 0.237 | 0.237 | - | - |

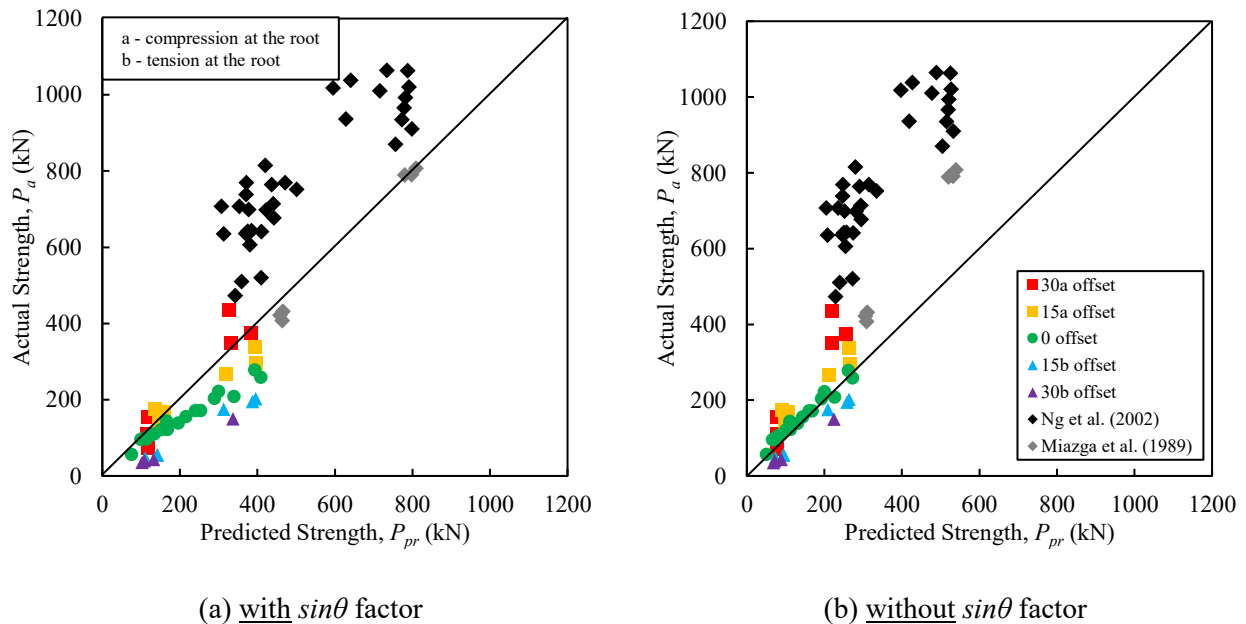


Fig. 5.11. Comparison of single-sided weld versus fillet welded lapped splice and cruciform test strengths using CSA S16:19

5.3.2. COMPARISONS TO FILLET WELDED HSS TEST RESULTS

To evaluate the behaviour of single-sided fillet welds in relation to fillet welded HSS connections, the ETLCC test results are compared to the results of tests on RHS-to-rigid end plate connections (experimental and FE tests) from Oatway (2014), Frater (1986) & Tousignant and Packer (2017) and CHS-to-rigid end plate connections (experimental and FE tests) from Tousignant and Packer (2017). The databases compiled for tests by these authors are provided in Appendix F. In Fig. 5.12, the actual strength (P_a) is again plotted versus the predicted strength (P_{pr}) according to CSA S16:19 both with and without the $\sin\theta$ factor. Table 5.8 summarizes the mean values of COVs for the tests. It is clear from Table 5.8 (and, perhaps, the figure) the single-sided welds in ETLCCs share remarkable similar strengths to single-sided fillet welds in RHS-to-rigid end plate connections and slightly less than CHS-to-rigid end plate connections – likely because the latter are curved, rather than straight, elements.

Table 5.8. Summary of δ_P and V_P values for CSA S16-19, AISC 360-16, and EN1993-1-8:2005 for single-sided fillet welds and welds in HSS-to-rigid end plate connections

| Offset, S | CSA S16:19 | | AISC 360-16 | | EN1993-1-8:2005 | | |
|------------------------------|-------------------|----------------------|-------------------|----------------------|-----------------|--------------|--------------------------|
| | with $\sin\theta$ | without $\sin\theta$ | with $\sin\theta$ | without $\sin\theta$ | Directional | Simplified | |
| 30a | δ_P = | 1.043 | 1.564 | 1.164 | 1.746 | 1.314 | 1.706 |
| | V_P = | 0.255 | 0.255 | 0.255 | 0.255 | 0.247 | 0.251 |
| 15a | δ_P = | 0.955 | 1.432 | 1.066 | 1.599 | 1.232 | 1.573 |
| | V_P = | 0.208 | 0.208 | 0.208 | 0.208 | 0.259 | 0.237 |
| 0b | δ_P = | 0.761 | 1.141 | 0.849 | 1.274 | 0.979 | 1.260 |
| | V_P = | 0.120 | 0.120 | 0.120 | 0.120 | 0.106 | 0.129 |
| 15b | δ_P = | 0.463 | 0.695 | 0.517 | 0.776 | 0.624 | 0.756 |
| | V_P = | 0.155 | 0.155 | 0.155 | 0.155 | 0.131 | 0.122 |
| 30b | δ_P = | 0.370 | 0.555 | 0.413 | 0.620 | 0.511 | 0.615 |
| | V_P = | 0.142 | 0.142 | 0.142 | 0.142 | 0.116 | 0.110 |
| All single-sided welds | δ_P = | 0.748 | 1.123 | 0.836 | 1.253 | 0.967 | 1.234 |
| | V_P = | 0.343 | 0.343 | 0.343 | 0.343 | 0.329 | 0.345 |
| RHS-to-rigid end plate welds | δ_P = | 0.737 | 1.106 | 0.824 | 1.234 | 1.151 | 1.357¹ |
| | V_P = | 0.135 | 0.135 | 0.135 | 0.136 | 0.132 | 0.090 ¹ |
| CHS-to-rigid end plate welds | δ_P = | 0.840 | 1.260 | 0.938 | 1.407 | 1.233 | 1.521 |
| | V_P = | 0.081 | 0.081 | 0.082 | 0.082 | 0.077 | 0.0591 |

¹Based on tests from Tousignant and Packer (2017) only

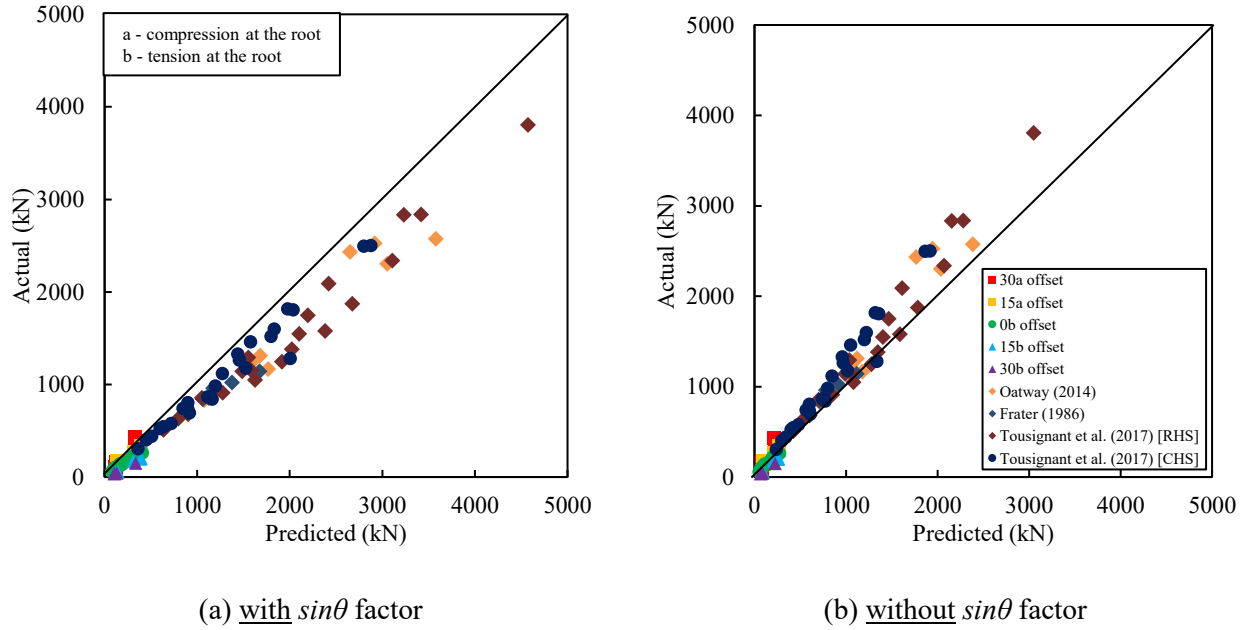


Fig. 5.12. Comparison of single-sided weld versus fillet welded HSS test strengths using CSA S16:19

5.4. INTRODUCTION AND EVALUATION OF NEW THEORETICAL MODEL

To better predict the strength of single-sided fillet welded connections, the induced stress at the weld root caused by eccentricity must be considered. Therefore, a new model is introduced to include this stress by adopting an approach like that given by Tuominen (2018) (see Section 2.3.5.), which breaks the applied force on the weld into its normal and longitudinal components to the weld throat plane. A bending stress component is then added to the normal stress component to include the effect of eccentricity as shown in Eqn. (5.5):

$$P_{pr} = \frac{X_u A_w}{\sqrt{\left[\cos \alpha + \frac{k\lambda(S+e)}{t_w} \right]^2 + 3\sin^2 \alpha}} = \frac{X_u A_w}{d} \quad (5.5)$$

where P_{pr} = predicted strength for single-sided fillet weld; A_w = effective throat area of weld ($= t_w \times l_w$); X_u = ultimate tensile strength of weld metal; α = angle of inclination of the weld throat plane (measured perpendicular to weld axis); k = 6 (for elastic distribution) and 4 (for plastic distribution); λ = stiffness factor for single-sided fillet welded connection [Eqn. (5.6)]; S = branch plate offset (“negative” if in direction causing compression at the root, and “positive” if in direction causing tension at the root); e = centre-to-centre distance between the branch plate and the weld throat plane; d = substitute for denominator; and t_w = weld throat size.

The variable d is used as a substitution for the denominator of Eqn. (5.5), for simplicity. To predict the strength of the ETLCC specimens according to the new theoretical model, a plastic failure distribution ($k = 4$) is assumed. P_{pr}/A_w vs. d for each test is plotted on the following graph, Fig. 5.13, for comparison. The variable

d accounts for eccentricity, weld throat angle, and weld throat thickness for each ETLCC test. All ETLCC values of λ (Table D.2 column 3) and $A_w (= t_w \times l_w)$ (Table 4.3. column 4 & Table 4.2. column 6, respectively) were used to plot all data points in Fig. 5.13 & Fig. 5.14.

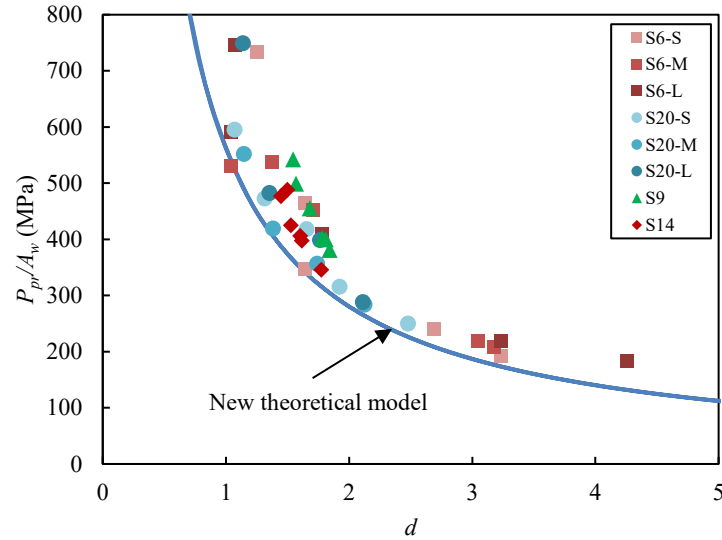


Fig. 5.13. Correlation of new theoretical method to ETLCC tests

Fig. 5.14, which plots the stiffness factor, λ , against the ratio t_w/t_v , shows there is a strong correlation between λ and t_w/t_v – as noted in Section 5.1.4. If a linear relationship is assumed, t_w/t_v can be used to predict the value of λ . As such, the recommended expression for λ in Eqn. (5.6) is as follows:

$$\lambda = 0.16 \left(\frac{t_w}{t_v} \right) \text{ where } 0.12 \leq t_w/t_v \leq 0.64 \quad (5.6)$$

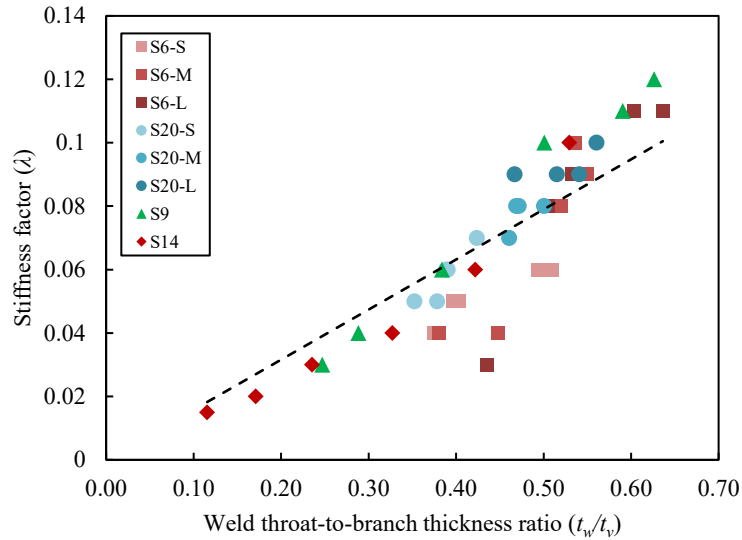
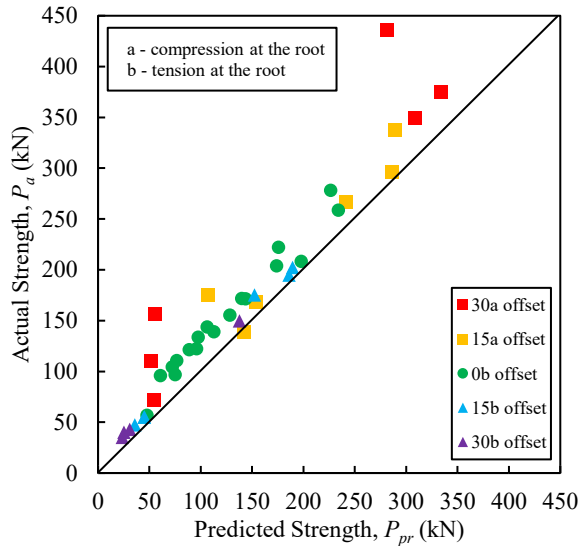


Fig. 5.14. Relationship between stiffness factor (λ) and weld throat-to-branch thickness ratio (t_w/t_v)

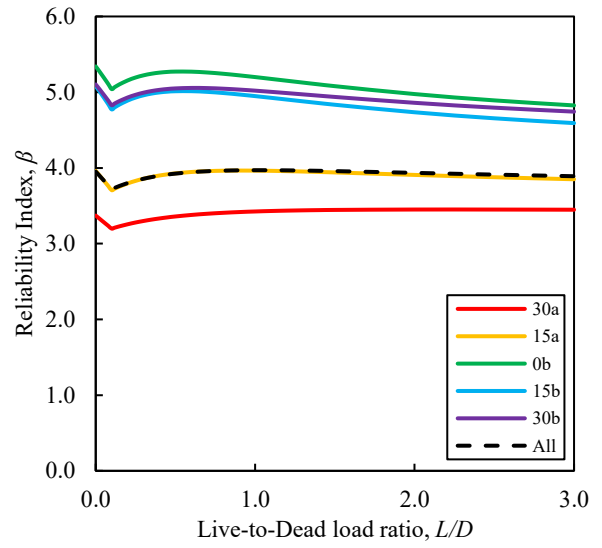
Figs. 5.15a-b shows the correlation plots and the reliability indices (β) calculated in accordance with the CSA S408-11/CSA S6:19 approach for the new theoretical model, assuming a resistance factor, $\phi = 0.67$. Table 5.9. summarizes the mean values, COVs and reliability indexes for the tests. Based on these graphs, the new theoretical model achieves adequate reliability, when observing all ETLCCs specimens together. All λ values were calculated using Eqn. (5.6) for Table 5.9. and Fig. 5.15.

Table 5.9. Summary of δ_P and V_P values using the new theoretical model and β values according to CSA S408-11/ CSA S6:19 and the Separation-factor approach for single-sided fillet welds

| Offset, S | δ_P | V_P | β | |
|-------------|--------------|--------------|---------------------------|-------------------------------|
| | | | CSA S408-11/ CSA S6:19 | Separation-factor approach |
| 30a | 1.680 | 0.403 | 3.20-3.45 | 5.11 |
| 15a | 1.169 | 0.206 | 3.71-3.97 | 5.78 |
| 0b | 1.277 | 0.101 | 4.83-5.34 | 8.27 |
| 15b | 1.172 | 0.090 | 4.59-5.08 | 7.74 |
| 30b | 1.389 | 0.155 | 4.74-5.10 | 7.88 |
| All | 1.317 | 0.248 | 3.72-3.97 | 5.87 |



(a) Correlation plot



(b) Reliability chart

Fig. 5.15. Comparison of actual strengths and predicted strengths & reliability using the new theoretical model

Chapter 6: CONCLUSIONS AND RECOMMENDATIONS

6.1. INTRODUCTION

In this chapter, conclusions and recommendations are given based on this experimental program and other past experimental programs examined.

6.2. SUMMARY

In North American steel design codes, a “directional strength enhancement” (or “ $\sin\theta$ ”) factor is used to increase the predicted strength of fillet welds subjected to tension-induced shear. CSA and AISC code committees have expressed concerns about this factor being potentially unsafe for single-sided fillet welds; however, due to a paucity of physical tests on such welds, only cautionary, but vague, statements to address this issue exist in codes, as was outlined in Chapter 1. A review of relevant studies on transverse fillet welds and single-sided fillet welds and current design methods for fillet welds according to CSA S16, AISC 360 and EN1993-1-8 steel design codes were outlined in Chapter 2 and Chapter 3, respectively.

An experimental program (Chapter 4) was therefore developed at Dalhousie University to test 40 single-sided fillet welds in cruciform connections subjected to branch axial tension. The connections varied the fillet weld size, branch-plate thickness, and loading eccentricity, to investigate the effects of these parameters on the weld strength. Using ultimate loads, a first-order reliability analysis was performed to determine the inherent safety index (β) of North American fillet weld design procedures over a practical range of live-to-dead load (L/D) ratios for elements in steel buildings ($0 \leq L/D \leq 3$). The results (Chapter 5) show that current provisions meet/exceed the target safety index (i.e. $\beta = 4.0$) specified by North American codes (e.g. CSA S16 and AISC 360) provided that: (i) the “ $\sin\theta$ ” factor is not used and (ii) tension at the weld root is avoided. A new theoretical model for single-sided fillet welds is also introduced to account for weld eccentricity (i.e. induced stress due to the bending of the weld).

6.3. CONCLUSIONS

Based on the results of this experimental program consisting of 40 ETLCCs with single-sided welds, and examination of other experimental programs consisting of connections with double-sided fillet welds (lapped-spliced connections, cruciform connections) and single-sided fillet welds (to HSS), the following conclusions are made with respect to single-sided fillets in transverse shear:

- Fillet weld size and branch plate thickness (examined independently) were found to have a small effect on single-sided fillet weld strength when observing all ETLCCs.
- Fillet weld eccentricity (magnitude and direction) has a significant effect on single-sided fillet weld strength:
 - eccentricity causing compression at the weld root increases strength, while
 - eccentricity causing tension at the weld root decreases strength.
- Fillet weld throat-to-branch plate thickness ratio can be used to help predict fillet weld strength according to the new theoretical model proposed herein (see Section 5.4.). Similar findings were made by Tousignant and Packer (2017), who related the strength of welds in HSS connections to the ratio t_w/t_b (see Section 2.3.4.).
- DIC results demonstrate that bending occurs in the branch plates when single-sided fillet welds are subject to transverse loading. Thinner branch plates exhibited far greater bending strains when compared to thicker branch plates.
- For the CSA S16:19 and AISC 360-16 fillet weld design approaches, when the $\sin\theta$ factor is used, predictions of strength are unsafe for all single-sided fillet welds (with compression or tension at the weld root). When the $\sin\theta$ factor is not used, predictions of strength are safe for single-sided fillet welds with compression at the weld root.
- For the EN 1993-1-8:2005 fillet weld design approaches, when the Directional Method is used, predictions of strength are marginally unsafe for single-sided fillet welds with compression at the weld root. When the Simplified Method is used, predictions of strength are safe for single-sided fillet welds with compression at the weld root.
- Single-sided fillet welds in ETLCCs are almost always weaker (regardless of whether there is tension or compression at the weld root) when compared to double-sided fillet welds in lapped-splice and cruciform connection tests from Miazga and Kennedy (1989) and Ng et al. (2002).
- Single-sided fillet welds in ETLCCs show remarkably similar strengths when compared to single-sided fillet welds in RHS-to-rigid end plate connection tests from Frater (1986), Oatway (2014), and Tousignant and Packer (2017). ETLCCs are slightly weaker than CHS-to-rigid end plate connections.

In general, the results of this study show that current North American fillet weld design provisions meet/exceed the target safety index (i.e. $\beta = 4.0$) specified by North American codes (e.g. CSA S16 and AISC 360) provided that: (i) the “ $\sin\theta$ ” factor is not used and (ii) tension at the weld root is avoided.

In addition to the above findings, the following proposed theoretical model [a variation of the model from Tuominen (2018)] was proposed and shown to provide adequate reliability, when observing all single-sided fillet welds in ETLCCs (with *either* compression or tension at the weld root).

$$P_{pr} = \frac{X_u A_w}{\sqrt{\left[\cos \alpha + \frac{k \lambda (S + e)}{t_w} \right]^2 + 3 \sin^2 \alpha}}$$

with:

$$\lambda = 0.16 \left(\frac{t_w}{t_v} \right) \text{ where } 0.12 \leq t_w/t_v \leq 0.64$$

6.4. RECOMMENDATIONS AND FUTURE WORK

The recommendations for each steel design code are the following:

- Using CSA S16:19 & AISC 360-16 for single-sided fillet welded connections, (i) the “sin θ ” factor should not be used and (ii) tension at the weld root should be avoided
- Using EN1993-1-8:2005 single-sided fillet welded connections, (i) only the simplified method should be used and (ii) tension at the weld root should be avoided

Recommendations for future work would be to perform further research (either through experimental or FE tests) to better understand the stiffness factor (λ) for the new theoretical model. The larger variance for predicting strength of single-sided fillet welds with compression at the root, compared to tension at the root, suggest further calibration for λ is needed before this model could be put into practice. The DIC results for the ETLCCs can be used to calibrate future FE models.

REFERENCES

- American Institute of Steel Construction (AISC) 2016. ANSI/AISC 360-16. Specification for structural steel buildings. Chicago, IL, USA.
- American Institute of Steel Construction (AISC). 2021. ANSI/AISC 360-xx. Specification for structural steel buildings. Public review draft dated August 3, 2020. Chicago, IL, USA.
- ASTM International. (2021). *E8/E8M-21 Standard Test Methods for Tension Testing of Metallic Materials*.
- American Welding Society (AWS). 2015. AWS D1.1/D1.1M:2015. Structural welding code – Steel, 23rd ed., Miami, FL, USA.
- Butler, L. J., and Kulak, G. L. (1971). “Strength of Fillet Welds as a Function of Direction of Load.” *Welding Research Supplement, Welding Journal*, 50(5), pp. 231- 234.
- Butler, L. J., Pal, S., and Kulak, G. L. 1972. Eccentrically loaded welded connections. *ASCE Journal of the Structural Division*, 98(ST5): 989 - 1005.
- Canadian Institute of Steel Construction (CISC). 2016. Handbook of steel construction, 11th ed., Toronto, Canada: Canadian Institute of Steel Construction.
- Canadian Standards Association (CSA) 2014. CSA S16-14. Design of steel structures. Toronto, Canada: Canadian Standards Association.
- Canadian Standards Association (CSA) 2019. CSA S16:19. Design of steel structures. Toronto, Canada: Canadian Standards Association.
- Canadian Standards Association (CSA) 2018. CSA W59-18. *Welded Steel Construction* (metal arc welding). Toronto, Canada: Canadian Standards Association.
- Callele, L. J., Driver, R. G., and Grondin, G. Y. (2009). “Design and Behavior of Multi-Orientation Fillet Weld Connections.” *AISC Engineering Journal*, (4), pp. 257- 272.

- Cassidy, C. E. (1993). Effective weld length for HSS T, Y, and X connections. Master of Applied Science Thesis. Toronto, Canada: University of Toronto.
- Chen, Y., Shen, Z. Y., Zheng, Q., & Chen, C. (2001). Experimental study on the performance of single weld joints in H-shaped steel members. *International Journal of Steel Structures*, 1(3), 201-211.
- CSA. 2011. Guidelines for the development of limit states design standards. CSA S408-11, Canadian Standards Association, Toronto, Canada.
- Dale, F., and Laurie, K. D. J. (1988). "Ultimate Strength of Eccentrically Loaded Fillet Weld Connections." Structural Engineering Report No. 159, University of Alberta, Department of Civil and Environmental Engineering, 90.
- EFIG. 1995. Compilation of air-pollutant emission factors. In Volume 1. Stationary-point and area sources, Supplement A. Research Triangle Park, NC: Office of Air Quality Planning and Standards, Office of Air and Radiation, & U.S. Environmental Protection Agency.
- European Committee for Standardization (CEN) 2005. EN 1993-1-8:2005. Eurocode 3: Design of steel structures – Part 1-8: Design of joints. Brussels, Belgium.
- Frater, G. S. (1986). "Weldment design for hollow structural section joints." M.A.Sc. thesis, Univ. of Toronto, Toronto.
- Gallow, M. S. (2019). *Behavior of Fillet Welds in Skewed Joints* (Doctoral dissertation, The University of Alabama at Birmingham).
- Iwankiw, N. R. (1997). "Rational Basis for Increased Fillet Weld Strength." AISC Engineering Journal, (2), pp. 68- 70.
- Kulak, G. L., and Timler, P. A. 1984. Tests on eccentrically loaded fillet welds. Structural Engineering Report No. 124, Department of Civil Engineering, University of Alberta, Edmonton, Alta.
- Lesik, D. F., and Kennedy, D. J. L. (1988). "Ultimate Strength of Eccentrically Loaded Fillet Welded Connections." University of Alberta.
- Lesik, D. F. & Kennedy, D. J. (1990). Ultimate strength of fillet welded connections loaded in plane. *Canadian Journal of Civil Engineering* 17(1): 55-67.

- Linnert, George E. (1967). *Welding Metallurgy*. Vol. 1, Fundamentals. Miami, Florida: American Welding Society.
- Luo, P., Asada, H., Uang, C. M., & Tanaka, T. (2020). Directionality Effect on Strength of Partial-Joint-Penetration Groove Weld Joints. *Journal of Structural Engineering*, 146(4), 04020030.
- MacPhedran, Ian, & Grondin, Gilbert Y. (2011). A simple steel beam design curve. *Canadian Journal of Civil Engineering*, 38(2), 141-153.
- McFadden, M. (2012). *Effective weld properties for RHS-to-RHS moment T-connections* (Doctoral dissertation).
- Miazga, G. S. & Kennedy, D. J. L. (1986). Behaviour of fillet welds as a function of the angle of loading. Structural Engineering Report 133, Department of Civil Engineering, University of Alberta, Edmonton, AB.
- Miazga, G. S. & Kennedy, D. J. (1989). Behaviour of fillet welds as a function of the angle of loading. *Canadian Journal of Civil Engineering* 16(4): 583-599.
- Miller, D. K. (1998). "Consider Direction of Loading When Sizing Fillet Welds." *Welding Innovation*, 15(2).
- Newcomb, B., & Tousignant, K. (2021). Optimized Design of Fillet Welds in RHS Joints for EN 1993-1-8. *Steel Construction Design and Research*, 14. Manuscript submitted for publication.
- Ng, A. K. F., Deng, K., Grondin, G. Y. & Driver, R. G. (2004a). "Behaviour of transverse fillet welds: experimental program", *AISC Engineering Journal* 41(2): 39-54.
- Ng, A. K. F., Deng, K., Grondin, G. Y. & Driver, R. G. (2004b). "Behaviour of transverse fillet welds: Parametric and reliability analyses", *AISC Engineering Journal* 41(2): 55-67.
- Oatway, P. (2014). "Fillet-welded end-plate connections to square and rectangular HSS." M.Eng. thesis, Univ. of Toronto, Toronto.
- O'Brien, Annette. (1991). *Welding Handbook, Welding Processes*. Vol. 2, AWS WHB-2.9. Miami, FL: American Welding Society.
- Packer, J. A., Sun, M., & Tousignant, K. (2016). "Experimental evaluation of design procedure for fillet welds to hollow structural sections", *ASCE Journal of Structural Engineering* 142(5): 0416007-1 – 04016007-12.
- Packer, J.A. (2019, Winter). "HSS Joint Welding", *Advantage Steel* 63: 12-13.

- Rasmussen, K. J. R., Ha, J., Lam, K., & Lam, Y. (1999). *Strength of eccentrically loaded incomplete penetration butt welds*. N.S.W., Australia.
- Swannell, P., and Skewes, I. C. 1979a. The design of welded brackets loaded in in-plane: elastic and ultimate load techniques - AWRA Report P6-8-77. Australian Welding Research, 7: 28-59.
- Swannell, P., and Skewes, I. C. 1979b. The design of welded brackets loaded in-plane: general theoretical ultimate load techniques and experimental programme - AWRA Report P6-1-78. Australian Welding Research, 7: 55 -70.
- Tousignant, K. & Packer, J. A. (2017). "Numerical investigation of fillet welds in HSS-to-rigid end-plate connections", *ASCE Journal of Structural Engineering* 143(12): 04017165-1 – 04017165-16.
- Tousignant, K. & Packer, J. A. (2019). Weld effective lengths for round HSS cross-connections under branch axial loading. *Engineering Journal, American Institute of Steel Construction*, 56(3): 173-186.
- Wang, W., Gu, Q., Ma, X., and Wang, J. (2015). "Axial tensile behavior and strength of welds for CHS branches to SHS chord joints." *J. Constr. Steel Res.*, 115, 303–315.

Appendix A: ETLCC SPECIMEN & METAL COUPON FABRICATION DRAWINGS

Appendix A includes the list of fabrication drawings for the ETLCC test specimens, Instrumentation and metal coupons, and the drawings themselves are provided herein.

Table A.1. List of ETLCC specimen fabrication drawings

| Sheet No. | Description |
|-----------|--------------------------------------|
| 1 | Welded section overview |
| 2 | S6-30a & S6-15a |
| 3 | S6-0 & S6-15b |
| 4 | S6-30b & S20-30a |
| 5 | S20-15a & S20-0 |
| 6 | S20-15b & S20-30b |
| 7 | S9-0 |
| 8 | S14-0 |
| 9 | Test & trial specimens |
| 10 | Instrumentation |
| 11 | Base metal & weld metal test coupons |

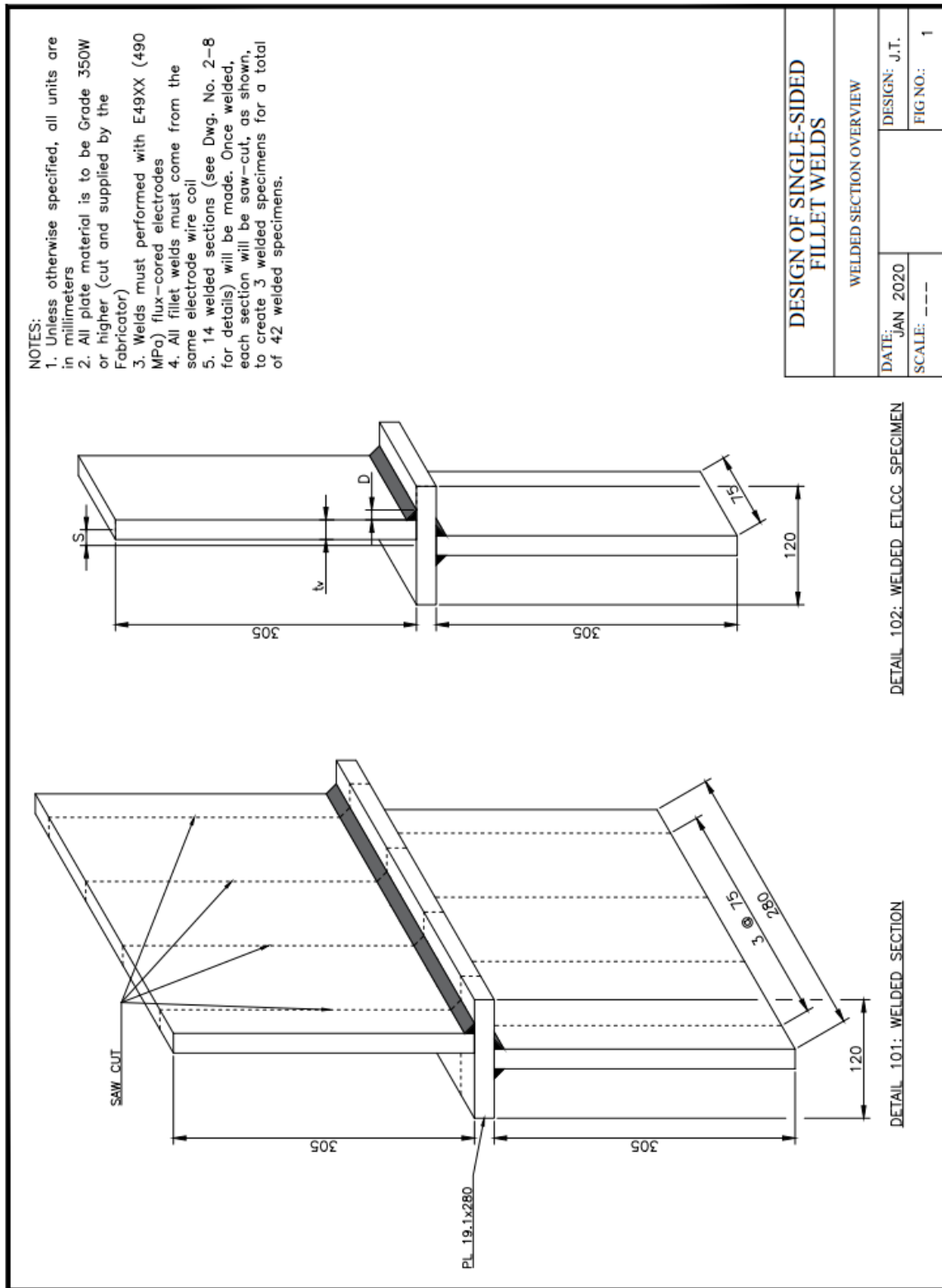


Fig. A.1. Welded section overview

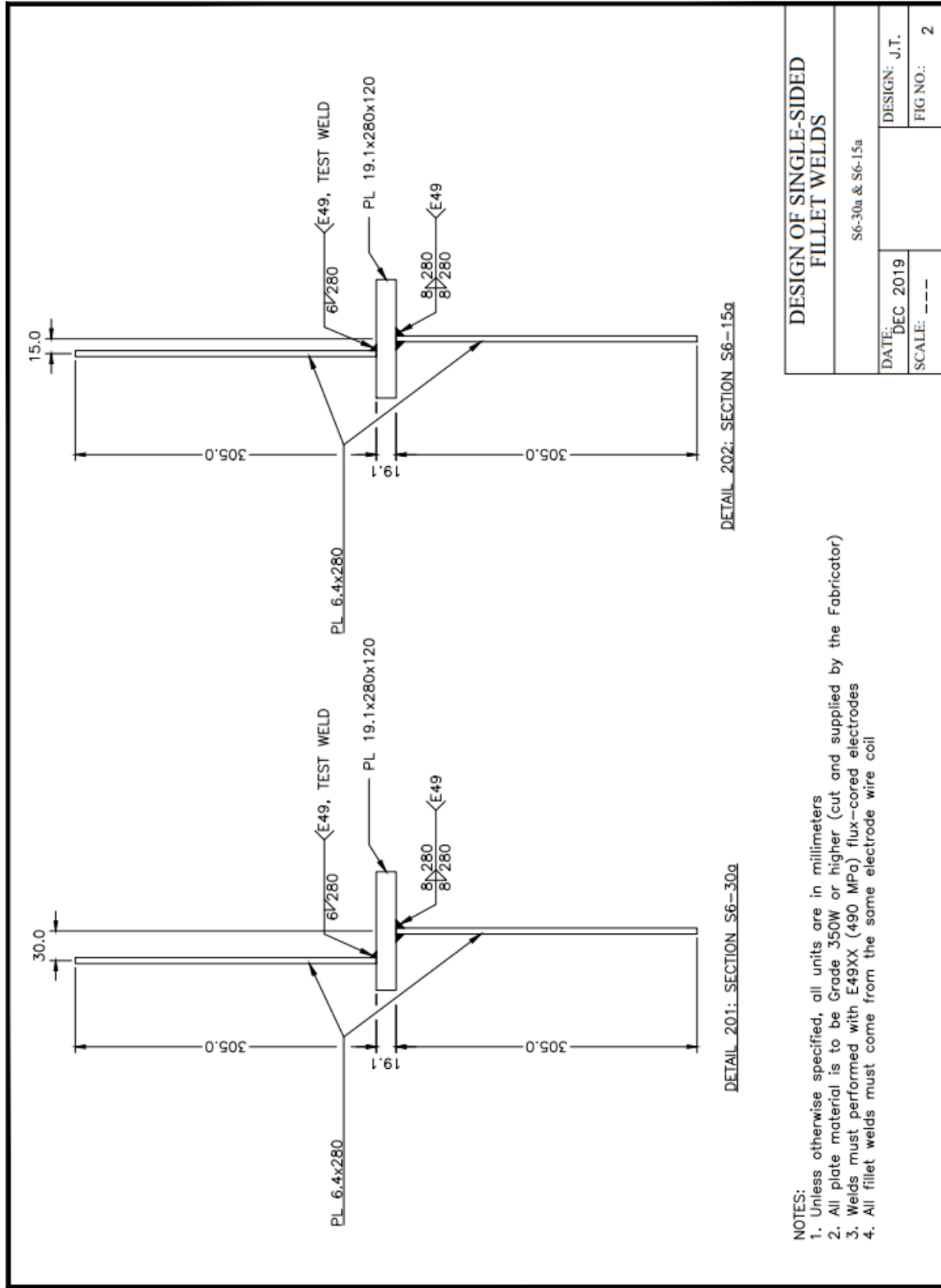


Fig. A.2. S6-30a & S6-15a sections

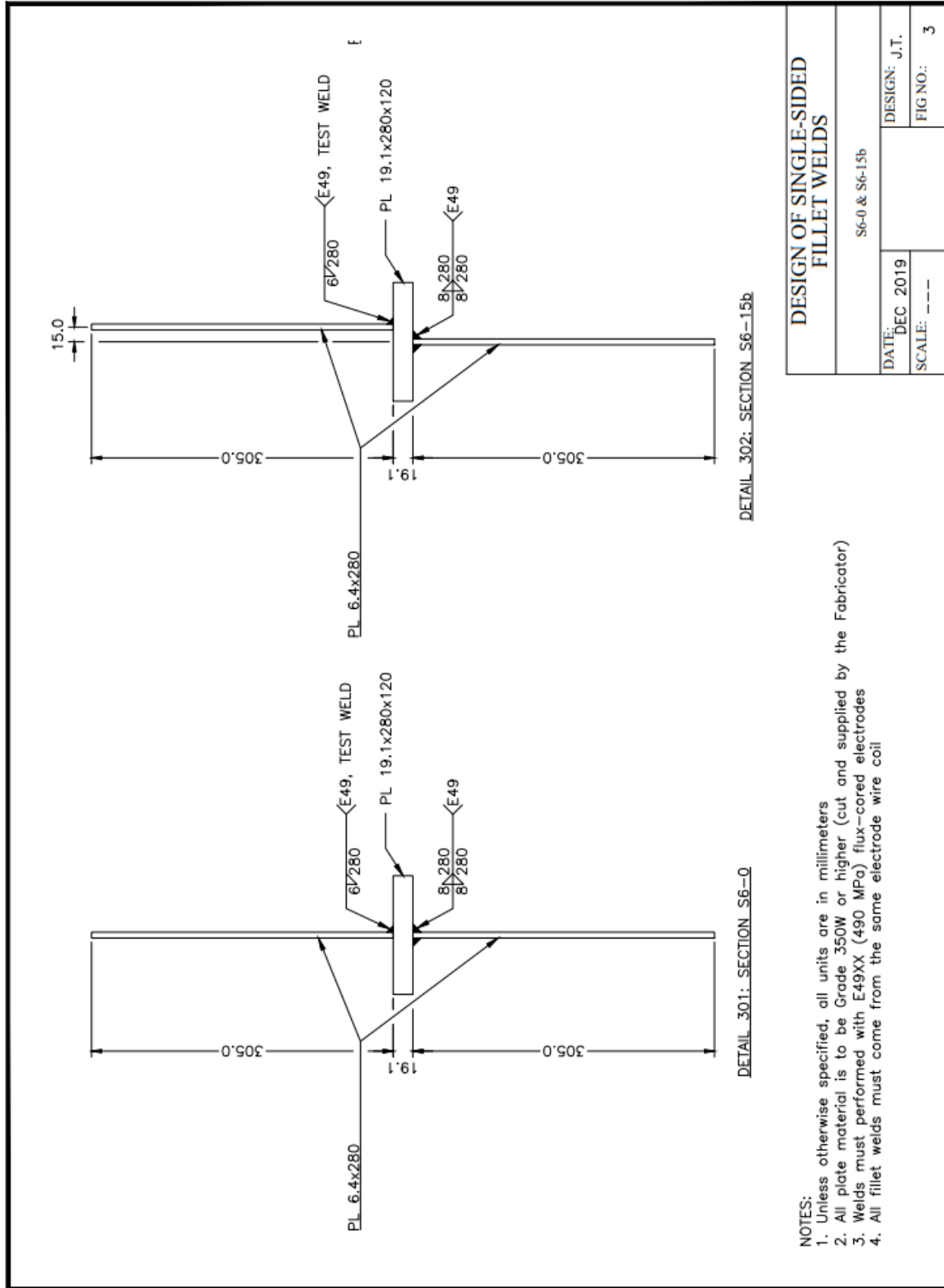


Fig. A.3. S6-0 & S6-15b sections

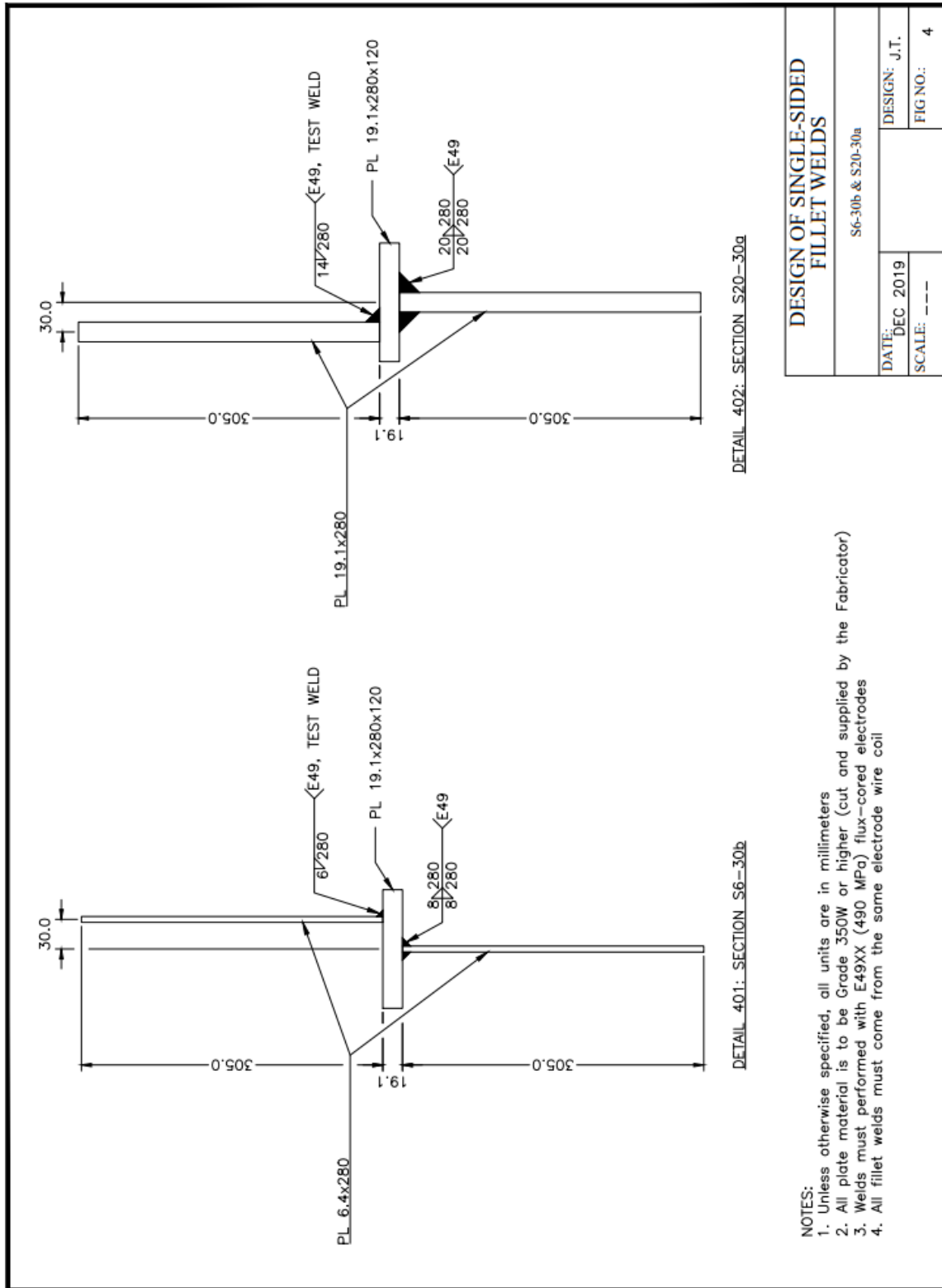


Fig. A.4. S6-30b & S20-30a sections

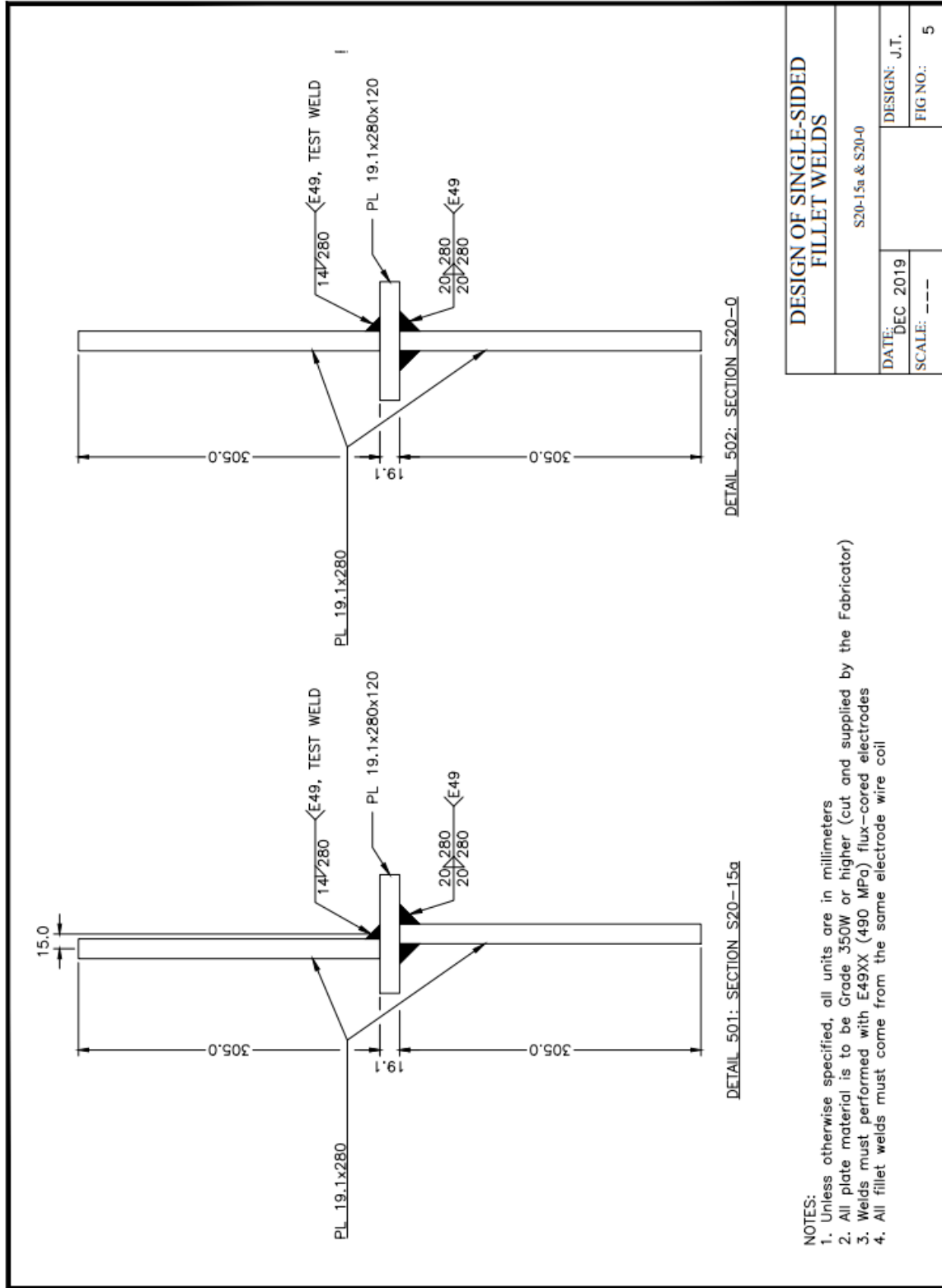


Fig. A.5. S20-15a & S20-0 sections

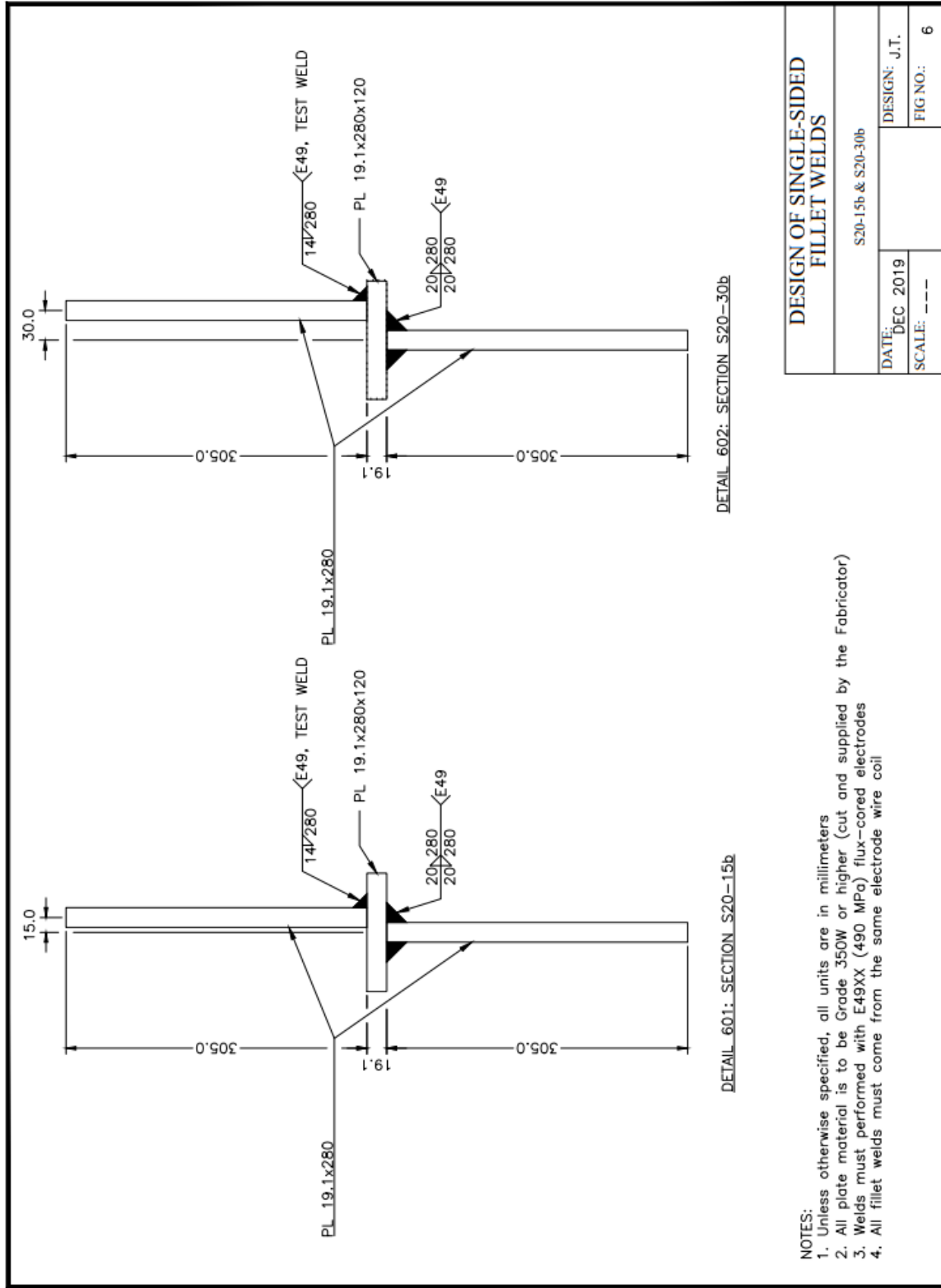


Fig. A.6. S20-15b & S20-30b sections

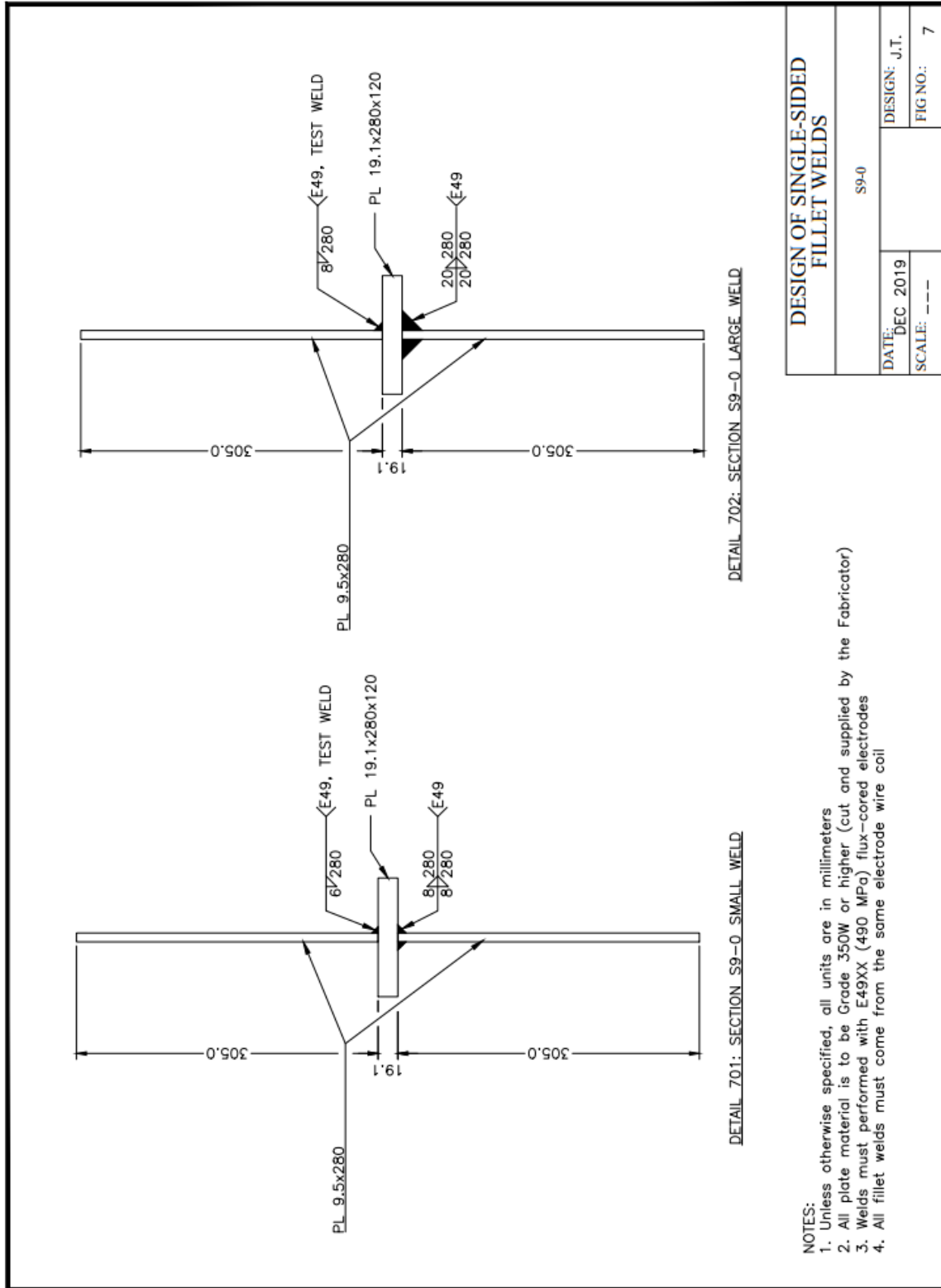


Fig. A.7. S9-0 section

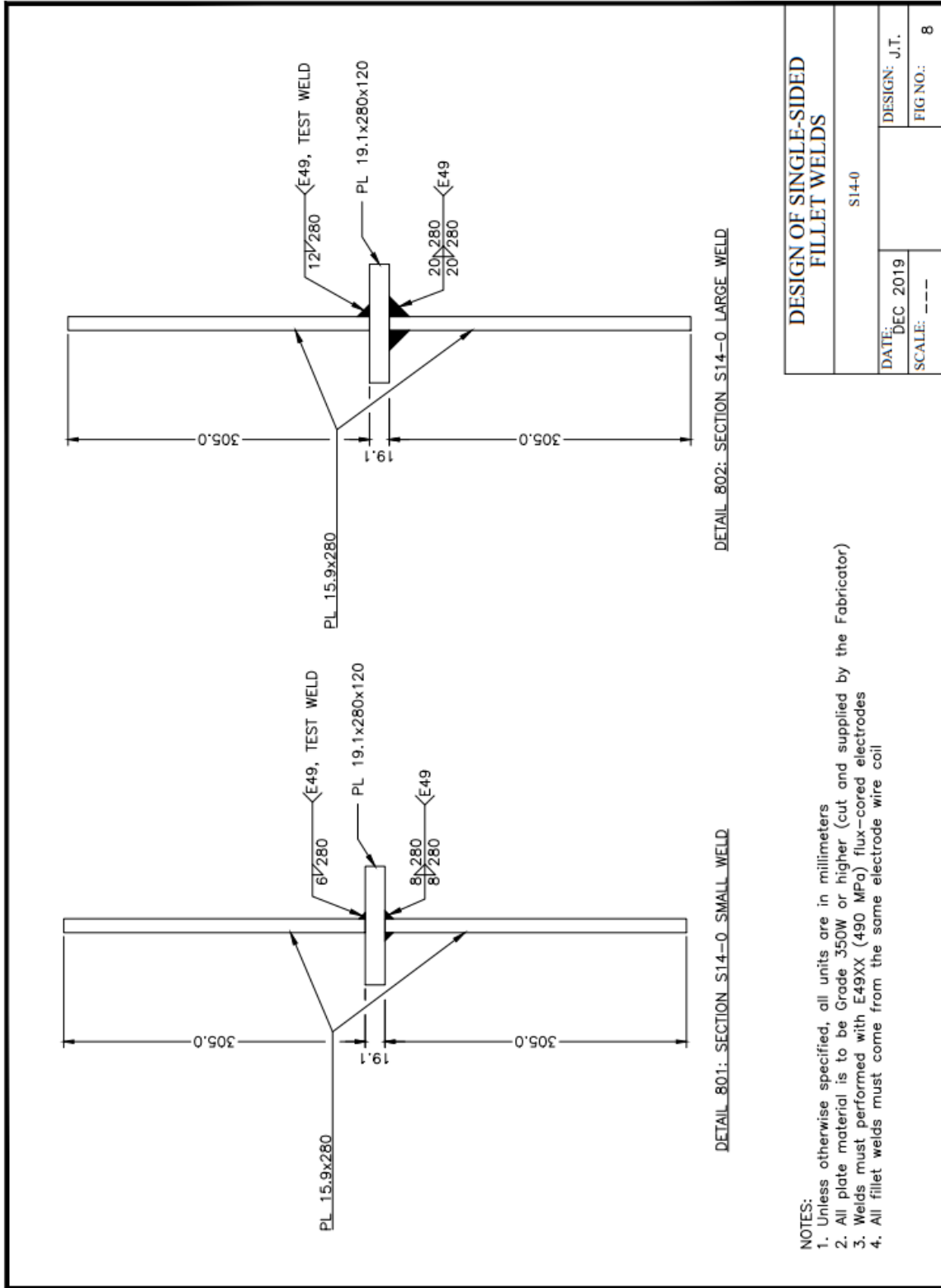


Fig. A.8. S14-0 section

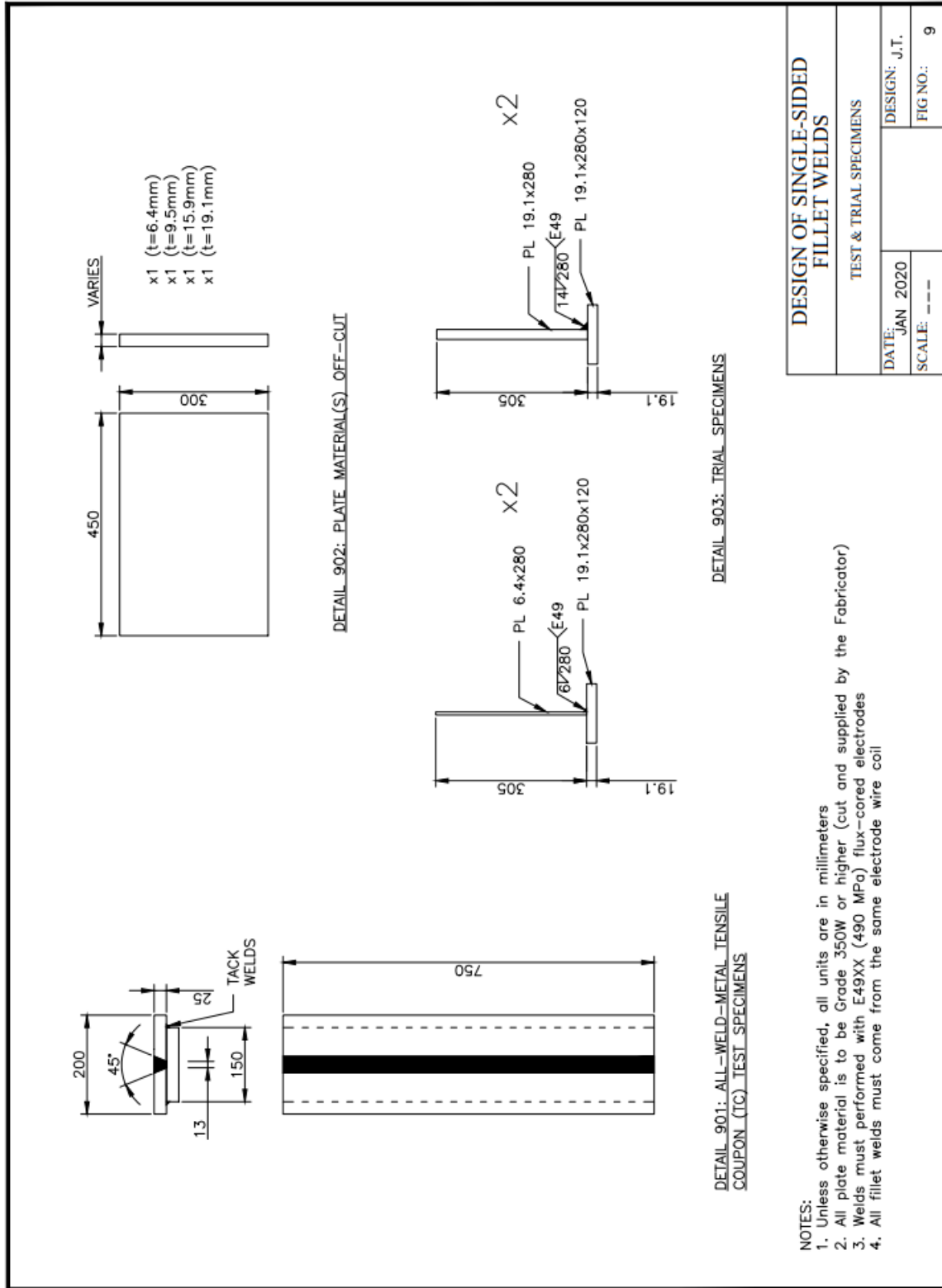


Fig. A.9. Test & trial specimens

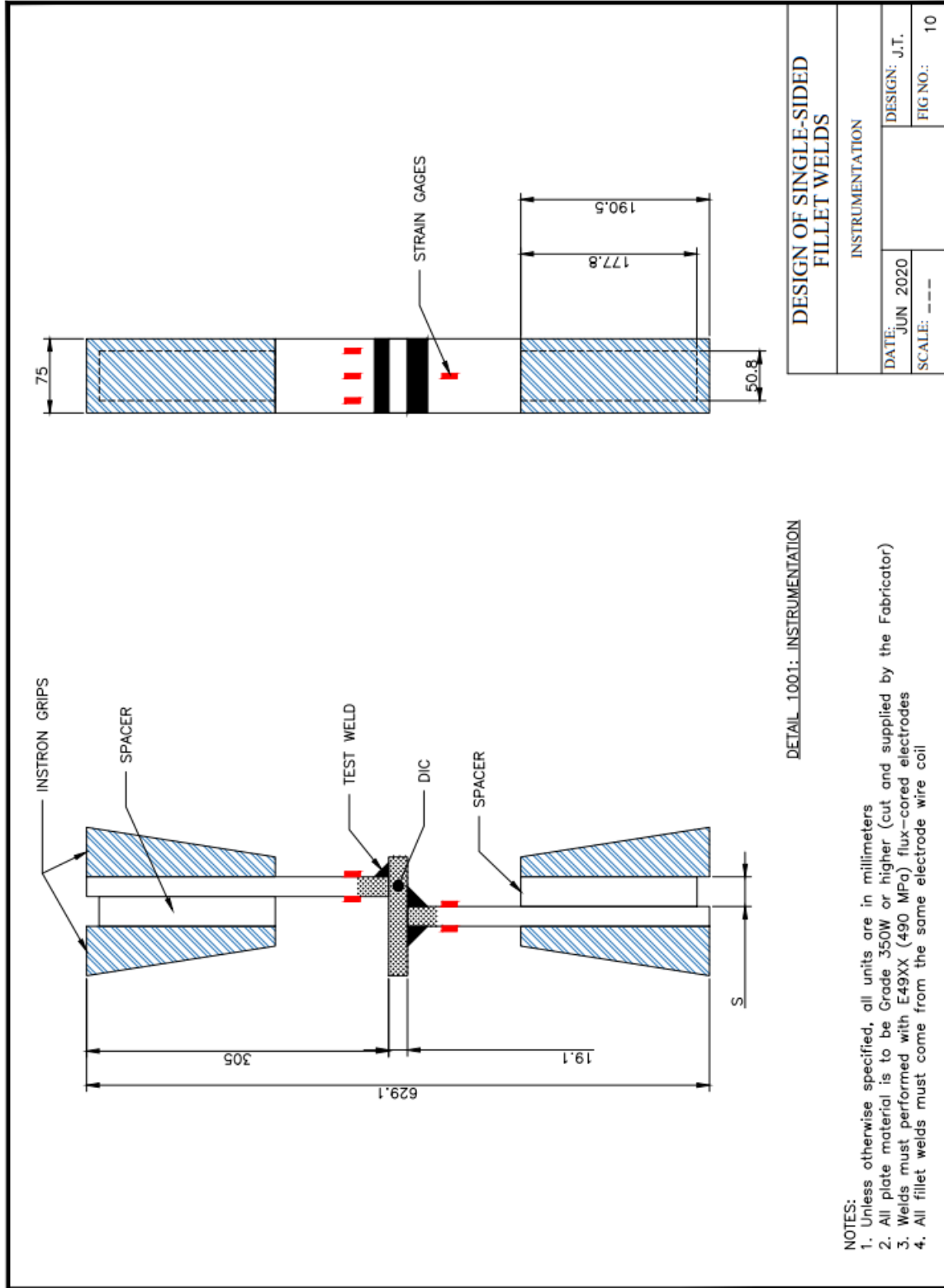


Fig. A.10. Instrumentation

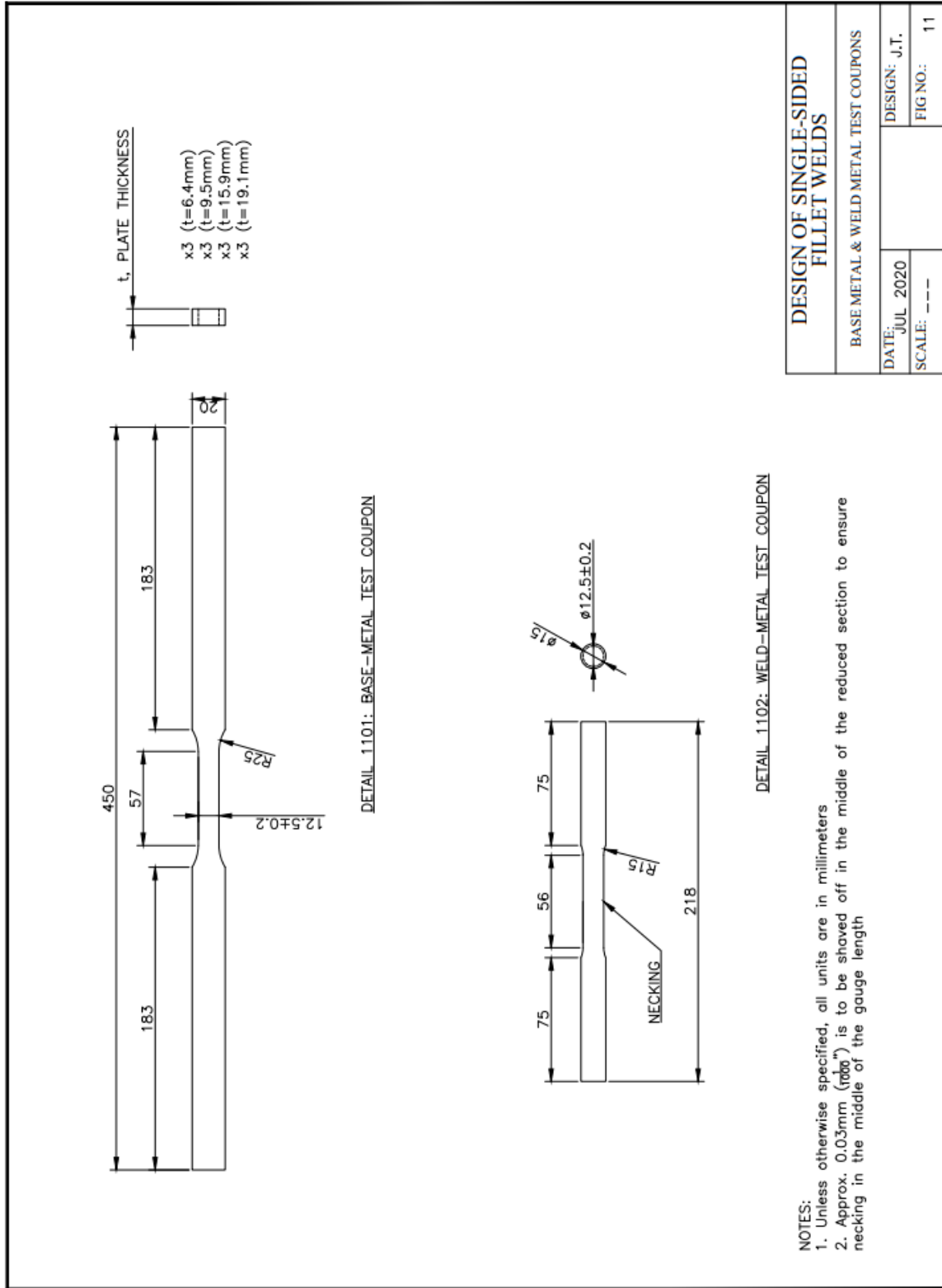


Fig. A.11. Base metal & weld metal test coupons

Appendix B: WELD PRE-RUPTURE AND POST-RUPTURE MEASUREMENTS

Appendix B provides the pre-rupture and post-rupture measurements of the weld leg and weld throats for the ETLCC specimens.

B.1. PRE-RUPTURE MEASUREMENTS

All weld throat and leg measurements using the weld gage before the single-sided welds of the ETLCC specimens were ruptured.

Table B.1. Pre-rupture measurements for ETLCC specimens

| Specimen designation | Shear leg, l_v (mm) | Tension leg, l_h (mm) | Weld throat (measured), t_{wm} (mm) | Weld throat (calculated), t_w (mm) |
|----------------------|-----------------------|-------------------------|---------------------------------------|--------------------------------------|
| S6-S-30a | 2.9 | 2.8 | 2.1 | 2.0 |
| | 3.0 | 2.9 | 2.1 | 2.1 |
| | 2.9 | 3.0 | 2.2 | 2.1 |
| | 2.9 | 2.9 | 2.2 | 2.1 |
| | 3.1 | 3.2 | 2.4 | 2.2 |
| Avg. | 2.96 | 2.96 | 2.20 | 2.09 |
| S6-S-15a | 3.2 | 3.2 | 2.1 | 2.3 |
| | 3.2 | 3.2 | 2.1 | 2.3 |
| | 3.2 | 3.2 | 2 | 2.3 |
| | 3.1 | 3.1 | 2 | 2.2 |
| | 3 | 3 | 2 | 2.1 |
| Avg. | 3.14 | 3.14 | 2.04 | 2.22 |
| S6-S-0 | 2.8 | 3.2 | 2.2 | 2.1 |
| | 2.9 | 3.3 | - | 2.2 |
| | 3.3 | 3.3 | - | 2.3 |
| | 3.3 | 3.2 | - | 2.3 |
| | 3.2 | 3.2 | 2.6 | 2.3 |
| Avg. | 3.10 | 3.24 | 2.40 | 2.24 |
| S6-S-15b | 3.3 | 3.3 | 2 | 2.3 |
| | 3.3 | 3.3 | 2.1 | 2.3 |
| | 3.3 | 3.2 | 2.1 | 2.3 |
| | 3.2 | 3.1 | 2 | 2.2 |
| | 3.2 | 3.1 | 2 | 2.2 |
| Avg. | 3.26 | 3.20 | 2.04 | 2.28 |

Table B.1. (cont.) Pre-rupture measurements for ETLCC specimens

| Specimen designation | Shear leg, l_v (mm) | Tension leg, l_h (mm) | Weld throat (measured), t_w (mm) | Weld throat (calculated), t_w (mm) |
|----------------------|-----------------------|-------------------------|------------------------------------|--------------------------------------|
| S6-S-30b | 3 | 2.8 | 2 | 2.0 |
| | 3.2 | 3 | 2.1 | 2.2 |
| | 3.2 | 3 | 2.1 | 2.2 |
| | 3.1 | 2.9 | 2.1 | 2.1 |
| | 3.2 | 2.9 | 2.2 | 2.1 |
| Avg. | 3.14 | 2.92 | 2.10 | 2.14 |
| S6-M-30a | 3.8 | 3.9 | 2.9 | 2.7 |
| | 4.1 | 4.1 | 3 | 2.9 |
| | 4.1 | 4 | 3 | 2.9 |
| | 3.9 | 4.1 | 3 | 2.8 |
| | 3.8 | 4.2 | 3 | 2.8 |
| Avg. | 3.94 | 4.06 | 2.98 | 2.83 |
| S6-M-15a | 4 | 4.1 | 2.4 | 2.9 |
| | 4.2 | 4 | 2.5 | 2.9 |
| | 4.3 | 4.1 | 2.5 | 3.0 |
| | 4.3 | 4.2 | 2.6 | 3.0 |
| | 4.1 | 4.2 | 2.6 | 2.9 |
| Avg. | 4.18 | 4.12 | 2.52 | 2.93 |
| S6-M-0 | 3.7 | 3.8 | 2.5 | 2.7 |
| | 3.8 | 3.8 | - | 2.7 |
| | 3.6 | 3.8 | - | 2.6 |
| | 3.8 | 3.8 | - | 2.7 |
| | 3.7 | 3.8 | 2.7 | 2.7 |
| Avg. | 3.72 | 3.80 | 2.60 | 2.66 |
| S6-M-15b | 3.8 | 3.8 | 2.7 | 2.7 |
| | 4.2 | 4.1 | 2.8 | 2.9 |
| | 4.2 | 4.1 | 2.9 | 2.9 |
| | 3.9 | 4 | 2.8 | 2.8 |
| | 4 | 4.1 | 2.7 | 2.9 |
| Avg. | 4.02 | 4.02 | 2.78 | 2.84 |
| S6-M-30b | 3.7 | 3.6 | 2.5 | 2.6 |
| | 3.5 | 3.6 | 2.3 | 2.5 |
| | 3.9 | 3.7 | 2.7 | 2.7 |
| | 4 | 3.7 | 2.6 | 2.7 |
| | 4 | 3.6 | 2.7 | 2.7 |
| Avg. | 3.82 | 3.64 | 2.56 | 2.63 |
| S6-L-30a | 4.8 | 4.9 | 3.3 | 3.4 |
| | 4.8 | 4.8 | 3.3 | 3.4 |
| | 5.1 | 4.8 | 3.4 | 3.5 |
| | 4.8 | 4.8 | 3.4 | 3.4 |
| | 4.6 | 4.7 | 3.2 | 3.3 |
| Avg. | 4.82 | 4.80 | 3.32 | 3.40 |

Table B.1. (cont.) Pre-rupture measurements for ETLCC specimens

| Specimen designation | Shear leg, l_v (mm) | Tension leg, l_h (mm) | Weld throat (measured), t_w (mm) | Weld throat (calculated), t_w (mm) |
|----------------------|-----------------------|-------------------------|------------------------------------|--------------------------------------|
| S6-L-15a | 5 | 4.9 | 3 | 3.5 |
| | 4.9 | 5 | 3.2 | 3.5 |
| | 5 | 5 | 3.2 | 3.5 |
| | 4.8 | 4.8 | 3.1 | 3.4 |
| | 4.8 | 4.9 | 3.1 | 3.4 |
| | Avg. | 4.90 | 4.92 | 3.12 |
| S6-L-0 | 4.8 | 4.7 | 3.2 | 3.4 |
| | 4.8 | 4.8 | - | 3.4 |
| | 4.9 | 4.8 | - | 3.4 |
| | 4.9 | 4.8 | - | 3.4 |
| | 4.7 | 5 | 3.4 | 3.4 |
| | Avg. | 4.82 | 4.82 | 3.30 |
| S6-L-15b | 5 | 4.7 | 3.1 | 3.4 |
| | 5 | 4.7 | 3.2 | 3.4 |
| | 5.1 | 4.8 | 3.3 | 3.5 |
| | 5.1 | 4.8 | 3.3 | 3.5 |
| | 5 | 4.8 | 3.1 | 3.5 |
| | Avg. | 5.04 | 4.76 | 3.20 |
| S6-L-30b | 4.5 | 4.5 | 2.9 | 3.2 |
| | 4.6 | 4.6 | 3.2 | 3.3 |
| | 4.8 | 4.7 | 3.3 | 3.4 |
| | 4.7 | 4.6 | 3.2 | 3.3 |
| | 4.5 | 4.6 | 3.2 | 3.2 |
| | Avg. | 4.62 | 4.60 | 3.16 |
| S9-XS-0 | 3.2 | 3.2 | 2.1 | 2.3 |
| | 3.2 | 3.1 | 2.3 | 2.2 |
| | 3.2 | 3.2 | 2.3 | 2.3 |
| | 3.3 | 3.2 | 2.2 | 2.3 |
| | 3.2 | 3.1 | 2.2 | 2.2 |
| | Avg. | 3.22 | 3.16 | 2.22 |
| S9-S-0 | 4.1 | 4 | 2.7 | 2.9 |
| | 4 | 4.1 | 2.7 | 2.9 |
| | 4.1 | 4.1 | 2.8 | 2.9 |
| | 4.2 | 4 | 2.8 | 2.9 |
| | 4.2 | 4 | 2.6 | 2.9 |
| | Avg. | 4.12 | 4.04 | 2.72 |
| S9-M-0 | 5.1 | 5 | 3.2 | 3.6 |
| | 5.2 | 4.9 | - | 3.6 |
| | 5.2 | 4.9 | - | 3.6 |
| | 5 | 5.1 | - | 3.6 |
| | 4.9 | 5.2 | 3.4 | 3.6 |
| | Avg. | 5.08 | 5.02 | 3.30 |

Table B.1. (cont.) Pre-rupture measurements for ETLCC specimens

| Specimen designation | Shear leg, l_v (mm) | Tension leg, l_h (mm) | Weld throat (measured), t_w (mm) | Weld throat (calculated), t_w (mm) |
|----------------------|-----------------------|-------------------------|------------------------------------|--------------------------------------|
| S9-L-0 | 5.7 | 5.5 | 4.2 | 4.0 |
| | 5.8 | 5.7 | - | 4.1 |
| | 5.7 | 6 | - | 4.1 |
| | 5.8 | 5.9 | - | 4.1 |
| | 5.6 | 6 | 4.3 | 4.1 |
| Avg. | 5.72 | 5.82 | 4.25 | 4.08 |
| S9-XL-0 | 6.9 | 7.1 | 4.9 | 4.9 |
| | 7 | 7.1 | - | 5.0 |
| | 7 | 7.1 | - | 5.0 |
| | 7 | 7.1 | - | 5.0 |
| | 7.1 | 7.2 | 5.1 | 5.1 |
| Avg. | 7.00 | 7.12 | 5.00 | 4.99 |
| S9-XXL-0 | 7.7 | 7.9 | 5.4 | 5.5 |
| | 7.7 | 8 | - | 5.5 |
| | 7.8 | 8 | - | 5.6 |
| | 7.9 | 7.9 | - | 5.6 |
| | 7.8 | 7.9 | 5.5 | 5.6 |
| Avg. | 7.78 | 7.94 | 5.45 | 5.56 |
| S14-XS-0 | 2.8 | 3.2 | 1.8 | 2.1 |
| | 3 | 3.2 | 1.9 | 2.2 |
| | 2.9 | 3.2 | 2 | 2.1 |
| | 2.9 | 3.1 | 1.8 | 2.1 |
| | 3.1 | 3.1 | 2 | 2.2 |
| Avg. | 2.94 | 3.16 | 1.90 | 2.15 |
| S14-S-0 | 4 | 3.5 | 2.6 | 2.6 |
| | 4.1 | 3.6 | 2.8 | 2.7 |
| | 4 | 3.7 | 2.8 | 2.7 |
| | 3.9 | 3.7 | 2.8 | 2.7 |
| | 4 | 3.9 | 3 | 2.8 |
| Avg. | 4.00 | 3.68 | 2.80 | 2.71 |
| S14-M-0 | 5.1 | 4.5 | 3.4 | 3.4 |
| | 5.1 | 4.7 | 3.5 | 3.5 |
| | 4.8 | 4.7 | 3.4 | 3.4 |
| | 4.9 | 4.6 | 3.4 | 3.4 |
| | 5 | 4.9 | 3.5 | 3.5 |
| Avg. | 4.98 | 4.68 | 3.44 | 3.41 |
| S14-L-0 | 7.7 | 7.9 | 5.1 | 5.5 |
| | 8.1 | 8.1 | 5.6 | 5.7 |
| | 8.1 | 8.1 | 5.6 | 5.7 |
| | 8.1 | 8 | 5.6 | 5.7 |
| | 7.8 | 7.9 | 5.5 | 5.6 |
| Avg. | 7.96 | 8.00 | 5.48 | 5.64 |

Table B.1. (cont.) Pre-rupture measurements for ETLCC specimens

| Specimen designation | Shear leg, l_v (mm) | Tension leg, l_h (mm) | Weld throat (measured), t_w (mm) | Weld throat (calculated), t_w (mm) |
|----------------------|-----------------------|-------------------------|------------------------------------|--------------------------------------|
| S14-XL-0 | 10.1 | 10 | 6.9 | 7.1 |
| | 10.2 | 9.8 | 7 | 7.1 |
| | 10.3 | 9.9 | 7 | 7.1 |
| | 10.5 | 9.9 | 7 | 7.2 |
| | 10.3 | 9.9 | 7 | 7.1 |
| Avg. | 10.28 | 9.90 | 6.98 | 7.13 |
| S14-XXL-0 | 11.2 | 11.6 | 8.4 | 8.1 |
| | 11.4 | 11.6 | 8.5 | 8.1 |
| | 11.4 | 11.8 | 8.6 | 8.2 |
| | 11.5 | 11.6 | 8.6 | 8.2 |
| | 11.2 | 11.5 | 8.5 | 8.0 |
| Avg. | 11.34 | 11.62 | 8.52 | 8.12 |
| S20-S-30a | 10.3 | 10.1 | 7 | 7.2 |
| | 10.3 | 10.5 | 7.1 | 7.4 |
| | 10.2 | 10.1 | 7.1 | 7.2 |
| | 10 | 10.2 | 7 | 7.1 |
| | 9.9 | 10.5 | 7 | 7.2 |
| Avg. | 10.14 | 10.28 | 7.04 | 7.22 |
| S20-S-15a | 10.1 | 9.7 | 7 | 7.0 |
| | 10 | 9.8 | 7.3 | 7.0 |
| | 10.1 | 9.9 | 7.2 | 7.1 |
| | 10 | 9.8 | 7.2 | 7.0 |
| | 10 | 9.9 | 7 | 7.0 |
| Avg. | 10.04 | 9.82 | 7.14 | 7.02 |
| S20-S-0 | 10.1 | 9.5 | 6.8 | 6.9 |
| | 9.8 | 9.6 | 7 | 6.9 |
| | 9.9 | 9.6 | 7 | 6.9 |
| | 10.1 | 9.8 | 7 | 7.0 |
| | 9.7 | 9.8 | 6.8 | 6.9 |
| Avg. | 9.92 | 9.66 | 6.92 | 6.92 |
| S20-S-15b | 10 | 10.2 | 6.9 | 7.1 |
| | 9.8 | 9.9 | 7.2 | 7.0 |
| | 10.1 | 9.8 | 7.1 | 7.0 |
| | 10 | 10.2 | 7.3 | 7.1 |
| | 9.9 | 10.2 | 7.2 | 7.1 |
| Avg. | 9.96 | 10.06 | 7.14 | 7.08 |
| S20-S-30b | 9.8 | 10 | 7 | 7.0 |
| | 9.7 | 10.2 | 7 | 7.0 |
| | 9.8 | 10.2 | 7 | 7.1 |
| | 9.8 | 10 | 7.1 | 7.0 |
| | 10 | 10 | 6.8 | 7.1 |
| Avg. | 9.82 | 10.08 | 6.98 | 7.03 |

Table B.1. (cont.) Pre-rupture measurements for ETLCC specimens

| Specimen designation | Shear leg, l_v (mm) | Tension leg, l_h (mm) | Weld throat (measured), t_w (mm) | Weld throat (calculated), t_w (mm) |
|----------------------|-----------------------|-------------------------|------------------------------------|--------------------------------------|
| S20-M-30a | 11.8 | 11.7 | 8.6 | 8.3 |
| | 11.3 | 11.8 | 8.5 | 8.2 |
| | 11.3 | 11.6 | 8.2 | 8.1 |
| | 11.5 | 11.3 | 8.2 | 8.1 |
| | 11.5 | 11.5 | 8.5 | 8.1 |
| Avg. | 11.48 | 11.58 | 8.40 | 8.15 |
| S20-M-15a | 11.6 | 11.8 | 8.2 | 8.3 |
| | 11.8 | 12.1 | 8.5 | 8.4 |
| | 11.9 | 11.9 | 8.5 | 8.4 |
| | 12.2 | 11.8 | 8.5 | 8.5 |
| | 12 | 11.9 | 8.5 | 8.4 |
| Avg. | 11.90 | 11.90 | 8.44 | 8.41 |
| S20-M-0 | 12.2 | 11.8 | 8.8 | 8.5 |
| | 11.8 | 12 | 8.8 | 8.4 |
| | 11.7 | 11.5 | 8.7 | 8.2 |
| | 12.1 | 11.5 | 8.5 | 8.3 |
| | 12.2 | 11.8 | 8.5 | 8.5 |
| Avg. | 12.00 | 11.72 | 8.66 | 8.38 |
| S20-M-15b | 12 | 12.1 | 8 | 8.5 |
| | 12.3 | 12.1 | 8.2 | 8.6 |
| | 12.1 | 11.9 | 8.2 | 8.5 |
| | 12 | 12 | 8.3 | 8.5 |
| | 12.1 | 11.9 | 8.1 | 8.5 |
| Avg. | 12.10 | 12.00 | 8.16 | 8.52 |
| S20-L-30a | 14.2 | 13.9 | 10 | 9.9 |
| | 14 | 13.8 | 10 | 9.8 |
| | 13.8 | 13.8 | 10.1 | 9.8 |
| | 13.7 | 13.8 | 10 | 9.7 |
| | 13.8 | 13.8 | 10 | 9.8 |
| Avg. | 13.90 | 13.82 | 10.02 | 9.80 |
| S20-L-15a | 13.8 | 13.5 | 9.9 | 9.7 |
| | 14 | 13.8 | 10 | 9.8 |
| | 13.9 | 13.8 | 10 | 9.8 |
| | 14 | 13.8 | 10 | 9.8 |
| | 14.1 | 13.8 | 9.8 | 9.9 |
| Avg. | 13.96 | 13.74 | 9.94 | 9.79 |
| S20-L-0 | 14 | 13.9 | 9.8 | 9.9 |
| | 14.1 | 14 | 9.9 | 9.9 |
| | 14.1 | 13.9 | 9.9 | 9.9 |
| | 13.8 | 14 | 9.9 | 9.8 |
| | 13.5 | 13.6 | 9.6 | 9.6 |
| Avg. | 13.90 | 13.88 | 9.82 | 9.82 |

Table B.1. (cont.) Pre-rupture measurements for ETLCC specimens

| Specimen designation | Shear leg, l_v (mm) | Tension leg, l_h (mm) | Weld throat (measured), t_w (mm) | Weld throat (calculated), t_w (mm) |
|----------------------|-----------------------|-------------------------|------------------------------------|--------------------------------------|
| S20-L-15b | 13.4 | 13.8 | 10 | 9.6 |
| | 13.8 | 13.9 | 9.9 | 9.8 |
| | 13.9 | 13.9 | 10 | 9.8 |
| | 13.9 | 13.8 | 9.8 | 9.8 |
| | 13.9 | 13.6 | 10 | 9.7 |
| Avg. | 13.78 | 13.80 | 9.94 | 9.75 |

B.2. POST-RUPTURE MEASUREMENTS

All weld throat and leg measurements from the macro-etch examinations after the single-sided welds of the ETLCC specimens were ruptured.

Table B.2. Post-rupture measurements of ETLCC specimens

| Specimen designation | Shear leg, l_v (mm) | Tension leg, l_h (mm) | Weld throat (measured), t_{wm} (mm) | Weld throat (calculated), t_w (mm) |
|----------------------|-----------------------|-------------------------|---------------------------------------|--------------------------------------|
| S6-S-30a | 4.0 | 3.5 | 3.0 | 2.6 |
| | 3.8 | 2.5 | 2.0 | 2.1 |
| | 4.8 | 3.4 | 2.5 | 2.8 |
| | 3.7 | 3.1 | 2.2 | 2.4 |
| | 4.2 | 4.0 | 3.2 | 2.9 |
| Avg. | 4.10 | 3.30 | 2.58 | 2.55 |
| S6-S-15a | 4.0 | 4.1 | 3.1 | 2.9 |
| | 3.9 | 4.2 | 3.3 | 2.9 |
| | 4.0 | 3.3 | 3 | 2.5 |
| | 3.9 | 5.0 | 3.4 | 3.1 |
| | - | - | - | - |
| Avg. | 3.95 | 4.15 | 3.20 | 2.84 |
| S6-S-0 | - | - | - | - |
| | 4.6 | 3.9 | 3.1 | 3.0 |
| | 4.3 | 4.0 | 3.3 | 2.9 |
| | 4.4 | 4.2 | 3.1 | 3.0 |
| | - | - | - | - |
| Avg. | 4.43 | 4.03 | 3.17 | 2.98 |
| S6-S-15b | 3.2 | 3.8 | 2.4 | 2.4 |
| | 4.0 | 3.4 | 2.6 | 2.6 |
| | 3.6 | 4.3 | 2.9 | 2.8 |
| | 3.0 | 4.1 | 2.6 | 2.4 |
| | 2.9 | 3.2 | 2.2 | 2.1 |
| Avg. | 3.34 | 3.76 | 2.54 | 2.47 |

Table B.2. (cont.) Post-rupture measurements of ETLCC specimens

| Specimen designation | Shear leg, l_v (mm) | Tension leg, l_h (mm) | Weld throat (measured), t_w (mm) | Weld throat (calculated), t_w (mm) |
|----------------------|-----------------------|-------------------------|------------------------------------|--------------------------------------|
| S6-S-30b | 3.1 | 3.4 | 2.5 | 2.3 |
| | 3.8 | 3.7 | 2.8 | 2.7 |
| | 3.3 | 3.2 | 2.4 | 2.3 |
| | 3.3 | 2.7 | 2.3 | 2.1 |
| | 2.4 | 2.6 | 2.1 | 1.8 |
| | Avg. | 3.18 | 3.12 | 2.42 |
| S6-M-30a | 4.9 | 4.8 | 3.8 | 3.4 |
| | 4.9 | 4.3 | 3.3 | 3.2 |
| | 3.9 | 2.9 | 2.2 | 2.3 |
| | 3.2 | 3.6 | 2.6 | 2.4 |
| | 4.2 | 3.3 | 2.4 | 2.6 |
| | Avg. | 4.22 | 3.78 | 2.86 |
| S6-M-15a | - | - | - | - |
| | - | - | - | - |
| | 5.7 | 4.5 | 3.5 | 3.5 |
| | 5.8 | 4.3 | 3.5 | 3.5 |
| | 5.4 | 3.7 | 3.3 | 3.1 |
| | Avg. | 5.63 | 4.17 | 3.43 |
| S6-M-0 | 7.1 | 4.3 | 4 | 3.7 |
| | 5.3 | 3.2 | 3 | 2.7 |
| | 5.3 | 3.9 | 3.3 | 3.1 |
| | 5.1 | 4.1 | 3.9 | 3.2 |
| | 4.9 | 3.7 | 3.4 | 3.0 |
| | Avg. | 5.54 | 3.84 | 3.52 |
| S6-M-15b | 4.6 | 4.7 | 3.3 | 3.3 |
| | 4.7 | 4.2 | 3.4 | 3.1 |
| | 4.9 | 4.2 | 3.6 | 3.2 |
| | 4.9 | 4.0 | 3.2 | 3.1 |
| | 3.7 | 4.4 | 3.2 | 2.8 |
| | Avg. | 4.56 | 4.30 | 3.34 |
| S6-M-30b | 5.2 | 4.0 | 3.2 | 3.2 |
| | 2.5 | 3.5 | 2.3 | 2.0 |
| | 2.4 | 3.0 | 1.9 | 1.9 |
| | 2.8 | 3.2 | 2.4 | 2.1 |
| | 3.6 | 3.6 | 2.5 | 2.5 |
| | Avg. | 3.30 | 3.46 | 2.46 |
| S6-L-30a | 6.1 | 5.4 | 3.5 | 4.0 |
| | 6.1 | 4.8 | 3.1 | 3.8 |
| | 6.3 | 4.7 | 3.3 | 3.8 |
| | 5.4 | 3.2 | 2.4 | 2.8 |
| | 4.4 | 2.9 | 1.9 | 2.4 |
| | Avg. | 5.66 | 4.20 | 2.84 |

Table B.2. (cont.) Post-rupture measurements of ETLCC specimens

| Specimen designation | Shear leg, l_v (mm) | Tension leg, l_h (mm) | Weld throat (measured), t_w (mm) | Weld throat (calculated), t_w (mm) |
|----------------------|-----------------------|-------------------------|------------------------------------|--------------------------------------|
| S6-L-15a | 5.1 | 5.2 | 4.2 | 3.6 |
| | 6.4 | 4.6 | 4 | 3.7 |
| | 6.5 | 4.4 | 3.8 | 3.6 |
| | 6.8 | 4.7 | 3.8 | 3.9 |
| | 5.7 | 3.8 | 3.5 | 3.2 |
| Avg. | 6.10 | 4.54 | 3.86 | 3.61 |
| S6-L-0 | 6.5 | 4.4 | 3.8 | 3.6 |
| | 5.7 | 4.6 | 4.1 | 3.6 |
| | 5.6 | 5.3 | 4.4 | 3.8 |
| | 6.1 | 4.8 | 4.2 | 3.8 |
| | 6.6 | 4.3 | 3.7 | 3.6 |
| Avg. | 6.10 | 4.68 | 4.04 | 3.69 |
| S6-L-15b | 3.3 | 2.6 | 2 | 2.0 |
| | 4.8 | 5.3 | 3.9 | 3.6 |
| | 4.7 | 5.7 | 4 | 3.6 |
| | 4.9 | 5.7 | 4 | 3.7 |
| | 3.9 | 4.3 | 3.2 | 2.9 |
| Avg. | 4.32 | 4.72 | 3.42 | 3.17 |
| S6-L-30b | 4.2 | 5.3 | 3.3 | 3.3 |
| | 3.8 | 4.0 | 2.9 | 2.8 |
| | 4.9 | 4.8 | 3.6 | 3.4 |
| | 3.7 | 4.5 | 3.4 | 2.9 |
| | 4.1 | 4.7 | 3 | 3.1 |
| Avg. | 4.14 | 4.66 | 3.24 | 3.08 |
| S9-XS-0 | 3.6 | 2.5 | 2.1 | 2.1 |
| | 4.5 | 2.7 | 2.3 | 2.3 |
| | 3.6 | 3.5 | 2.9 | 2.5 |
| | 3.8 | 3.1 | 2.7 | 2.4 |
| | 3.4 | 2.2 | 1.9 | 1.8 |
| Avg. | 3.78 | 2.80 | 2.38 | 2.23 |
| S9-S-0 | 4.9 | 3.3 | 2.6 | 2.7 |
| | 5.3 | 3.8 | 3.1 | 3.1 |
| | 4.6 | 3.2 | 2.8 | 2.6 |
| | 5.3 | 3.2 | 2.9 | 2.7 |
| | 4.8 | 2.8 | 2.4 | 2.4 |
| Avg. | 4.98 | 3.26 | 2.76 | 2.72 |
| S9-M-0 | 5.2 | 5.4 | 4 | 3.7 |
| | 5.8 | 5.6 | 4.3 | 4.0 |
| | 5.6 | 4.5 | 3.6 | 3.5 |
| | 5.1 | 3.5 | 3 | 2.9 |
| | 6.3 | 3.9 | 3.6 | 3.3 |
| Avg. | 5.60 | 4.58 | 3.70 | 3.50 |

Table B.2. (cont.) Post-rupture measurements of ETLCC specimens

| Specimen designation | Shear leg, l_v (mm) | Tension leg, l_h (mm) | Weld throat (measured), t_w (mm) | Weld throat (calculated), t_w (mm) |
|----------------------|-----------------------|-------------------------|------------------------------------|--------------------------------------|
| S9-L-0 | 5.7 | 7.4 | 4.8 | 4.5 |
| | 5.2 | 6.0 | 4.6 | 3.9 |
| | 5.8 | 6.1 | 4.6 | 4.2 |
| | 6.2 | 6.0 | 5.1 | 4.3 |
| | 6.2 | 6.0 | 5 | 4.3 |
| Avg. | 5.82 | 6.30 | 4.82 | 4.25 |
| S9-XL-0 | 8.6 | 7.1 | 6.2 | 5.5 |
| | 8.8 | 6.7 | 5.6 | 5.3 |
| | 8.3 | 6.7 | 5.5 | 5.2 |
| | 6.8 | 6.7 | 5.6 | 4.8 |
| | 8.3 | 6.7 | 5.5 | 5.2 |
| Avg. | 8.16 | 6.78 | 5.68 | 5.20 |
| S9-XXL-0 | 10.0 | 8.1 | 6.7 | 6.3 |
| | 9.2 | 7.1 | 6 | 5.6 |
| | 8.0 | 8.0 | 5.9 | 5.7 |
| | 7.2 | 7.8 | 6.3 | 5.3 |
| | 7.4 | 6.2 | 5.1 | 4.8 |
| Avg. | 8.36 | 7.44 | 6.00 | 5.52 |
| S14-XS-0 | 3.7 | 3.1 | 2.5 | 2.4 |
| | 2.6 | 1.9 | 1.6 | 1.5 |
| | 2.7 | 3.0 | 2 | 2.0 |
| | 2.6 | 2.6 | 1.8 | 1.8 |
| | 2.2 | 1.7 | 1.3 | 1.3 |
| Avg. | 2.76 | 2.46 | 1.84 | 1.82 |
| S14-S-0 | 5.9 | 4.1 | 3.4 | 3.4 |
| | 4.2 | 3.3 | 2.6 | 2.6 |
| | 4.7 | 2.9 | 2.5 | 2.5 |
| | 5.1 | 3.3 | 2.8 | 2.8 |
| | 4.6 | 2.5 | 2.3 | 2.2 |
| Avg. | 4.90 | 3.22 | 2.72 | 2.68 |
| S14-M-0 | 6.9 | 5.4 | 4.4 | 4.3 |
| | 6.0 | 4.5 | 3.7 | 3.6 |
| | 6.4 | 4.6 | 3.8 | 3.7 |
| | 5.9 | 4.2 | 3.5 | 3.4 |
| | 5.5 | 3.9 | 3.3 | 3.2 |
| Avg. | 6.14 | 4.52 | 3.74 | 3.64 |
| S14-L-0 | 8.4 | 7.6 | 5.9 | 5.6 |
| | 7.0 | 7.5 | 5.3 | 5.1 |
| | 7.6 | 7.8 | 5.3 | 5.4 |
| | 7.9 | 7.5 | 5.5 | 5.4 |
| | 5.3 | 5.9 | 4 | 3.9 |
| Avg. | 7.24 | 7.26 | 5.20 | 5.12 |

Table B.2. (cont.) Post-rupture measurements of ETLCC specimens

| Specimen designation | Shear leg, l_v (mm) | Tension leg, l_h (mm) | Weld throat (measured), t_w (mm) | Weld throat (calculated), t_w (mm) |
|----------------------|-----------------------|-------------------------|------------------------------------|--------------------------------------|
| S14-XL-0 | 11.0 | 8.9 | 6.8 | 6.9 |
| | 10.2 | 9.0 | 6.8 | 6.7 |
| | 10.8 | 8.9 | 7 | 6.9 |
| | 10.2 | 8.8 | 6.8 | 6.7 |
| | 8.7 | 8.5 | 6.1 | 6.1 |
| Avg. | 10.18 | 8.82 | 6.70 | 6.66 |
| S14-XXL-0 | 13.1 | 11.2 | 8.5 | 8.5 |
| | 12.9 | 11.3 | 8.6 | 8.5 |
| | 12.5 | 11.1 | 8.5 | 8.3 |
| | 10.8 | 11.3 | 8.6 | 7.8 |
| | 11.5 | 10.5 | 7.9 | 7.8 |
| Avg. | 12.16 | 11.08 | 8.42 | 8.17 |
| S20-S-30a | 13.6 | 8.6 | 7.5 | 7.3 |
| | 12.6 | 10.6 | 8.2 | 8.1 |
| | 12.4 | 9.7 | 8.2 | 7.6 |
| | 12.1 | 9.8 | 8.1 | 7.6 |
| | 12.0 | 6.7 | 5.9 | 5.8 |
| Avg. | 12.54 | 9.08 | 7.58 | 7.30 |
| S20-S-15a | 11.6 | 8.3 | 7.2 | 6.8 |
| | 11.9 | 9.4 | 7.9 | 7.4 |
| | 12.3 | 10.6 | 8.4 | 8.0 |
| | 11.9 | 11.3 | 8.7 | 8.2 |
| | 10.3 | 6.8 | 5.7 | 5.7 |
| Avg. | 11.60 | 9.28 | 7.58 | 7.21 |
| S20-S-0 | 12.1 | 7.7 | 6.4 | 6.5 |
| | 9.4 | 7.8 | 6.8 | 6.0 |
| | 9.6 | 10.2 | 7.7 | 7.0 |
| | 8.5 | 9.8 | 7.4 | 6.4 |
| | 9.2 | 8.3 | 6 | 6.2 |
| Avg. | 9.76 | 8.76 | 6.86 | 6.41 |
| S20-S-15b | 10.2 | 11.8 | 7.8 | 7.7 |
| | 9.6 | 11.4 | 7.4 | 7.3 |
| | 9.7 | 11.5 | 7.7 | 7.4 |
| | 9.9 | 10.8 | 7.3 | 7.3 |
| | 9.2 | 10.0 | 6.8 | 6.8 |
| Avg. | 9.72 | 11.10 | 7.40 | 7.31 |
| S20-S-30b | 11.2 | 12.5 | 8.4 | 8.3 |
| | 10.1 | 12.9 | 8.1 | 8.0 |
| | 10.7 | 11.9 | 8.6 | 8.0 |
| | 10.1 | 11.1 | 7.7 | 7.5 |
| | 11.7 | 12.0 | 8.3 | 8.4 |
| Avg. | 10.76 | 12.08 | 8.22 | 8.02 |

Table B.2. (cont.) Post-rupture measurements of ETLCC specimens

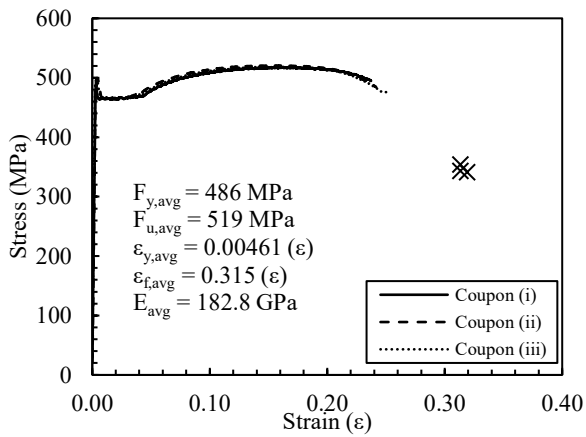
| Specimen designation | Shear leg, l_v (mm) | Tension leg, l_h (mm) | Weld throat (measured), t_w (mm) | Weld throat (calculated), t_w (mm) |
|----------------------|-----------------------|-------------------------|------------------------------------|--------------------------------------|
| S20-M-30a | 13.1 | 10.2 | 9 | 8.0 |
| | 13.7 | 10.9 | 9.3 | 8.5 |
| | 12.6 | 11.7 | 9.1 | 8.6 |
| | 12.9 | 11.4 | 8.9 | 8.5 |
| | 12.8 | 9.9 | 8.7 | 7.8 |
| Avg. | 13.02 | 10.82 | 9.00 | 8.30 |
| S20-M-15a | 12.6 | 10.7 | 8.9 | 8.2 |
| | 12.7 | 11.9 | 9.6 | 8.7 |
| | 13.2 | 12.1 | 9.6 | 8.9 |
| | 13.2 | 11.6 | 9.4 | 8.7 |
| | 11.0 | 11.2 | 8.6 | 7.8 |
| Avg. | 12.54 | 11.50 | 9.22 | 8.46 |
| S20-M-0 | 13.7 | 11.3 | 9.8 | 8.7 |
| | 12.4 | 11.6 | 9.7 | 8.5 |
| | 13.8 | 12.2 | 9.8 | 9.1 |
| | 12.5 | 12.5 | 9.7 | 8.8 |
| | 13.4 | 11.9 | 9.7 | 8.9 |
| Avg. | 13.16 | 11.90 | 9.74 | 8.81 |
| S20-M-15b | 12.6 | 12.0 | 9.4 | 8.7 |
| | 10.3 | 12.0 | 9.3 | 7.8 |
| | 11.2 | 12.2 | 8.9 | 8.3 |
| | 11.0 | 12.4 | 9.1 | 8.2 |
| | 10.7 | 12.0 | 8.8 | 8.0 |
| Avg. | 11.16 | 12.12 | 9.10 | 8.19 |
| S20-L-30a | 12.9 | 11.1 | 9.8 | 8.4 |
| | 12.8 | 11.3 | 9 | 8.5 |
| | 13.1 | 11.8 | 9.3 | 8.8 |
| | 12.8 | 10.7 | 8.5 | 8.2 |
| | 13.1 | 10.3 | 9 | 8.1 |
| Avg. | 12.94 | 11.04 | 9.12 | 8.39 |
| S20-L-15a | 17.3 | 12.5 | 10.6 | 10.1 |
| | 14.8 | 13.2 | 11 | 9.9 |
| | 15.2 | 12.0 | 9.5 | 9.4 |
| | 15.7 | 14.2 | 11.5 | 10.5 |
| | 13.8 | 14.5 | 11.8 | 10.0 |
| Avg. | 15.36 | 13.28 | 10.88 | 9.99 |
| S20-L-0 | 17.1 | 12.1 | 9.6 | 9.9 |
| | 13.9 | 14.5 | 11.2 | 10.0 |
| | 13.8 | 15.0 | 11.1 | 10.2 |
| | 14.4 | 13.9 | 10.6 | 10.0 |
| | 14.1 | 9.8 | 7.5 | 8.0 |
| Avg. | 14.66 | 13.06 | 10.00 | 9.62 |

Table B.2. (cont.) Post-rupture measurements of ETLCC specimens

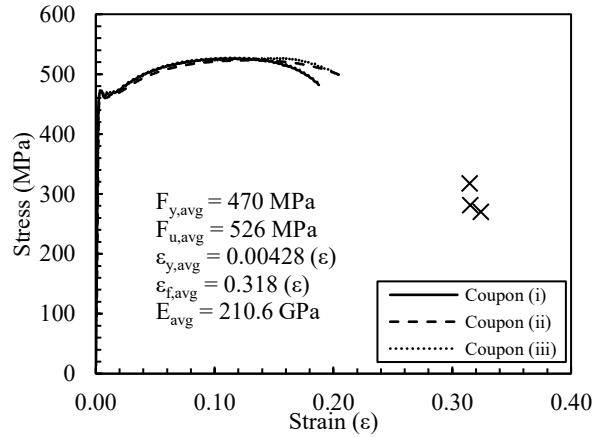
| Specimen designation | Shear leg, l_v (mm) | Tension leg, l_h (mm) | Weld throat (measured), t_w (mm) | Weld throat (calculated), t_w (mm) |
|----------------------|-----------------------|-------------------------|------------------------------------|--------------------------------------|
| S20-L-15b | 14.8 | 10.4 | 12.9 | 9.7 |
| | 13.5 | 10.4 | 13.3 | 9.5 |
| | 14.5 | 10.8 | 13.6 | 9.9 |
| | 14.5 | 10.2 | 12.9 | 9.6 |
| | 14.2 | 10.8 | 13.9 | 9.9 |
| Avg. | 14.30 | 10.52 | 13.32 | 9.74 |

Appendix C: MATERIAL PROPERTY TEST RESULTS

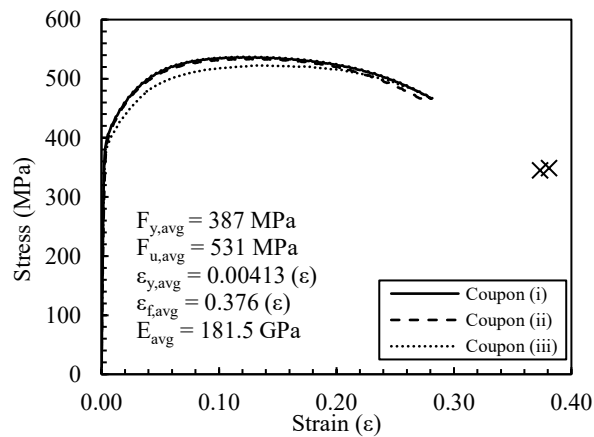
Appendix C provides the tensile coupon test results which determine the material properties of the weld and base metal used in the ETLCC test specimens.



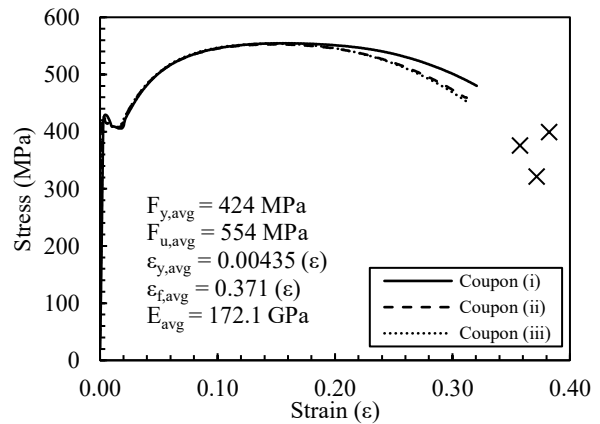
(a) Results for base metal coupons ($t = 6.4 \text{ mm}$)



(b) Results for base metal coupons ($t = 9.5 \text{ mm}$)



(c) Results for base metal coupons ($t = 15.9 \text{ mm}$)



(d) Results for base metal coupons ($t = 19.1 \text{ mm}$)

Fig. C.1. Base metal rectangular tensile coupon results

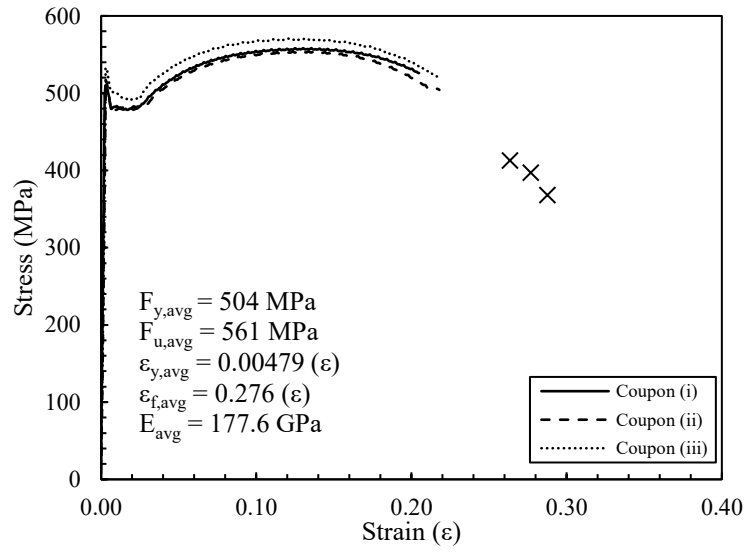


Fig. C.2. Weld metal round tensile coupon results

Appendix D: ETLCC EXPERIMENTAL TEST RESULTS

Appendix D provides the ETLCC experimental test results for Section 4.6. which include the actual and predicted strengths for all 40 ETLCC tests for CSA S16:19, AISC 360-16 and EN1993-1-8:2005.

Table D.1. ETLCC experimental test results with comparison to CSA S16:19, AISC 360-16 and EN1993-1-8:2005

| S | t_w/t_v | P_a kN | P_{pr} | | | | | | | | | | | |
|------------|------------|-------------|-------------------|-------|----------------------|-------|-------------------|-------|----------------------|-------|-----------------|-------|------------|-------|
| | | | CSA S16:19 | | | | AISC 360-16 | | | | EN1993-1-8:2005 | | | |
| | | | with $\sin\theta$ | | without $\sin\theta$ | | with $\sin\theta$ | | without $\sin\theta$ | | Directional | | Simplified | |
| kN | (A/P) | kN | (A/P) | kN | (A/P) | kN | (A/P) | kN | (A/P) | kN | (A/P) | | | |
| <u>30a</u> | 0.40 | 72.0 | 117.0 | 0.62 | 78.0 | 0.92 | 104.7 | 0.69 | 69.8 | 1.03 | 89.6 | 0.80 | 69.1 | 1.04 |
| | 0.45 | 109.9 | 115.1 | 0.95 | 76.8 | 1.43 | 103.1 | 1.07 | 68.7 | 1.60 | 85.7 | 1.28 | 68.0 | 1.62 |
| | 0.44 | 155.8 | 117.8 | 1.32 | 78.6 | 1.98 | 105.5 | 1.48 | 70.4 | 2.21 | 92.6 | 1.68 | 69.6 | 2.24 |
| | 0.40 | 349.6 | 331.2 | 1.06 | 220.8 | 1.58 | 296.6 | 1.18 | 197.7 | 1.77 | 278.8 | 1.25 | 208.8 | 1.67 |
| | 0.47 | 374.9 | 383.1 | 0.98 | 255.4 | 1.47 | 343.1 | 1.09 | 228.7 | 1.64 | 310.4 | 1.21 | 241.5 | 1.55 |
| | 0.48 | 435.7 | 327.9 | 1.33 | 218.6 | 1.99 | 293.6 | 1.48 | 195.8 | 2.23 | 263.8 | 1.65 | 206.7 | 2.11 |
| | δ_p | = | | 1.043 | | 1.564 | | 1.164 | | 1.746 | | 1.314 | | 1.706 |
| V_p | = | | 0.255 | | 0.255 | | 0.255 | | 0.255 | | 0.247 | | 0.251 | |
| <u>15a</u> | 0.48 | 175.2 | 128.5 | 1.36 | 85.6 | 2.05 | 115.0 | 1.52 | 76.7 | 2.28 | 96.6 | 1.81 | 79.6 | 2.20 |
| | 0.54 | 138.4 | 147.1 | 0.94 | 98.1 | 1.41 | 131.7 | 1.05 | 87.8 | 1.58 | 115.2 | 1.20 | 86.9 | 1.59 |
| | 0.60 | 168.0 | 160.0 | 1.05 | 106.6 | 1.58 | 143.2 | 1.17 | 95.5 | 1.76 | 124.9 | 1.34 | 94.5 | 1.78 |
| | 0.40 | 267.1 | 318.4 | 0.84 | 212.3 | 1.26 | 285.1 | 0.94 | 190.1 | 1.41 | 261.4 | 1.02 | 200.7 | 1.33 |
| | 0.48 | 295.6 | 397.7 | 0.74 | 265.1 | 1.11 | 356.1 | 0.83 | 237.4 | 1.25 | 313.7 | 0.94 | 250.7 | 1.18 |
| | 0.57 | 337.4 | 394.4 | 0.86 | 263.0 | 1.28 | 353.2 | 0.96 | 235.5 | 1.43 | 316.0 | 1.07 | 248.6 | 1.36 |
| | δ_p | = | | 0.965 | | 1.448 | | 1.078 | | 1.617 | | 1.232 | | 1.573 |
| V_p | = | | 0.229 | | 0.229 | | 0.229 | | 0.229 | | 0.259 | | 0.237 | |
| <u>0</u> | 0.49 | 110.5 | 133.9 | 0.82 | 89.3 | 1.24 | 119.9 | 0.92 | 79.9 | 1.38 | 99.2 | 1.11 | 79.1 | 1.40 |
| | 0.55 | 121.2 | 151.2 | 0.80 | 100.8 | 1.20 | 135.4 | 0.90 | 90.3 | 1.34 | 120.2 | 1.01 | 89.3 | 1.36 |
| | 0.63 | 122.3 | 168.1 | 0.73 | 112.1 | 1.09 | 150.5 | 0.81 | 100.4 | 1.22 | 130.2 | 0.94 | 99.3 | 1.23 |
| | 0.36 | 222.2 | 299.7 | 0.74 | 199.8 | 1.11 | 268.4 | 0.83 | 179.0 | 1.24 | 237.7 | 0.93 | 188.9 | 1.18 |
| | 0.51 | 258.7 | 409.1 | 0.63 | 272.7 | 0.95 | 366.4 | 0.71 | 244.2 | 1.06 | 324.0 | 0.80 | 257.9 | 1.00 |
| | 0.52 | 278.0 | 393.1 | 0.71 | 262.1 | 1.06 | 352.0 | 0.79 | 234.7 | 1.18 | 313.1 | 0.89 | 247.8 | 1.12 |
| | 0.25 | 95.9 | 99.7 | 0.96 | 66.5 | 1.44 | 89.3 | 1.07 | 59.5 | 1.61 | 79.2 | 1.21 | 59.7 | 1.61 |
| | 0.29 | 104.4 | 118.0 | 0.89 | 78.6 | 1.33 | 105.6 | 0.99 | 70.4 | 1.48 | 96.7 | 1.08 | 70.6 | 1.48 |
| | 0.39 | 133.7 | 165.6 | 0.81 | 110.4 | 1.21 | 148.3 | 0.90 | 98.9 | 1.35 | 128.2 | 1.04 | 99.1 | 1.35 |
| | 0.51 | 139.0 | 195.9 | 0.71 | 130.6 | 1.06 | 175.5 | 0.79 | 117.0 | 1.19 | 140.9 | 0.99 | 117.3 | 1.19 |
| | 0.60 | 171.8 | 240.8 | 0.71 | 160.5 | 1.07 | 215.7 | 0.80 | 143.8 | 1.19 | 185.0 | 0.93 | 144.1 | 1.19 |

Table D.1. (cont.) ETLCC experimental test results with comparison to CSA S16:19, AISC 360-16 and EN1993-1-8:2005

| <i>S</i> | t_w/t_v | P_a kN | P_{pr} | | | | | | | | | | | |
|------------|------------|-------------|-------------------|-------|----------------------|-------|-------------------|-------|----------------------|-------|-----------------|-------|------------|-------|
| | | | CSA S16:19 | | | | AISC 360-16 | | | | EN1993-1-8:2005 | | | |
| | | | with $\sin\theta$ | | without $\sin\theta$ | | with $\sin\theta$ | | without $\sin\theta$ | | Directional | | Simplified | |
| kN | (A/P) | kN | (A/P) | kN | (A/P) | kN | (A/P) | kN | (A/P) | kN | (A/P) | kN | (A/P) | |
| <u>Q</u> | 0.63 | 171.3 | 253.4 | 0.68 | 168.9 | 1.01 | 226.9 | 0.75 | 151.3 | 1.13 | 191.2 | 0.90 | 151.6 | 1.13 |
| | 0.12 | 56.8 | 75.4 | 0.75 | 50.3 | 1.13 | 67.5 | 0.84 | 45.0 | 1.26 | 57.7 | 0.99 | 45.6 | 1.25 |
| | 0.17 | 96.8 | 114.6 | 0.85 | 76.4 | 1.27 | 102.6 | 0.94 | 68.4 | 1.42 | 94.8 | 1.02 | 69.2 | 1.40 |
| | 0.24 | 143.6 | 165.9 | 0.87 | 110.6 | 1.30 | 148.6 | 0.97 | 99.1 | 1.45 | 133.2 | 1.08 | 100.3 | 1.43 |
| | 0.33 | 155.2 | 215.5 | 0.72 | 143.7 | 1.08 | 193.0 | 0.80 | 128.6 | 1.21 | 159.1 | 0.98 | 130.2 | 1.19 |
| | 0.42 | 203.7 | 289.0 | 0.70 | 192.7 | 1.06 | 258.8 | 0.79 | 172.5 | 1.18 | 221.7 | 0.92 | 174.6 | 1.17 |
| | 0.53 | 208.3 | 339.4 | 0.61 | 226.3 | 0.92 | 304.0 | 0.69 | 202.6 | 1.03 | 257.0 | 0.81 | 205.1 | 1.02 |
| | δ_p | = | | 0.761 | | 1.141 | | 0.849 | | 1.274 | | 0.979 | | 1.260 |
| V_p | = | | 0.120 | | 0.120 | | 0.120 | | 0.120 | | 0.106 | | 0.129 | |
| <u>15b</u> | 0.40 | 47.4 | 111.0 | 0.43 | 74.0 | 0.64 | 99.4 | 0.48 | 66.3 | 0.72 | 78.0 | 0.61 | 65.5 | 0.72 |
| | 0.52 | 55.0 | 141.2 | 0.39 | 94.2 | 0.58 | 126.5 | 0.43 | 84.3 | 0.65 | 103.6 | 0.53 | 83.4 | 0.66 |
| | 0.53 | 55.1 | 142.1 | 0.39 | 94.7 | 0.58 | 127.3 | 0.43 | 84.8 | 0.65 | 101.3 | 0.54 | 83.9 | 0.66 |
| | 0.39 | 175.2 | 312.9 | 0.56 | 208.6 | 0.84 | 280.2 | 0.63 | 186.8 | 0.94 | 234.0 | 0.75 | 197.2 | 0.89 |
| | 0.48 | 194.8 | 387.4 | 0.50 | 258.2 | 0.75 | 346.9 | 0.56 | 231.3 | 0.84 | 292.9 | 0.66 | 244.2 | 0.80 |
| | 0.55 | 202.3 | 395.6 | 0.51 | 263.7 | 0.77 | 354.3 | 0.57 | 236.2 | 0.86 | 311.0 | 0.65 | 249.4 | 0.81 |
| | δ_p | = | | 0.463 | | 0.695 | | 0.517 | | 0.776 | | 0.624 | | 0.756 |
| | V_p | = | | 0.155 | | 0.155 | | 0.155 | | 0.155 | | 0.131 | | 0.122 |
| <u>30b</u> | 0.38 | 35.1 | 102.9 | 0.34 | 68.6 | 0.51 | 92.1 | 0.38 | 61.4 | 0.57 | 74.7 | 0.47 | 60.8 | 0.58 |
| | 0.38 | 40.0 | 108.0 | 0.37 | 72.0 | 0.55 | 96.8 | 0.41 | 64.5 | 0.62 | 76.5 | 0.52 | 63.8 | 0.63 |
| | 0.51 | 43.0 | 132.3 | 0.32 | 88.2 | 0.49 | 118.4 | 0.36 | 79.0 | 0.54 | 92.9 | 0.46 | 78.1 | 0.55 |
| | 0.43 | 149.8 | 337.4 | 0.44 | 224.9 | 0.67 | 302.1 | 0.50 | 201.4 | 0.74 | 253.3 | 0.59 | 212.7 | 0.70 |
| | δ_p | = | | 0.370 | | 0.555 | | 0.413 | | 0.620 | | 0.511 | | 0.615 |
| | V_p | = | | 0.142 | | 0.142 | | 0.142 | | 0.142 | | 0.116 | | 0.110 |

Table D.2. ETLCC experimental test results with comparison to new theoretical model

| <i>S</i> | t_w/t_v | λ | P_a | P_{pr} | | |
|------------|-----------|------------|-------|-----------------|-------|-------|
| | | | | Tuominen (2018) | | |
| | | | kN | kN | (A/P) | |
| <u>30a</u> | 0.40 | 0.06 | 72.0 | 55.0 | 1.31 | |
| | 0.45 | 0.07 | 109.9 | 51.1 | 2.15 | |
| | 0.44 | 0.07 | 155.8 | 55.2 | 2.82 | |
| | 0.39 | 0.06 | 349.6 | 309.2 | 1.13 | |
| | 0.46 | 0.07 | 374.9 | 334.4 | 1.12 | |
| | 0.47 | 0.07 | 435.7 | 281.7 | 1.55 | |
| | | δ_p | = | | | 1.680 |
| | V_p | = | | | 0.403 | |
| <u>15a</u> | 0.51 | 0.08 | 175.2 | 106.8 | 1.64 | |
| | 0.54 | 0.09 | 138.4 | 142.2 | 0.97 | |
| | 0.60 | 0.10 | 168.0 | 153.6 | 1.09 | |
| | 0.39 | 0.06 | 267.1 | 241.0 | 1.11 | |
| | 0.47 | 0.08 | 295.6 | 286.4 | 1.03 | |
| | 0.56 | 0.09 | 337.4 | 289.5 | 1.17 | |
| | | δ_p | = | | | 1.169 |
| | V_p | = | | | 0.206 | |
| <u>0</u> | 0.49 | 0.08 | 110.5 | 76.8 | 1.44 | |
| | 0.55 | 0.09 | 121.2 | 88.8 | 1.37 | |
| | 0.64 | 0.10 | 122.3 | 96.1 | 1.27 | |
| | 0.35 | 0.06 | 222.2 | 175.8 | 1.26 | |
| | 0.50 | 0.08 | 258.7 | 233.9 | 1.11 | |
| | 0.52 | 0.08 | 278.0 | 226.4 | 1.23 | |
| | 0.25 | 0.04 | 95.9 | 60.8 | 1.58 | |
| | 0.29 | 0.05 | 104.4 | 72.4 | 1.44 | |
| | 0.38 | 0.06 | 133.7 | 97.5 | 1.37 | |
| | 0.50 | 0.08 | 139.0 | 112.9 | 1.23 | |
| | 0.59 | 0.09 | 171.8 | 139.8 | 1.23 | |
| | 0.63 | 0.10 | 171.3 | 143.7 | 1.19 | |
| | 0.12 | 0.02 | 56.8 | 47.8 | 1.19 | |
| | 0.17 | 0.03 | 96.8 | 75.0 | 1.29 | |
| | 0.24 | 0.04 | 143.6 | 106.3 | 1.35 | |
| | 0.33 | 0.05 | 155.2 | 128.4 | 1.21 | |
| | 0.42 | 0.07 | 203.7 | 173.9 | 1.17 | |
| | 0.53 | 0.08 | 208.3 | 197.9 | 1.05 | |
| | | δ_p | = | | | 1.277 |
| | | V_p | = | | | 0.101 |
| <u>15b</u> | 0.40 | 0.06 | 47.4 | 35.7 | 1.33 | |
| | 0.52 | 0.08 | 55.0 | 44.9 | 1.22 | |
| | 0.53 | 0.09 | 55.1 | 45.3 | 1.22 | |

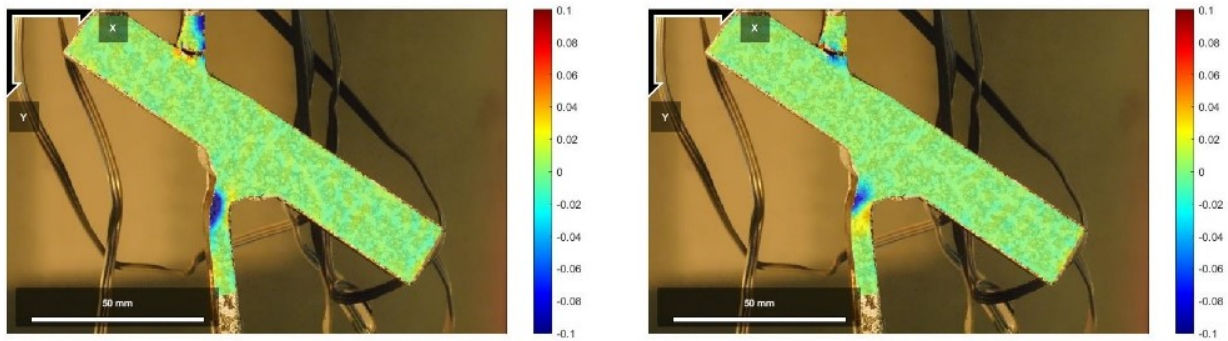
Table D.2. (cont.) ETLCC experimental test results with comparison to new theoretical model

| <i>S</i> | t_w/t_v | λ | P_a kN | P_{pr} Tuominen (2018) | |
|------------|------------|-----------|-------------|-----------------------------|-------|
| | | | | kN | (A/P) |
| <u>15b</u> | 0.38 | 0.06 | 175.2 | 152.3 | 1.15 |
| | 0.47 | 0.07 | 194.8 | 185.9 | 1.05 |
| | 0.54 | 0.09 | 202.3 | 189.3 | 1.07 |
| | δ_p | = | | | 1.172 |
| | V_p | = | | | 0.090 |
| <u>30b</u> | 0.38 | 0.06 | 35.1 | 23.7 | 1.48 |
| | 0.38 | 0.06 | 40.0 | 25.1 | 1.59 |
| | 0.50 | 0.08 | 43.0 | 30.7 | 1.40 |
| | 0.42 | 0.07 | 149.8 | 137.6 | 1.09 |
| | δ_p | = | | | 1.389 |
| | V_p | = | | | 0.155 |

Appendix E: DIGITAL IMAGE CORRELATION & STRAIN GAGE RESULTS

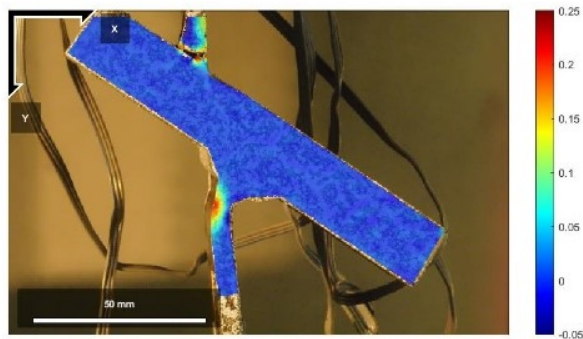
E.1. DIGITAL IMAGE CORRELATION RESULTS

Appendix E provides the digital image correlation (DIC) results for 16 (out of 40) chosen ETLCC tests. 14 tests each vary in either branch plate thickness (t_v) or branch plate offset (S). Two more tests, which vary only in weld size were chosen, to confirm similar bending behaviour across fillet weld sizes. Digital correlation plots were performed using Ncorr digital correlation software. All strains displayed are Eulerian-Almansi strains to show the image of the specimens in their deformed state. All plots showed are taken within five seconds before rupture.



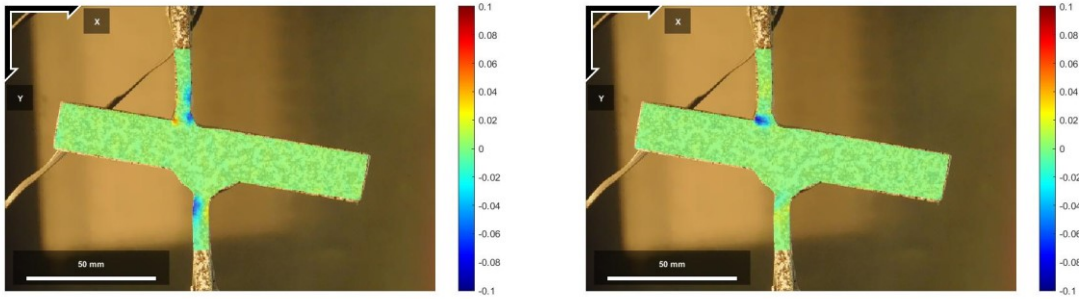
(a) x-axis strain (ϵ_{xx}) plot

(b) shear strain (ϵ_{xy}) plot



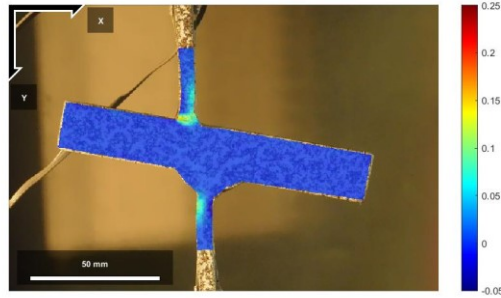
(c) y-axis strain (ϵ_{yy}) plot

Fig. E.1. DIC strain plots for test S6-L-30a



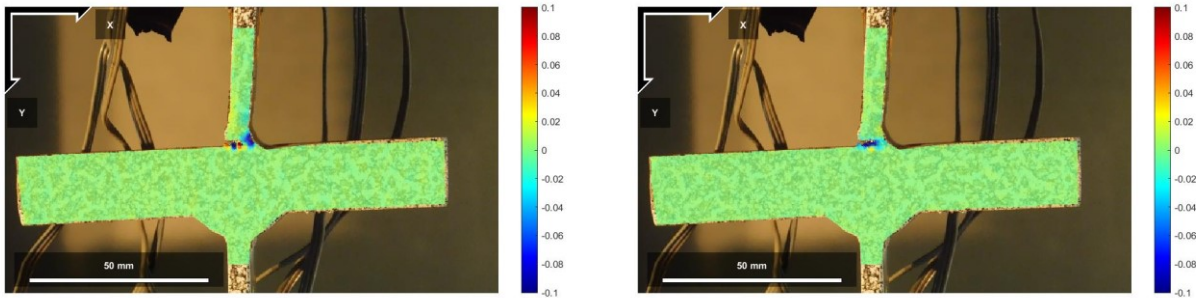
(a) x-axis strain (ϵ_{xx}) plot

(b) shear strain (ϵ_{xy}) plot



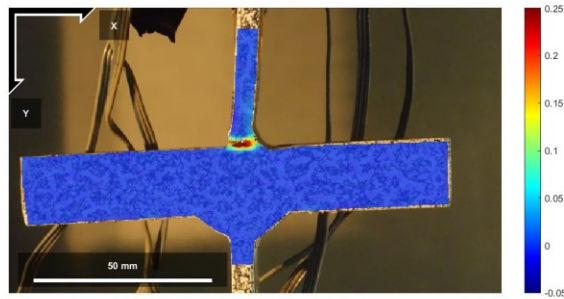
(c) y-axis strain (ϵ_{yy}) plot

Fig. E.2. DIC strain plots for test S6-S-15a



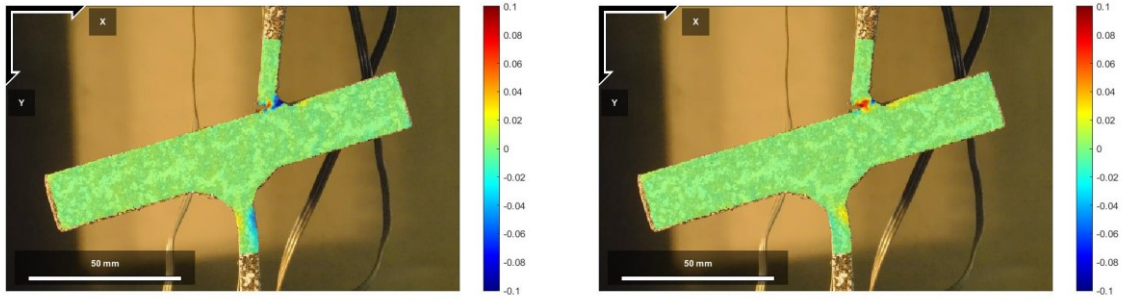
(a) x-axis strain (ϵ_{xx}) plot

(b) shear strain (ϵ_{xy}) plot



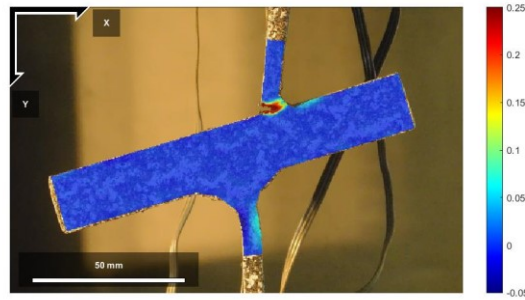
(c) y-axis strain (ϵ_{yy}) plot

Fig. E.3. DIC strain plots for test S6-S-0



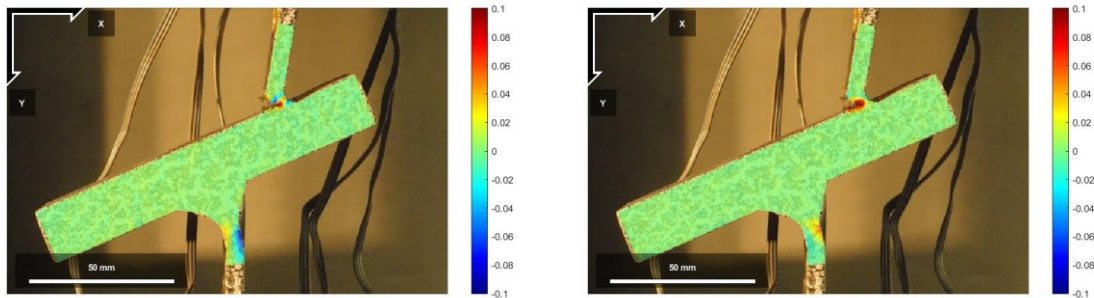
(a) x-axis strain (ϵ_{xx}) plot

(b) shear strain (ϵ_{xy}) plot



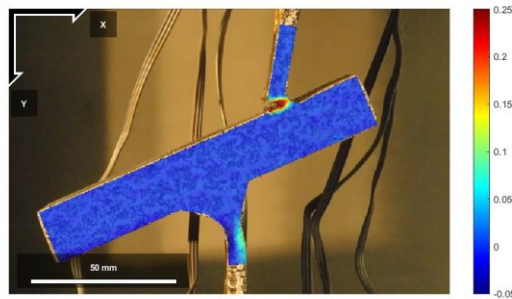
(c) y-axis strain (ϵ_{yy}) plot

Fig. E.4. DIC strain plots for test S6-S-15b



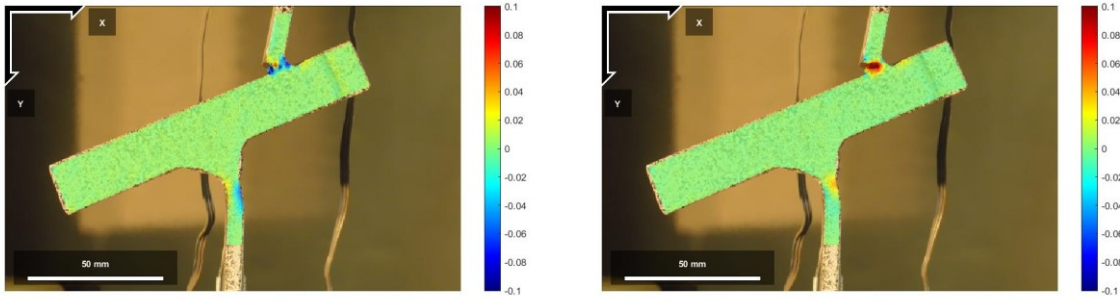
(a) x-axis strain (ϵ_{xx}) plot

(b) shear strain (ϵ_{xy}) plot



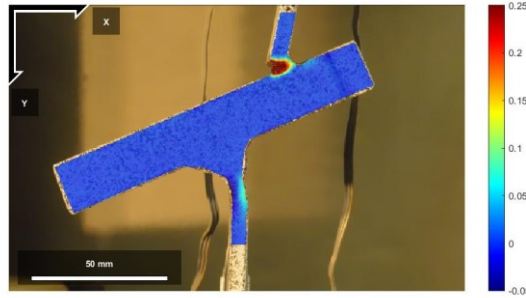
(c) y-axis strain (ϵ_{yy}) plot

Fig. E.5. DIC strain plots for test S6-S-30b



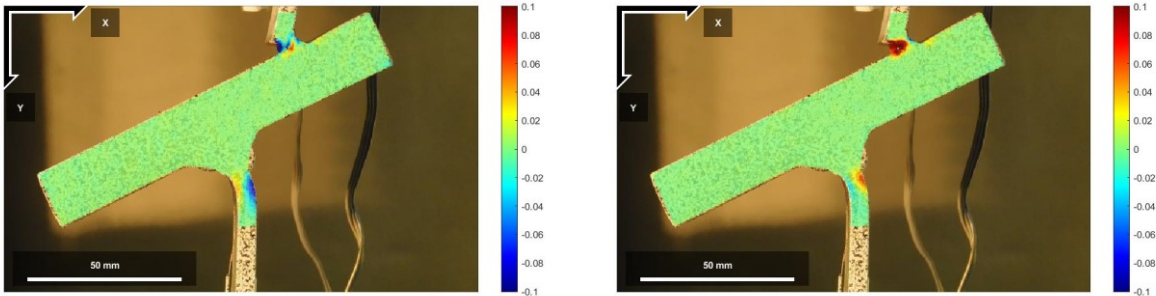
(a) x-axis strain (ϵ_{xx}) plot

(b) shear strain (ϵ_{xy}) plot



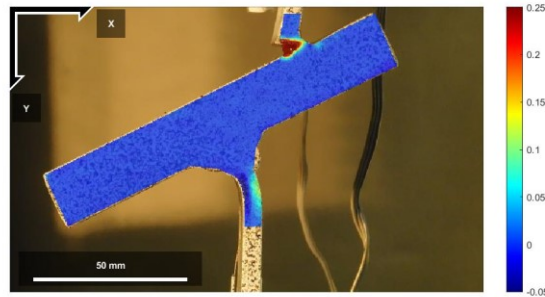
(c) y-axis strain (ϵ_{yy}) plot

Fig. E.6. DIC strain plots for test S6-M-30b



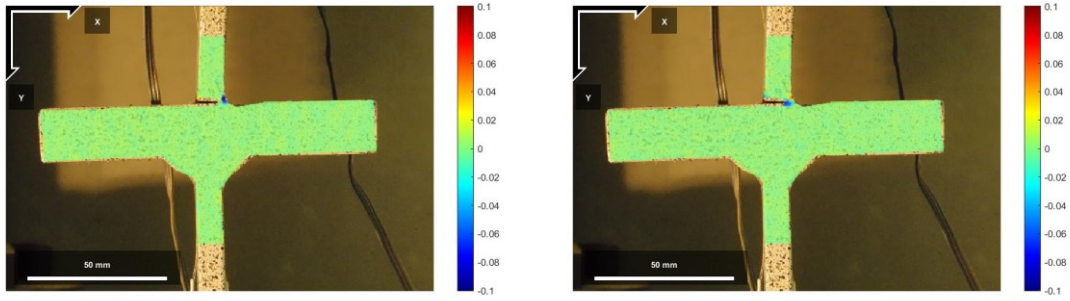
(a) x-axis strain (ϵ_{xx}) plot

(b) shear strain (ϵ_{xy}) plot



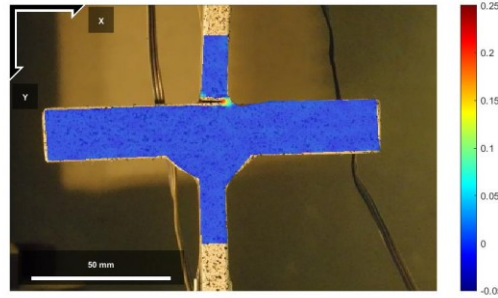
(c) y-axis strain (ϵ_{yy}) plot

Fig. E.7. DIC strain plots for test S6-L-30b



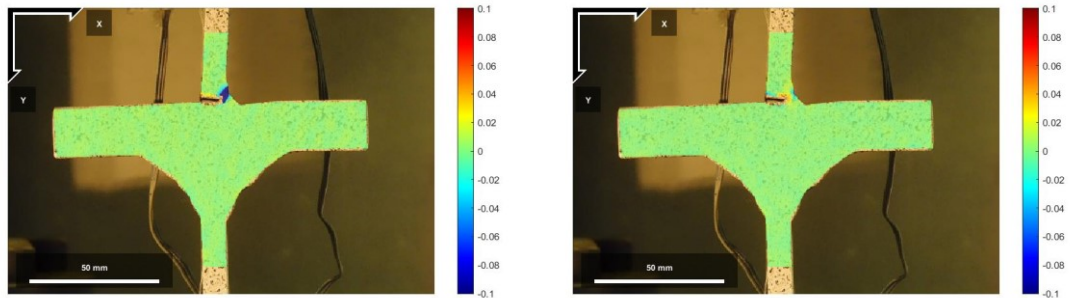
(a) x-axis strain (ϵ_{xx}) plot

(b) shear strain (ϵ_{xy}) plot



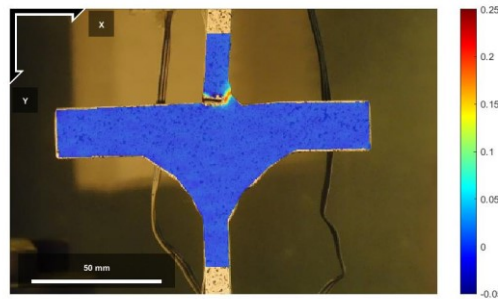
(c) y-axis strain (ϵ_{yy}) plot

Fig. E.8. DIC strain plots for test S9-XS-0



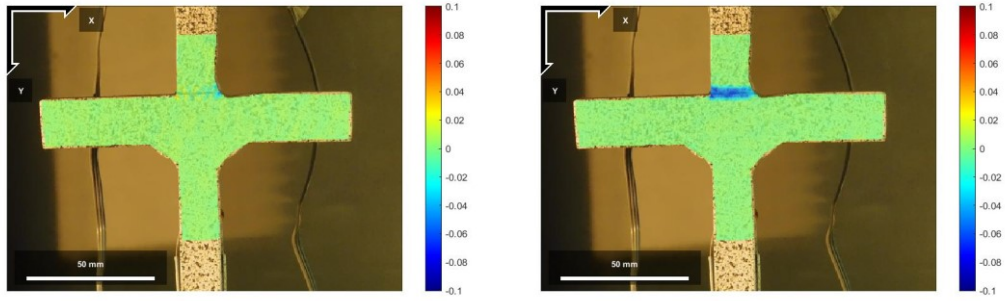
(a) x-axis strain (ϵ_{xx}) plot

(b) shear strain (ϵ_{xy}) plot



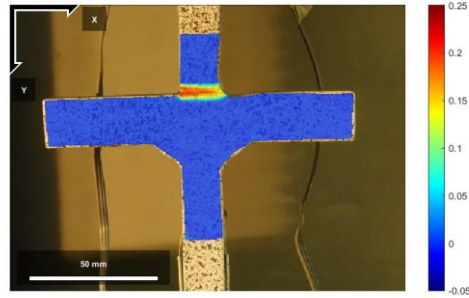
(c) y-axis strain (ϵ_{yy}) plot

Fig E.9. DIC strain plots for test S9-L-0



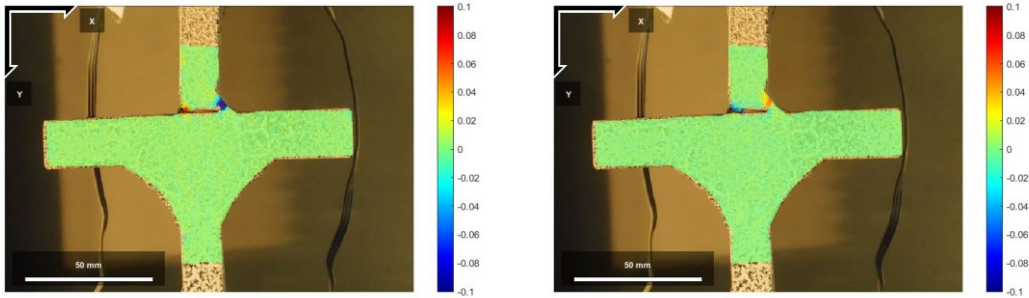
(a) x-axis strain (ϵ_{xx}) plot

(b) shear strain (ϵ_{xy}) plot



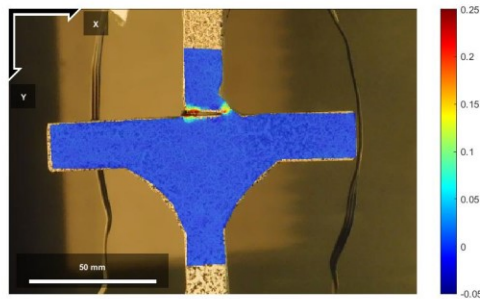
(c) y-axis strain (ϵ_{yy}) plot

Fig. E.10. DIC strain plots for test S14-XS-0



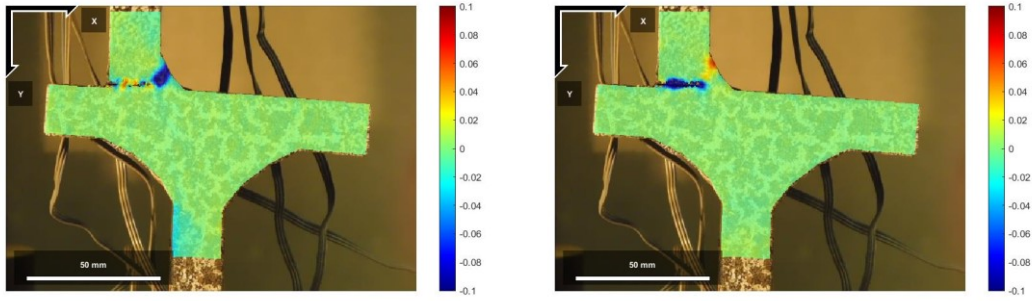
(a) x-axis strain (ϵ_{xx}) plot

(b) shear strain (ϵ_{xy}) plot



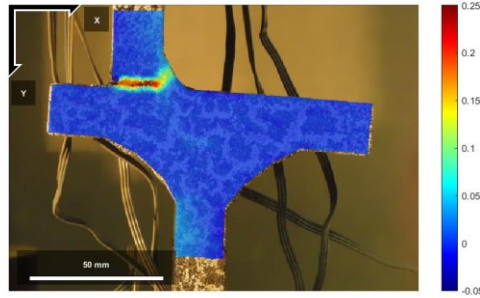
(c) y-axis strain (ϵ_{yy}) plot

Fig. E.11. DIC strain plots for test S14-L-0



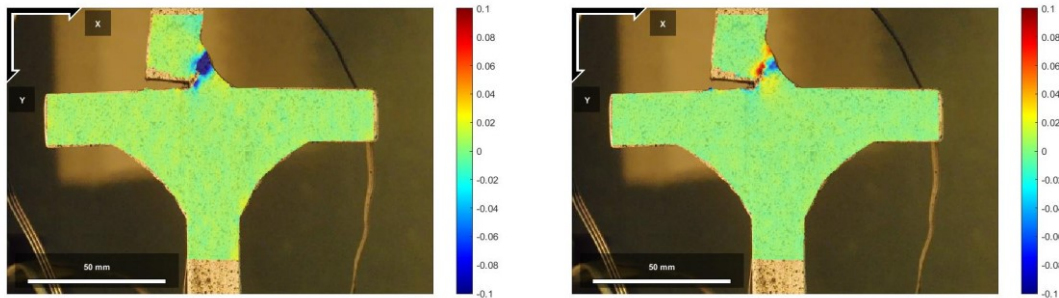
(a) x-axis strain (ϵ_{xx}) plot

(b) shear strain (ϵ_{xy}) plot



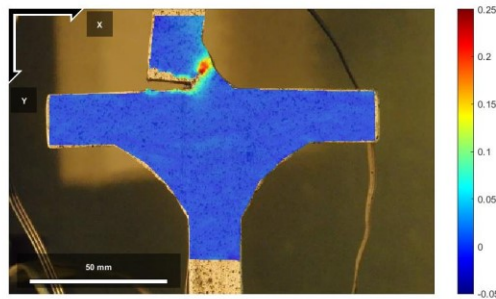
(c) y-axis strain (ϵ_{yy}) plot

Fig. E.12. DIC strain plots for test S20-S-30a



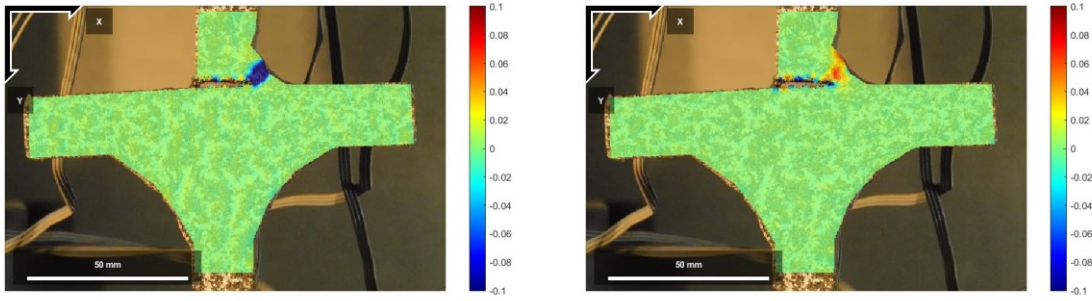
(a) x-axis strain (ϵ_{xx}) plot

(b) shear strain (ϵ_{xy}) plot



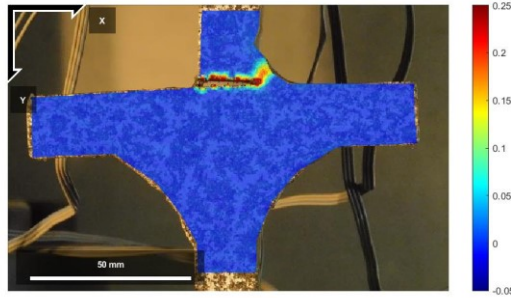
(c) y-axis strain (ϵ_{yy}) plot

Fig. E.13. DIC strain plots for test S20-L-15a



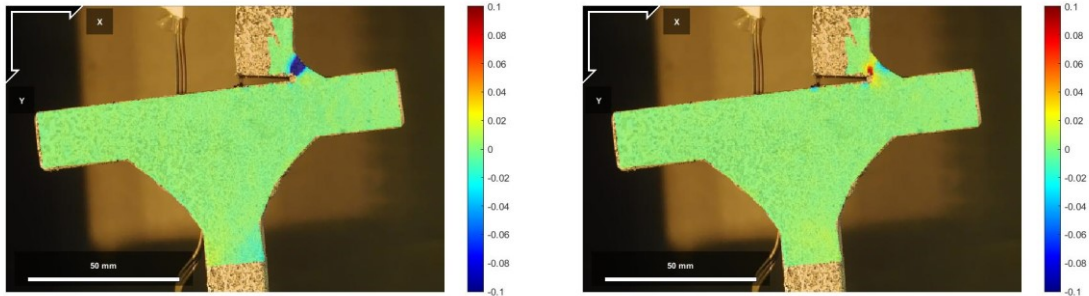
(a) x-axis strain (ϵ_{xx}) plot

(b) shear strain (ϵ_{xy}) plot



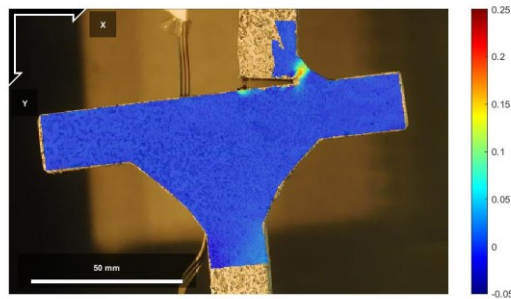
(c) y-axis strain (ϵ_{yy}) plot

Fig. E.14. DIC strain plots for test S20-S-0



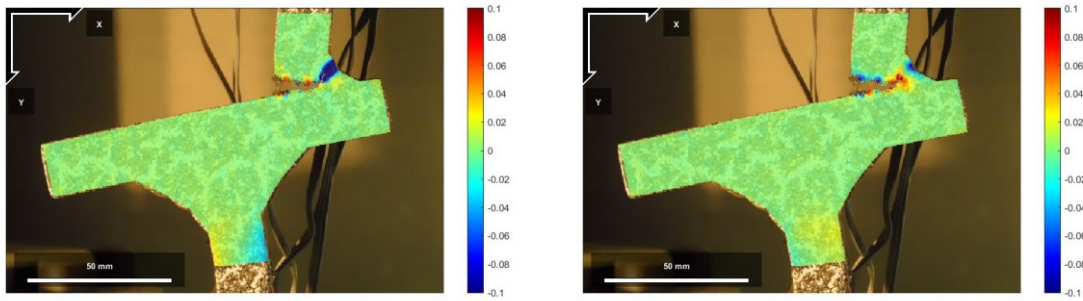
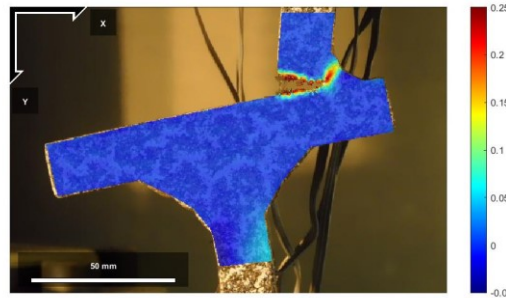
(a) x-axis strain (ϵ_{xx}) plot

(b) shear strain (ϵ_{xy}) plot



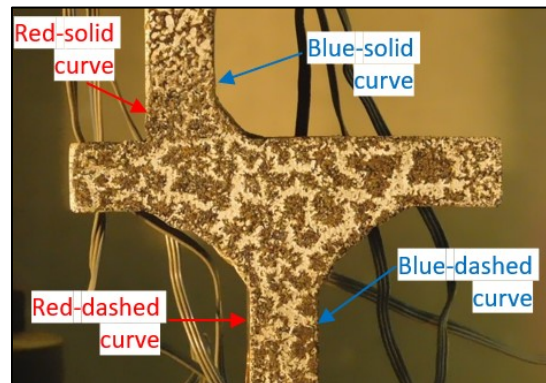
(c) y-axis strain (ϵ_{yy}) plot

Fig. E.15. DIC strain plots for test S20-S-15b

(a) x-axis strain (ϵ_{xx}) plot(b) shear strain (ϵ_{xy}) plot(c) y-axis strain (ϵ_{yy}) plot**Fig. E.16.** DIC strain plots for test S20-S-30b

E.2. STRAIN GAGE RESULTS

Results for ETLCC strain gages accompanying the DIC results. On the strain gage graphs, all strain gages are represented by a 'solid' or 'dashed' curve along with a 'red' or 'blue' colour. A solid line or a dashed curve represents a location on the top or bottom branch plate, respectively, and 'red' or 'blue' colour represents being located on the left or right sides (as shown in the figure), respectively (i.e. a blue-dashed curve means the strain gage is located on the right side of the bottom branch plate). Refer to Fig. E.17. to determine the locations of each strain gage from the strain gage graphs, below.

**Fig. E.17.** Legend for locations of strain gages for ETLCC tests

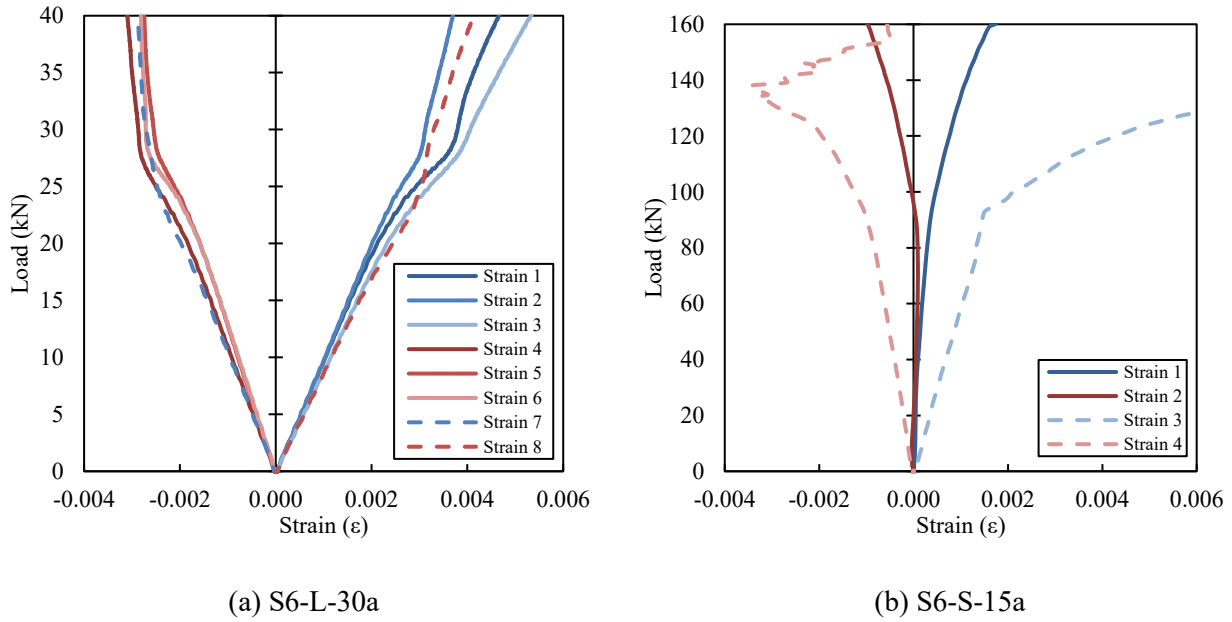


Fig. E.18. Strain gage graphs for S6-L-30a & S6-S-15a

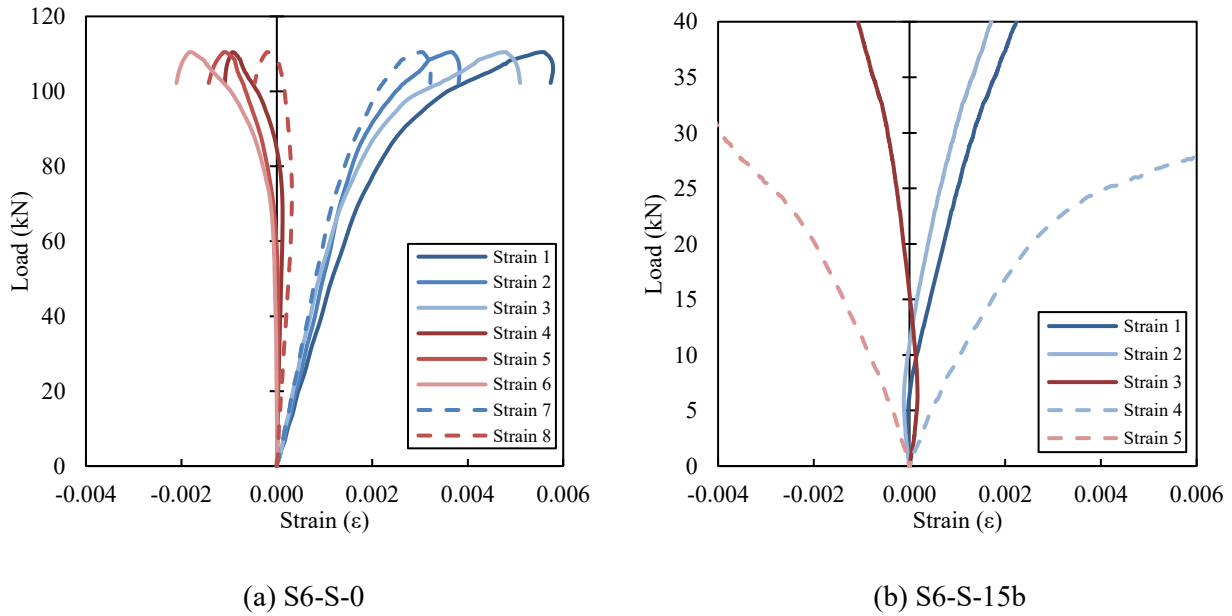


Fig. E.19. Strain gage graphs for S6-S-0 & S6-S-15b

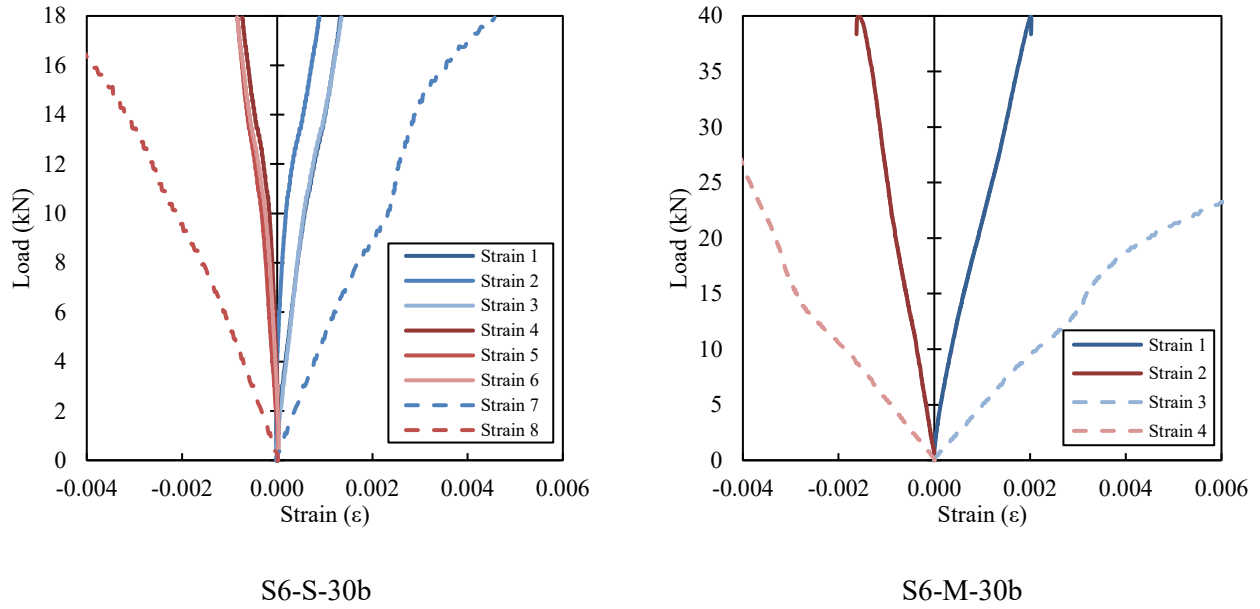


Fig. E.20. Strain gage graphs for S6-S-30b & S6-M-30b

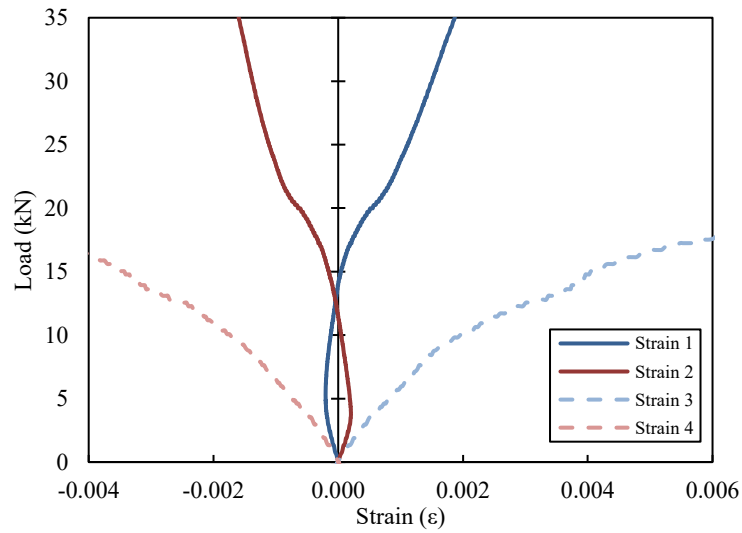


Fig. E.21. Strain gage graphs for S6-L-30b

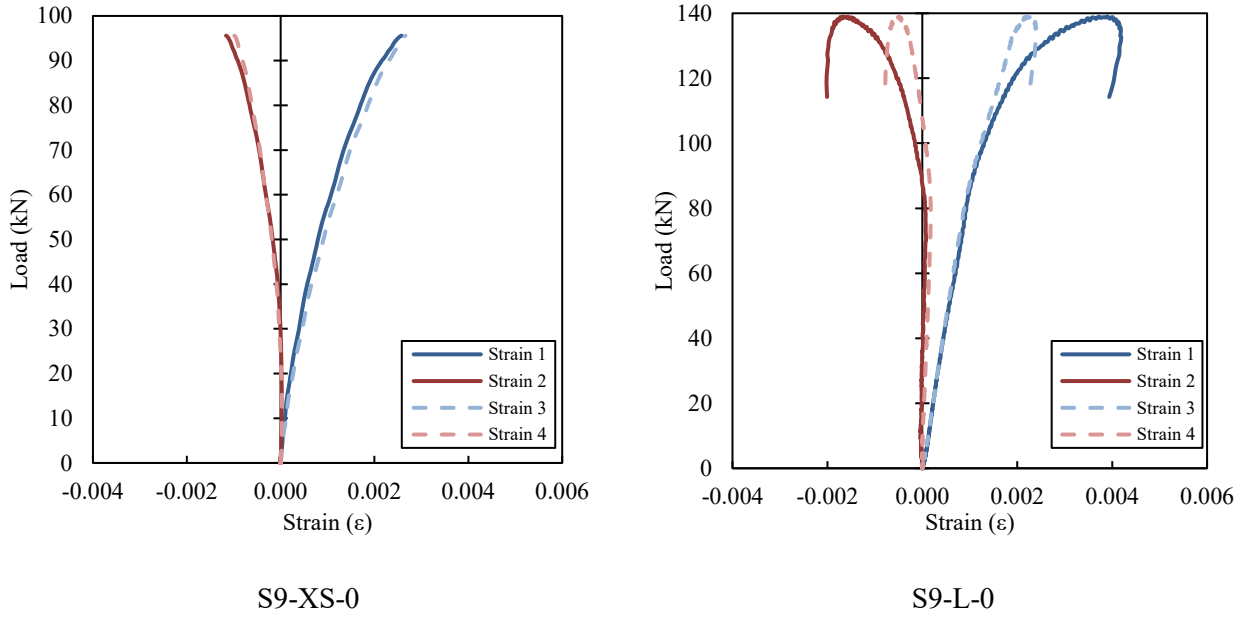


Fig. E.22. Strain gage graphs for S9-XS-0 & S9-L-0

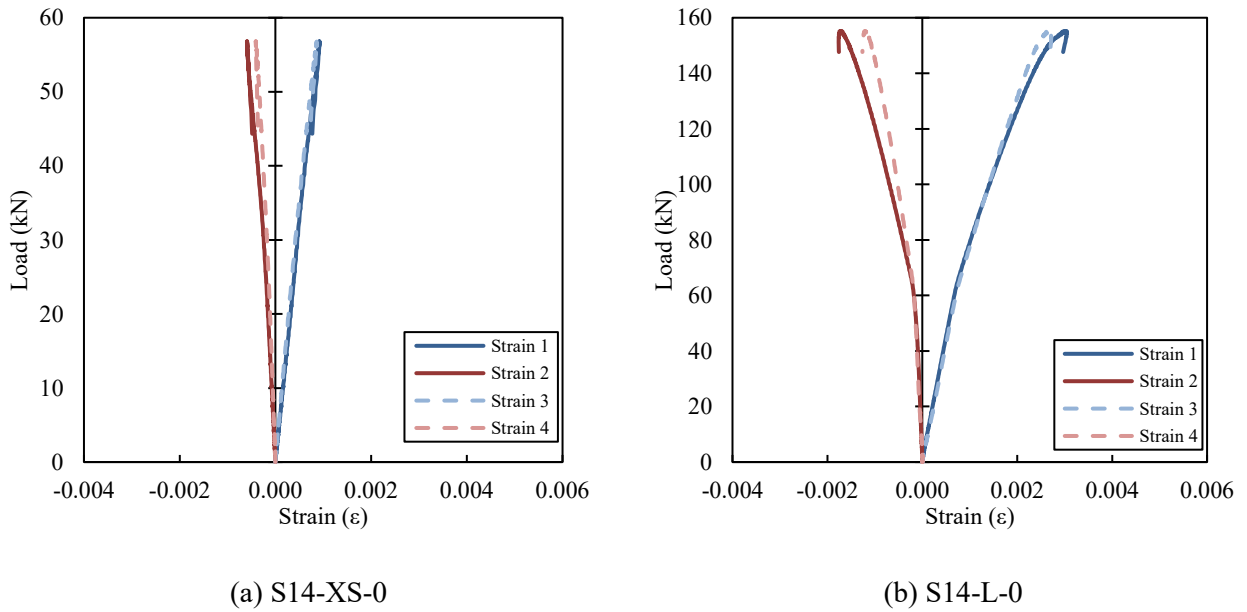


Fig. E.23. Strain gage graphs for S14-XS-0 & S14-L-0

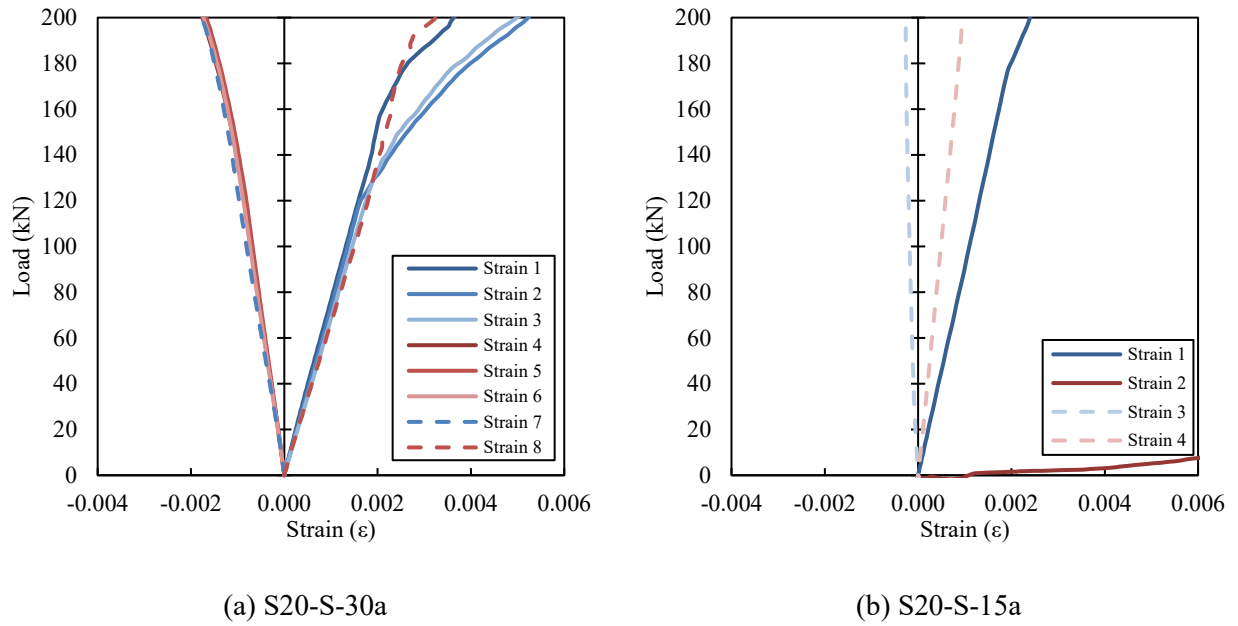


Fig. E.24. Strain gage graphs for S20-S-30a & S20-S-15a

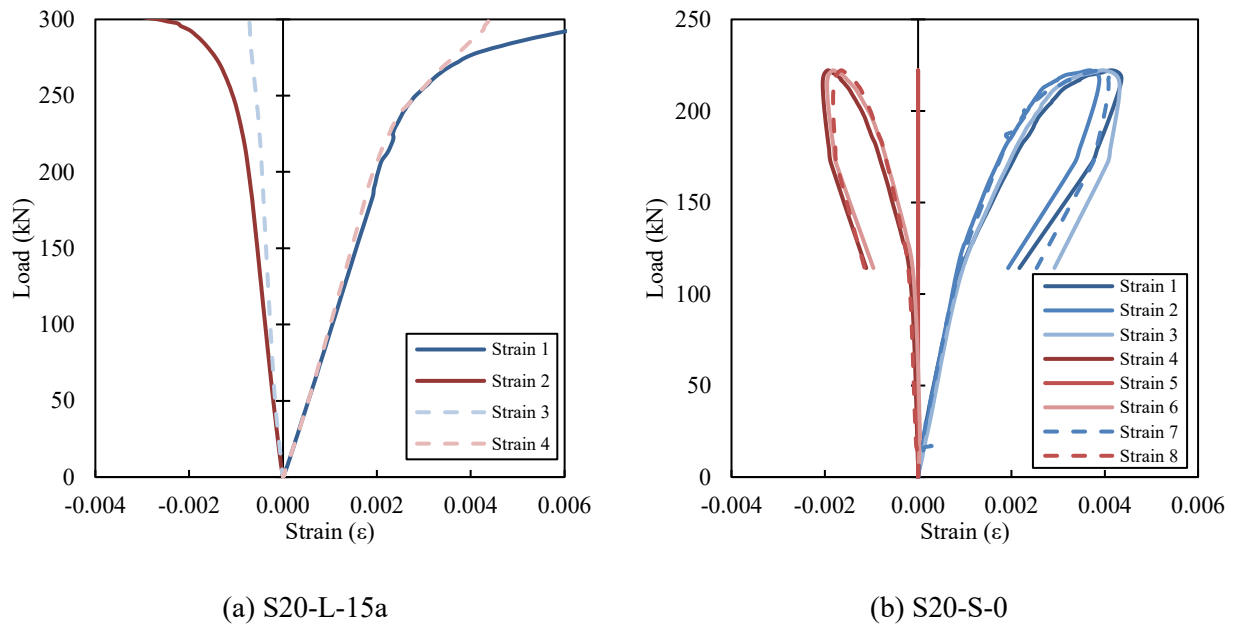
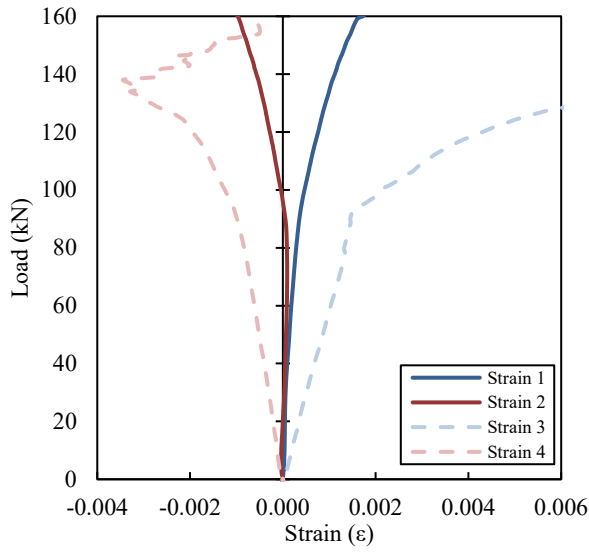
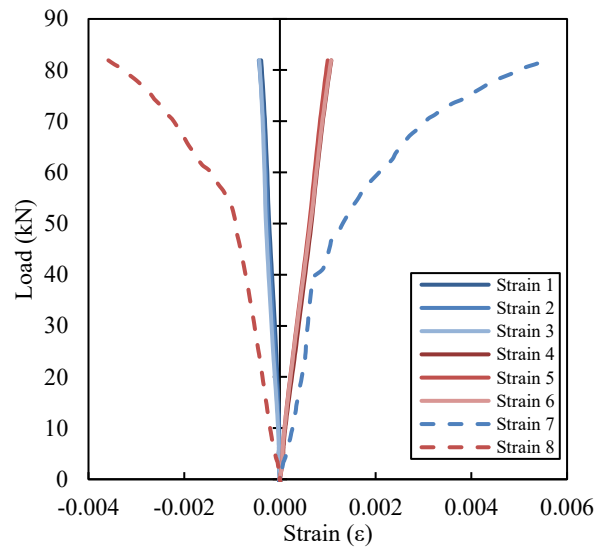


Fig. E.25. Strain gage graphs for S20-L-15a & S20-S-0



(a) S20-S-15b



(b) S20-S-30b

Fig. E.26. Strain gage graphs for S20-S-15b & S20-S-30b

Appendix F: OTHER EXPERIMENTAL PROGRAM TEST DATA

Appendix F provides test data used from other experimental programs on fillet welded RHS-to-rigid end plate connection tests from Frater (1986), Oatway (2014) & Tousignant and Packer (2017), RHS-to-rigid end plate connection tests from Tousignant and Packer (2017) and fillet welded lapped-splice and cruciform connection tests from Miazga and Kennedy (1989) & Ng et al. (2002).

Table F.1. Experimental program test data for fillet welded RHS-to-rigid end plate connection tests

| Author | t_w/t_v | P_a | P_{pr} | | | | | | | | | | | |
|------------------------------|-----------|-------------------|-------------------|------|----------------------|------|-------------------|------|----------------------|------|-----------------|------|------------|------|
| | | | CSA S16:19 | | | | AISC 360-16 | | | | EN1993-1-8:2005 | | | |
| | | | with $\sin\theta$ | | without $\sin\theta$ | | with $\sin\theta$ | | without $\sin\theta$ | | Directional | | Simplified | |
| kN | (A/P) | kN | (A/P) | kN | (A/P) | kN | (A/P) | kN | (A/P) | kN | (A/P) | | | |
| Frater (1986) | 0.44 | 1020 | 1377 | 0.74 | 918 | 1.11 | 1234 | 0.83 | 822 | 1.24 | 737 | 1.38 | - | - |
| | 0.37 | 960 | 1171 | 0.82 | 781 | 1.23 | 1048 | 0.92 | 699 | 1.37 | 619 | 1.55 | - | - |
| | 0.34 | 840 | 1063 | 0.79 | 708 | 1.19 | 952 | 0.88 | 634 | 1.32 | 555 | 1.51 | - | - |
| | 0.50 | 1140 | 1672 | 0.68 | 1115 | 1.02 | 1497 | 0.76 | 998 | 1.14 | 856 | 1.33 | - | - |
| | 0.60 | 1200 ¹ | 2007 | 0.60 | 1338 | 0.90 | 1798 | 0.67 | 1198 | 1.00 | 1065 | 1.13 | - | - |
| | 0.57 | 1207 ¹ | 1919 | 0.63 | 1279 | 0.94 | 1719 | 0.70 | 1146 | 1.05 | 1002 | 1.20 | - | - |
| | 0.81 | 1494 ² | 2720 | 0.55 | 1813 | 0.82 | 2436 | 0.61 | 1624 | 0.92 | 1432 | 1.04 | - | - |
| | 0.98 | 1578 ² | 3291 | 0.48 | 2194 | 0.72 | 2948 | 0.54 | 1965 | 0.80 | 1741 | 0.91 | - | - |
| | 1.13 | 1788 ² | 3548 | 0.50 | 2366 | 0.76 | 3178 | 0.56 | 2119 | 0.84 | 2019 | 0.89 | - | - |
| Oatway (2014) | 0.46 | 831 | 1074 | 0.77 | 716 | 1.16 | 962 | 0.86 | 641 | 1.30 | 670 | 1.24 | - | - |
| | 0.76 | 1166 | 1768 | 0.66 | 1179 | 0.99 | 1584 | 0.74 | 1056 | 1.10 | 1063 | 1.10 | - | - |
| | 0.68 | 1235 | 1583 | 0.78 | 1055 | 1.17 | 1418 | 0.87 | 945 | 1.31 | 1059 | 1.17 | - | - |
| | 0.72 | 1311 | 1679 | 0.78 | 1119 | 1.17 | 1503 | 0.87 | 1002 | 1.31 | 1132 | 1.16 | - | - |
| | 0.51 | 2433 | 2651 | 0.92 | 1768 | 1.38 | 2374 | 1.02 | 1583 | 1.54 | 1661 | 1.46 | - | - |
| | 0.69 | 2574 | 3578 | 0.72 | 2385 | 1.08 | 3204 | 0.80 | 2136 | 1.20 | 2304 | 1.12 | - | - |
| | 0.56 | 2525 | 2917 | 0.87 | 1945 | 1.30 | 2612 | 0.97 | 1742 | 1.45 | 2175 | 1.16 | - | - |
| | 0.59 | 2302 | 3054 | 0.75 | 2036 | 1.13 | 2735 | 0.84 | 1823 | 1.26 | 2104 | 1.09 | - | - |
| Tousignant and Packer (2017) | 0.35 | 508 | 638 | 0.80 | 425 | 1.19 | 571 | 0.89 | 381 | 1.33 | 438 | 1.16 | 357 | 1.42 |
| | 0.50 | 679 | 902 | 0.75 | 602 | 1.13 | 808 | 0.84 | 539 | 1.26 | 619 | 1.10 | 505 | 1.34 |
| | 0.71 | 911 | 1276 | 0.71 | 851 | 1.07 | 1143 | 0.80 | 762 | 1.20 | 875 | 1.04 | 715 | 1.27 |
| | 0.90 | 1049 | 1624 | 0.65 | 1083 | 0.97 | 1455 | 0.72 | 970 | 1.08 | 1114 | 0.94 | 910 | 1.15 |
| | 1.06 | 1247 | 1914 | 0.65 | 1276 | 0.98 | 1714 | 0.73 | 1143 | 1.09 | 1313 | 0.95 | 1072 | 1.16 |
| | 0.35 | 631 | 794 | 0.79 | 529 | 1.19 | 711 | 0.89 | 474 | 1.33 | 545 | 1.16 | 445 | 1.42 |
| | 0.50 | 855 | 1123 | 0.76 | 749 | 1.14 | 1006 | 0.85 | 670 | 1.28 | 770 | 1.11 | 629 | 1.36 |
| | 0.71 | 1147 | 1588 | 0.72 | 1059 | 1.08 | 1422 | 0.81 | 948 | 1.21 | 1089 | 1.05 | 890 | 1.29 |

¹Mixed failure mode of weld failure and partial plate failure

²End-plate failure along at least one weldment

Table F.1. (cont.) Experimental program test data for fillet welded RHS-to-rigid end plate connection tests

| Author | t_w/t_v | P_a kN | P_{pr} | | | | | | | | | | | | |
|---------------------------------|------------|-------------|-------------------|--------------|----------------------|--------------|-------------------|--------------|----------------------|--------------|-----------------|--------------|------------|--------------|--|
| | | | CSA S16:19 | | | | AISC 360-16 | | | | EN1993-1-8:2005 | | | | |
| | | | with $\sin\theta$ | | without $\sin\theta$ | | with $\sin\theta$ | | without $\sin\theta$ | | Directional | | Simplified | | |
| kN | (A/P) | kN | (A/P) | kN | (A/P) | kN | (A/P) | kN | (A/P) | kN | (A/P) | kN | (A/P) | | |
| Tousignant and Packer (2017) | 0.90 | 1380 | 2022 | 0.68 | 1348 | 1.02 | 1810 | 0.76 | 1207 | 1.14 | 1387 | 1.00 | 1132 | 1.22 | |
| | 1.06 | 1578 | 2382 | 0.66 | 1588 | 0.99 | 2134 | 0.74 | 1422 | 1.11 | 1634 | 0.97 | 1334 | 1.18 | |
| | 0.35 | 855 | 1052 | 0.81 | 701 | 1.22 | 942 | 0.91 | 628 | 1.36 | 721 | 1.19 | 589 | 1.45 | |
| | 0.50 | 1142 | 1487 | 0.77 | 991 | 1.15 | 1332 | 0.86 | 888 | 1.29 | 1020 | 1.12 | 833 | 1.37 | |
| | 0.71 | 1546 | 2103 | 0.74 | 1402 | 1.10 | 1883 | 0.82 | 1256 | 1.23 | 1443 | 1.07 | 1178 | 1.31 | |
| | 0.90 | 1872 | 2677 | 0.70 | 1785 | 1.05 | 2397 | 0.78 | 1598 | 1.17 | 1836 | 1.02 | 1499 | 1.25 | |
| | 0.35 | 1291 | 1553 | 0.83 | 1036 | 1.25 | 1391 | 0.93 | 927 | 1.39 | 1066 | 1.21 | 870 | 1.48 | |
| | 0.50 | 1748 | 2197 | 0.80 | 1465 | 1.19 | 1967 | 0.89 | 1312 | 1.33 | 1507 | 1.16 | 1230 | 1.42 | |
| | 0.71 | 2338 | 3107 | 0.75 | 2071 | 1.13 | 2782 | 0.84 | 1855 | 1.26 | 2131 | 1.10 | 1740 | 1.34 | |
| | 0.35 | 2088 | 2419 | 0.86 | 1612 | 1.29 | 2166 | 0.96 | 1444 | 1.45 | 1659 | 1.26 | 1355 | 1.54 | |
| | 0.50 | 2836 | 3420 | 0.83 | 2280 | 1.24 | 3063 | 0.93 | 2042 | 1.39 | 2346 | 1.21 | 1916 | 1.48 | |
| | 0.35 | 2831 | 3234 | 0.88 | 2156 | 1.31 | 2896 | 0.98 | 1931 | 1.47 | 2218 | 1.28 | 1811 | 1.56 | |
| | 0.50 | 3804 | 4573 | 0.83 | 3049 | 1.25 | 4095 | 0.93 | 2730 | 1.39 | 3137 | 1.21 | 2561 | 1.49 | |
| | δ_p | = | | 0.840 | | 1.260 | | 0.938 | | 1.407 | | 1.233 | | 1.521 | |
| | V_p | = | | 0.081 | | 0.081 | | 0.082 | | 0.082 | | 0.077 | | 0.059 | |

Table F.2. Experimental program test data for fillet welded CHS-to-rigid end plate connection tests

| Author | P_a kN | P_{pr} | | | | | | | | | | | |
|---------------------------------|-------------------|-------------------|-------|----------------------|-------|-------------------|-------|----------------------|-------|-----------------|-------|------------|------|
| | | CSA S16:19 | | | | AISC 360-16 | | | | EN1993-1-8:2005 | | | |
| | | with $\sin\theta$ | | without $\sin\theta$ | | with $\sin\theta$ | | without $\sin\theta$ | | Directional | | Simplified | |
| kN | (A/P) | kN | (A/P) | kN | (A/P) | kN | (A/P) | kN | (A/P) | kN | (A/P) | | |
| Tousignant and Packer (2017) | 1261 ¹ | 1455 | 0.87 | 970 | 1.30 | 1303 | 0.97 | 869 | 1.45 | 1017 | 1.24 | - | - |
| | 1279 ¹ | 2006 | 0.64 | 1337 | 0.96 | 1796 | 0.71 | 1197 | 1.07 | 1395 | 0.92 | - | - |
| | 1459 ¹ | 1577 | 0.93 | 1051 | 1.39 | 1412 | 1.03 | 942 | 1.55 | 1069 | 1.36 | - | - |
| | 1597 ¹ | 1833 | 0.87 | 1222 | 1.31 | 1641 | 0.97 | 1094 | 1.46 | 1226 | 1.30 | - | - |
| | 841 ¹ | 1161 | 0.72 | 774 | 1.09 | 1040 | 0.81 | 693 | 1.21 | 710 | 1.18 | - | - |
| | 864 ¹ | 1113 | 0.78 | 742 | 1.16 | 997 | 0.87 | 664 | 1.30 | 706 | 1.22 | - | - |
| | 508 | 638 | 0.80 | 425 | 1.19 | 571 | 0.89 | 381 | 1.33 | 438 | 1.16 | 357 | 1.42 |
| | 679 | 902 | 0.75 | 602 | 1.13 | 808 | 0.84 | 539 | 1.26 | 619 | 1.10 | 505 | 1.34 |
| | 911 | 1276 | 0.71 | 851 | 1.07 | 1143 | 0.80 | 762 | 1.20 | 875 | 1.04 | 715 | 1.27 |
| | 1049 | 1624 | 0.65 | 1083 | 0.97 | 1455 | 0.72 | 970 | 1.08 | 1114 | 0.94 | 910 | 1.15 |
| | 1247 | 1914 | 0.65 | 1276 | 0.98 | 1714 | 0.73 | 1143 | 1.09 | 1313 | 0.95 | 1072 | 1.16 |
| | 631 | 794 | 0.79 | 529 | 1.19 | 711 | 0.89 | 474 | 1.33 | 545 | 1.16 | 445 | 1.42 |
| | 855 | 1123 | 0.76 | 749 | 1.14 | 1006 | 0.85 | 670 | 1.28 | 770 | 1.11 | 629 | 1.36 |
| | 1147 | 1588 | 0.72 | 1059 | 1.08 | 1422 | 0.81 | 948 | 1.21 | 1089 | 1.05 | 890 | 1.29 |
| | 1380 | 2022 | 0.68 | 1348 | 1.02 | 1810 | 0.76 | 1207 | 1.14 | 1387 | 1.00 | 1132 | 1.22 |
| | 1578 | 2382 | 0.66 | 1588 | 0.99 | 2134 | 0.74 | 1422 | 1.11 | 1634 | 0.97 | 1334 | 1.18 |
| | 855 | 1052 | 0.81 | 701 | 1.22 | 942 | 0.91 | 628 | 1.36 | 721 | 1.19 | 589 | 1.45 |
| | 1142 | 1487 | 0.77 | 991 | 1.15 | 1332 | 0.86 | 888 | 1.29 | 1020 | 1.12 | 833 | 1.37 |
| | 1546 | 2103 | 0.74 | 1402 | 1.10 | 1883 | 0.82 | 1256 | 1.23 | 1443 | 1.07 | 1178 | 1.31 |

¹Experimental test (others are FE tests)

Table F.2. (cont.) Experimental program test data for fillet welded CHS-to-rigid end plate connection tests

| Author | P_a kN | P_{pr} | | | | | | | | | | | |
|---------------------------------|-------------|-------------------|------|----------------------|------|-------------------|------|----------------------|------|-----------------|------|--------------|------|
| | | CSA S16:19 | | | | AISC 360-16 | | | | EN1993-1-8:2005 | | | |
| | | with $\sin\theta$ | | without $\sin\theta$ | | with $\sin\theta$ | | without $\sin\theta$ | | Directional | | Simplified | |
| kN | kN | (A/P) | kN | (A/P) | kN | (A/P) | kN | (A/P) | kN | (A/P) | kN | (A/P) | |
| Tousignant and Packer (2017) | 1872 | 2677 | 0.70 | 1785 | 1.05 | 2397 | 0.78 | 1598 | 1.17 | 1836 | 1.02 | 1499 | 1.25 |
| | 1291 | 1553 | 0.83 | 1036 | 1.25 | 1391 | 0.93 | 927 | 1.39 | 1066 | 1.21 | 870 | 1.48 |
| | 1748 | 2197 | 0.80 | 1465 | 1.19 | 1967 | 0.89 | 1312 | 1.33 | 1507 | 1.16 | 1230 | 1.42 |
| | 2338 | 3107 | 0.75 | 2071 | 1.13 | 2782 | 0.84 | 1855 | 1.26 | 2131 | 1.10 | 1740 | 1.34 |
| | 2088 | 2419 | 0.86 | 1612 | 1.29 | 2166 | 0.96 | 1444 | 1.45 | 1659 | 1.26 | 1355 | 1.54 |
| | 2836 | 3420 | 0.83 | 2280 | 1.24 | 3063 | 0.93 | 2042 | 1.39 | 2346 | 1.21 | 1916 | 1.48 |
| | 2831 | 3234 | 0.88 | 2156 | 1.31 | 2896 | 0.98 | 1931 | 1.47 | 2218 | 1.28 | 1811 | 1.56 |
| | 3804 | 4573 | 0.83 | 3049 | 1.25 | 4095 | 0.93 | 2730 | 1.39 | 3137 | 1.21 | 2561 | 1.49 |
| δ_p | = | 0.737 | | 1.106 | | 0.824 | | 1.234 | | 1.151 | | 1.357 | |
| V_p | = | 0.135 | | 0.135 | | 0.135 | | 0.136 | | 0.132 | | 0.090 | |

Table F.3. Experimental program test data for fillet welded lapped-splice and cruciform connection tests

| Author | P_a kN | P_{pr} | | | | | | | |
|------------------------------|-------------|-------------------|-------|----------------------|-------|-------------------|-------|----------------------|-------|
| | | CSA S16:19 | | | | AISC 360-16 | | | |
| | | with $\sin\theta$ | | without $\sin\theta$ | | with $\sin\theta$ | | without $\sin\theta$ | |
| kN | kN | (A/P) | kN | (A/P) | kN | (A/P) | kN | (A/P) | |
| Miazga and Kennedy (1989) | 421.3 | 458.6 | 0.919 | 305.7 | 1.378 | 410.7 | 1.026 | 273.8 | 1.539 |
| | 431.4 | 465.5 | 0.927 | 310.4 | 1.390 | 416.9 | 1.035 | 277.9 | 1.552 |
| | 407.3 | 463.9 | 0.878 | 309.3 | 1.317 | 415.4 | 0.980 | 277.0 | 1.471 |
| | 789.2 | 780.4 | 1.011 | 520.2 | 1.517 | 698.8 | 1.129 | 465.9 | 1.694 |
| | 807.4 | 809.0 | 0.998 | 539.3 | 1.497 | 724.5 | 1.114 | 483.0 | 1.672 |
| | 790.5 | 797.4 | 0.991 | 531.6 | 1.487 | 714.1 | 1.107 | 476.1 | 1.660 |
| Ng. et al. (2002) | 510 | 359.2 | 1.42 | 239.4 | 2.13 | 320.8 | 1.59 | 213.8 | 2.39 |
| | 473 | 342.8 | 1.38 | 228.5 | 2.07 | 307.1 | 1.54 | 204.8 | 2.31 |
| | 520 | 409.4 | 1.27 | 273.0 | 1.91 | 366.2 | 1.42 | 244.1 | 2.13 |
| | 642 | 375.4 | 1.71 | 250.3 | 2.57 | 336.1 | 1.91 | 224.1 | 2.87 |
| | 636 | 369.8 | 1.72 | 246.5 | 2.58 | 331.3 | 1.92 | 220.8 | 2.88 |
| | 707 | 353.5 | 2.00 | 235.7 | 3.00 | 317.0 | 2.23 | 211.4 | 3.35 |
| | 635 | 312.8 | 2.03 | 208.5 | 3.05 | 279.7 | 2.27 | 186.5 | 3.41 |
| | 698 | 423.0 | 1.65 | 282.0 | 2.48 | 377.3 | 1.85 | 251.5 | 2.78 |
| | 815 | 420.1 | 1.94 | 280.1 | 2.91 | 375.6 | 2.17 | 250.4 | 3.26 |
| | 764 | 436.6 | 1.75 | 291.0 | 2.63 | 389.8 | 1.96 | 259.9 | 2.94 |
| | 677 | 442.5 | 1.53 | 295.0 | 2.30 | 395.9 | 1.71 | 263.9 | 2.57 |
| | 699 | 377.8 | 1.85 | 251.9 | 2.78 | 339.3 | 2.06 | 226.2 | 3.09 |
| | 606 | 381.1 | 1.59 | 254.1 | 2.39 | 342.4 | 1.77 | 228.2 | 2.66 |
| | 752 | 501.3 | 1.50 | 334.2 | 2.25 | 450.3 | 1.67 | 300.2 | 2.51 |
| 769 | 471.8 | 1.63 | 314.5 | 2.45 | 422.5 | 1.82 | 281.7 | 2.73 | |
| 714 | 440.7 | 1.62 | 293.8 | 2.43 | 394.5 | 1.81 | 263.0 | 2.72 | |
| 738 | 370.9 | 1.99 | 247.2 | 2.99 | 330.9 | 2.23 | 220.6 | 3.35 | |

Table F.3. (Cont.) Experimental program test data for fillet welded lapped-splice and cruciform connection tests

| Author | P_a kN | P_{pr} | | | | | | | | |
|-------------------|-------------|-------------------|------|----------------------|------|-------------------|------|----------------------|------|--------------|
| | | CSA S16:19 | | | | AISC 360-16 | | | | |
| | | with $\sin\theta$ | | without $\sin\theta$ | | with $\sin\theta$ | | without $\sin\theta$ | | |
| | kN | (A/P) | kN | (A/P) | kN | (A/P) | kN | (A/P) | | |
| Ng. et al. (2002) | 707 | 307.4 | 2.30 | 204.9 | 3.45 | 275.1 | 2.57 | 183.4 | 3.86 | |
| | 769 | 371.5 | 2.07 | 247.7 | 3.11 | 332.9 | 2.31 | 221.9 | 3.47 | |
| | 870 | 756.5 | 1.15 | 504.3 | 1.73 | 674.4 | 1.29 | 449.6 | 1.94 | |
| | 966 | 779.0 | 1.24 | 519.4 | 1.86 | 695.0 | 1.39 | 463.3 | 2.09 | |
| | 936 | 628.2 | 1.49 | 418.8 | 2.24 | 563.9 | 1.66 | 375.9 | 2.49 | |
| | 935 | 772.7 | 1.21 | 515.2 | 1.82 | 692.6 | 1.35 | 461.7 | 2.03 | |
| | 1010 | 716.3 | 1.41 | 477.5 | 2.12 | 639.2 | 1.58 | 426.2 | 2.37 | |
| | 1020 | 790.7 | 1.29 | 527.1 | 1.94 | 708.3 | 1.44 | 472.2 | 2.16 | |
| | 1063 | 787.4 | 1.35 | 524.9 | 2.03 | 704.0 | 1.51 | 469.3 | 2.27 | |
| | 910 | 798.2 | 1.14 | 532.2 | 1.71 | 710.9 | 1.28 | 474.0 | 1.92 | |
| | 993 | 781.9 | 1.27 | 521.3 | 1.91 | 699.3 | 1.42 | 466.2 | 2.13 | |
| | 1064 | 733.8 | 1.45 | 489.2 | 2.18 | 656.8 | 1.62 | 437.9 | 2.43 | |
| | 1018 | 595.3 | 1.71 | 396.9 | 2.57 | 533.0 | 1.91 | 355.3 | 2.87 | |
| | 1038 | 640.7 | 1.62 | 427.2 | 2.43 | 573.5 | 1.81 | 382.3 | 2.72 | |
| | 643 | 385.0 | 1.67 | 256.7 | 2.51 | 345.7 | 1.86 | 230.5 | 2.79 | |
| | 641 | 410.9 | 1.56 | 273.9 | 2.34 | 368.4 | 1.74 | 245.6 | 2.61 | |
| | | δ_p | = | 1.493 | | 2.240 | | 1.668 | | 2.502 |
| | | V_p | = | 0.237 | | 0.237 | | 0.237 | | 0.237 |

Appendix G: MACRO-ETCH EXAMINATIONS

Appendix G provides macro-etch examination data used to determine the post-rupture measurements of the single-sided fillet welds of ETLCC specimens.

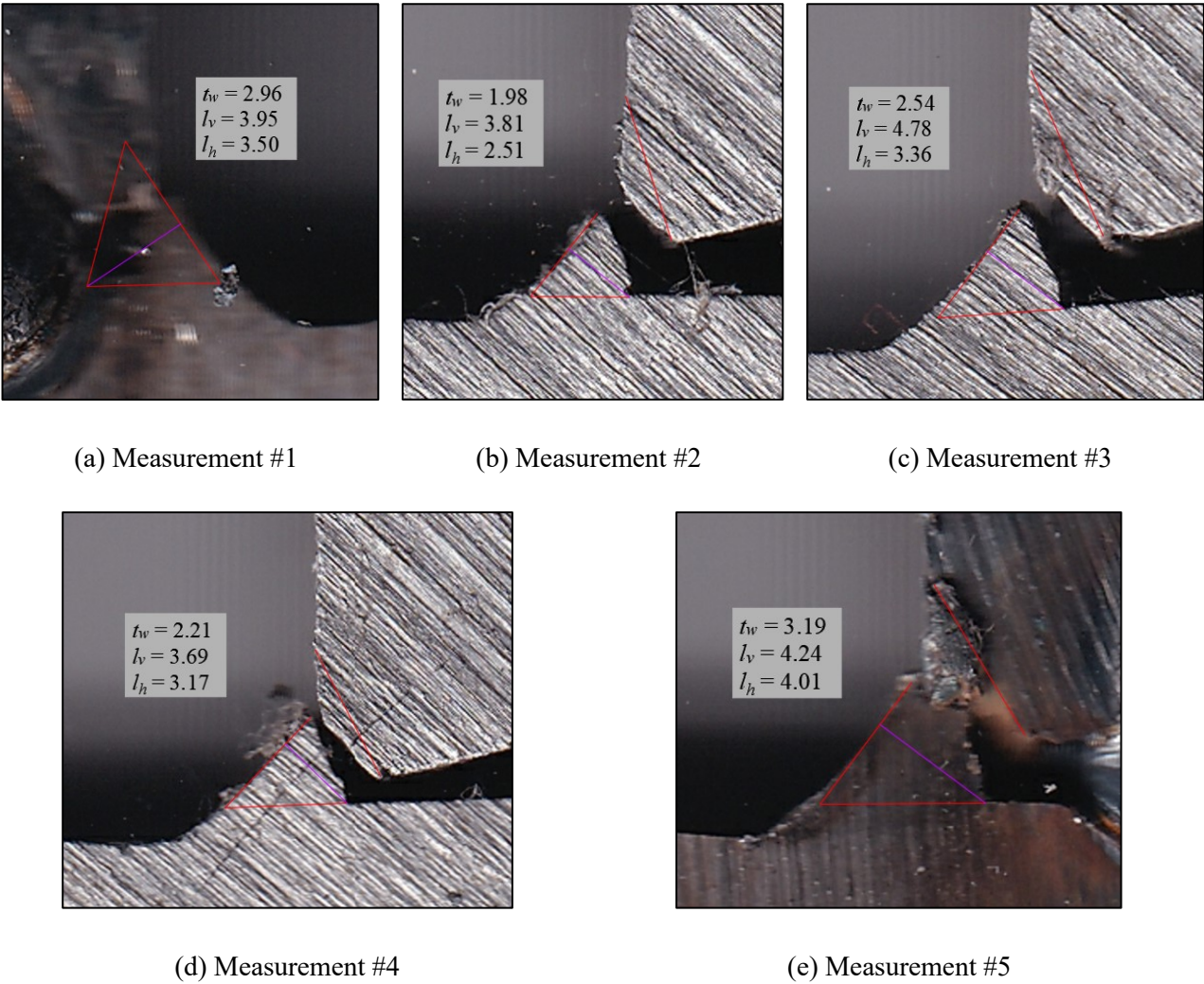
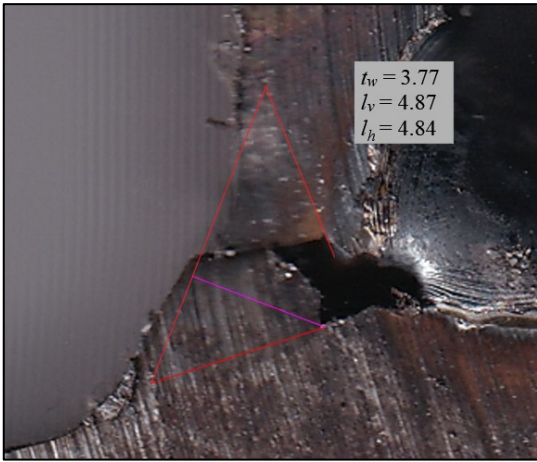
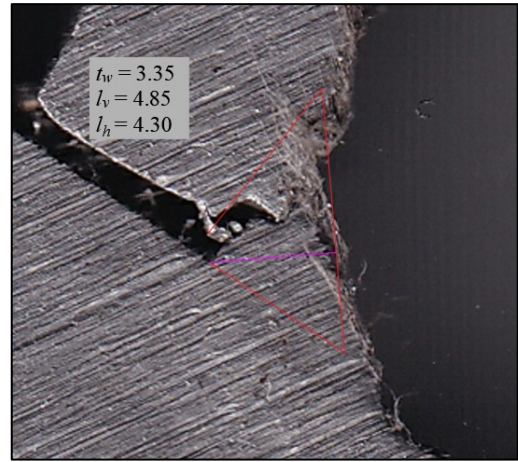


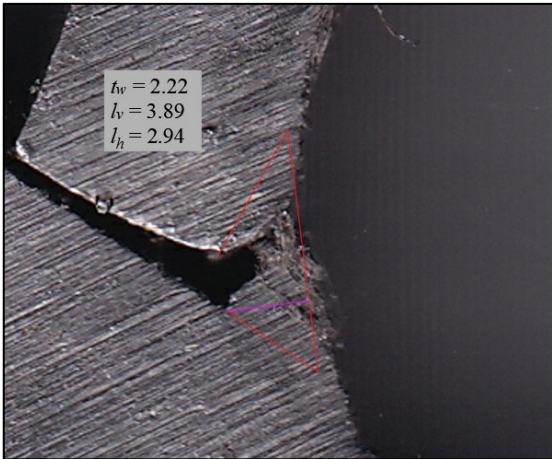
Fig. G.1. Macro-etch examinations for specimen S6-S-30a



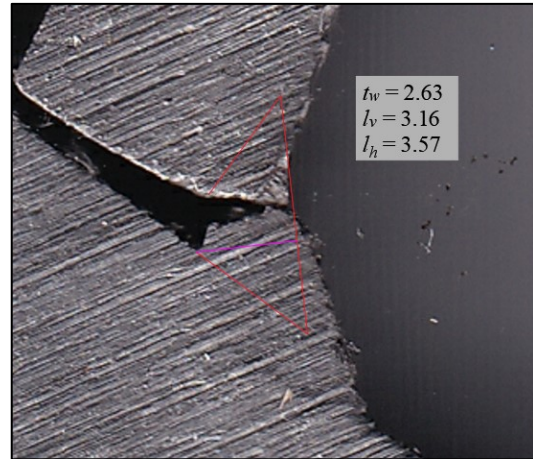
(a) Measurement #1



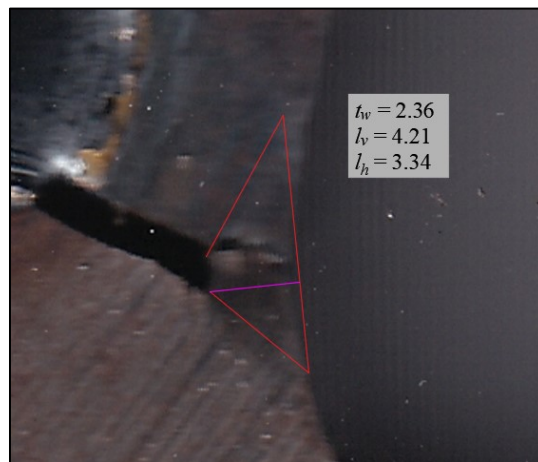
(b) Measurement #2



(c) Measurement #3

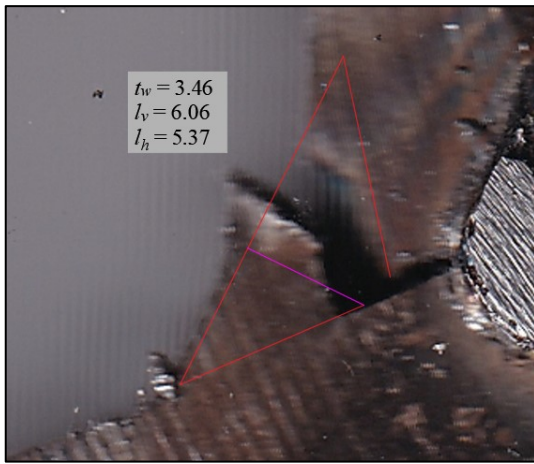


(d) Measurement #4

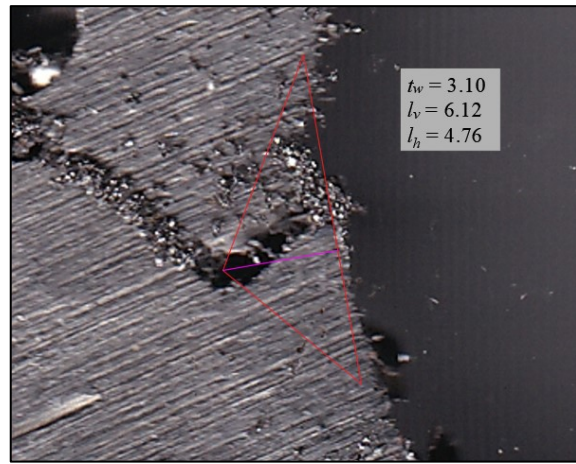


(e) Measurement #5

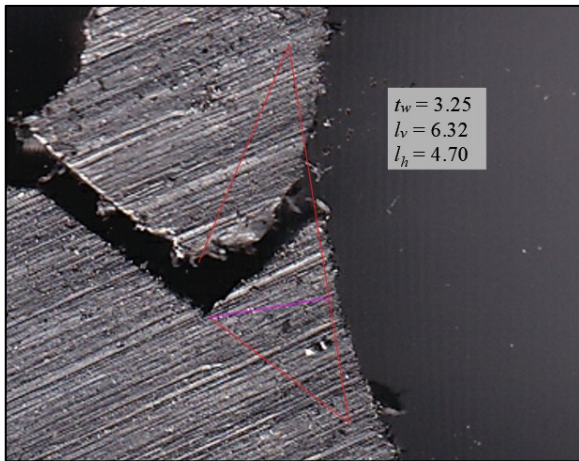
Fig. G.2. Macro-etch examinations for specimen S6-M-30a



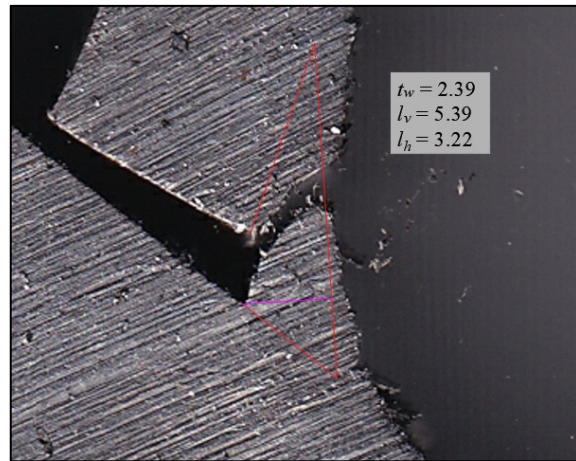
(a) Measurement #1



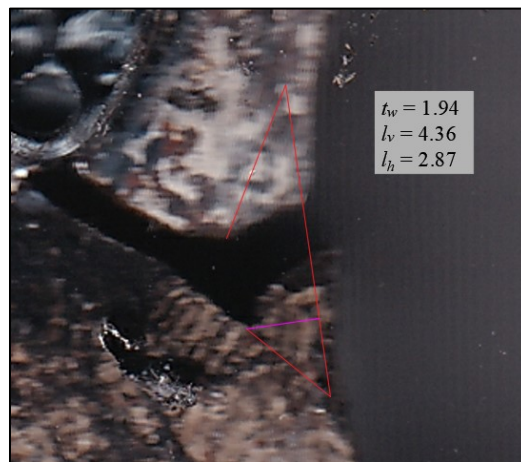
(b) Measurement #2



(c) Measurement #3

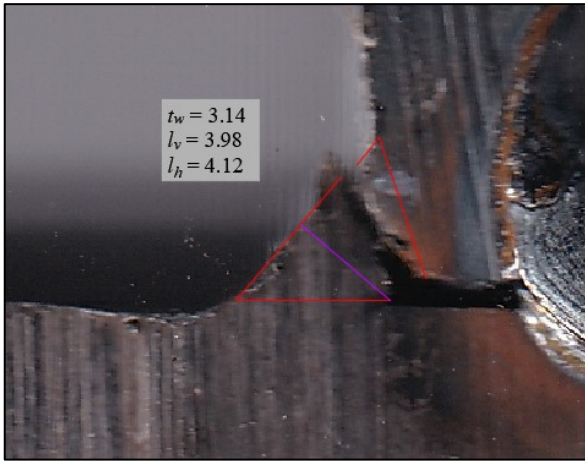


(d) Measurement #4

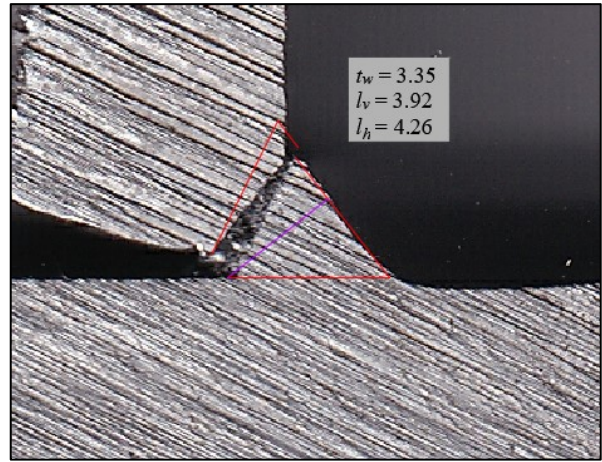


(e) Measurement #5

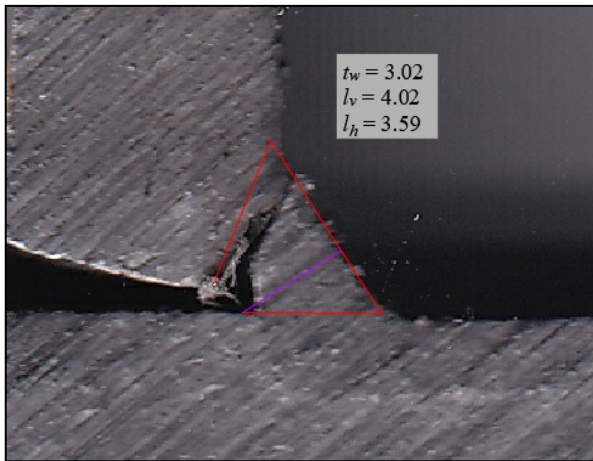
Fig. G.3. Macro-etch examinations for specimen S6-L-30a



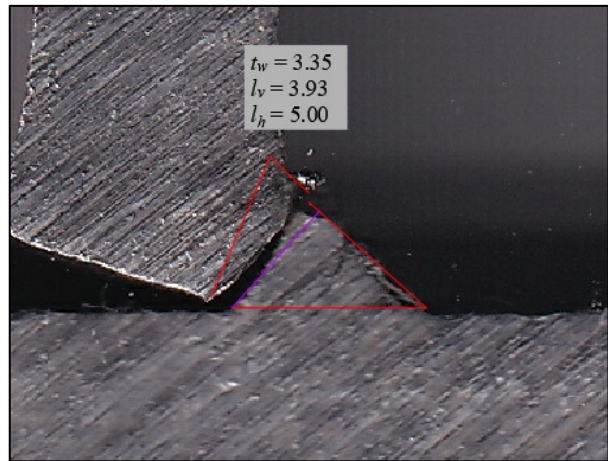
(a) Measurement #1



(b) Measurement #2



(c) Measurement #3

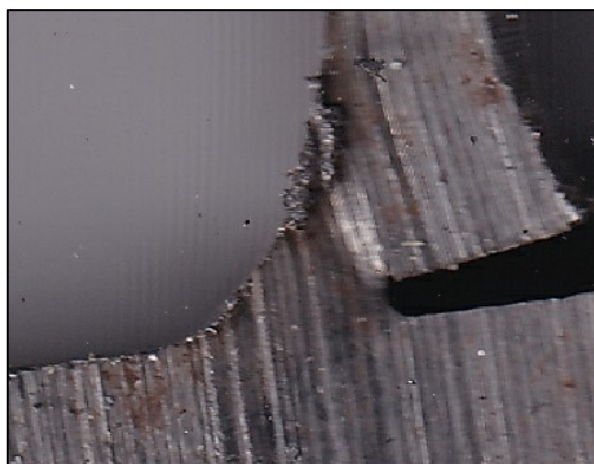


(d) Measurement #4

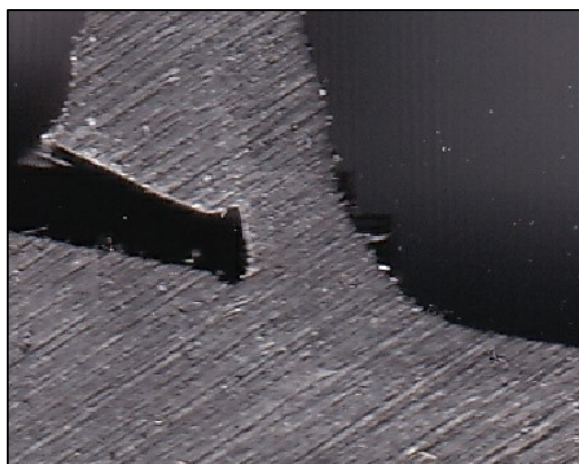


(e) Measurement #5

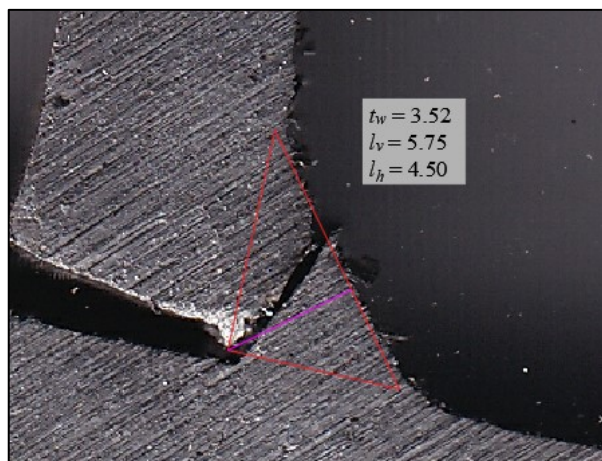
Fig. G.4. Macro-etch examinations for specimen S6-S-15a



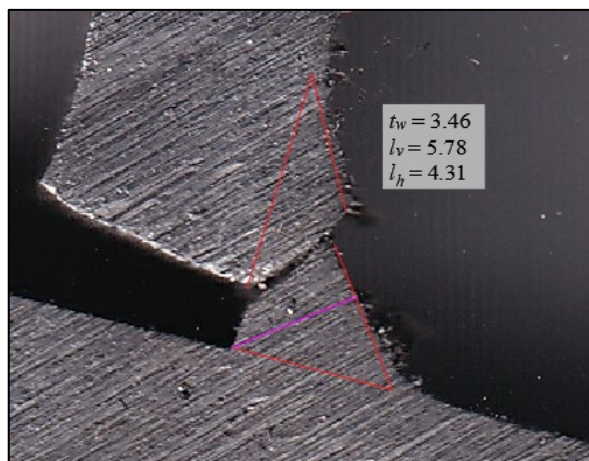
(a) Measurement #1



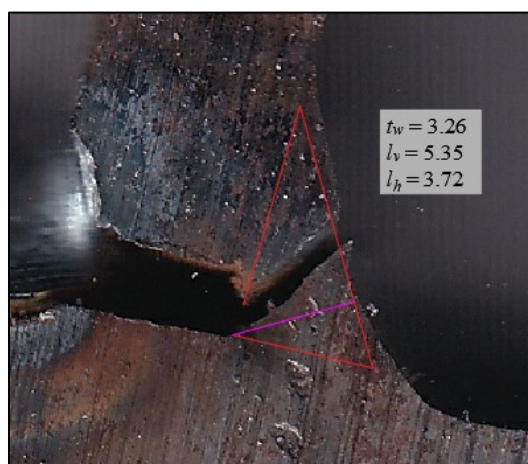
(b) Measurement #2



(c) Measurement #3

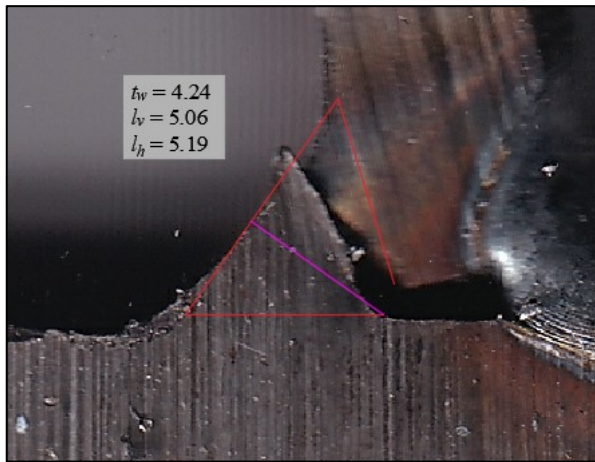


(d) Measurement #4

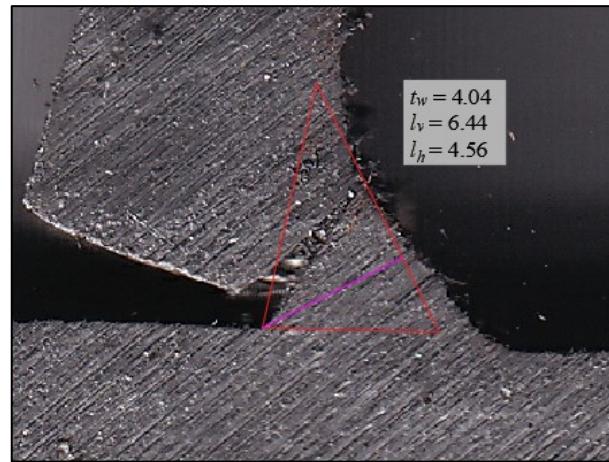


(e) Measurement #5

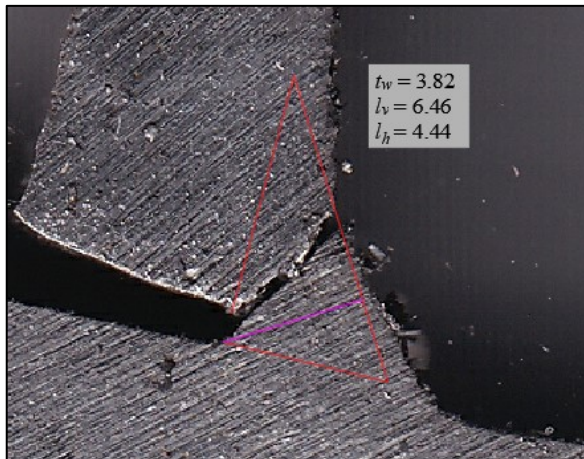
Fig. G.5. Macro-etch examinations for specimen S6-M-15a



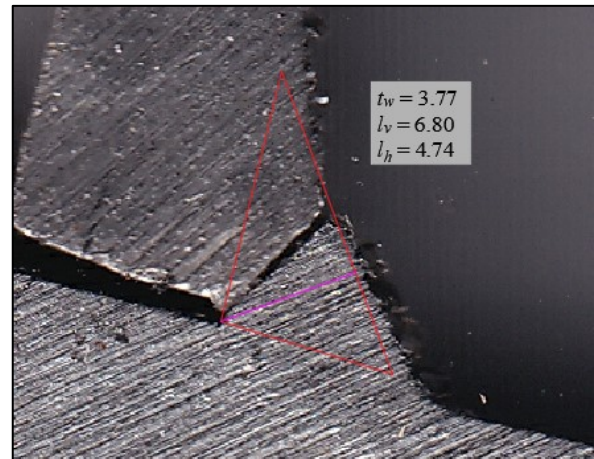
(a) Measurement #1



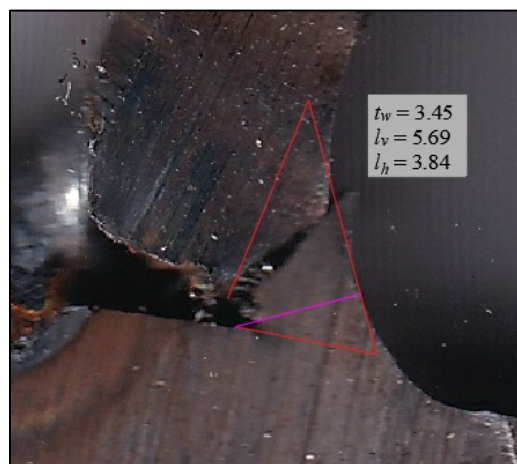
(b) Measurement #2



(c) Measurement #3



(d) Measurement #4

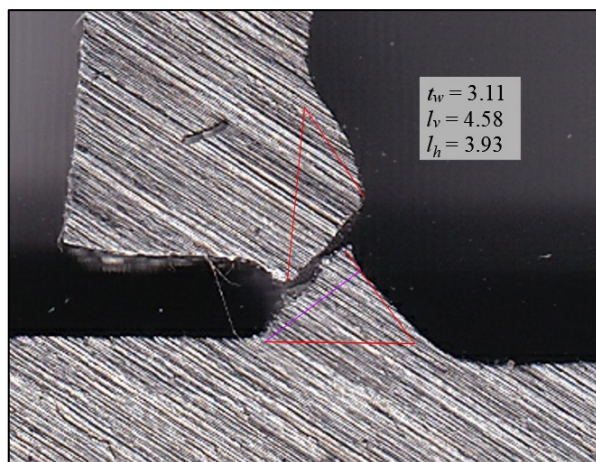


(e) Measurement #5

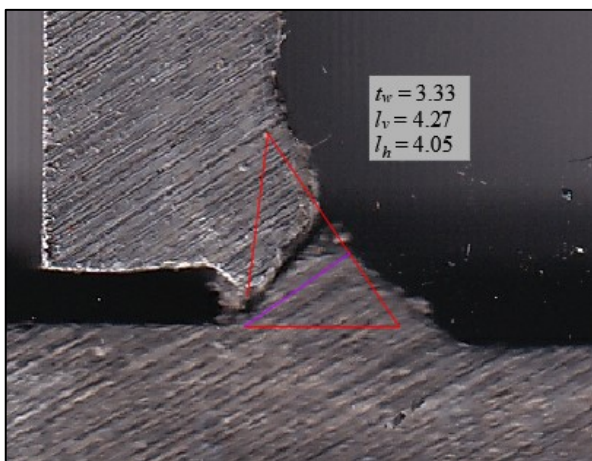
Fig. G.6. Macro-etch examinations for specimen S6-L-15a



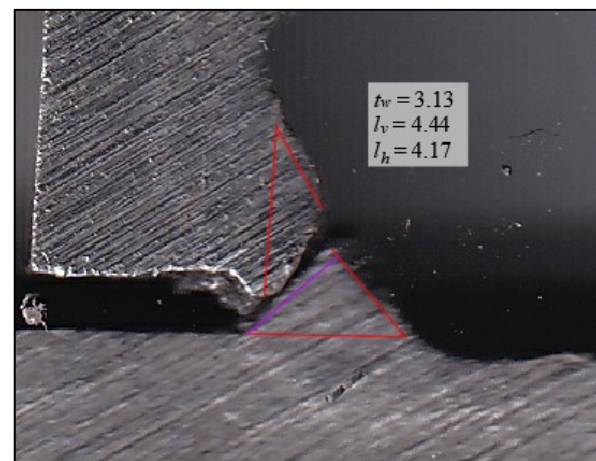
(a) Measurement #1



(b) Measurement #2



(c) Measurement #3

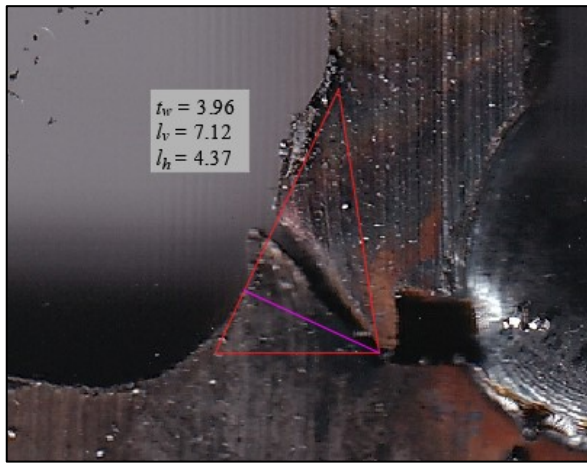


(d) Measurement #4

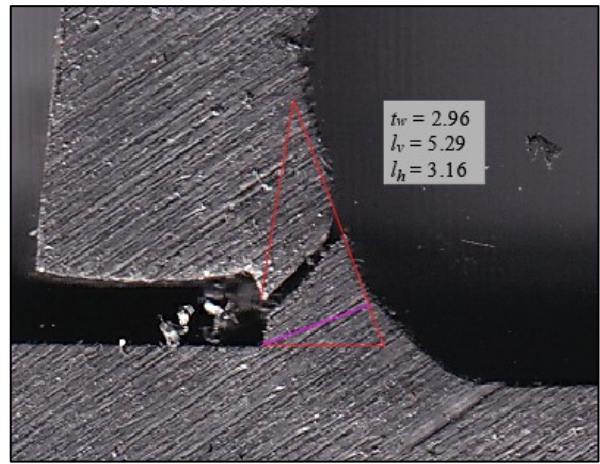


(e) Measurement #5

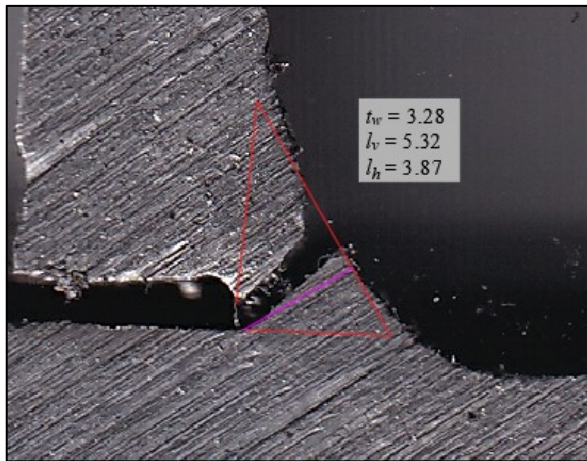
Fig. G.7. Macro-etch examinations for specimen S6-S-0



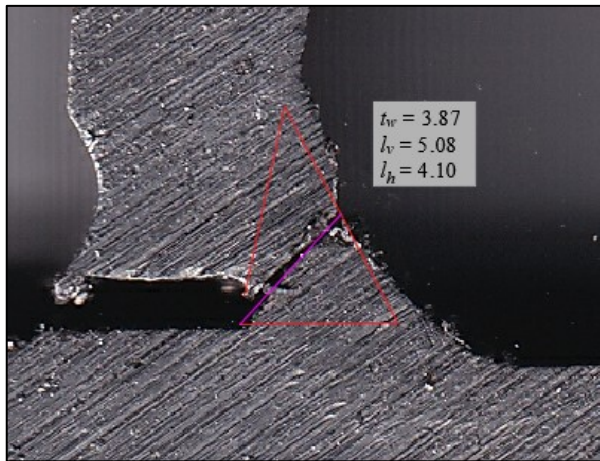
(a) Measurement #1



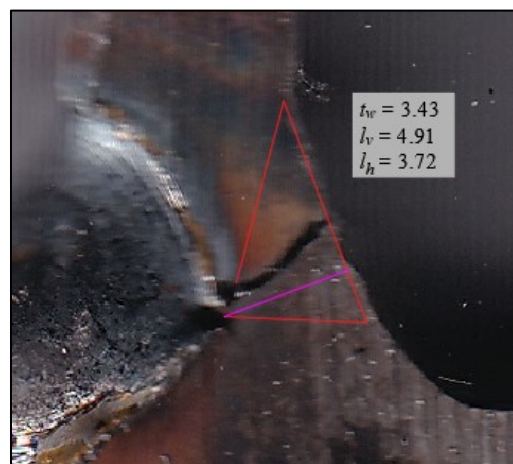
(b) Measurement #2



(c) Measurement #3

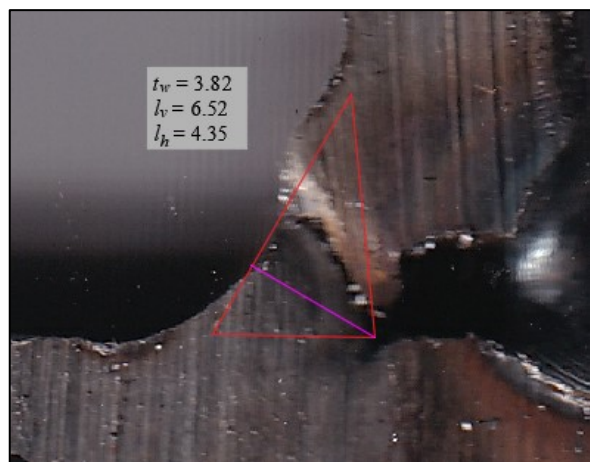


(d) Measurement #4

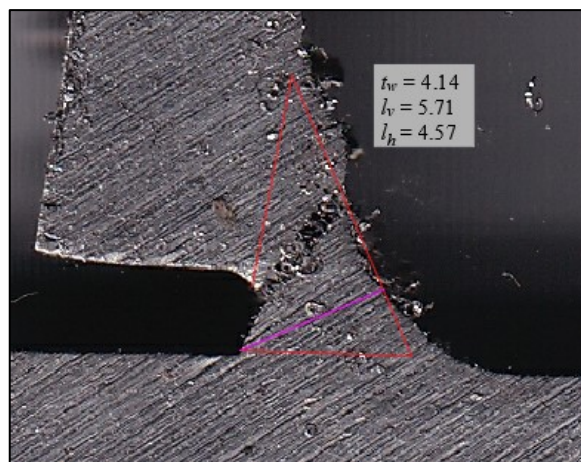


(e) Measurement #5

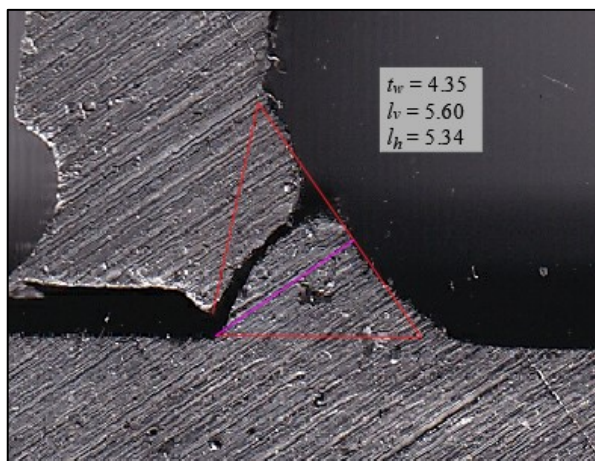
Fig. G.8. Macro-etch examinations for specimen S6-M-0



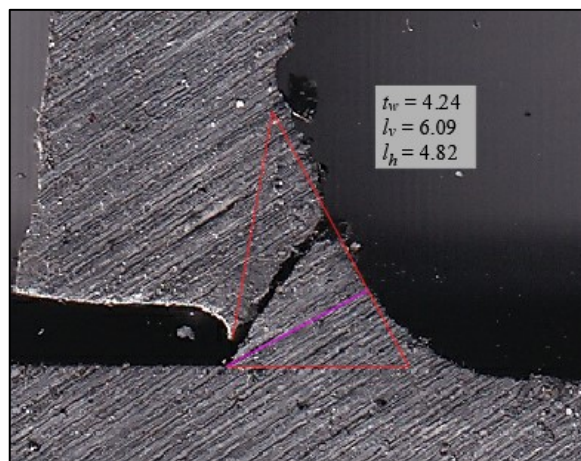
(a) Measurement #1



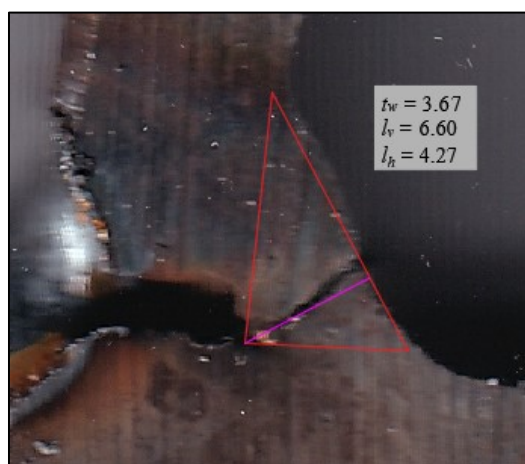
(b) Measurement #2



(c) Measurement #3

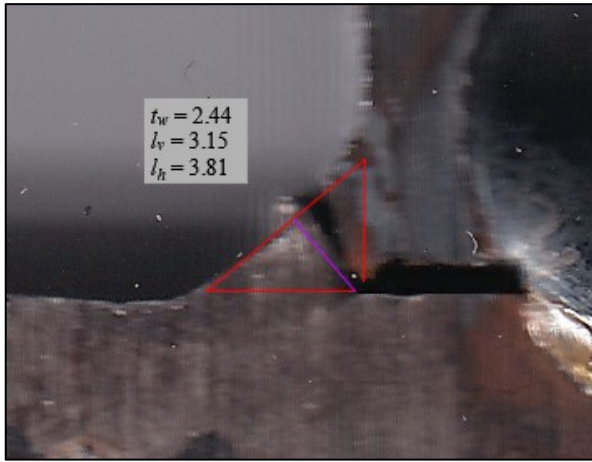


(d) Measurement #4

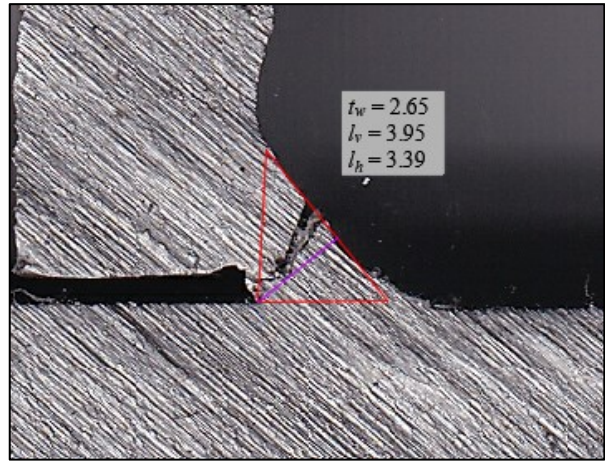


(e) Measurement #5

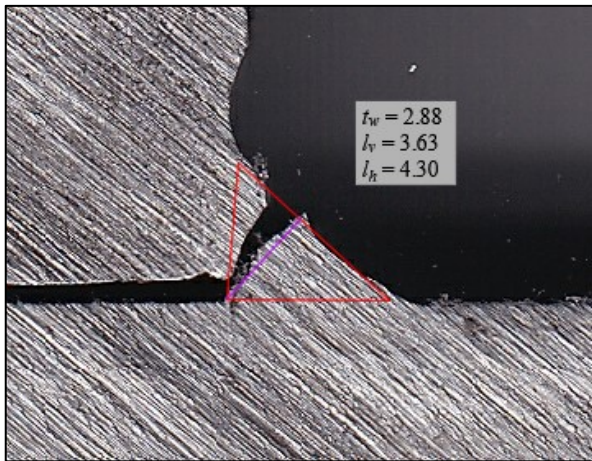
Fig. G.9. Macro-etch examinations for specimen S6-L-0



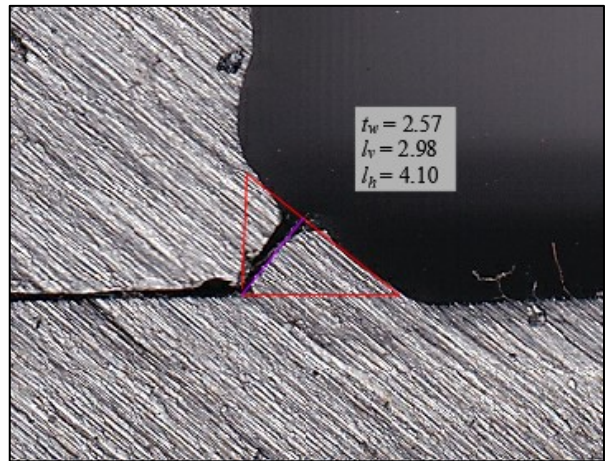
(a) Measurement #1



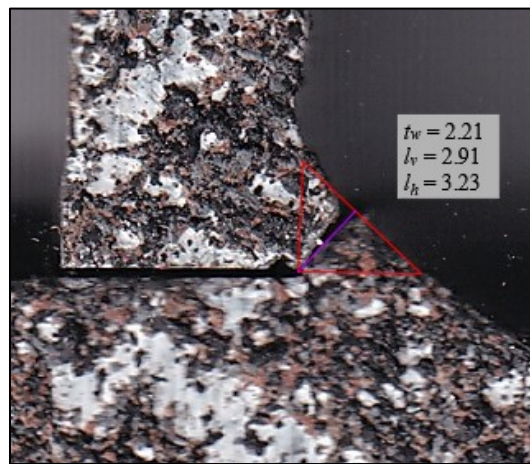
(b) Measurement #2



(c) Measurement #3

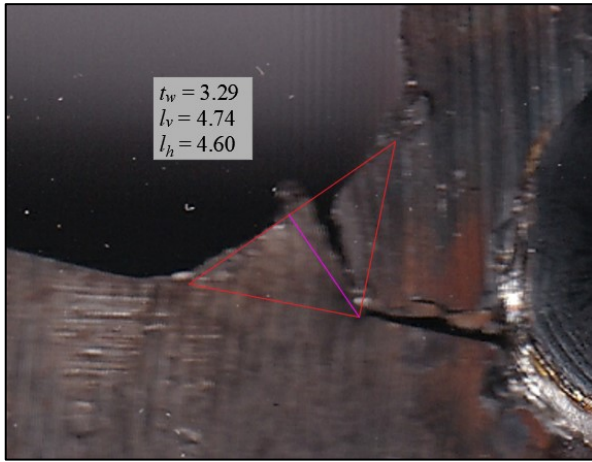


(d) Measurement #4

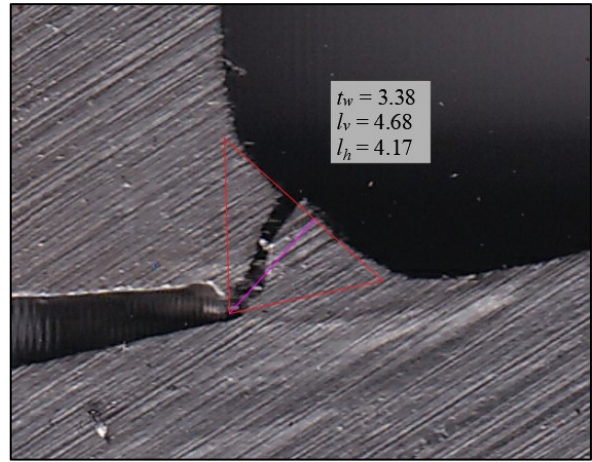


(e) Measurement #5

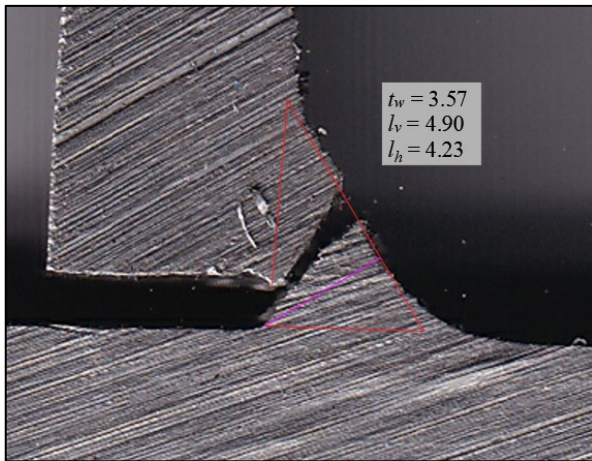
Fig. G.10. Macro-etch examinations for specimen S6-S-15b



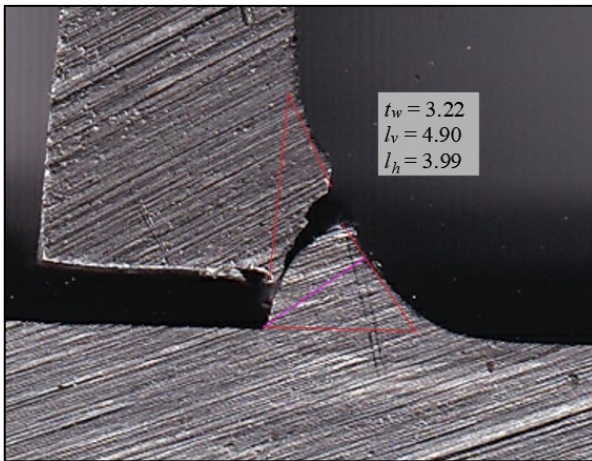
(a) Measurement #1



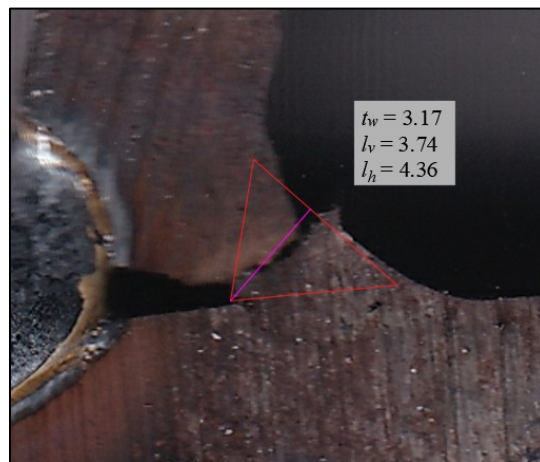
(b) Measurement #2



(c) Measurement #3

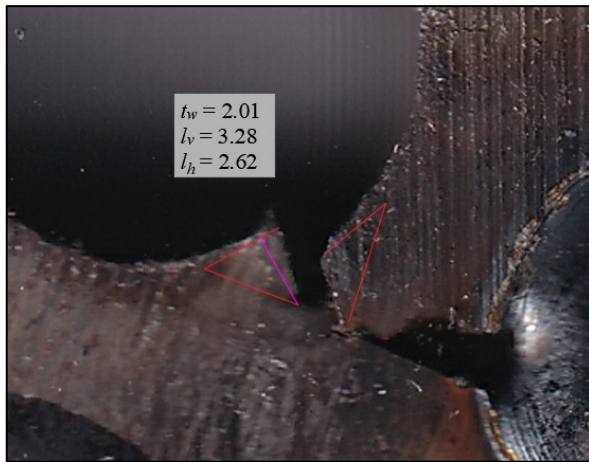


(d) Measurement #4

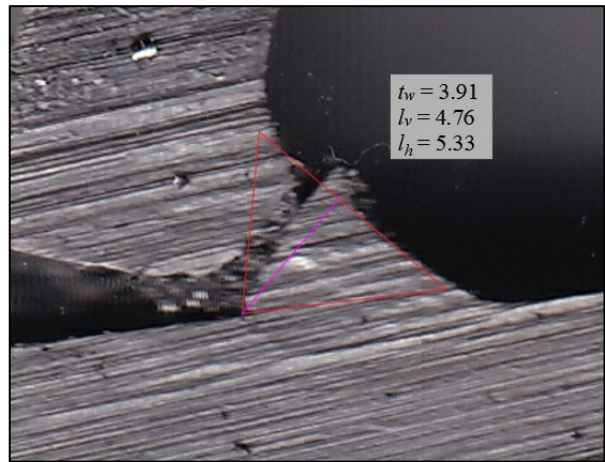


(e) Measurement #5

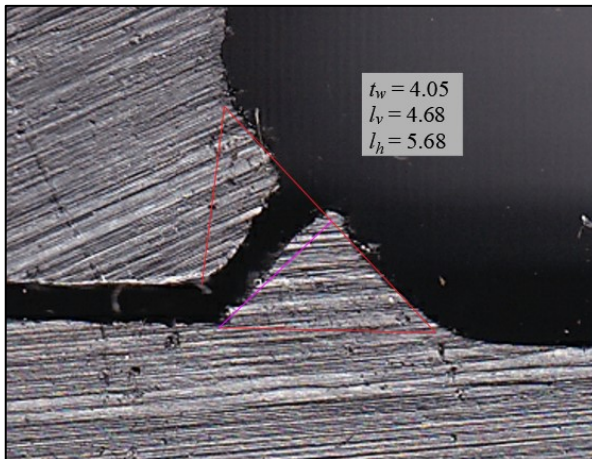
Fig. G.11. Macro-etch examinations for specimen S6-M-15b



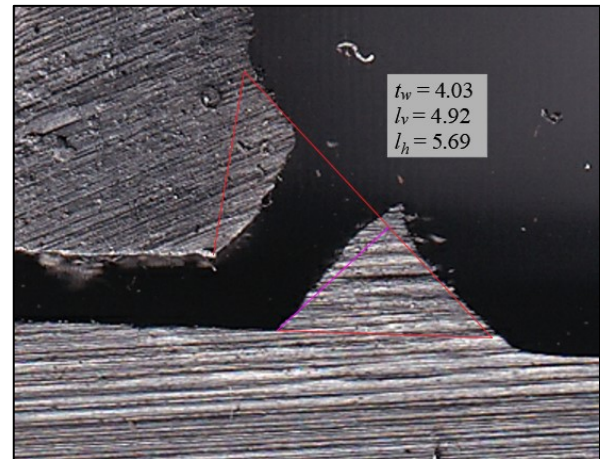
(a) Measurement #1



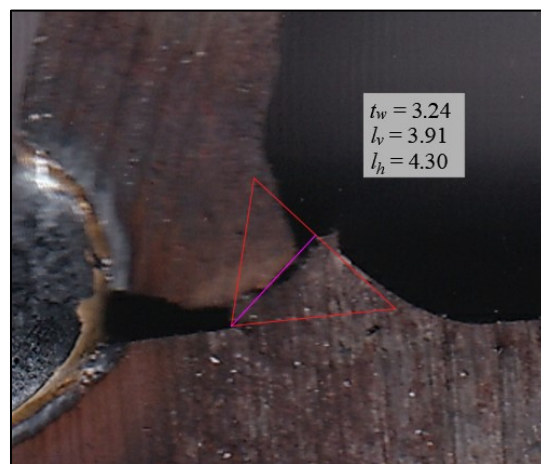
(b) Measurement #2



(c) Measurement #3

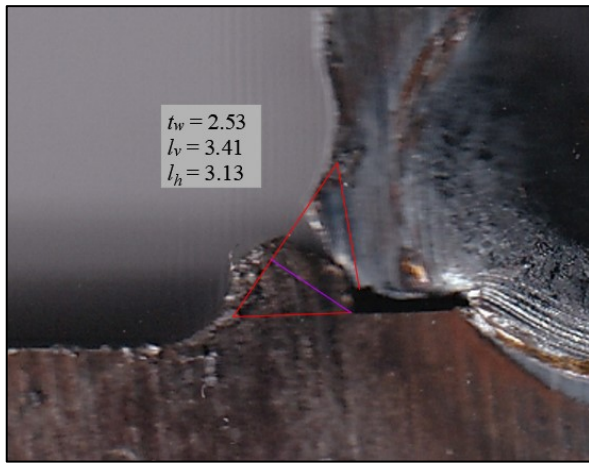


(d) Measurement #4

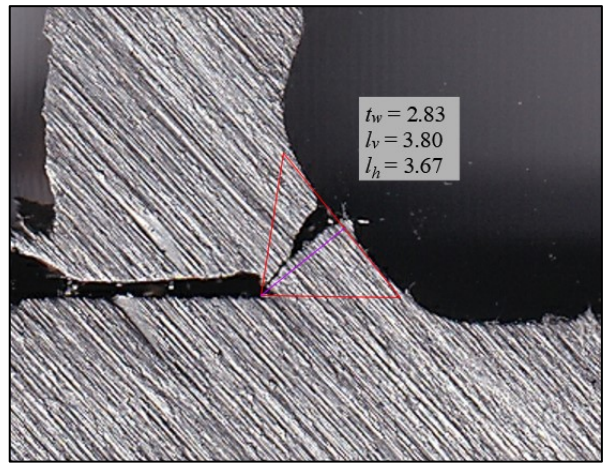


(e) Measurement #5

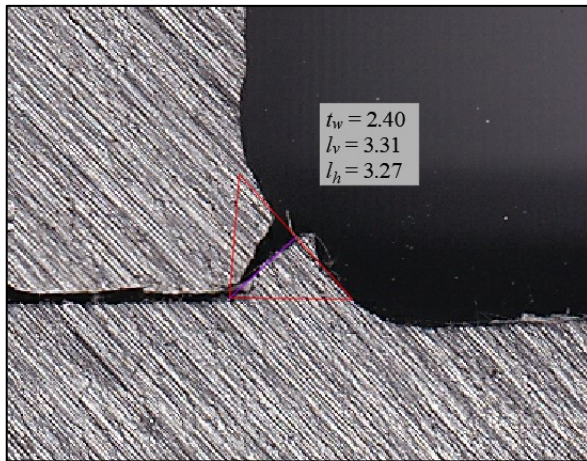
Fig. G.12. Macro-etch examinations for specimen S6-L-15b



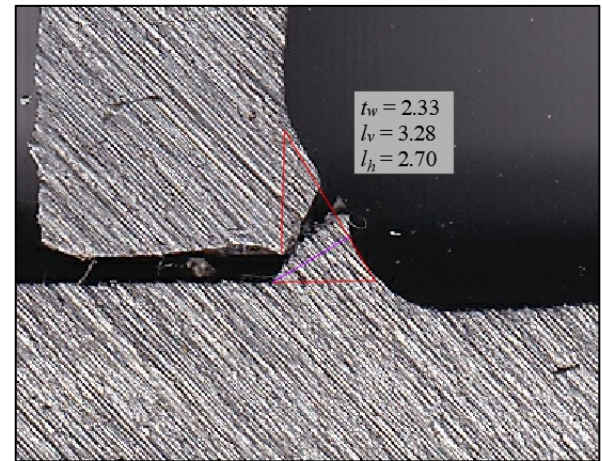
(a) Measurement #1



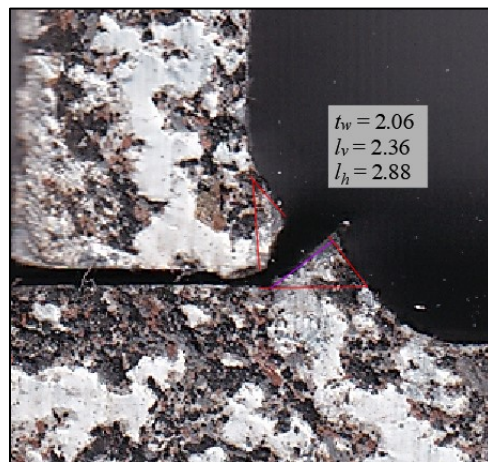
(b) Measurement #2



(c) Measurement #3

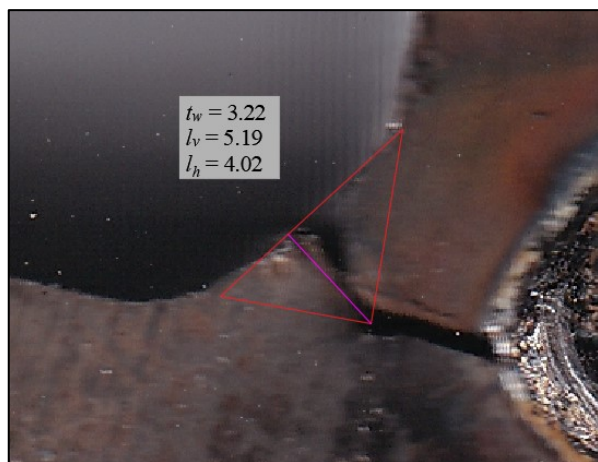


(d) Measurement #4

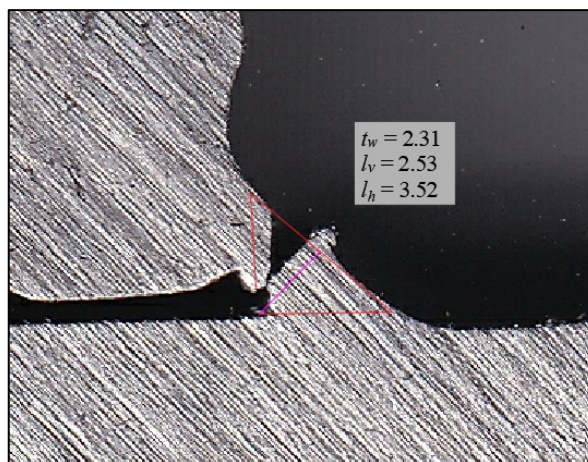


(e) Measurement #5

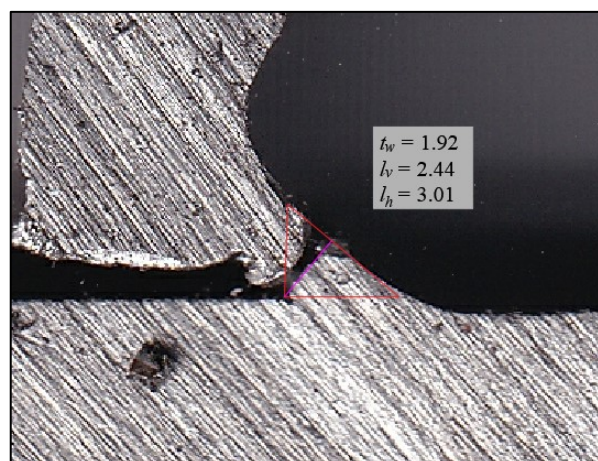
Fig. G.13. Macro-etch examinations for specimen S6-S-30b



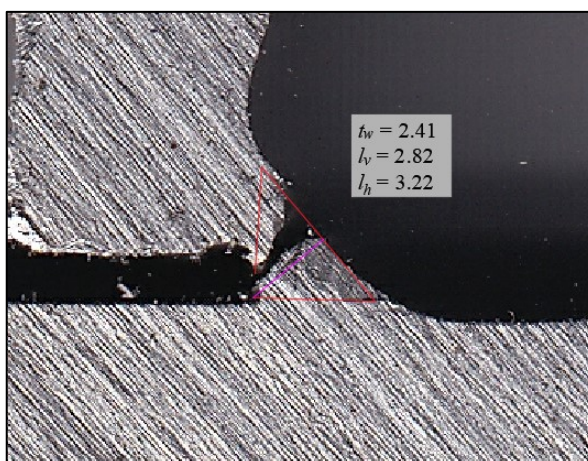
(a) Measurement #1



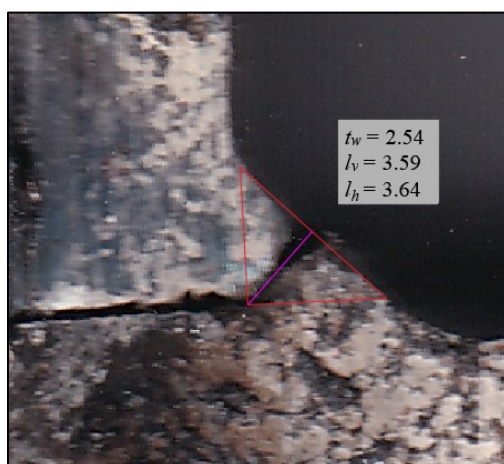
(b) Measurement #2



(c) Measurement #3

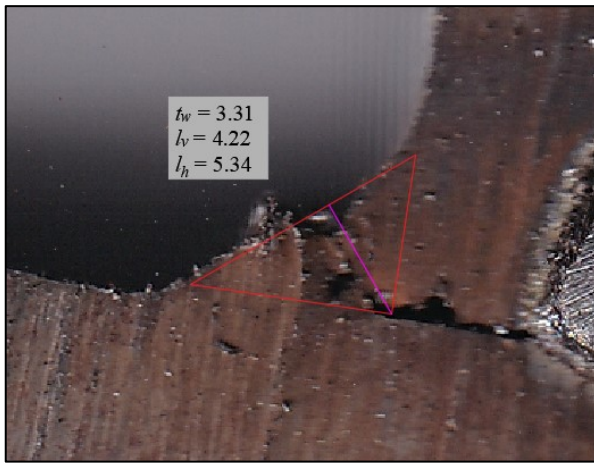


(d) Measurement #4

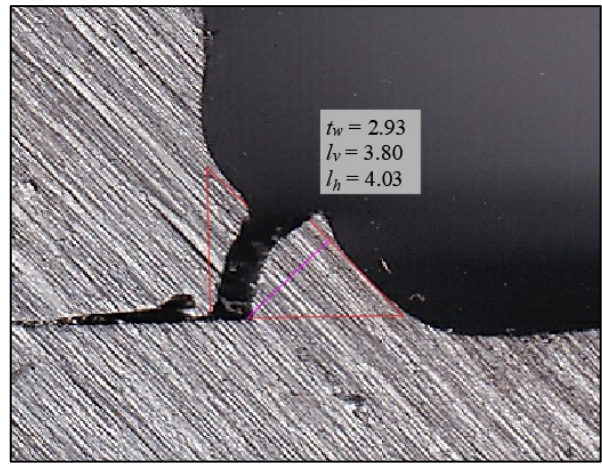


(e) Measurement #5

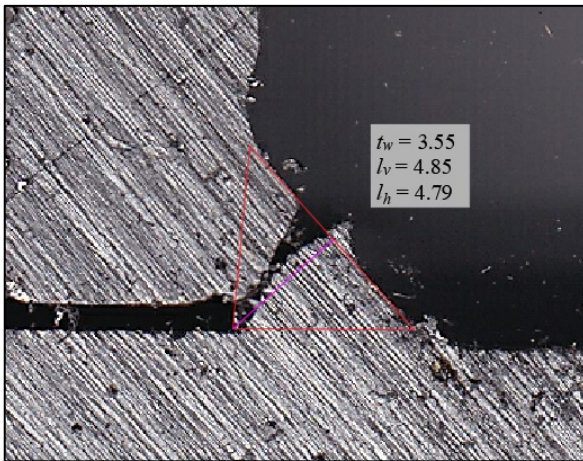
Fig. G.14. Macro-etch examinations for specimen S6-M-30b



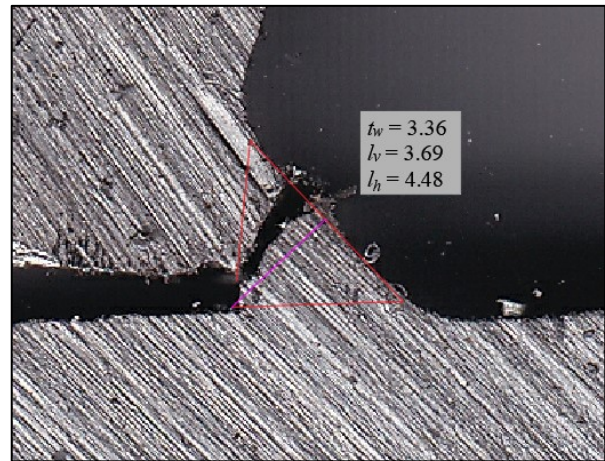
(a) Measurement #1



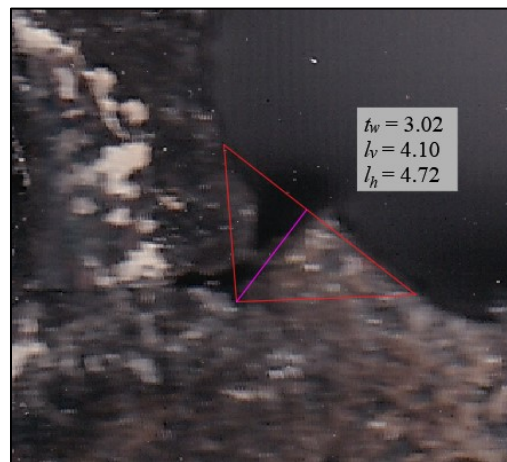
(b) Measurement #2



(c) Measurement #3

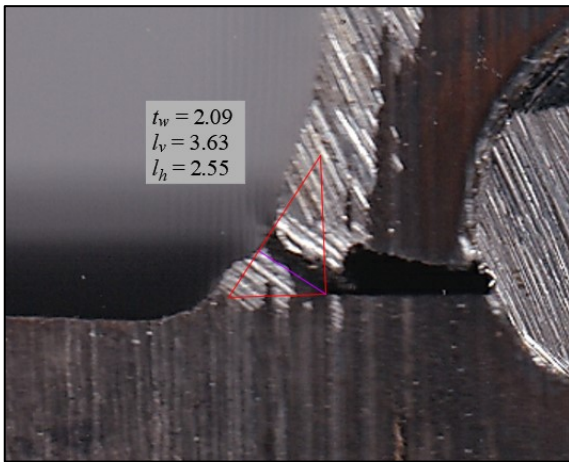


(d) Measurement #4

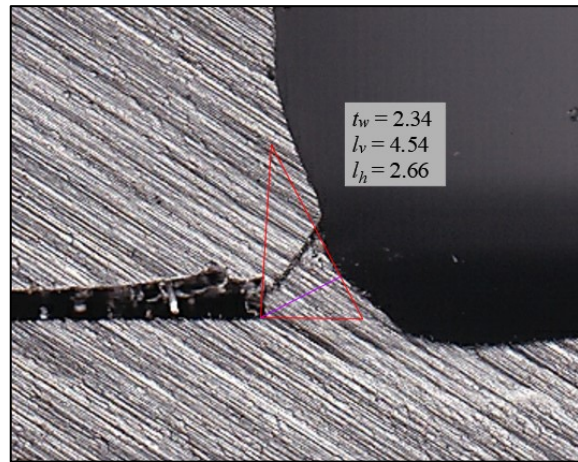


(e) Measurement #5

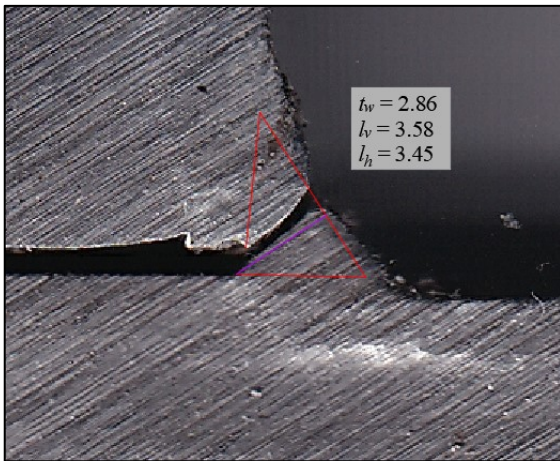
Fig. G.15. Macro-etch examinations for specimen S6-L-30b



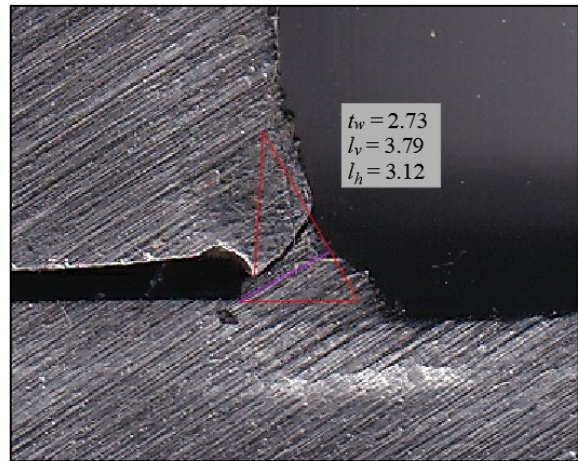
(a) Measurement #1



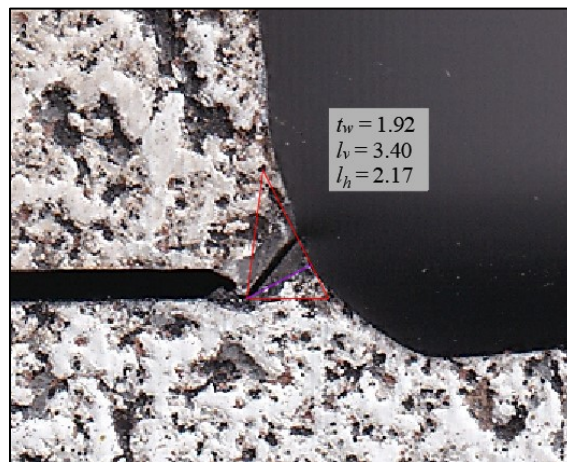
(b) Measurement #2



(c) Measurement #3

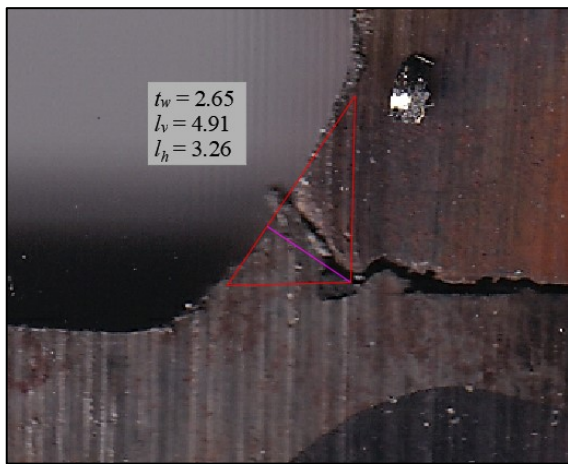


(d) Measurement #4

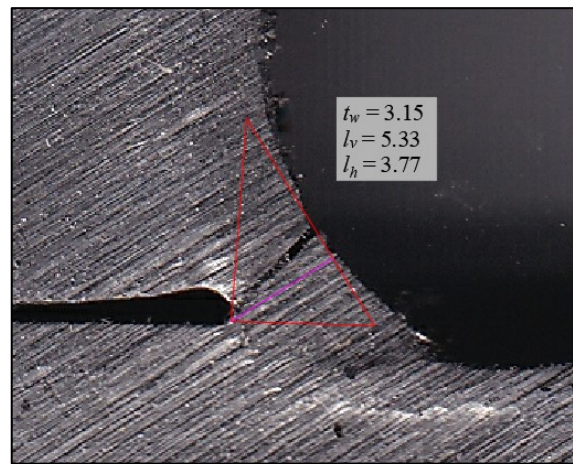


(e) Measurement #5

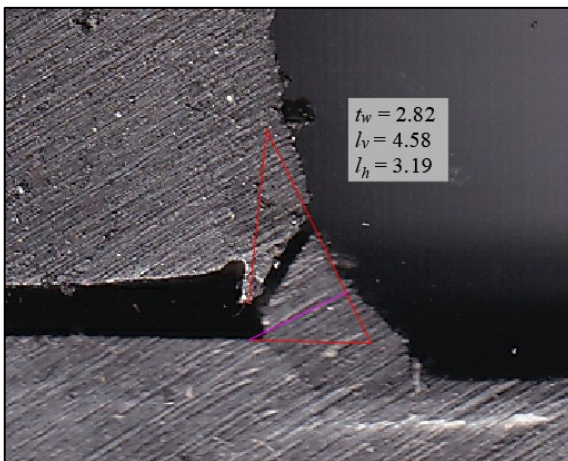
Fig. G.16. Macro-etch examinations for specimen S9-XS-0



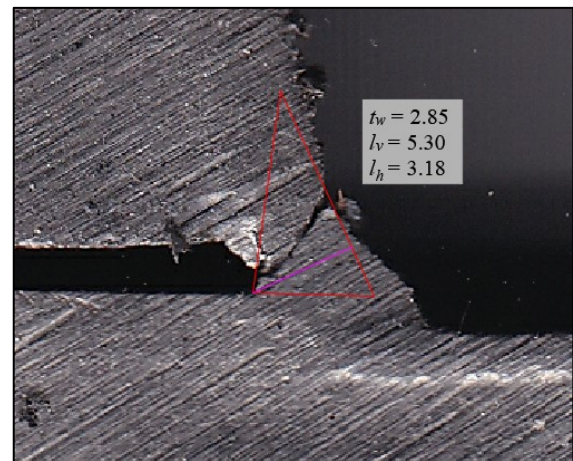
(a) Measurement #1



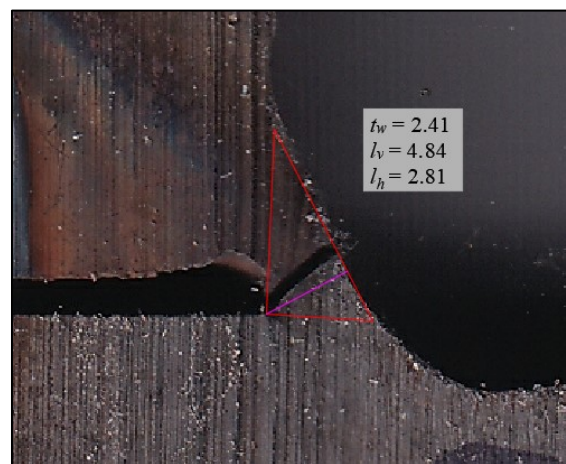
(b) Measurement #2



(c) Measurement #3

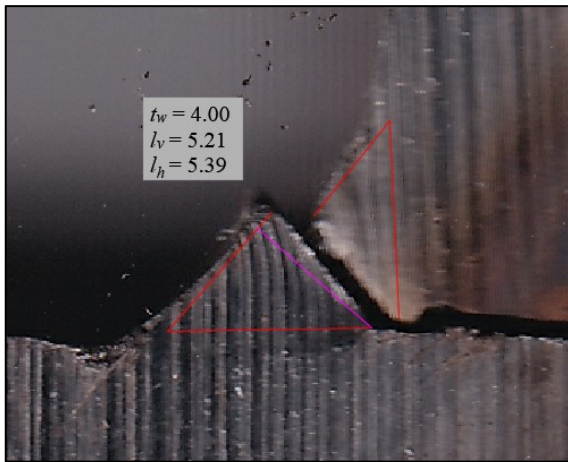


(d) Measurement #4

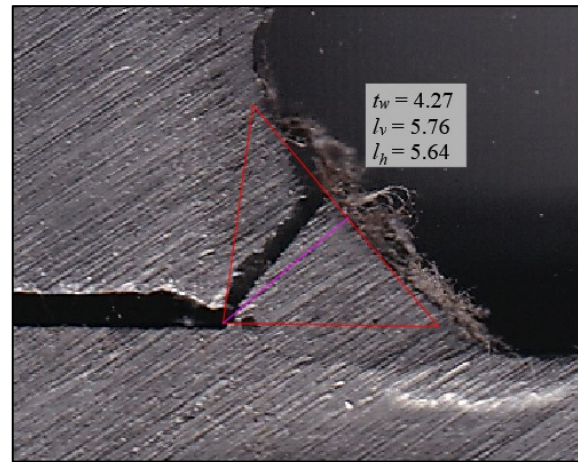


(e) Measurement #5

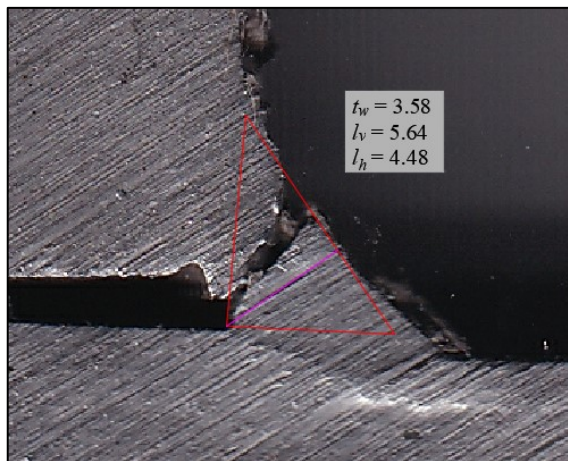
Fig. G.17. Macro-etch examinations for specimen S9-S-0



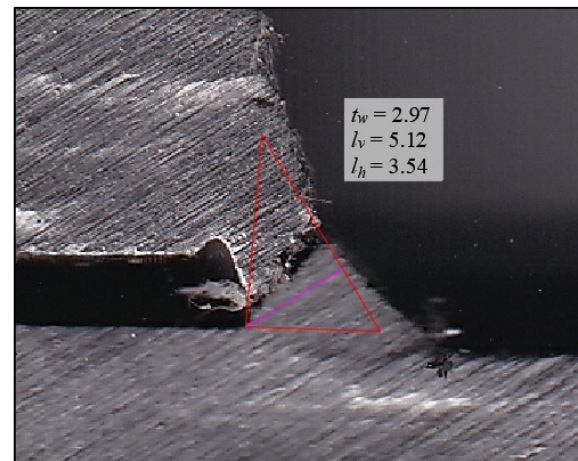
(a) Measurement #1



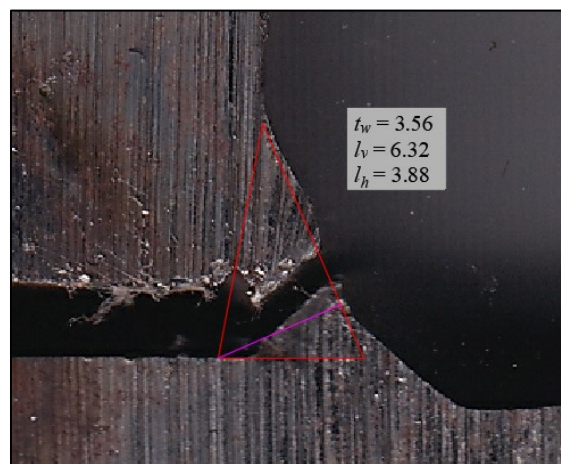
(b) Measurement #2



(c) Measurement #3

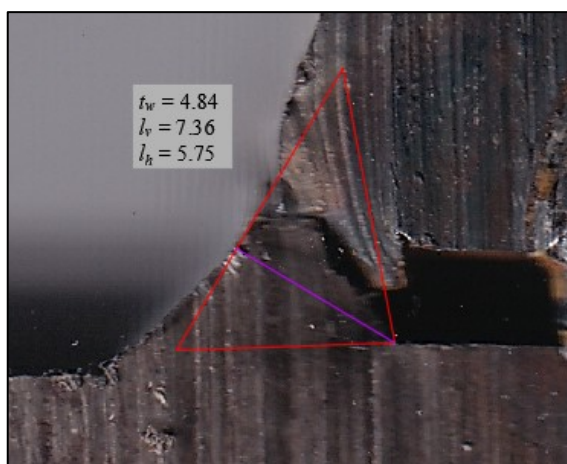


(d) Measurement #4

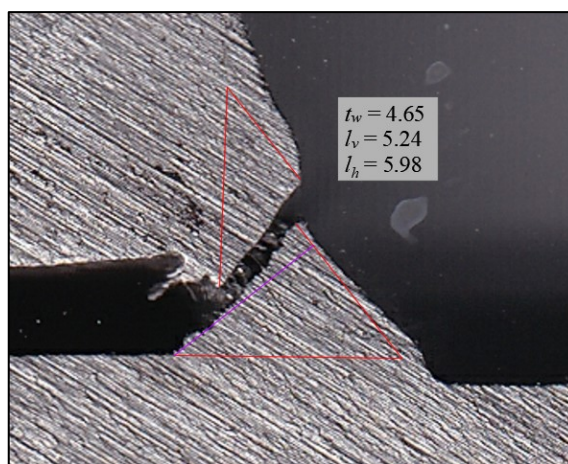


(e) Measurement #5

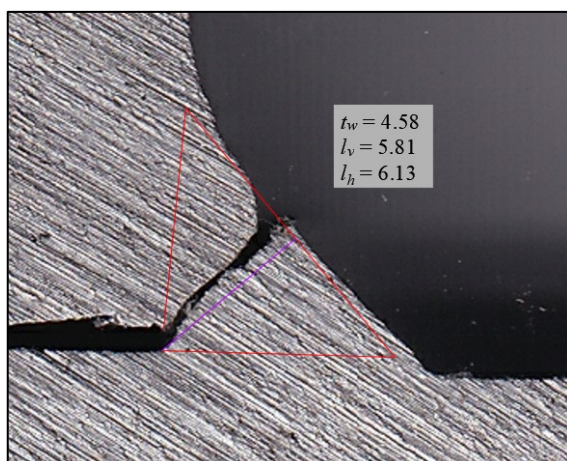
Fig. G.18. Macro-etch examinations for specimen S9-M-0



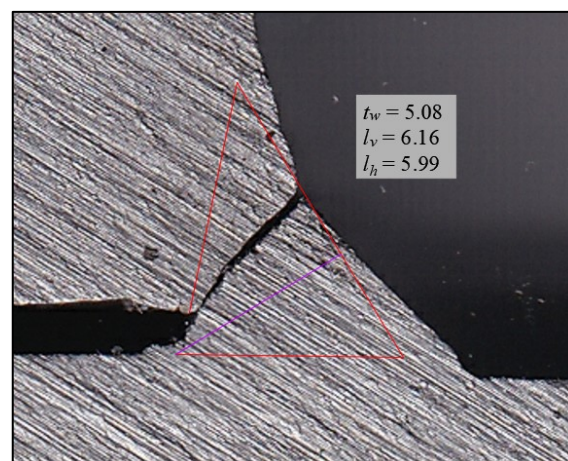
(a) Measurement #1



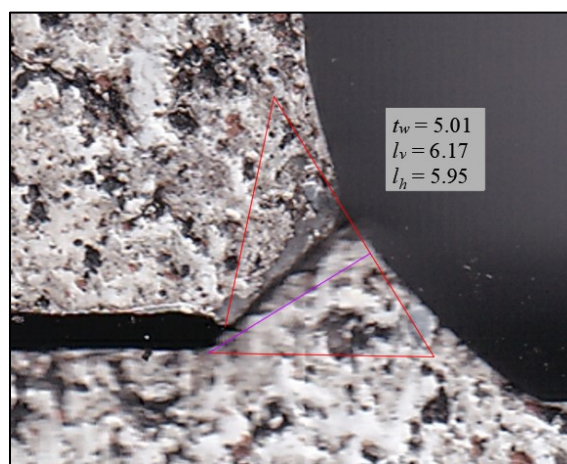
(b) Measurement #2



(c) Measurement #3

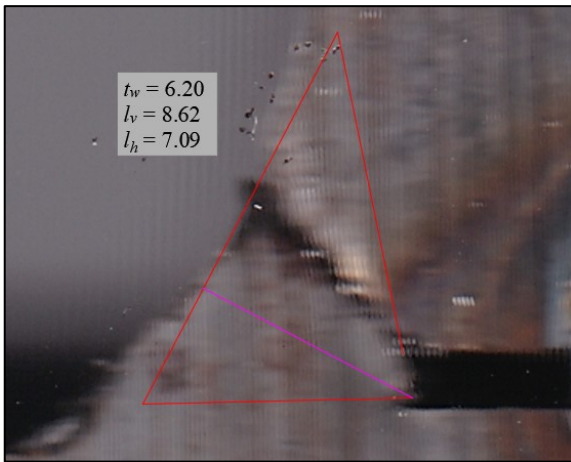


(d) Measurement #4

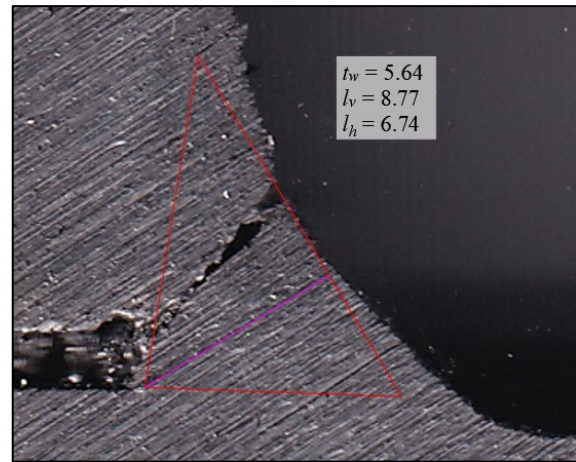


(e) Measurement #5

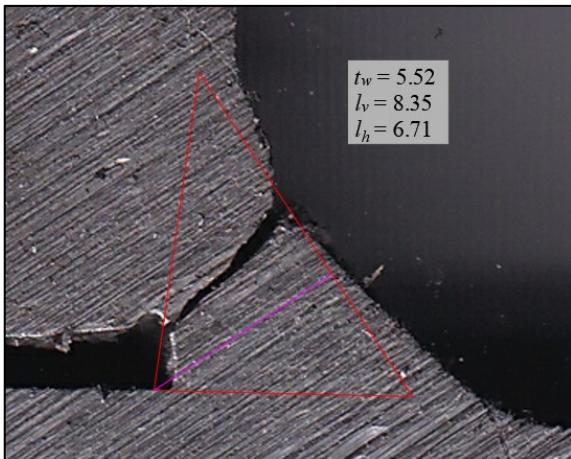
Fig. G.19. Macro-etch examinations for specimen S9-L-0



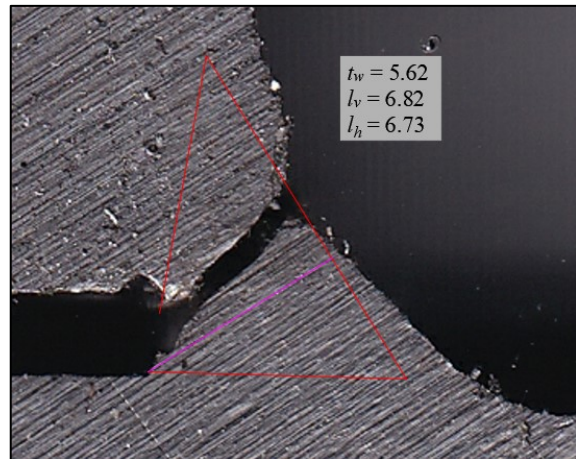
(a) Measurement #1



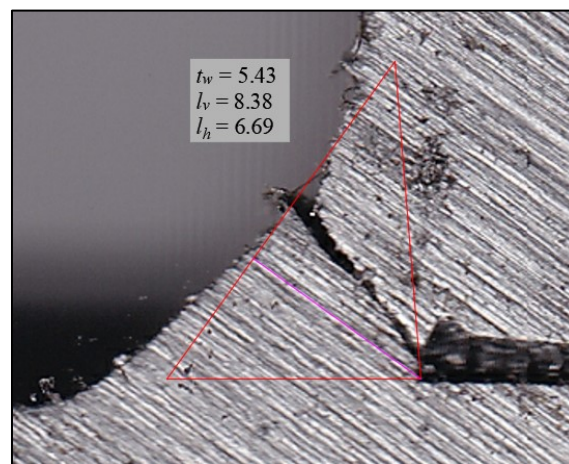
(b) Measurement #2



(c) Measurement #3

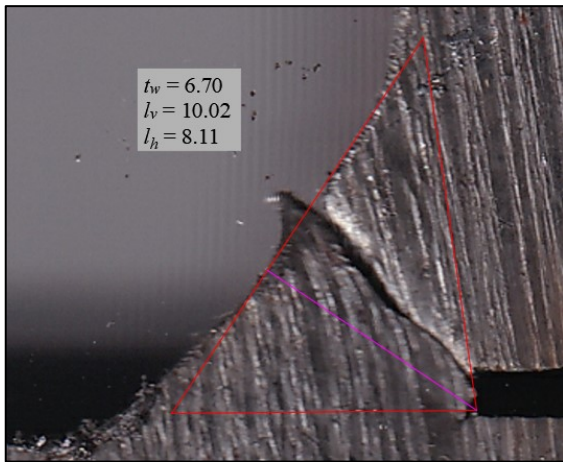


(d) Measurement #4

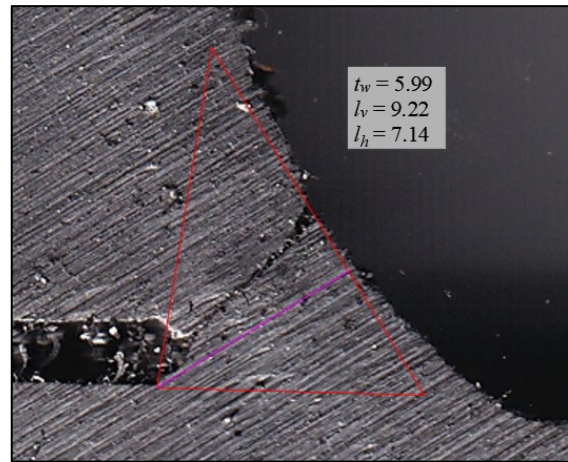


(e) Measurement #5

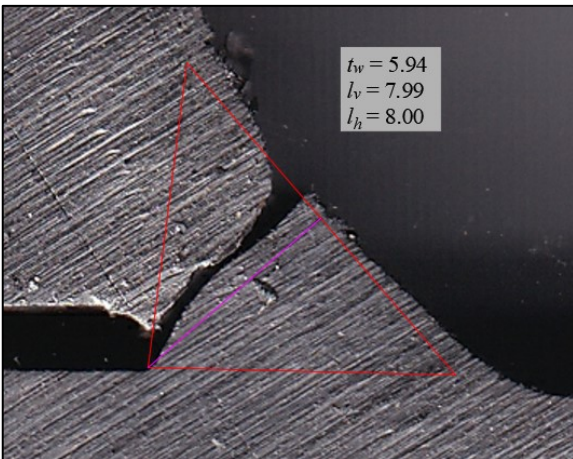
Fig. G.20. Macro-etch examinations for specimen S9-XL-0



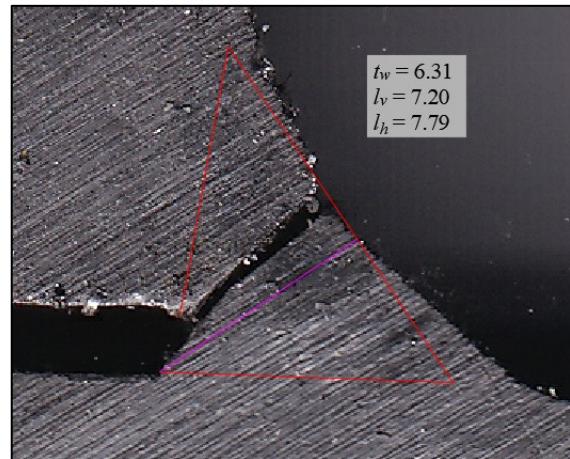
(a) Measurement #1



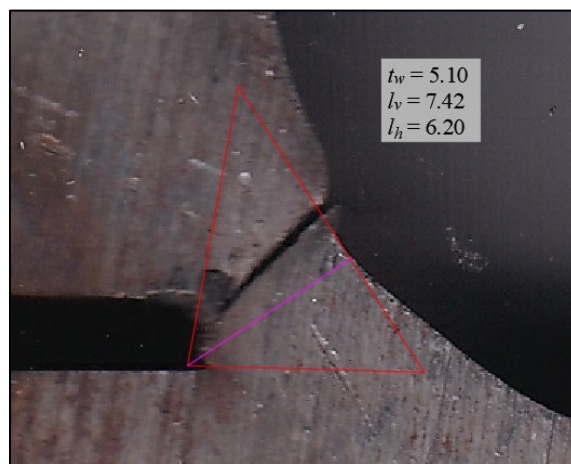
(b) Measurement #2



(c) Measurement #3

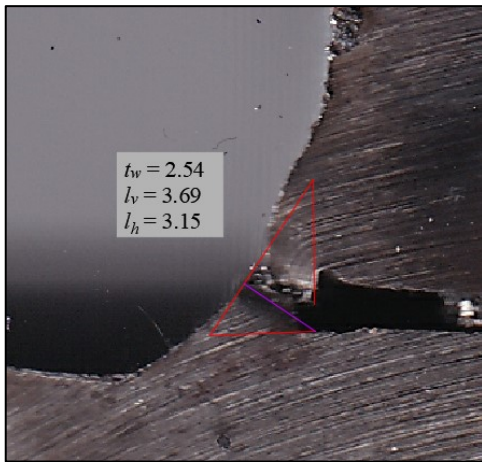


(d) Measurement #4

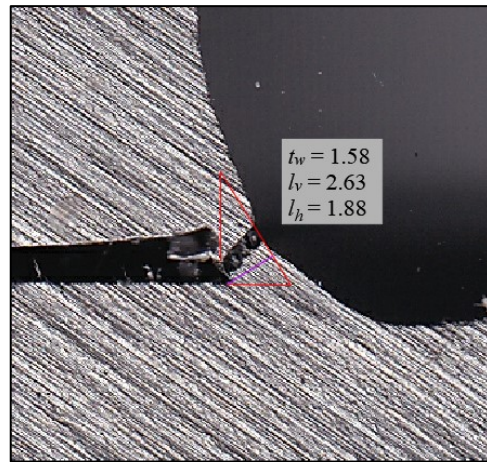


(e) Measurement #5

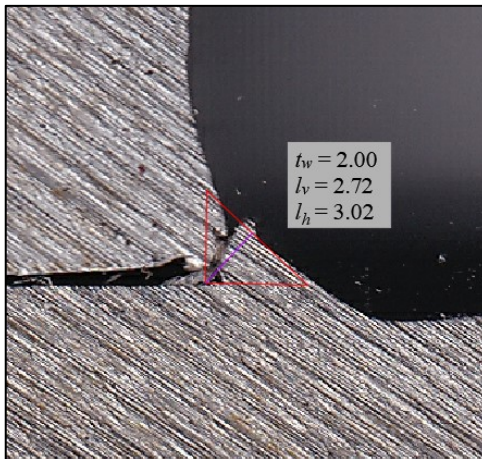
Fig. G.21. Macro-etch examinations for specimen S9-XXL-0



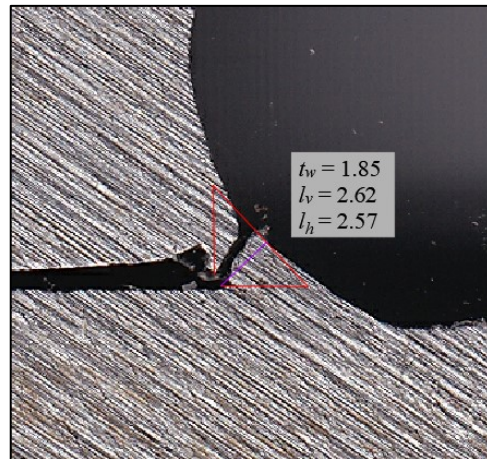
(a) Measurement #1



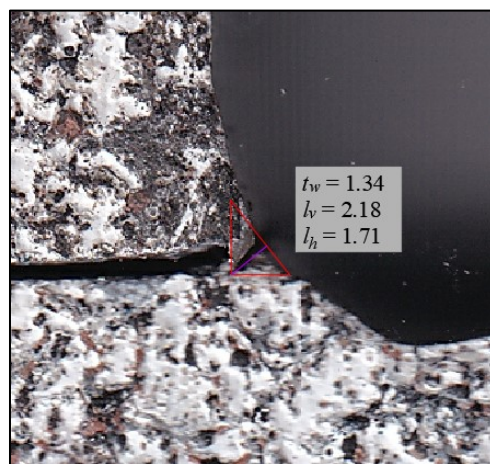
(b) Measurement #2



(c) Measurement #3

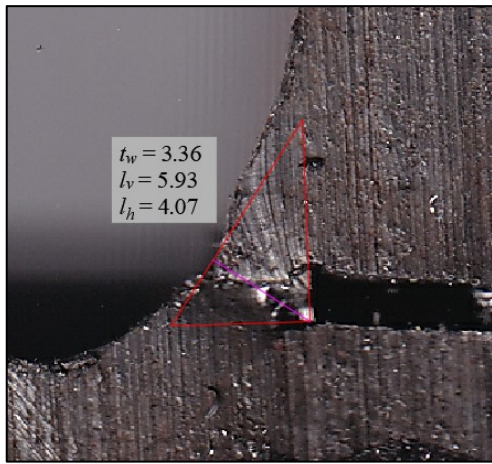


(d) Measurement #4

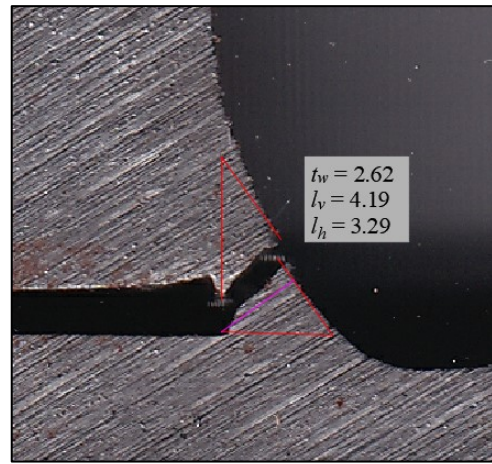


(e) Measurement #5

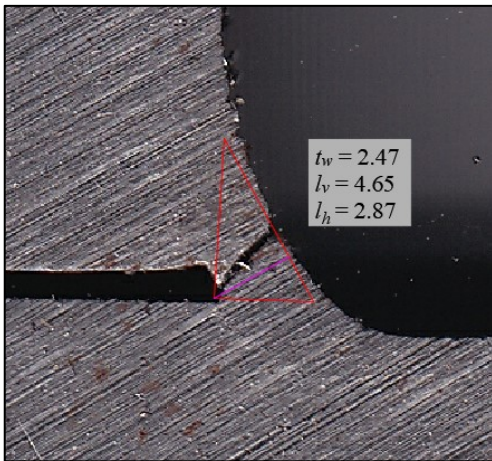
Fig. G.22. Macro-etch examinations for specimen S14-XS-0



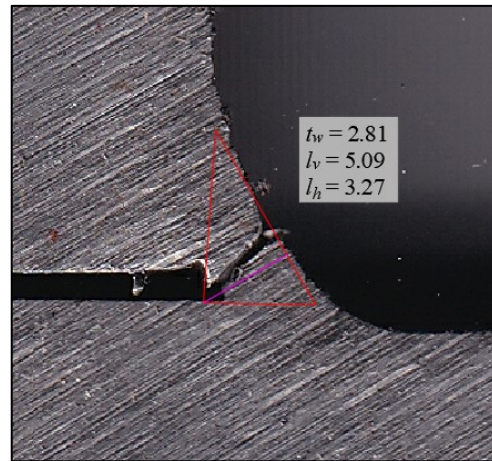
(a) Measurement #1



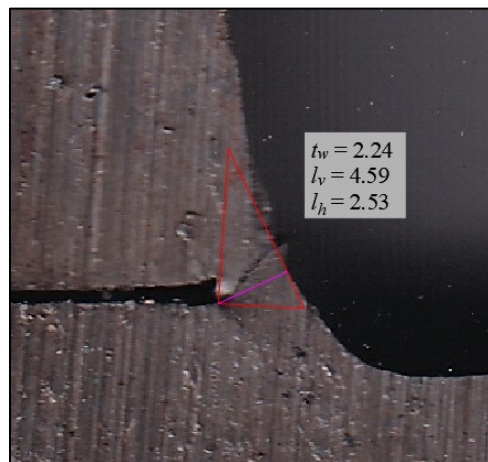
(b) Measurement #2



(c) Measurement #3

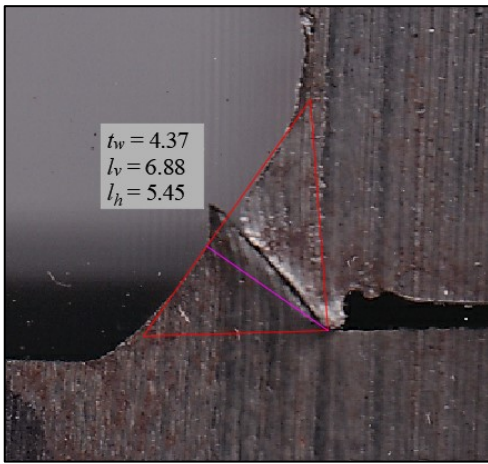


(d) Measurement #4

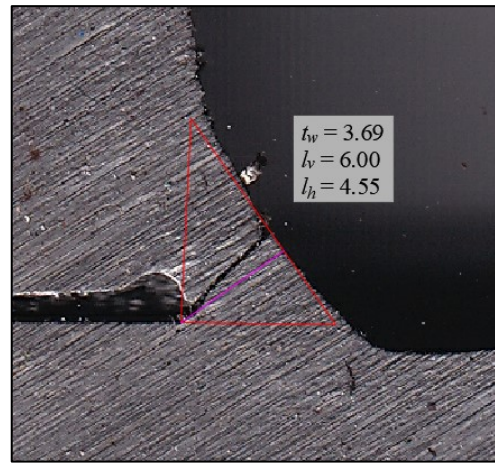


(e) Measurement #5

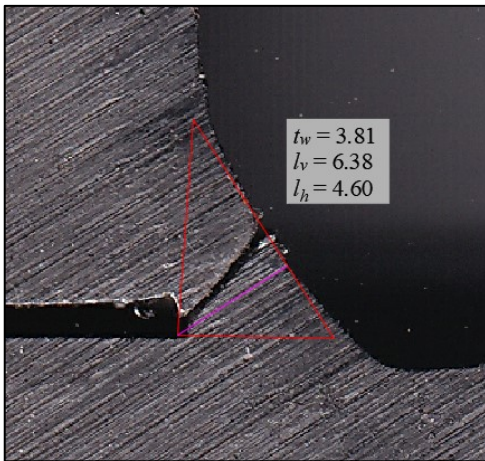
Fig. G.23. Macro-etch examinations for specimen S14-S-0



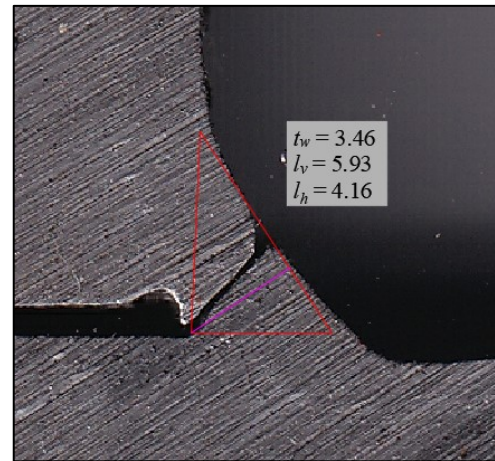
(a) Measurement #1



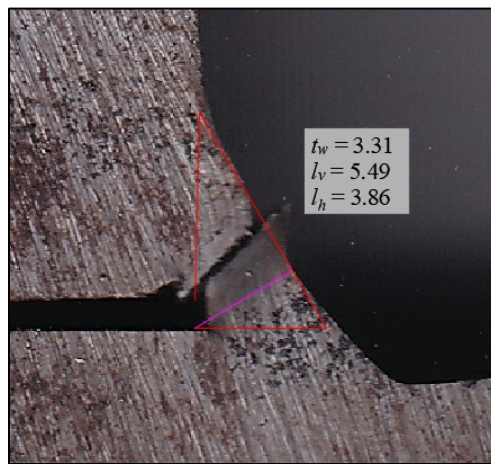
(b) Measurement #2



(c) Measurement #3

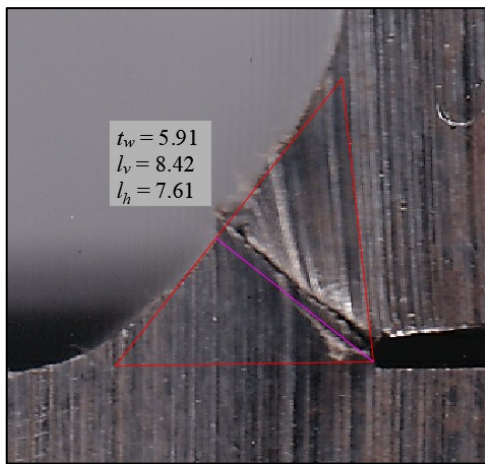


(d) Measurement #4

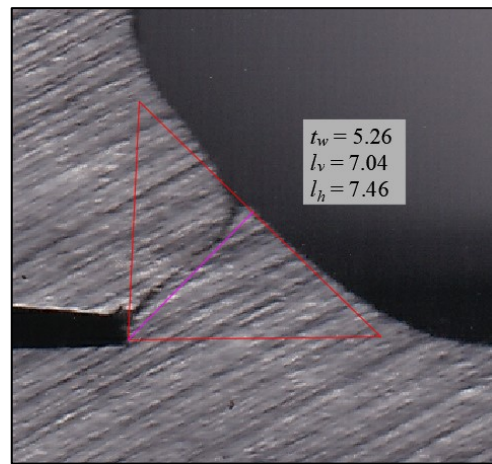


(e) Measurement #5

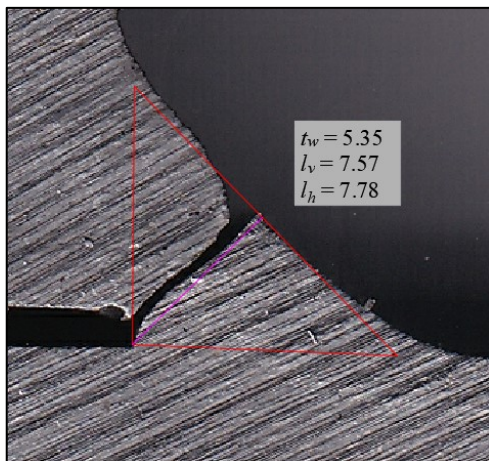
Fig. G.24. Macro-etch examinations for specimen S14-M-0



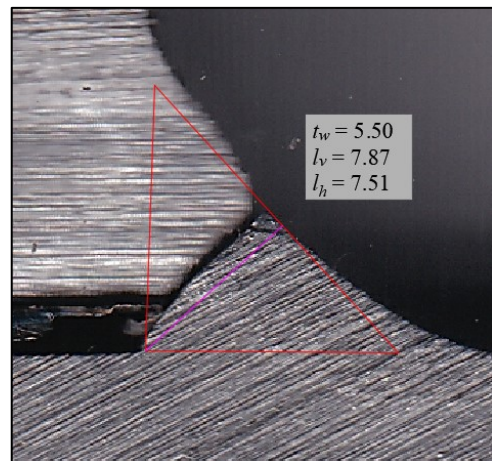
(a) Measurement #1



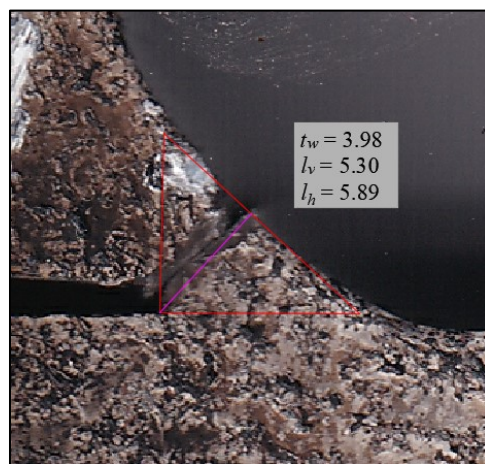
(b) Measurement #2



(c) Measurement #3

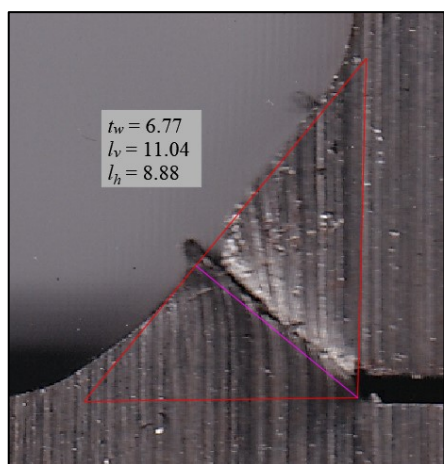


(d) Measurement #4

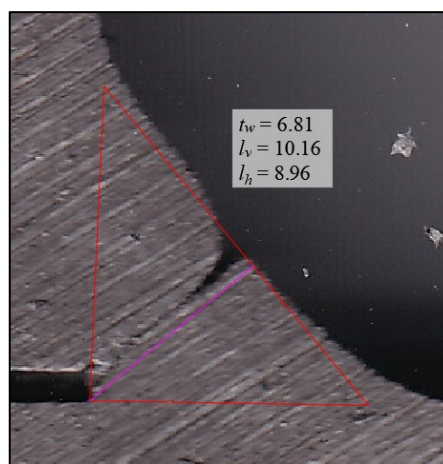


(e) Measurement #5

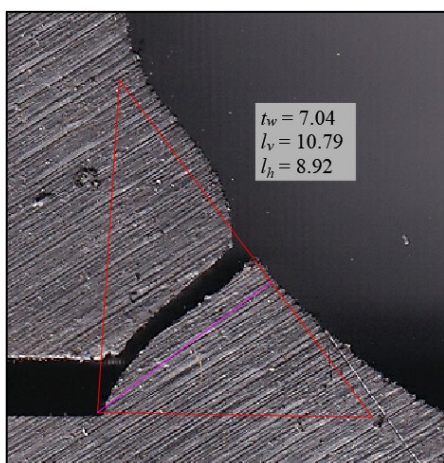
Fig. G.25. Macro-etch examinations for specimen S14-L-0



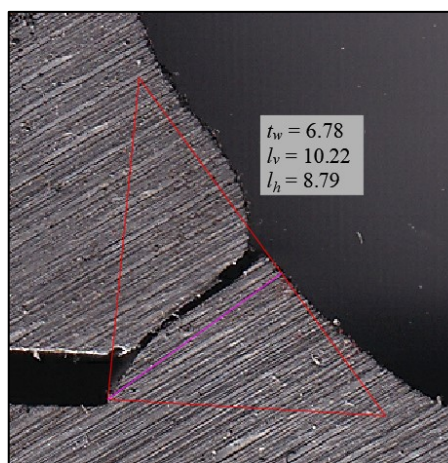
(a) Measurement #1



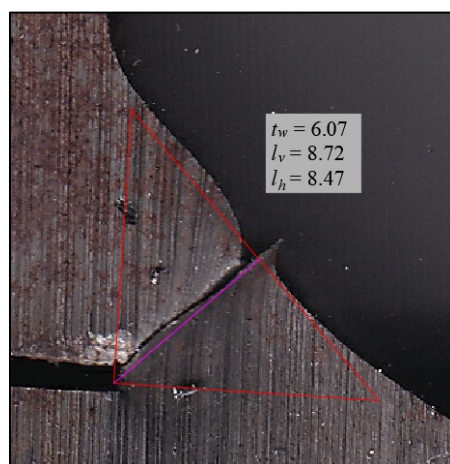
(b) Measurement #2



(c) Measurement #3

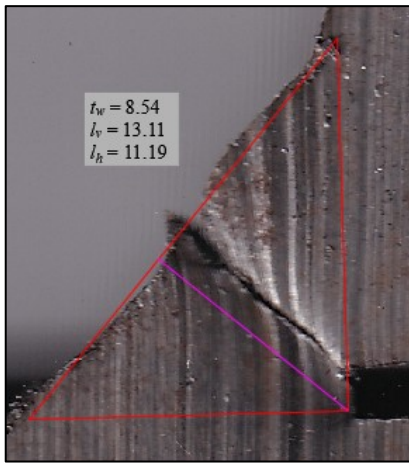


(d) Measurement #4

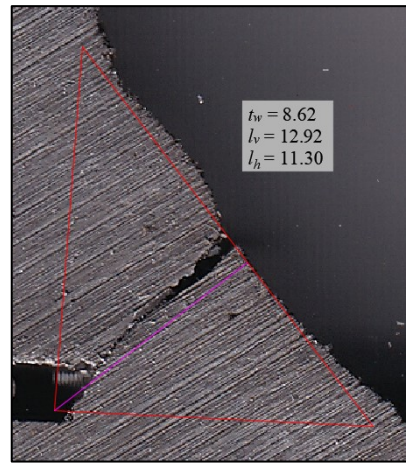


(e) Measurement #5

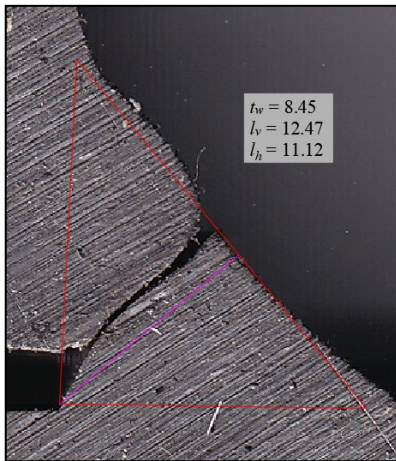
Fig. G.26. Macro-etch examinations for specimen S14-XL-0



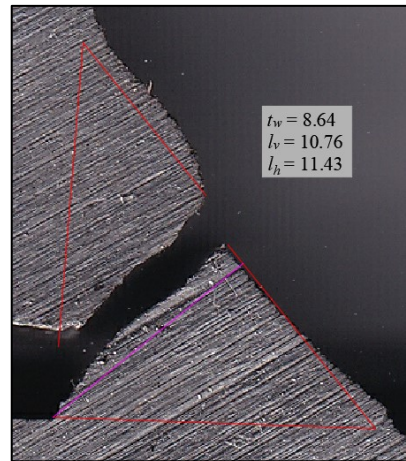
(a) Measurement #1



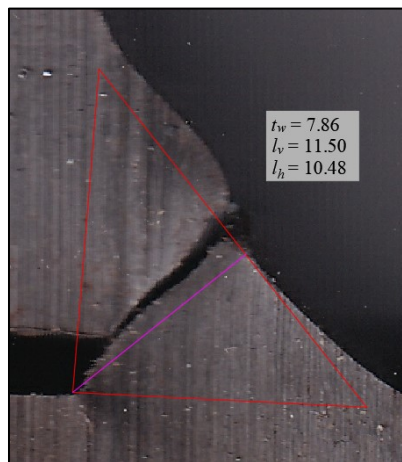
(b) Measurement #2



(c) Measurement #3

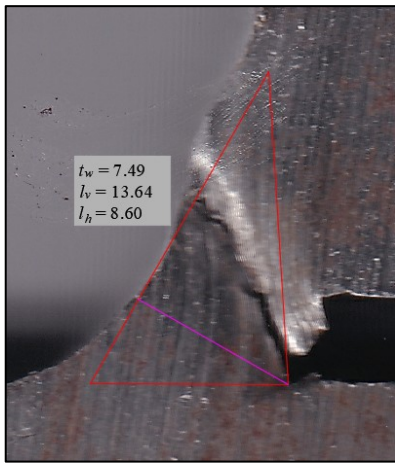


(d) Measurement #4

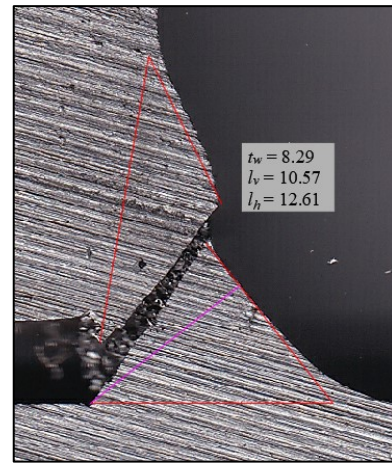


(e) Measurement #5

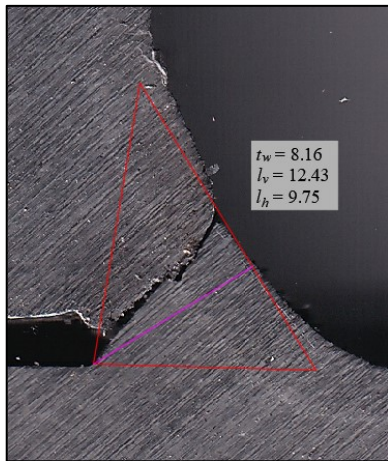
Fig. G.27. Macro-etch examinations for specimen S14-XXL-0



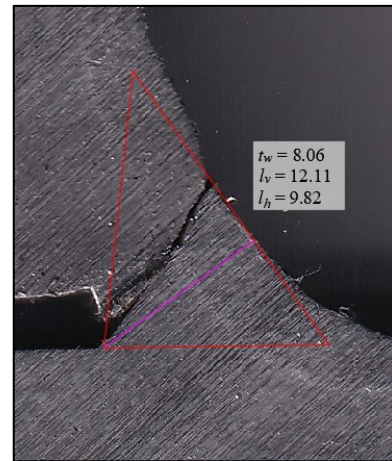
(a) Measurement #1



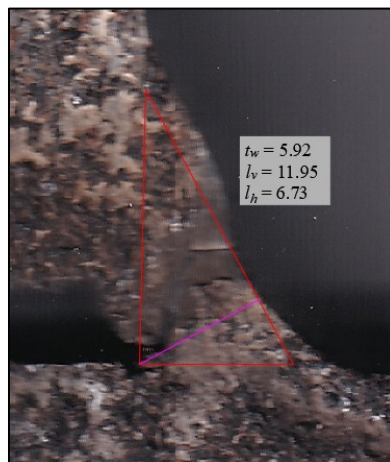
(b) Measurement #2



(c) Measurement #3

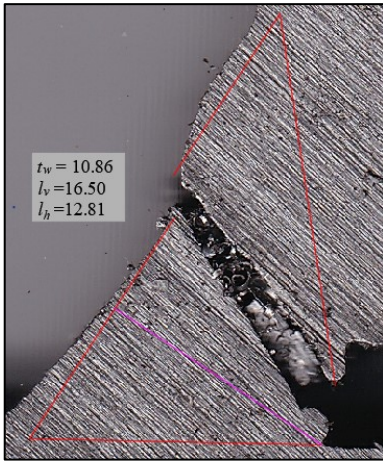


(d) Measurement #4

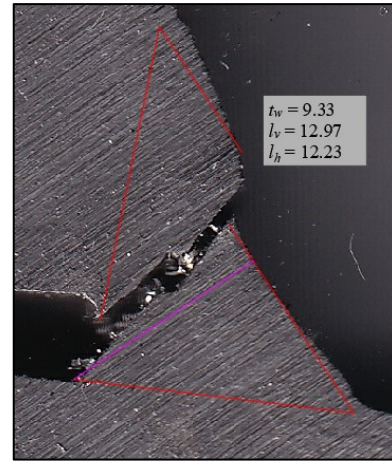


(e) Measurement #5

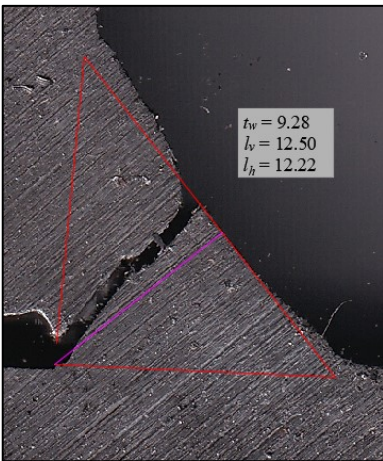
Fig. G.28. Macro-etch examinations for specimen S20-S-30a



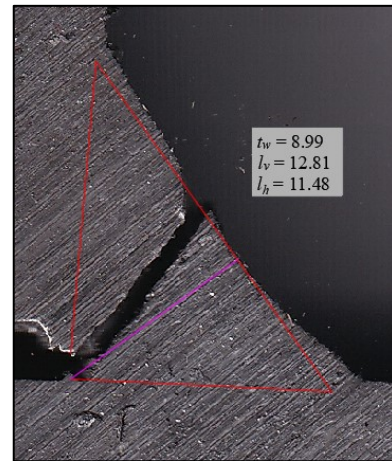
(a) Measurement #1



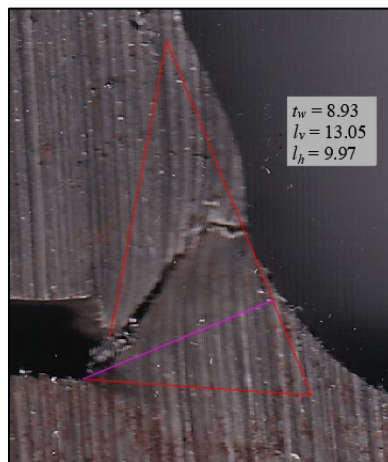
(b) Measurement #2



(c) Measurement #3

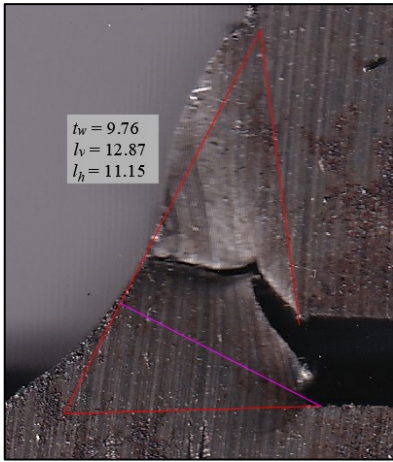


(d) Measurement #4

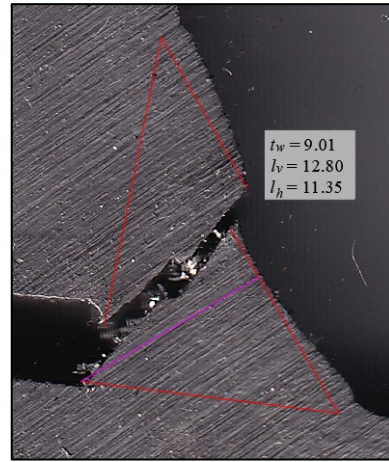


(e) Measurement #5

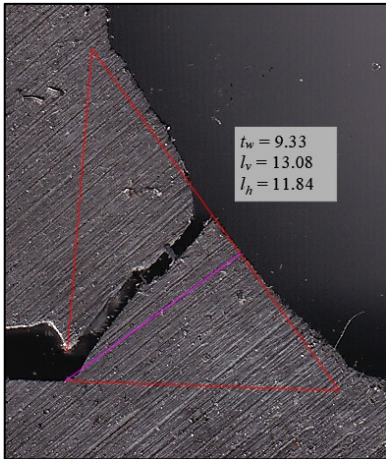
Fig. G.29. Macro-etch examinations for specimen S20-M-30a



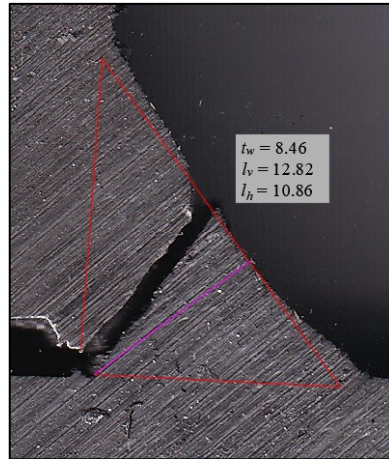
(a) Measurement #1



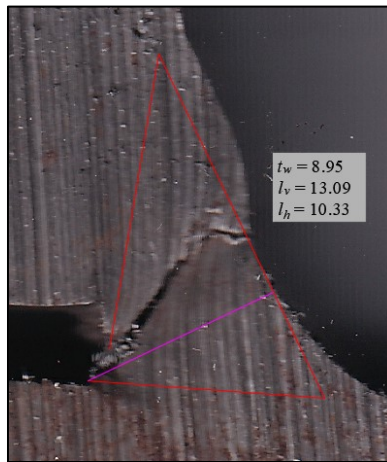
(b) Measurement #2



(c) Measurement #3

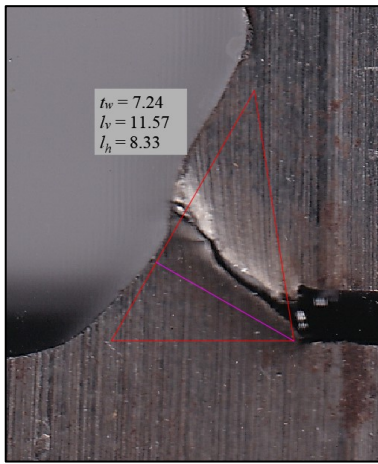


(d) Measurement #4

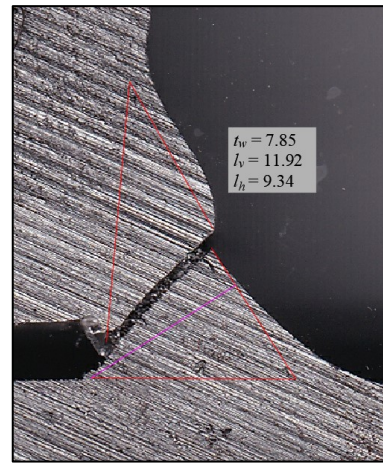


(e) Measurement #5

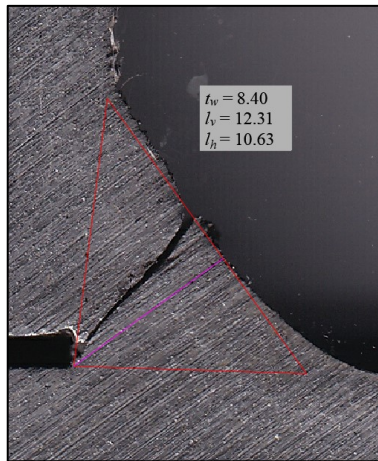
Fig. G.30. Macro-etch examinations for specimen S20-L-30a



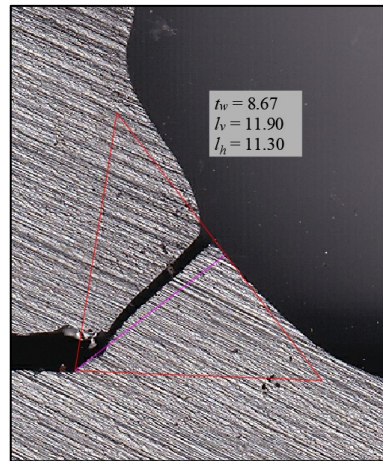
(a) Measurement #1



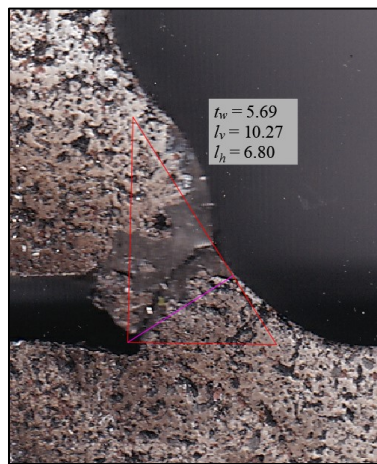
(b) Measurement #2



(c) Measurement #3

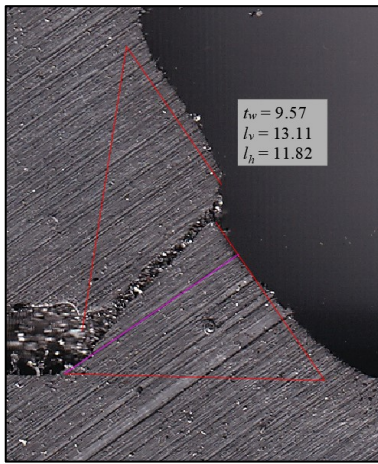


(d) Measurement #4

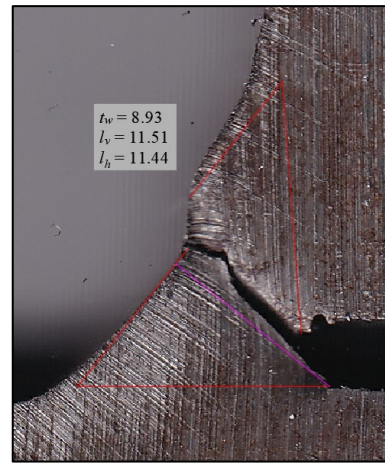


(e) Measurement #5

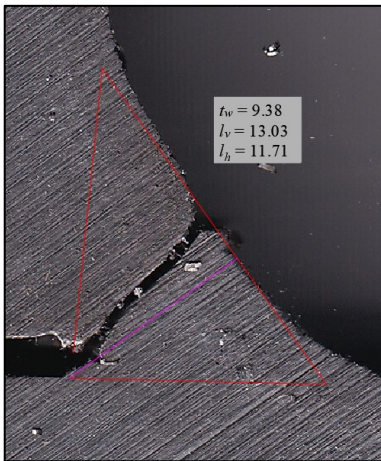
Fig. G.31. Macro-etch examinations for specimen S20-S-15a



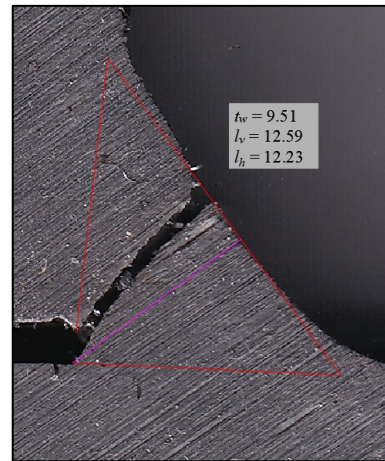
(a) Measurement #1



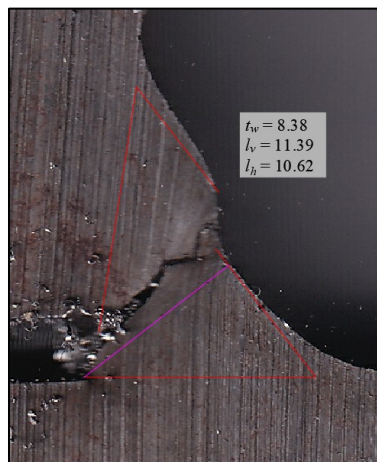
(b) Measurement #2



(c) Measurement #3

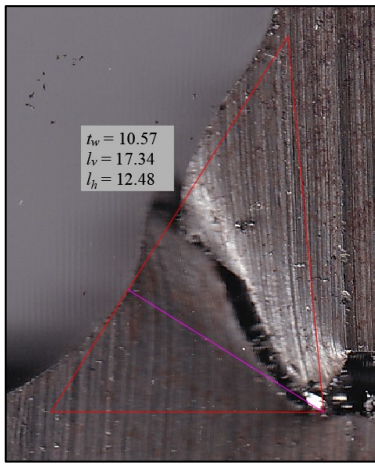


(d) Measurement #4

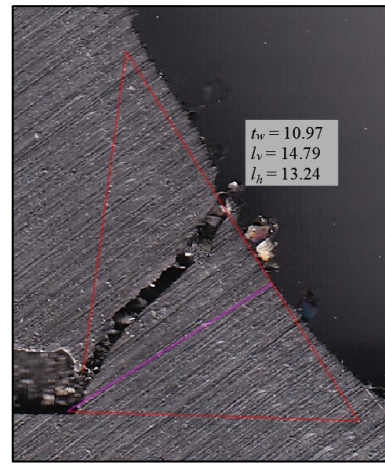


(e) Measurement #5

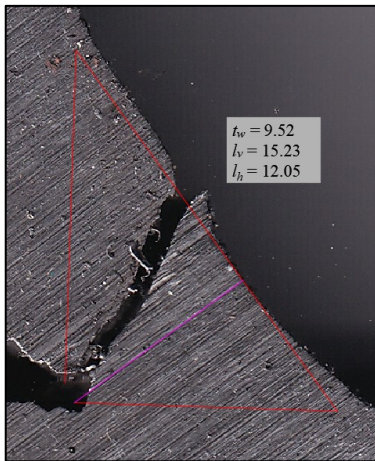
Fig. G.32. Macro-etch examinations for specimen S20-M-15a



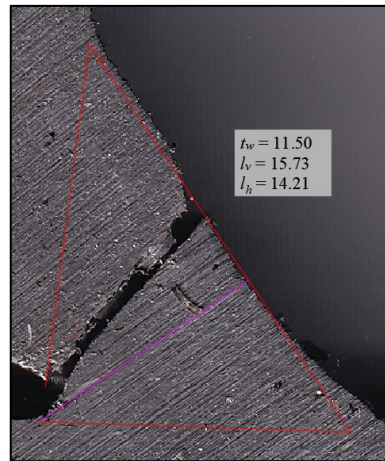
(a) Measurement #1



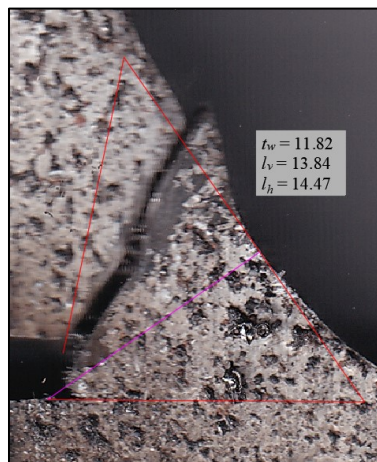
(b) Measurement #2



(c) Measurement #3

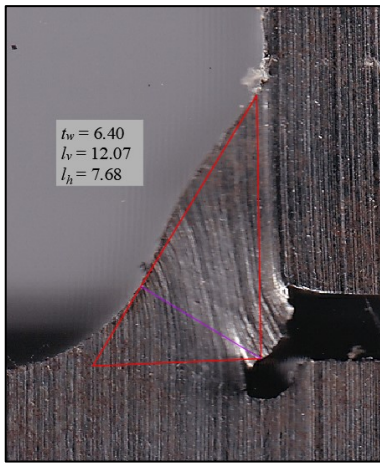


(d) Measurement #4

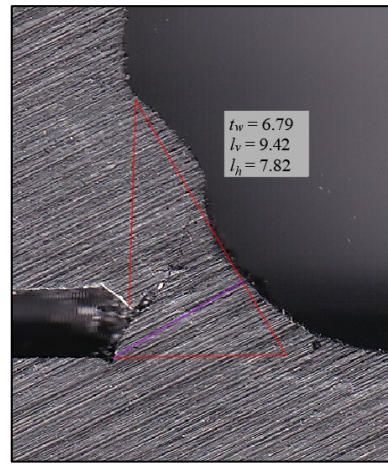


(e) Measurement #5

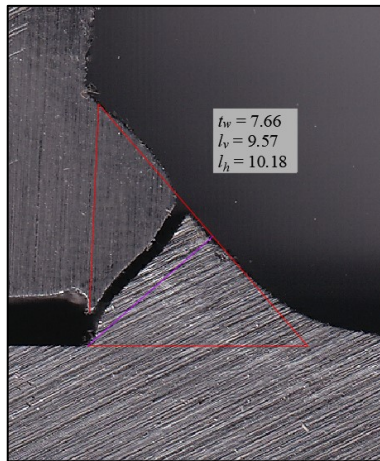
Fig. G.33. Macro-etch examinations for specimen S20-L-15a



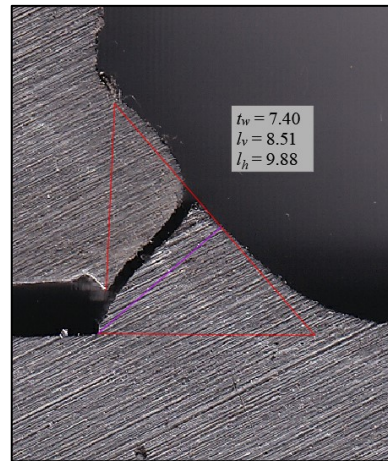
(a) Measurement #1



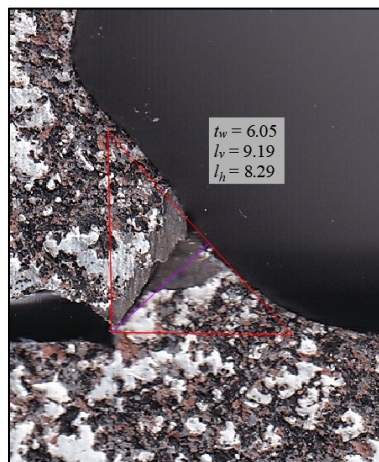
(b) Measurement #2



(c) Measurement #3

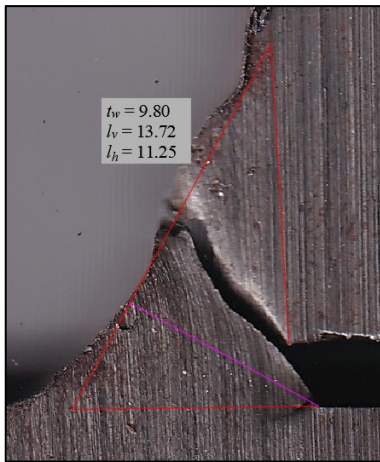


(d) Measurement #4

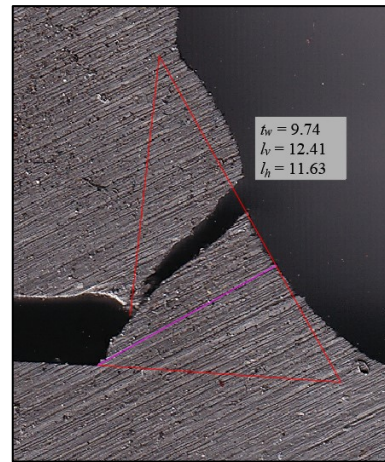


(e) Measurement #5

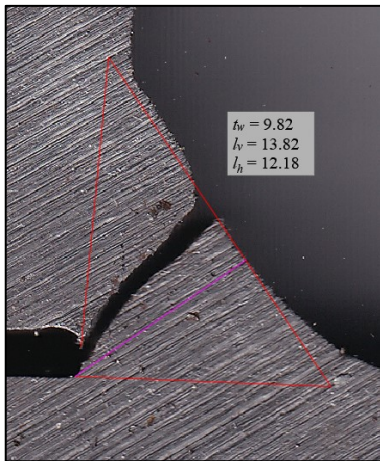
Fig. G.34. Macro-etch examinations for specimen S20-S-0



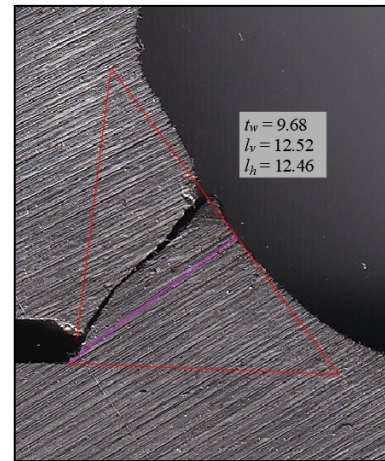
(a) Measurement #1



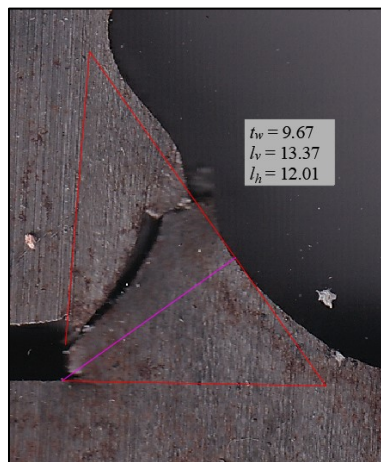
(b) Measurement #2



(c) Measurement #3

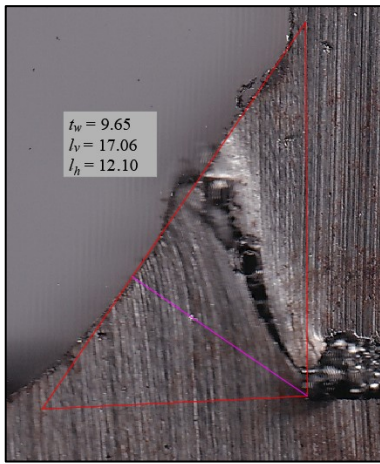


(d) Measurement #4

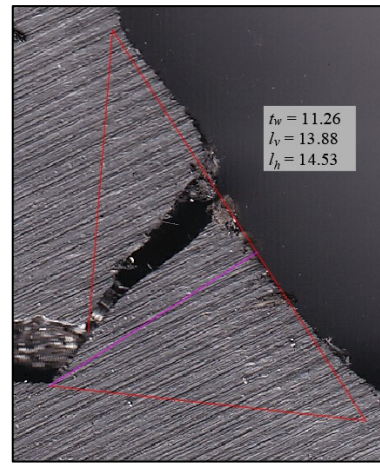


(e) Measurement #5

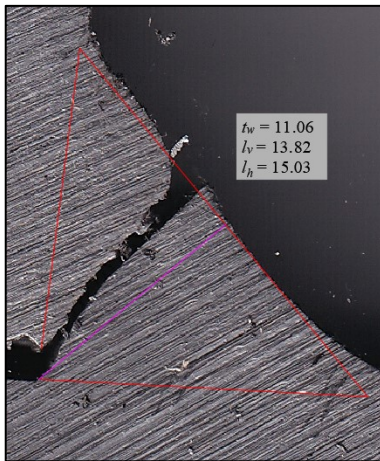
Fig. G.35. Macro-etch examinations for specimen S20-M-0



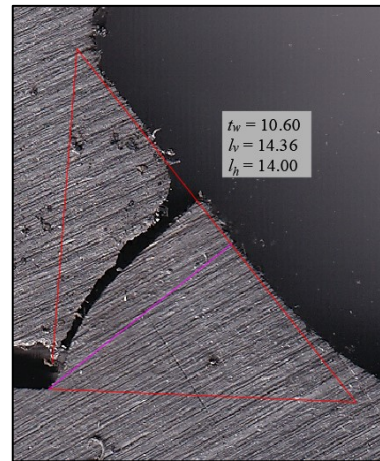
(a) Measurement #1



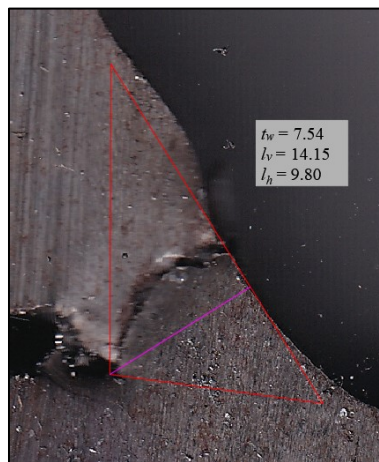
(b) Measurement #2



(c) Measurement #3

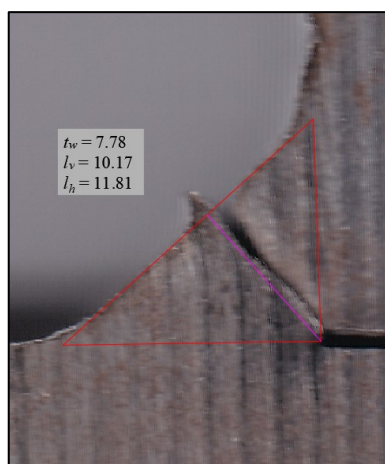


(d) Measurement #4

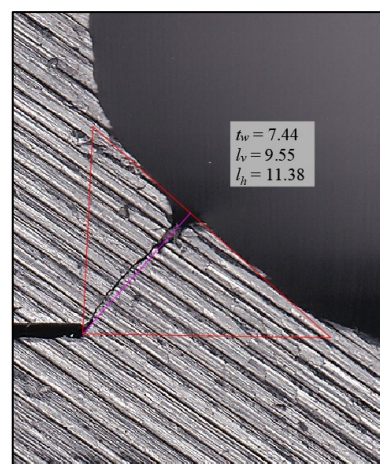


(e) Measurement #5

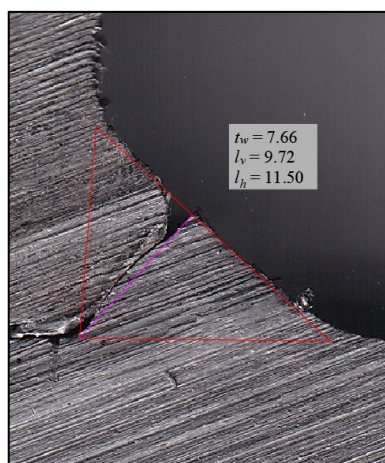
Fig. G.36. Macro-etch examinations for specimen S20-L-0



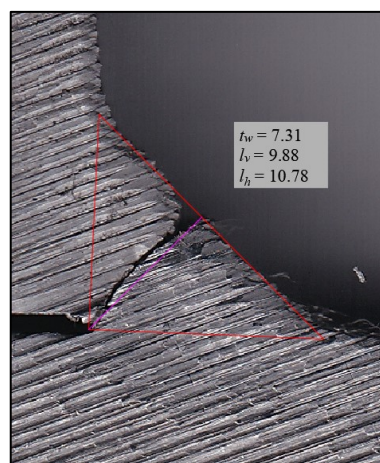
(a) Measurement #1



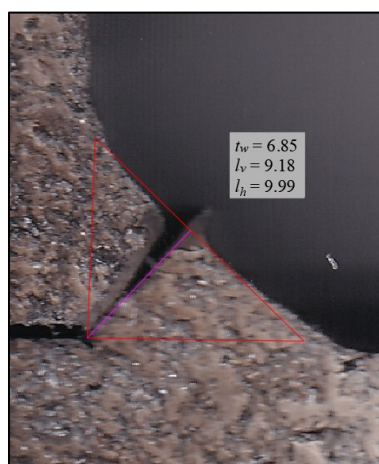
(b) Measurement #2



(c) Measurement #3

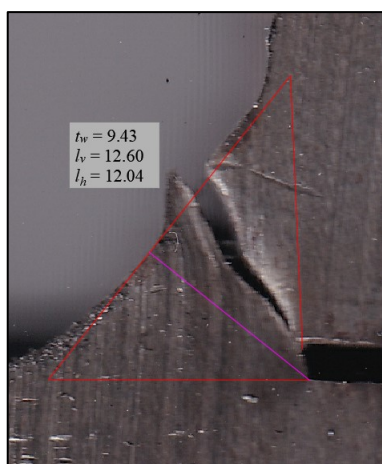


(d) Measurement #4

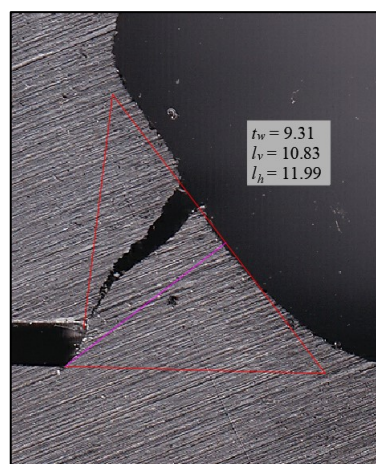


(e) Measurement #5

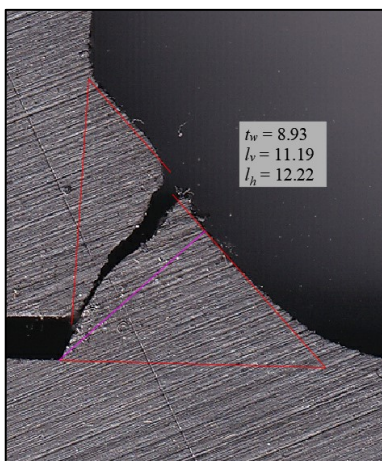
Fig. G.37. Macro-etch examinations for specimen S20-S-15b



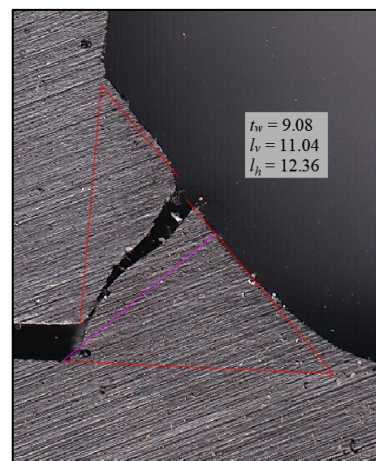
(a) Measurement #1



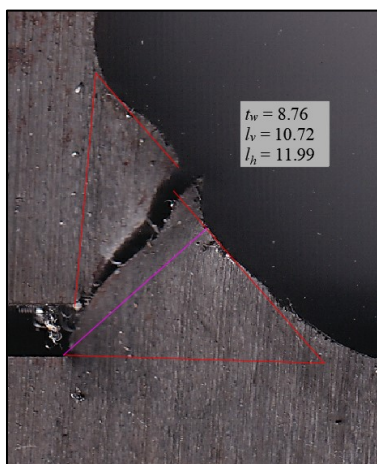
(b) Measurement #2



(c) Measurement #3

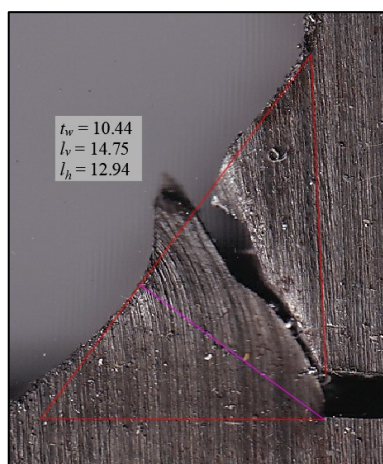


(d) Measurement #4

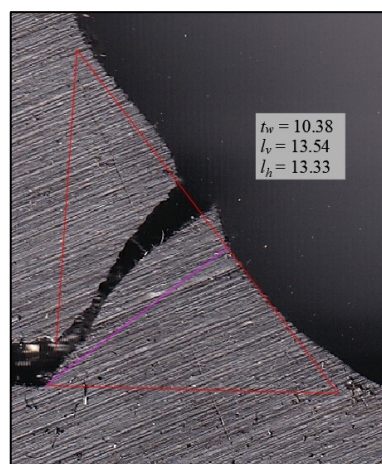


(e) Measurement #5

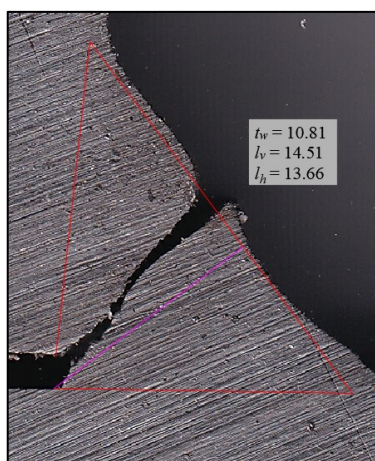
Fig. G.38. Macro-etch examinations for specimen S20-M-15b



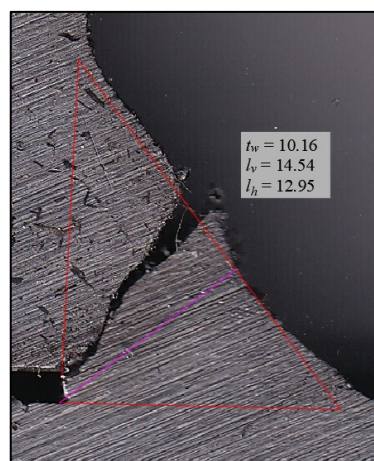
(a) Measurement #1



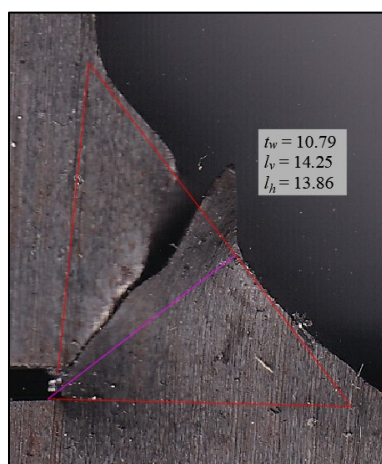
(b) Measurement #2



(c) Measurement #3

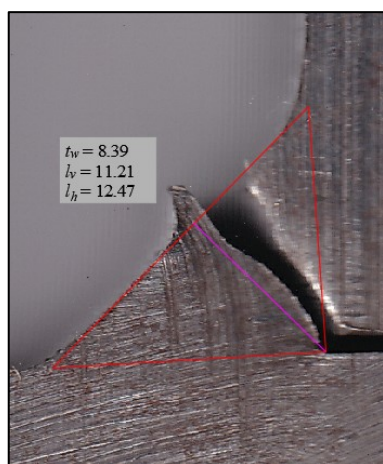


(d) Measurement #4

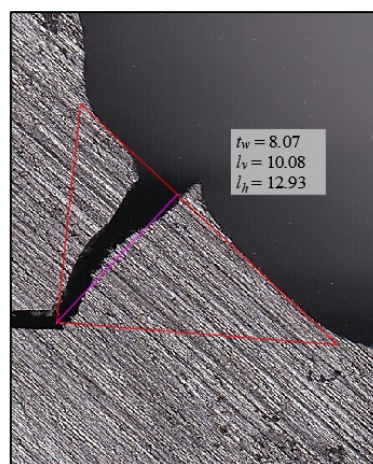


(e) Measurement #5

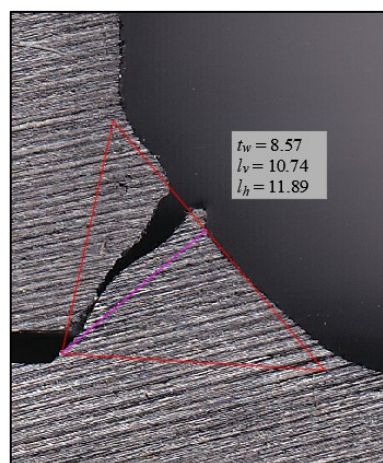
Fig. G.39. Macro-etch examinations for specimen S20-L-15b



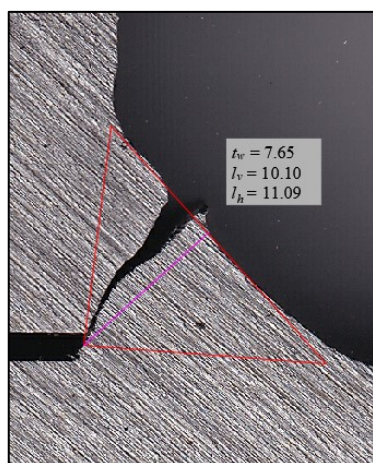
(a) Measurement #1



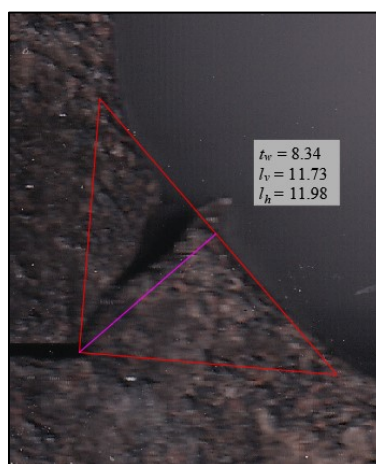
(b) Measurement #2



(c) Measurement #3



(d) Measurement #4



(e) Measurement #5

Fig. G.40. Macro-etch examinations for specimen S20-S-30b

Appendix H: DOCUMENTATION FROM MARID INDUSTRIES LTD

Appendix H includes documentation received from Marid Industries Ltd such as welder qualification, mill test reports and the welding procedure specification.

H.1. WELDER QUALIFICATION

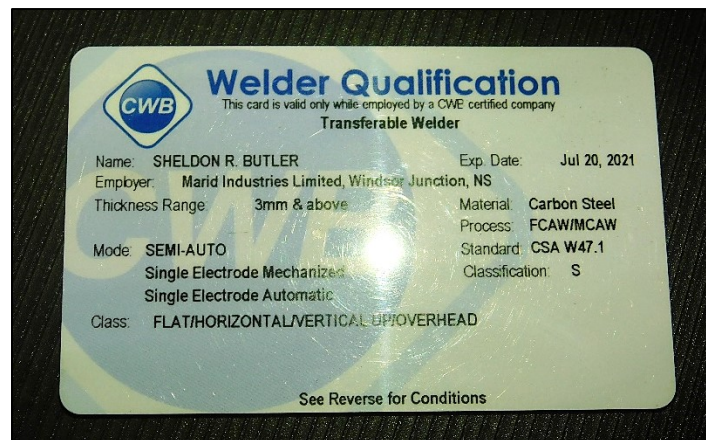


Fig. H.1. Welder's certification from Marid Industries Ltd

H.2. MILL TEST REPORTS

Printable Test Report

12/18/2018

ArcelorMittal Dofasco G.P.
P.O. Box 2468
Hamilton, Ontario
L8M 3J5

TEST REPORT
RAPPORT D'ESSAI

Attention: [NAME]
Fax: [FAX]
Date: 12/18/2018

Page 1 of 1

Purchase Order/Bon de Commande
M02120189 6 3AM

Customer/Client
557628

Sales Order/Bon de Commande
PCS 359910014

Vendor/Vendeur

Bill of Lading/Connaissement
369728

Packing Slip/Bordereau de Charge
Vehicule or Carrier/Vehicule ou Transporteur

Sold To/Vendu A
RUSSEL METALS INC.
28 LAKESIDE PARK DRIVE
LAKESIDE, NS.
B3T 1A3

Ship To/Expédier A
COILEX - VARENNES
350 RUE JEAN COUTU, SUITE DOOR #1
VARENNES, QC.
J3X 0E1
CORNER DE L'ENERGIE/JEAN COUTU

Material Description/Description du Material
PLATE IN COIL FOR CONVERSION
STRUCTURAL STEEL
COILS
MILL EDGE PLAIN DRY
.2438 MIN .2530 X 48 X COIL
WEIGHT: 42590 LBS

Spec/Norm et Spec
DDF 640-21 44M/50M FOR CONV TO PLATE (01/11)
STANDARD THICKNESS TOLERANCE
TEST REPORTS REQUIRED
Code: 64501

Test Methods/Methods d'Essai
ASTM A370, E1019, E415

HEAT Chemical testing performed by an ISO/IEC 17025 certified laboratory

| COULEE | C | Mn | P | S | Si | Cu | Ni | Cr | Sn | Mo | Als | Alc | Co | V | Ti | Ca | N | B | O |
|--------|-----|-----|------|------|-----|-----|-----|-----|------|------|------|------|------|------|------|------|-------|-------|---|
| 755046 | .07 | .68 | .005 | .004 | .03 | .07 | .02 | .02 | .002 | .004 | .056 | .058 | .044 | .002 | .005 | .002 | .0061 | .0080 | |

MECHANICAL PROPERTIES/PROPRIETES MECANQUES

| SERIAL NUMBER | LIFT # | DIR | YIELD STRENGTH | ULTIMATE STRENGTH | ELONG |
|-----------------|---------|-----|------------------------------|--------------------------|----------|
| NUMERO DE SERIE | FARDEAU | DIR | RESISTANCE A LA D'ELASTICITE | RESISTANCE A LA TRACTION | ALLONG |
| A11570/00 | 4569573 | T | 63 | 71 | 29.8 (*) |

(*) Method of elongation calculation: at fracture. / Methode de calcul de l'allongement: au point de fracture.

0200 90910

As shipped from ArcelorMittal Dofasco G.P. as per John Duric, OMTL Supervisor 985_548_7200 x 6960
The Results Relate Only To The Items Tested
This Report Shall Not Be Reproduced Except In Full Without The Expressed Written Approval of The OMTL Supervisor.

This Contract Is Subject To The Terms And Conditions Of Sale Shown On The Order Acknowledgement.
Ce Contrat est Sujet aux Termes et Conditions de Vente Indiqués Sur l'Accuse de Reception de Commande.

Fig. H.2. Mill test report for 6.4 mm plate steel

Printable Test Report

12/12/2018

ArcelorMittal Dofasco G.P.
P.O. Box 2488
Hamilton, Ontario
L8N 3J5

TEST REPORT
RAPPORT D'ESSAI

Attention: [NAME]
Fax: [FAX]
Date: 12/07/2018

Page 1 of 1

Customer/Client: 557628
Sales Order/Bon de Commande: PCS 359913010
Vendor/Vendeur: _____

Bill of Lading/Connaissance: 364277
Packing Slip/Bordereau de Charge: _____
Vehicle or Carrier/Vehicule ou Transporteur: _____

Sold To/Vendu A:
RUSSEL METALS INC.
29 LAKESIDE PARK DRIVE
LAKESIDE, NS.
B3T 1A3

Ship To/Expédier A:
COILEX VARENNES
350 RUE JEAN COUTU, SUITE DOOR #1
VARENNES, QC.
J3X 0E1
CORNER DE L'ENERGIE/JEAN COUTU

Spec/Norm et Spec:
DDF 640.21 44M/50M FOR CONV TO PLATE (01/11)
STANDARD THICKNESS TOLERANCE
TEST REPORTS REQUIRED
Code: 64509

Material Description/Description du Material:
PLATE_IN_COIL FOR CONVERSION
STRUCTURAL STEEL
COILS
MILL EDGE PLAIN DRY
.3650 MIN .3780 X 48 X COIL
WEIGHT: 42770 LBS

Test Methods/Methods d'Essai:
ASTM A370, E1819, E415

HEAT Chemical testing performed by an ISO/IEC 17025 certified laboratory

| COULEE | C | Mn | P | S | Si | Cu | Ni | Cr | Sn | Mo | Als | Alt | Cb | V | Ti | Ca | N | B | O |
|--------|-----|-----|------|------|-----|-----|-----|-----|------|------|------|------|------|------|------|------|-------|-------|---|
| 754966 | .06 | .74 | .006 | .005 | .03 | .03 | .01 | .02 | .001 | .003 | .050 | .052 | .048 | .003 | .001 | .002 | .0034 | .0000 | |

MECHANICAL PROPERTIES/PROPRIETES MECANIKES

| SERIAL NUMBER | LIFT # | DIR | YIELD STRENGTH | ULTIMATE STRENGTH |
|-----------------|---------|------|---------------------------------|-------------------|
| NOMBRE DE SERIE | FARDEAU | | RESISTANCE A LA RESISTANCE A LA | ALLONG |
| | | | D'ELASTICITE | TRACTION |
| T98326/00 | 4556865 | T 59 | 77 | 31 (*) |

(*) Method of elongation calculation: at fracture. / Methode de calcul de l'allongement: au point de fracture.

0200 90895

As shipped from ArcelorMittal Dofasco G.P. as per John Duric, CMTL Supervisor 905_548_7200 x 6960
The Results Relate Only To The Items Tested

This Report Shall Not Be Reproduced Except In Full Without The Expressed Written Approval of The CMTL Supervisor.

This Contract Is Subject To The Terms And Conditions Of Sale Shown On The Order Acknowledgement.
Ce Contrat est Sujet aux Termes et Conditions de Vente Indiques Sur l'Accuse de Reception de Commande.

Fig. H.3. Mill test report for 9.5 mm plate steel

ESSAR STEEL

ESSAR STEEL ALGOMA INC., 105 West Street, Sault Ste. Marie, Ontario, Canada P6A 7B4

| | | | |
|---|---|---|-----------------------------------|
| BO No./Item & Date: 8095594 000090 2018/11/07 | Shipment No. & Date: 1200013981 2018/11/11 | TC No., Date & Time: ESA-527099 2018/11/11 - 14:49:24 | Customer PO No./Item: M0212070373 |
| Sold to Customer Name and Address: RUSSEL METALS INC LAKEVIEW PARK DRIVE 28 LAKEVIEW Nova Scotia, Canada | Ship to Customer Name and Address: RUSSEL METALS INC RUE JEAN COUTU 350 VARENNES, Quebec, Canada | Customer PO No./Item: 1200013981 | BOI NO.: 09209 |
| B31 1A3 | J3X 1P7 | Carrier: C P RAIL (CAD FUNDS) - FLUX 389970 | |

Customer Specification: HR STEEL SHEET HSLA 50 / SS 70 to the Chemistry of CSA G40.21 50W (2013) Top Semi Critical Surface Improved Shape Gauge Type NOM - 0.0039" +/- 0.0039"

Supplementary Instructions: Test Cert 1jharvey@usssteel.com

Map TR: Test Report For Info Only

Customer Use: RESALE IMPR SHAPE & SURF

ESSAR STEEL ALGOMA INC. HEREBY CERTIFIES THAT THE MATERIAL HEREIN DESCRIBED WAS MADE AND TESTED IN ACCORDANCE WITH THE RULES OF THE SPECIFICATION SHOWN. ALL RESULTS ARE RETURNED IN ACCORDANCE WITH THE COMPANY'S STANDARD RECORDING PROCEDURES. THE RESULTS OF THIS TEST REPORT ARE VALID ONLY IF YOU RECEIVE THIS DOCUMENT AND ARE NOT THE INTENDED RECEIVER. PLEASE CALL (709)946-4068 FOR CUSTOMER'S STANDARD RECORDING PROCEDURES. THIS TEST REPORT HAS BEEN GENERATED BY A COMPUTERIZED SYSTEM AND IS VALID WITHOUT A PHYSICAL SIGNATURE.

MECHANICAL TESTING RESULTS ARE PROVIDED FOR INFORMATION ONLY. COILS ARE EXCLUDED FROM QUALIFICATION TO THE APPLICABLE PLATE GRADE. APPROPRIATE TESTING IS REQUIRED WHEN COILS ARE PROCESSED INTO PLATE FROM REELS OR COILS.

ISO 9001 AND ENVIRONMENTAL CERTIFICATES AVAILABLE AT WWW.ALGOMA.COM

ALL HEATS OILY ROLLED.
HEATS INDICATED WITH (*) MEAN IN CANADA FOR NAFTA duty preference and NAFTA marking purposes

| | | | | |
|---|----------------------|--------------------------|-----------------------|------------|
| Dimensions (T x W x L) 0.6250" x 48.000" | Batch No. XC80708 | Heat No./MS 4825E4-01 | Quantity 41,238 LB | Pcs 1 |
| CHEMICAL PROPERTIES | | | | |
| Heat No. (mpsl) 4825E4* | C 0.17 | Min 0.98 | P 0.012 | S 0.005 |
| | Mn 0.30 | Si 0.02 | Cr 0.01 | Ni 0.03 |
| | Mo 0.00 | Al 0.031 | Nb 0.018 | V 0.000 |
| | Ti 0.001 | | | |

MECHANICAL PROPERTIES

| | | | | | | | | | | | | |
|----------|-----------|------|-----|--------|------|------|-----|-----|-------------|--------------|----------|----------|
| Heat No. | Batch No. | SRCE | LAB | GAUGE | COND | METH | DIR | LOC | YIELDING(S) | TENSILE(MSI) | EL SCALE | ELONG(%) |
| 4825E4 | | DSFC | ALG | 0.6250 | AR | 2 | T | F | 56.0 | 77.0 | 2" | 40 |

0200 90935

KASHIF REHMAN
MANAGER METALLURGICAL SERVICES

WARNING: THE TEST RESULTS AND VALUES REPORTED HEREIN INDICATE ONLY THAT (1) THE PARTICULAR STEEL FOR WHICH THIS CERTIFICATE IS ISSUED MEETS THE MINIMUM SPECIFIED YIELD STRENGTH AND (2) THE MINIMUM SPECIFIED TENSILE STRENGTH AND ELONGATION REQUIREMENTS. THESE VALUES ARE NOT TO BE USED TO QUALIFY THE STEEL FOR ANY APPLICATION OTHER THAN THE ONE INDICATED AND CAN NOT BE HELD UPON FOR ANY PURPOSE. (INCLUDING DESIGN OR CALCULATION) IN DETERMINING THE ACTUAL STRENGTH OF SUCH STEEL.

Date: 2018/11/12 Time: 18:50:50 Page no. 1 of 1

Fig. H.4. Mill test report for 15.9 mm plate steel

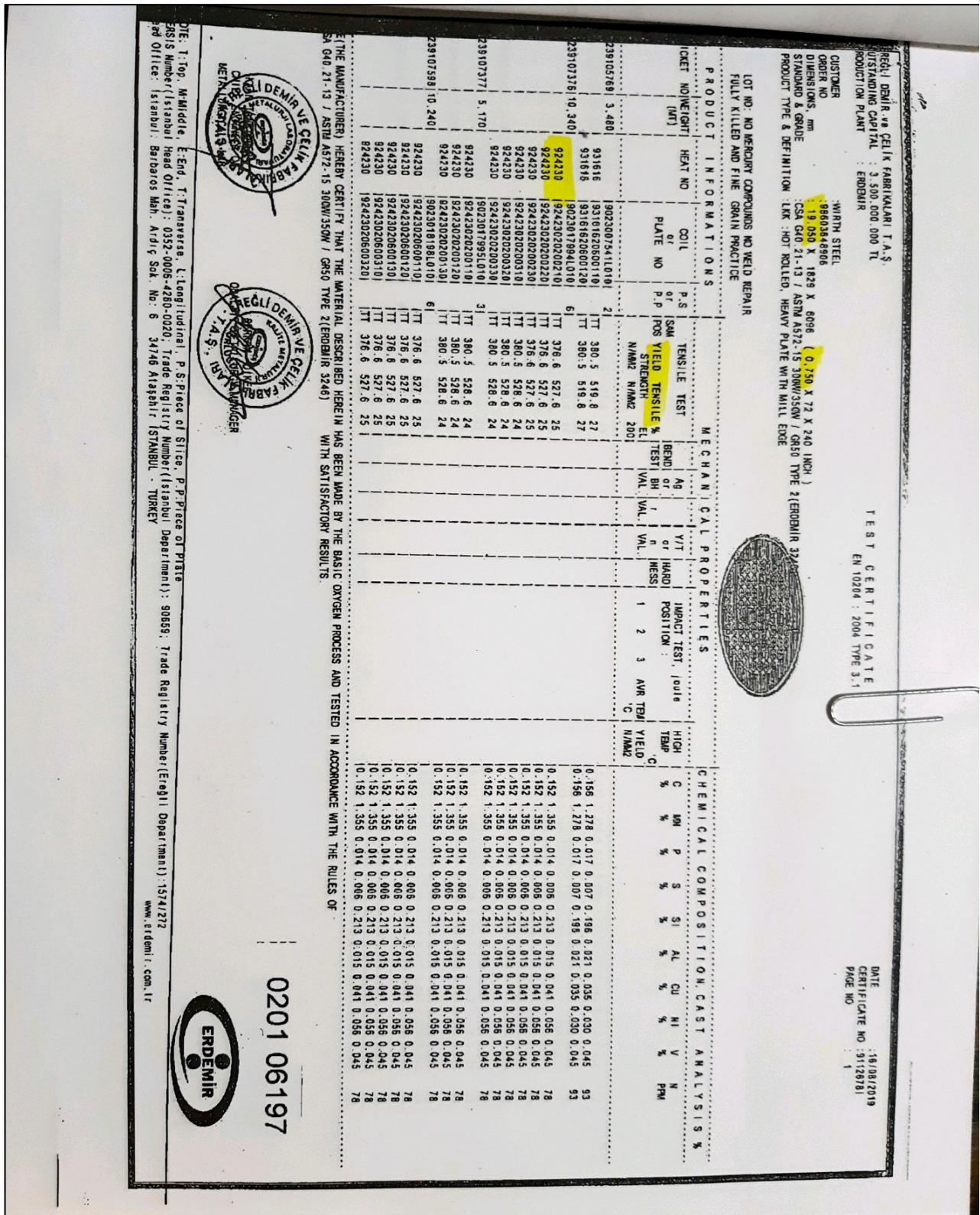


Fig. H.5. Mill test report for 19.1 mm plate steel

TEST CERTIFICATE
EN 10204 : 2004 TYPE 3.1

DATE: 30/07/2018
CERTIFICATE NO: 81133881
PAGE NO: 15

ERDEMİR DEĞİR VE ÇELİK FABRİKALARI T.A.Ş.
OUTSTANDING CAPITAL : 3.500.000.000 TL
PRODUCTION PLANT : ERDEMİR

WIRTH STEEL
ORDER NO : 88602270807
DIMENSIONS, mm : 25.400 X 2438 X 6096 (1.000 X 96 X 240 (INCH))
STANDARD & GRADE : CSA G40.21 / ASTM A572 300W/35W / GR50 TYPE 2 (ERDEMİR 3246)
PRODUCT TYPE & DEFINITION : LK : HOT ROLLED HEAVY PLATE WITH MILL EDGE

CUSTOMER : WIRTH STEEL
ORDER NO : 88602270807
DIMENSIONS, mm : 25.400 X 2438 X 6096 (1.000 X 96 X 240 (INCH))
STANDARD & GRADE : CSA G40.21 / ASTM A572 300W/35W / GR50 TYPE 2 (ERDEMİR 3246)
PRODUCT TYPE & DEFINITION : LK : HOT ROLLED HEAVY PLATE WITH MILL EDGE

LOT NO :
FULLY KILLED AND FINE GRAIN PRACTICE

| TICKET NO/WEIGHT (MT) | HEAT NO | COIL OR PLATE NO | P.S. or P.P. | SAM POS | TENSILE TEST | | BEND TEST | Y/T or HARDNESS | | IMPACT TEST POSITION | AIR TEMPERATURE | CHEMICAL COMPOSITION ANALYSIS % | | | | | | | | | | | | | | | | | | | |
|-----------------------|---------|------------------|--------------|---------|----------------------------------|------------------------------------|-----------|-----------------|-------|----------------------|-----------------|---------------------------------|-------|---------------|-------|-------|-------|-------|-------|-------|-------|-------|-------|-------|-------|-------|-------|-------|-------|-------|----|
| | | | | | YIELD STRENGTH N/MM ² | TENSILE STRENGTH N/MM ² | | ELONGATION % | VAL. | | | VAL. | VAL. | HIGH TEMP. °C | C | MN | P | S | SI | AL | CJ | NI | V | N | PM | | | | | | |
| 0238068848/12.420 | 814655 | 8023017914L010 | TT | 41 | 392.3 | 555.1 | 26 | TT | 403.1 | 559.0 | 27 | 0.195 | 1.207 | 0.019 | 0.010 | 0.168 | 0.037 | 0.044 | 0.041 | 0.072 | 45 | 0.195 | 1.207 | 0.019 | 0.010 | 0.168 | 0.037 | 0.044 | 0.041 | 0.072 | 45 |
| 0238068848/12.420 | 814655 | 81465520700110 | TT | 403.1 | 559.0 | 27 | TT | 403.1 | 559.0 | 27 | 0.195 | 1.207 | 0.019 | 0.010 | 0.168 | 0.037 | 0.044 | 0.041 | 0.072 | 45 | 0.195 | 1.207 | 0.019 | 0.010 | 0.168 | 0.037 | 0.044 | 0.041 | 0.072 | 45 | |
| 0238068848/12.420 | 814655 | 81465520800210 | TT | 397.2 | 556.0 | 27 | TT | 397.2 | 556.0 | 27 | 0.195 | 1.207 | 0.019 | 0.010 | 0.168 | 0.037 | 0.044 | 0.041 | 0.072 | 45 | 0.195 | 1.207 | 0.019 | 0.010 | 0.168 | 0.037 | 0.044 | 0.041 | 0.072 | 45 | |
| 0238068848/12.420 | 814655 | 8023017914L010 | TT | 41 | 397.2 | 556.0 | 27 | TT | 403.1 | 559.0 | 27 | 0.195 | 1.207 | 0.019 | 0.010 | 0.168 | 0.037 | 0.044 | 0.041 | 0.072 | 45 | 0.195 | 1.207 | 0.019 | 0.010 | 0.168 | 0.037 | 0.044 | 0.041 | 0.072 | 45 |
| 0238068848/12.420 | 814655 | 81465520700210 | TT | 387.2 | 556.0 | 27 | TT | 387.2 | 556.0 | 27 | 0.195 | 1.207 | 0.019 | 0.010 | 0.168 | 0.037 | 0.044 | 0.041 | 0.072 | 45 | 0.195 | 1.207 | 0.019 | 0.010 | 0.168 | 0.037 | 0.044 | 0.041 | 0.072 | 45 | |
| 0238068848/12.420 | 814655 | 81465520800110 | TT | 403.1 | 559.0 | 27 | TT | 403.1 | 559.0 | 27 | 0.195 | 1.207 | 0.019 | 0.010 | 0.168 | 0.037 | 0.044 | 0.041 | 0.072 | 45 | 0.195 | 1.207 | 0.019 | 0.010 | 0.168 | 0.037 | 0.044 | 0.041 | 0.072 | 45 | |
| 0238068848/12.420 | 814655 | 81465520800210 | TT | 397.2 | 556.0 | 27 | TT | 397.2 | 556.0 | 27 | 0.195 | 1.207 | 0.019 | 0.010 | 0.168 | 0.037 | 0.044 | 0.041 | 0.072 | 45 | 0.195 | 1.207 | 0.019 | 0.010 | 0.168 | 0.037 | 0.044 | 0.041 | 0.072 | 45 | |
| 0238068848/12.420 | 814655 | 81465520900210 | TT | 397.2 | 556.0 | 27 | TT | 397.2 | 556.0 | 27 | 0.195 | 1.207 | 0.019 | 0.010 | 0.168 | 0.037 | 0.044 | 0.041 | 0.072 | 45 | 0.195 | 1.207 | 0.019 | 0.010 | 0.168 | 0.037 | 0.044 | 0.041 | 0.072 | 45 | |
| 0238068848/12.420 | 814655 | 8023017914L010 | TT | 41 | 397.2 | 556.0 | 27 | TT | 403.1 | 559.0 | 27 | 0.195 | 1.207 | 0.019 | 0.010 | 0.168 | 0.037 | 0.044 | 0.041 | 0.072 | 45 | 0.195 | 1.207 | 0.019 | 0.010 | 0.168 | 0.037 | 0.044 | 0.041 | 0.072 | 45 |
| 0238068848/12.420 | 814655 | 81465520900110 | TT | 403.1 | 559.0 | 27 | TT | 403.1 | 559.0 | 27 | 0.195 | 1.207 | 0.019 | 0.010 | 0.168 | 0.037 | 0.044 | 0.041 | 0.072 | 45 | 0.195 | 1.207 | 0.019 | 0.010 | 0.168 | 0.037 | 0.044 | 0.041 | 0.072 | 45 | |
| 0238068848/12.420 | 814655 | 81465520900210 | TT | 403.1 | 559.0 | 27 | TT | 403.1 | 559.0 | 27 | 0.195 | 1.207 | 0.019 | 0.010 | 0.168 | 0.037 | 0.044 | 0.041 | 0.072 | 45 | 0.195 | 1.207 | 0.019 | 0.010 | 0.168 | 0.037 | 0.044 | 0.041 | 0.072 | 45 | |

WE (THE MANUFACTURER) HEREBY CERTIFY THAT THE MATERIAL DESCRIBED HEREIN HAS BEEN MADE BY THE BASIC OXYGEN PROCESS AND TESTED IN ACCORDANCE WITH THE RULES OF CSA G40.21 / ASTM A572 300W/35W / GR50 TYPE 2 (ERDEMİR 3246) WITH SATISFACTORY RESULTS.

KAAN-TANIRÖVER
CHIEF ENGINEER OF
METALLURGICAL LAB

ERDEMİR
QUALITY CONTROL

NOTE: Top, Middle, End, Transverse, L, Longitudinal, P, S, Piece of Slice, P, Piece of Plate
REGISTRY NUMBER: (Istanbul Head Office): 0252-0006-4260-0200; Trade Registry Number (Istanbul Department): 90659; Trade Registry Number (Erzincan Department): 15747272
Head Office: (Istanbul: Barbaros Mah. Ardiç Sok. No: 6 34746 Alipaşa / İSTANBUL - TÜRKİYE
www.erdemir.com.tr

Fig. H.6. Mill test report for 25.4 mm plate steel

H.3. WELDING PROCEDURE SPECIFICATION

Prepared by Skarborn Engineering Ltd.
For MARID INDUSTRIES LTD.

Welding Procedure
Specification No. 2/7
Page Number 10
Issue 2015-1
Page Revision —
Rev. Date —

WPS NO. 2/7 - APPENDIX B
PARAMETERS TO BE USED FOR WELDING PREQUALIFIED FCAW FILLET, AND COMPLETE AND PARTIAL PENETRATION GROOVE JOINTS, IN QUENCHED & TEMPERED MATERIALS, CSA W59, STEEL GROUP 6 OR 7 WITH 75/25% ARGON/CO₂ GAS & MATCHING CONSUMABLE
Applicable Standards: CSA W47.1 and W59

| | | | | |
|-------------------------------|--|--|--------------------------------|--|
| Check Type of Welding Process | <input type="checkbox"/> Manual (SMAW) <input type="checkbox"/> Solid-Wire (GMAW) <input checked="" type="checkbox"/> Flux-Cored (FCAW) <input type="checkbox"/> Metal-Cored (MCAW) | <input type="checkbox"/> Submerged-Arc (SAW) <input type="checkbox"/> Gas-Tungsten Arc (GTAW) | Welding Positions: | Electrode (Wire) Classification: AWS A5.29 E11XT5-K4M-H4 OR E11XT1-K3M-H4 (X = 1 or 0) SEE SPEC. CLAUSE 5.0 |
| Materials: | AS PER W59, TABLE 11.1 or 12.1, STEEL GROUP 7 | | PREHEAT: | SEE SPEC. CLAUSE 9.0 |
| Material Thickness: | 5 mm TO < 64 mm, UNLESS RESTRICTED BY CSA W59 FIG. 10.5 AND 10.6 | | MINIMUM Interpass Temperature: | AS ABOVE |
| | | | MAXIMUM Interpass Temperature: | AS ABOVE |

Joint Configurations: ALL FILLET WELDS AND ALL PREQUALIFIED COMPLETE AND PARTIAL JOINT PENETRATION WELDS AS PER CSA W59, FIGURE 10.5 AND 10.6.

Pass Criteria: (1) BUILD UP WELD SIZE AS REQUIRED USING TECHNIQUE AS PER CLAUSE 13.0.
(2) MAXIMUM SINGLE PASS FILLET WELD SIZE TO BE IN ACCORDANCE WITH CSA W59, TABLE 10.2.
(3) COMPLETE AND PARTIAL PENETRATION FIRST PASS TO BE LARGE ENOUGH TO MINIMIZE RISK OF CRACKING.

| | | | |
|---|---|---|--|
| COMPLETE JOINT PENETRATION GROOVE <input checked="" type="checkbox"/> Back-gouged to sound metal <input checked="" type="checkbox"/> Welded onto steel backing <input type="checkbox"/> Welded from one side without backing <input type="checkbox"/> Welded both sides without back gouging <input type="checkbox"/> Welded onto other than steel backing | FILLET WELD <input checked="" type="checkbox"/> Minimum per CSA W59 GROOVE WELD PARTIAL JOINT PENETRATION <input checked="" type="checkbox"/> Minimum per CSA W59 <input type="checkbox"/> Others (specify) | JOINT TYPE CSA W59 <input checked="" type="checkbox"/> Butt <input checked="" type="checkbox"/> Corner <input checked="" type="checkbox"/> Lap <input checked="" type="checkbox"/> Tee <input checked="" type="checkbox"/> Edge | Electrical Stickout: 15 - 25 mm Shielding Gas: 75/25% ARGON/CO ₂ (CWB CERTIFICATION REQ'D FOR GAS/WIRE COMBINATION) cu. ft. hr.: 35-45 |
|---|---|---|--|

| Material Thickness | | Positions | Side No. | Layer No. | Pass No. | Elect. Size | Current Polarity | Amperes | Wire Feed Speed | Volts | Arc Travel Speed | Heat Input |
|--------------------|--------|---------------|------------|-----------|----------|-------------|------------------|----------------|-----------------|--------------|------------------|------------|
| mm | in. | | | | | | | | | | | |
| ≥ 5 | ≥ 3/16 | F, H | 1 and/or 2 | ALL | ALL | 1.1 | DCRP | 230-280 | 500-550 | 25-31 | 250-400 | - |
| | | F, H, V-up, O | | | | | | | | | | |
| ≥ 6 | ≥ 1/4 | F, H | 1 and/or 2 | ALL | ALL | 1.3 | DCRP | 260-330 | 425-500 | 24-31 | 250-400 | - |
| | | F, H, V-up, O | | | | | | | | | | |
| ≥ 6 | ≥ 1/4 | F, H | 1 and/or 2 | ALL | ALL | 1.6 | DCRP | 320-380 | 325-350 | 24-30 | 250-400 | - |
| | | F, H, V-up, O | | | | | | | | | | |
| ≥ 12 | ≥ 1/2 | F, H | 1 and/or 2 | ALL | ALL | 2.4 | DCRP | 350-400 | 125-175 | 23-28 | 300-450 | - |

NOTES: 1) Wire speed, voltage and stickout will vary depending on consumable manufacturer. Consult manufacturer's recommendations, but maintain current range listed above. 2) Values in bold result in most economical welding for F and H.

| Revision Date | Explanation | CWB Acceptance |
|---------------|-------------|---------------------------|
| | | EXCLUDES IMPACT APPRAISAL |
| | | |
| | | |
| | | |
| | | |




Fig. H.7. Welding Procedure Specification (Pg. 1)

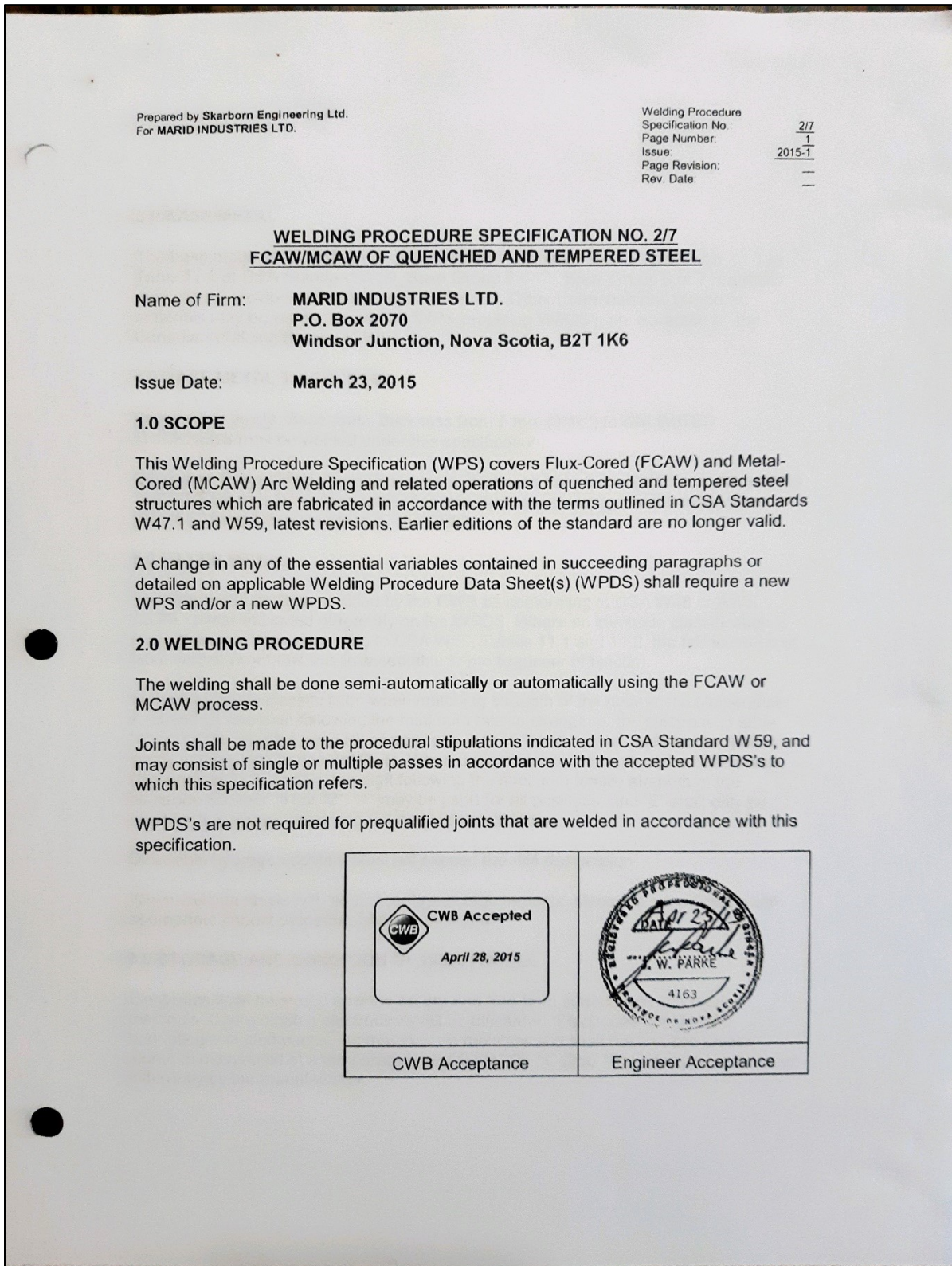


Fig. H.8. Welding Procedure Specification (Pg. 2)

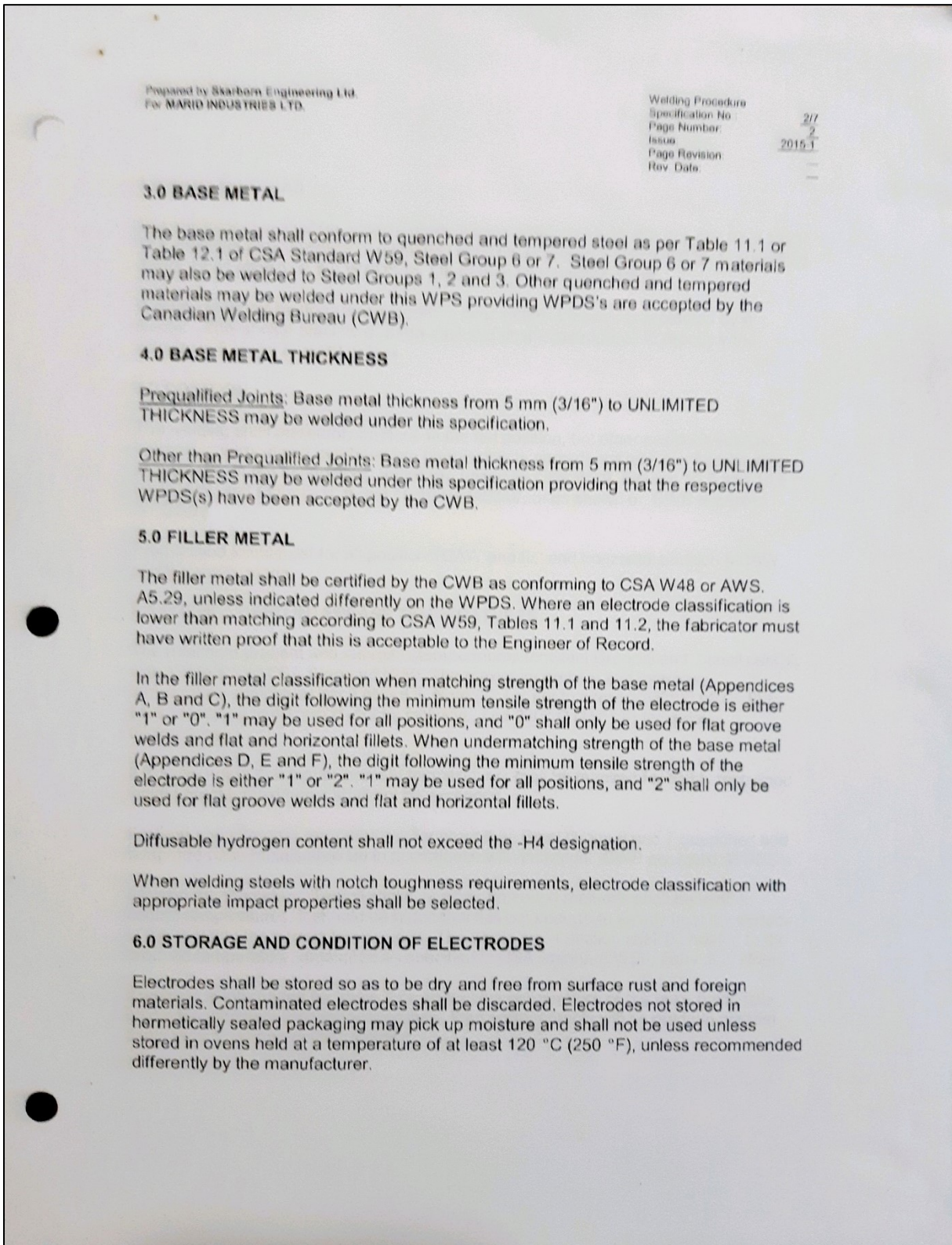


Fig. H.9. Welding Procedure Specification (Pg. 3)

| | | | | | | | | | | | |
|--|--|-------------------------------------|-----|--------------|---|--------|--------|----------------|---|------------|---|
| <p>Prepared by Skarborn Engineering Ltd For MARID INDUSTRIES LTD.</p> | <table border="0" style="width: 100%;"> <tr> <td style="padding-right: 10px;">Welding Procedure Specification No.</td> <td style="text-align: right;">2/7</td> </tr> <tr> <td>Page Number:</td> <td style="text-align: right;">2</td> </tr> <tr> <td>Issue:</td> <td style="text-align: right;">2015-1</td> </tr> <tr> <td>Page Revision:</td> <td style="text-align: right;">—</td> </tr> <tr> <td>Rev. Date:</td> <td style="text-align: right;">—</td> </tr> </table> | Welding Procedure Specification No. | 2/7 | Page Number: | 2 | Issue: | 2015-1 | Page Revision: | — | Rev. Date: | — |
| Welding Procedure Specification No. | 2/7 | | | | | | | | | | |
| Page Number: | 2 | | | | | | | | | | |
| Issue: | 2015-1 | | | | | | | | | | |
| Page Revision: | — | | | | | | | | | | |
| Rev. Date: | — | | | | | | | | | | |

7.0 SHIELDING GAS

The shielding gas shall be welding grade having a dew point of -40°C (-40°F) or lower. The shielding gas/electrode combination shall be as shown in this WPS for Prequalified Joints, or as shown on the WPDS for Other than Prequalified Joints.

Welding shall not be done in a draught or wind unless the weld is protected by a shelter. This shelter shall be of a material and shape appropriate to reduce wind velocity to 8 km/hr (5 mph) or less.

8.0 POSITION

The welding shall preferably be done in the flat position, but other positions such as horizontal, vertical and overhead are permissible in accordance with this specification as indicated in the appendices, which are based on CSA W59, Figures 10.5 and 10.6 for FCAW, and Figures 10.9 and 10.10 for MCAW, or as shown on CWB accepted WPDS(s).

Prequalified joints exist for all position FCAW and flat and horizontal position MCAW, spray transfer mode.

9.0 PREHEAT AND INTERPASS TEMPERATURES

The minimum preheat and interpass temperatures for Steel Group 6 and 7 shall comply with Table 5.3 of CSA Standard W59. The maximum preheat and interpass temperature shall be as per Table 5.3, Note (2), i.e. not to exceed 200°C (400°F) for thicknesses up to 40 mm (1-1/2 in) inclusive, and 230°C (450°F) for greater thicknesses.

It is to be noted that higher preheat temperatures may be required for highly restrained welds, but the maximums shall not be exceeded.

Preheat and interpass temperatures for other than Steel Group 6 and 7 quenched and tempered base metals shall be in accordance with individual, CWB accepted, WPDS's.

Infrared thermometers, Tempil sticks, or other approved methods shall be used to control temperatures. It should be noted that it is not enough to simply heat the surface of the metal to the correct temperature. The whole cross section shall be heated to the required temperature, measured as specified in CSA Standard W59, Table 5.3, Note 2.

If welding is interrupted for some time so that the temperature of the base metal falls below the minimum preheat temperature, then arrangements will be made to preheat again prior to recommencing welding.

Fig. H.10. Welding Procedure Specification (Pg. 4)

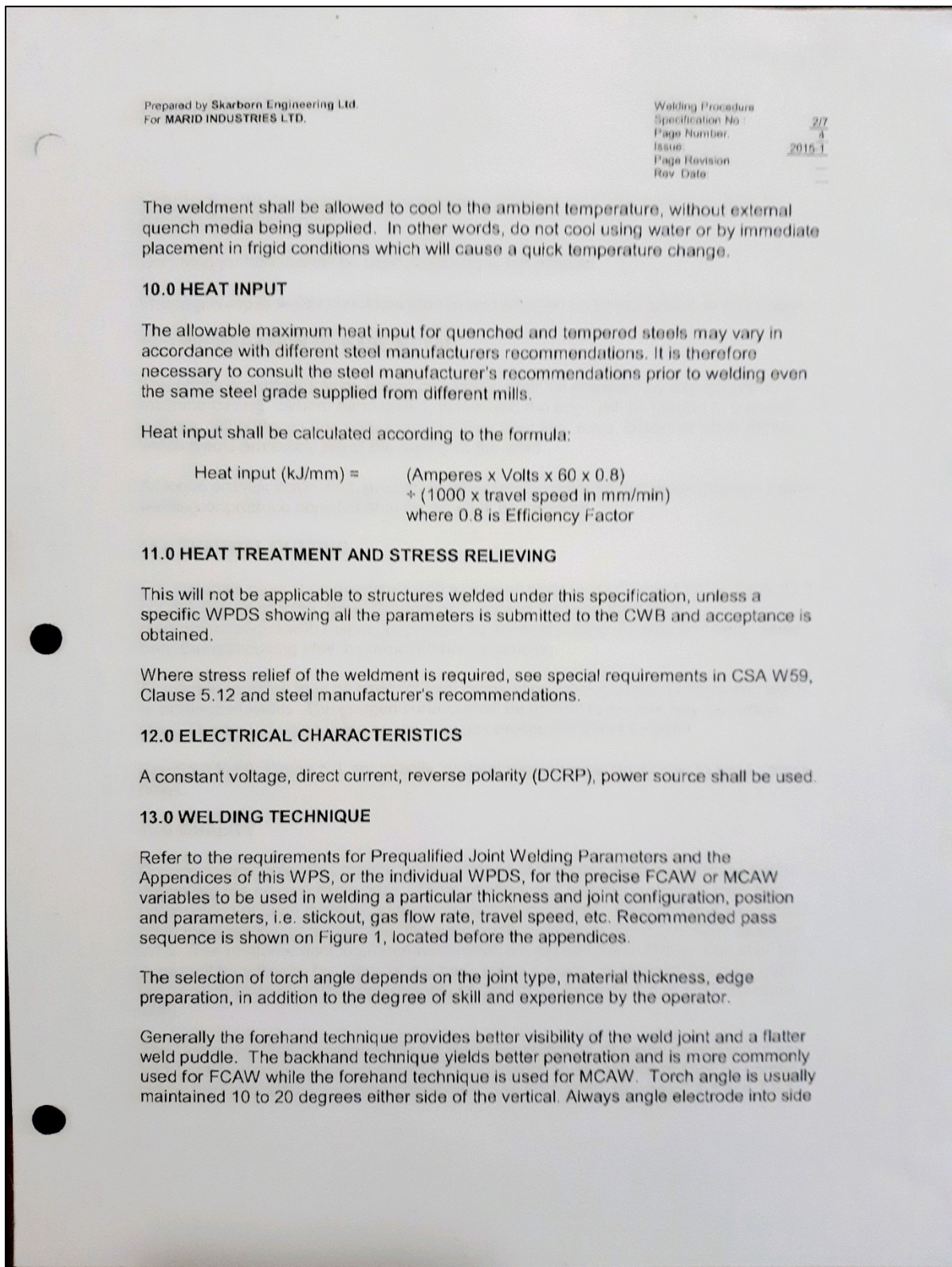


Fig. H.11. Welding Procedure Specification (Pg. 5)

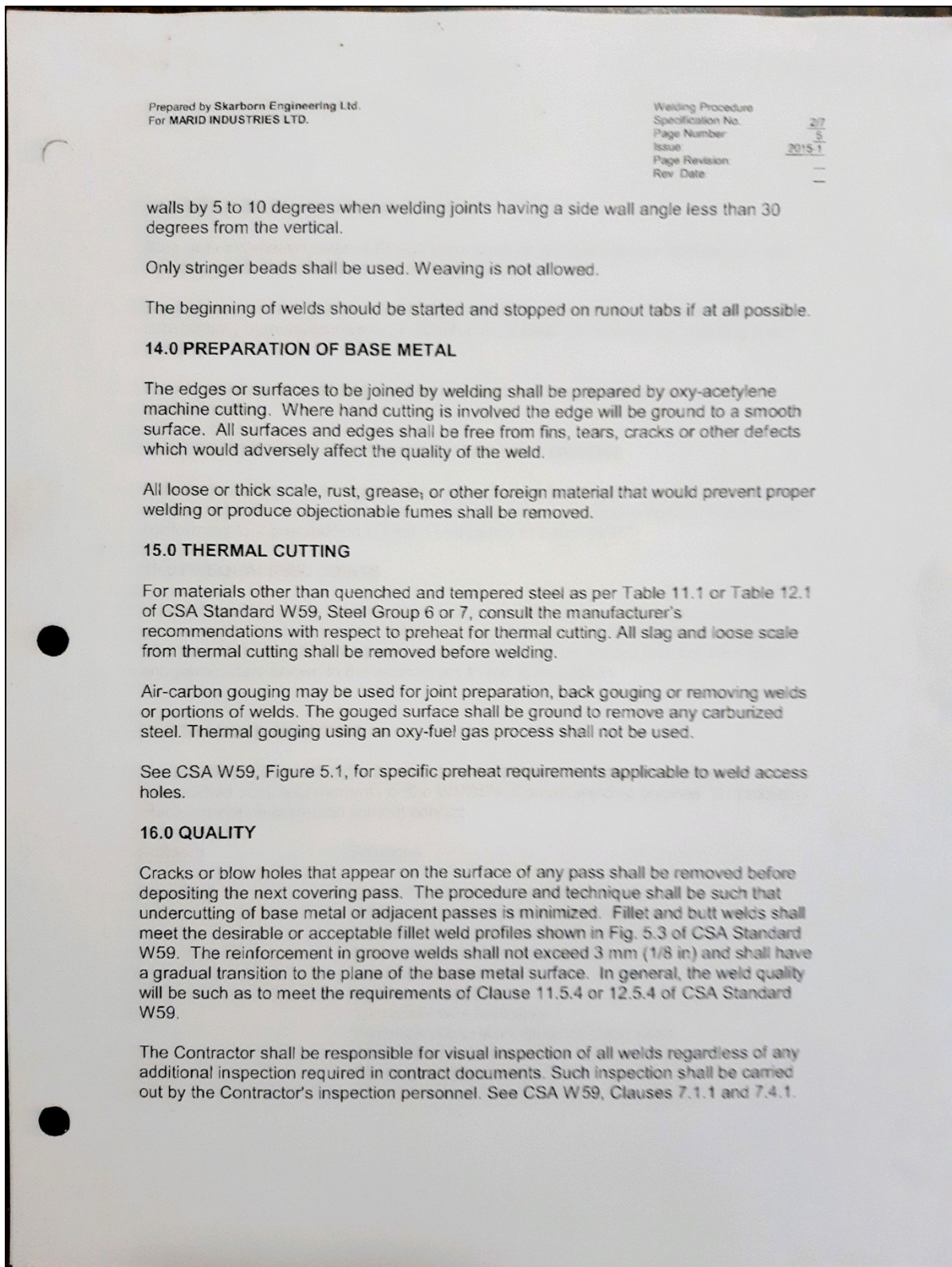


Fig. H.12. Welding Procedure Specification (Pg. 6)

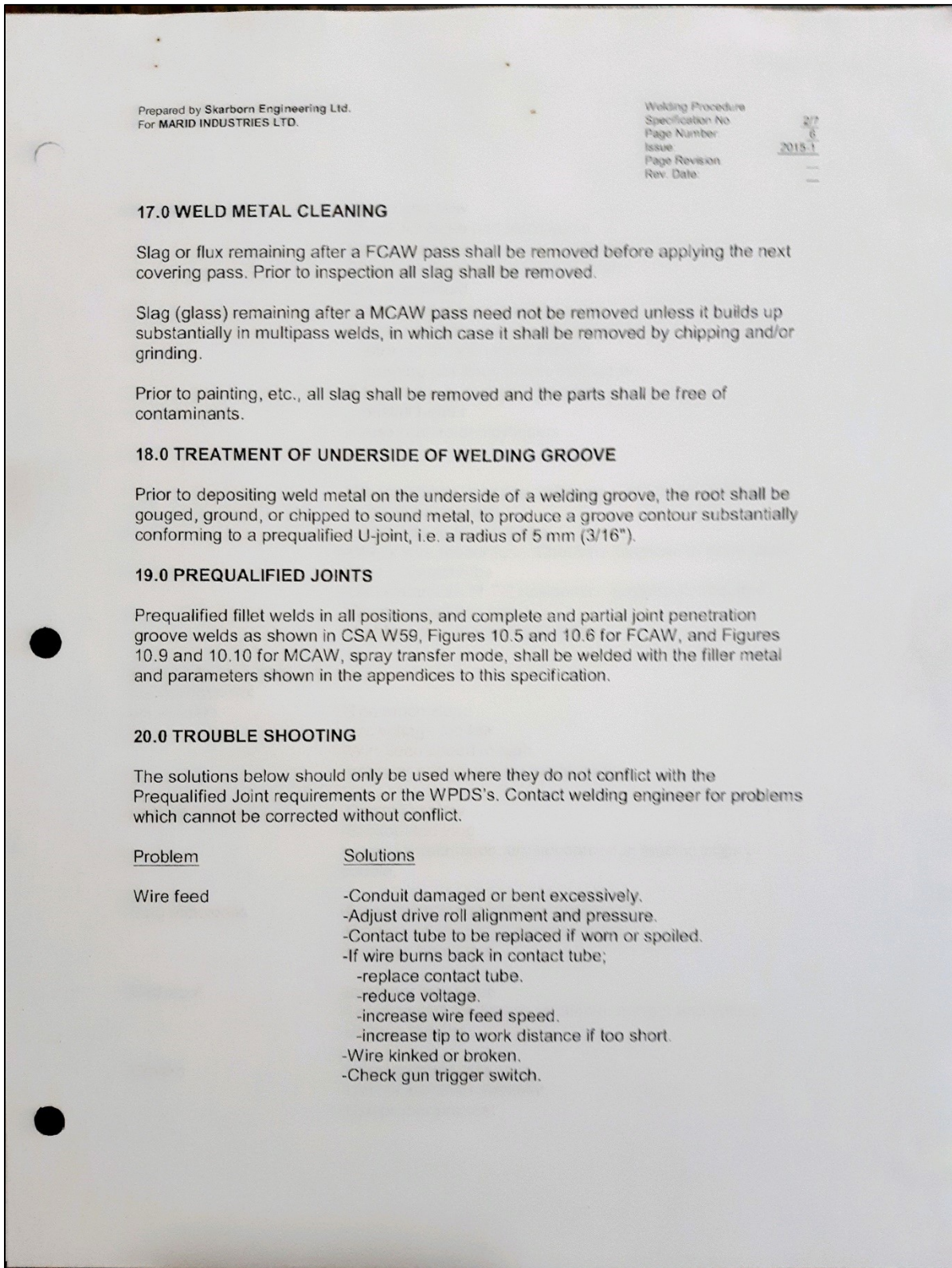


Fig. H.13. Welding Procedure Specification (Pg. 7)

| Prepared by Skarhorn Engineering Ltd. for MARID INDUSTRIES LTD. | | Welding Procedure Specification No. <u>2/7</u> Page Number <u>1</u> Issue <u>2015-1</u> Page Revision: <u>—</u> Rev. Date <u>—</u> | |
|--|--|---|--|
| Porosity | <ul style="list-style-type: none"> -Check gas flow. -Check for hose and torch leaks. -Shorten terminal distance if excessive. -Shield arc from strong wind or drafts. -Check solenoid. -Clean spatter from gun gas ports. -Starting porosity may be eliminated by ; <ul style="list-style-type: none"> -striking arc with short stickout. -purging gas lines before striking arc. -If flowmeter or regulator freezes; <ul style="list-style-type: none"> -install heater. -use manifolded cylinders. | | |
| Wire stubs and weld appearance not acceptable. | <ul style="list-style-type: none"> -When welding over rust, millscale and foreign matters; <ul style="list-style-type: none"> -clean base metal. -slow down travel speed. -Check wire feeder fuse. Check for overload or short circuit. -Clean contact tube. -Use electrodes of T-2 designation (procedure required) -Change shielding gas. -Welding over manual tack welds. | | |
| Lack of penetration. | <ul style="list-style-type: none"> -Too much slope. -Arc voltage too low. -Wire feed speed too high. -Irregular speed on wire feeder motor. | | |
| Slag inclusions. | <ul style="list-style-type: none"> -Current too low. -Stickout too long. -Improper technique; arc not carried at leading edge of puddle. | | |
| Undercut. | <ul style="list-style-type: none"> -Clean base metal prior too welding. -Remove all slag from previous pass. -Increase heat input. | | |
| Cracks. | <ul style="list-style-type: none"> -Improper technique. -Travel speed too high in relation to current and voltage. -Voltage too high. | | |
| | <ul style="list-style-type: none"> -Increase bead size. -Limit or eliminate restraint. -Use proper preheat | | |

Fig. H.14. Welding Procedure Specification (Pg. 8)

Prepared by Skarborn Engineering Ltd.
For MARID INDUSTRIES LTD.

Welding Procedure
Specification No. 2/7
Page Number. 8
Issue. 2015-1
Page Revision. —
Rev. Date. —

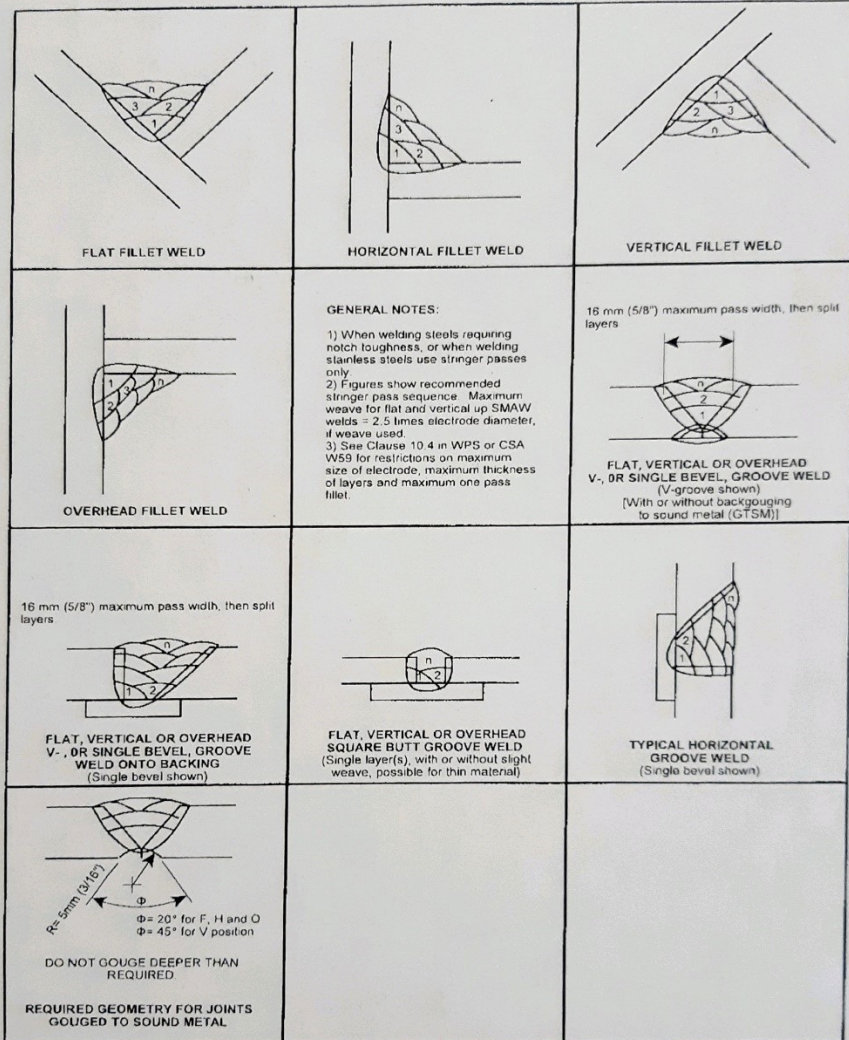


FIGURE 1 - RECOMMENDED PASS SEQUENCE
(Similar sequence recommended for other joint types)

Fig. H.15. Welding Procedure Specification (Pg. 9)